In-situ FTIR Spectroelectrochemical Studies on the Electrocatalytic Reduction of Carbon Dioxide by Some Ruthenium and Iron Complexes

A Thesis

forwarded to

Department of Applied Biology & Chemical Technology

in

Partial Fulfillment of the Requirements

for

the Degree of Master of Philosophy

at

The Hong Kong Polytechnic University

by

Pun So Ngan

May, 2001

Declaration

I hereby declare that the thesis summarizes my own work carried out since my registration for the Degree of Master of Philosophy in October, 1998, and that it has not been previously included in a thesis, dissertation or report submitted to this or any other institution for a degree, diploma or other qualification.

Pun So Ngan

May, 2001

Acknowledgements

I am deeply grateful to Prof. K. Y. Wong, my peerless supervisor, for his many intelligent and insightful suggestions and for the meticulous care he gave in the preparation of this thesis. His consistent support and empathic advice were instrumental in the completion of this project. I owe him my enduring gratitude.

Dr. C. H. Yeung is gratefully acknowledged to be my co-supervisor. I wish to thank a few friends and postgraduate colleagues for their abiding support throughout this project: Dr. W. H. Chung, Dr. K. W. Yeung. Dr. W. H. Fung, Dr. P. Guo, Dr. C. M. Chan, Dr. S. H. Lau, Mr. K. C. Cheung, Ms. M. Y. Chan, Ms. H. S. Tang. I must also acknowledge my family. My mother and sisters have given me the inestimable comfort and cheerful encouragement in the past two years.

Finally, I would like to thank the Research Committee of The Hong Kong Polytechnic University for the award of a tuition scholarship and a studentship in 1998-2001 and for a grant supporting my conference presentation in the 219th American Chemical Society National Meeting held in San Francisco in March, 1999. Last, but not least, the award of a postgraduate fellowship by the Sir Edward Youde Memorial Fund is gratefully acknowledged.

Abstract of thesis entitled "*In-situ* FTIR Spectroelectrochemical Studies on the Electrocatalytic Reduction of Carbon Dioxide by Some Ruthenium and Iron Complexes"

Submitted by Pun So Ngan

For the Degree of Master Philosophy

at The Hong Kong Polytechnic University

May, 2001

Abstract

The excessive production of CO_2 is a major environmental issue. The removal of CO_2 by reducing it to energetically rich raw materials is one way to recycle the carbon source. In the past two decades, much attention has been paid to the eletrocatalytic reduction of CO_2. In order to develope an efficient system to recycle CO_2, an in-depth understanding of the mechanism of CO_2 reduction is necessary.

In this study, we have synthesized and characterized two new ruthenium carbonyl complexes, namely $[Ru(bdmpp)(bpy)CO]^{2+}$ **[1]** and $[Ru(tpm)(bpy)CO]^{2+}$ **[2]** (bdmpp = 2,6'-bis(3,5-dimethylpyrazol)pyridine; tpm = tris(1-pyrazoyl)methane; bpy = 2,2'-bipyridine) that are electrocatalysts for CO_2 reduction. The mechanism for CO_2 reduction was investigated by cyclic voltammetry, constant potential electrolysis and *in-situ* FTIR spectroelectrochemistry. It was found that addition of protic sources significantly enhanced the rate of CO_2 reduction. In the presence of H_2O as proton source, CO was produced exclusively with current efficiency close to 98%. In the presence of protonated amine salts such as $Et_3NH^+Cl^-$, selective production of formate could be achieved with a current efficiency as high as 90%. Mechanistic studies by *in-situ* FTIR spectroelectrochemistry suggested that CO was afforded via a Ru-COOH intermediate in the presence of H_2O as proton source. CO was produced by protonation of the coordinated CO_2 by H_2O followed by the cleavage of one C-O bond and subsequent release of CO from the metal center. On the contrary, a Ru-H species was detected in the IR spectrum prior to the formation of the metalloformate species in the presence of $Et_3NH^+Cl^-$, which supported that the ruthenium formato species was formed via the insertion of CO_2 into a Ru-H moiety.

The effect of weak Brönsted acid on the electrocatalytic reduction of CO_2 by $[Fe(dophen)(N\text{-}MeIm)_2]^+$ **[3]** was also studied. Addition of weak Brönsted acids such as trifluoroethanol or methanol can enhance the rate of catalysis to yield a mixture of carbon monoxide, formate and oxalate. Monitoring the reduction process by *in-situ* FTIR showed the existence of both an iron carbonyl and an iron formato species. While CO and $HCOO^-$ were suggested to be produced by similar mechanisms as the ruthenium catalysts, the homolytic cleavage of the Fe-C bond of $Fe\text{-}COO^-$ will lead to the formation of $CO_2^{\bullet-}$ which will subsequently dimerize to yield oxalate. This is probably because the carbenoid character of $Fe\text{-}COO^-$ is weaker than that of $Ru\text{-}COO^-$ which leads to the release of $CO_2^{\bullet-}$ in an early stage of the catalytic process.

Structure of Ligands and Abbreviations

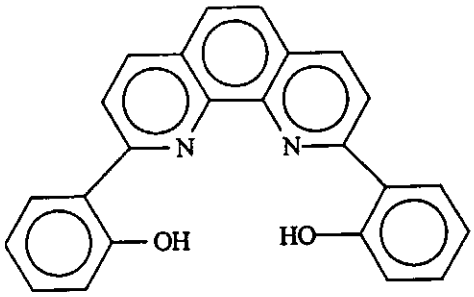

2,9-bis(2'-hydroxyphenyl)-1,10-phenanthroline) (H_2dophen)

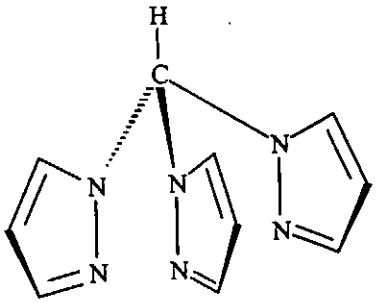

tris-(1-pyrazoyl)-methane (tpm)

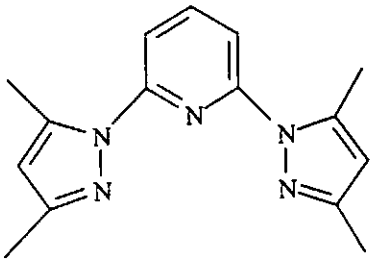

2,6-bis(3,5'-dimethylpyrazoyl)pyridine (bdmpp)

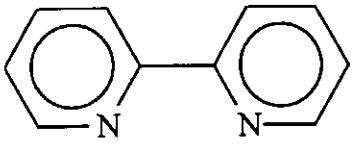

2,2'-bipyridine (bpy)

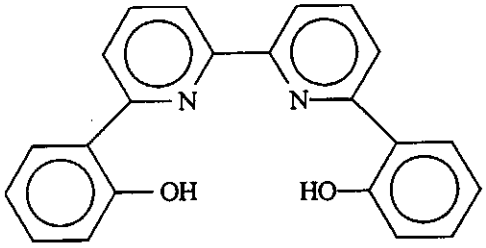

6,6'-bis(2'-hydroxy)-2,2'-bipyridine

(H_2dobpy)

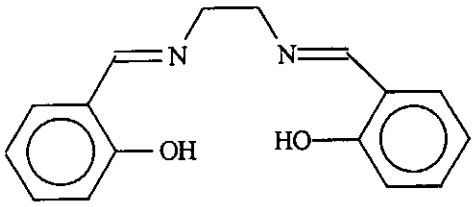

N,N'-bis(salicylidene)ethylenediamine

(H_2salen)

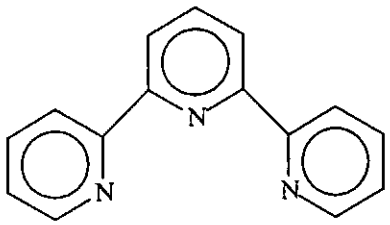

2,2':6',2"-terpyridine (terpy)

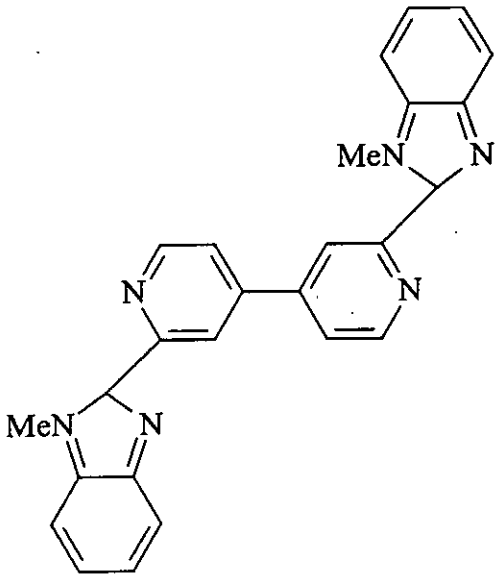

2,2'-bis(1-methyl-benzimidazol-2-yl)-4,4'-bipyridine (dmbbbpy)

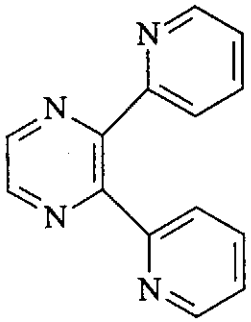

2,3-bis(2-pyridyl)pyrazine (dpp)

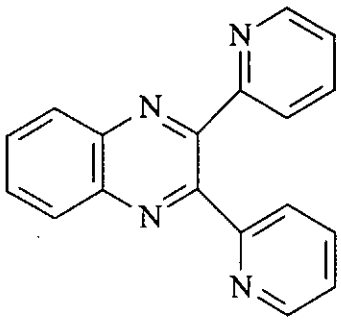

2,3-bis(pyridyl)quinoxaline (dpq)

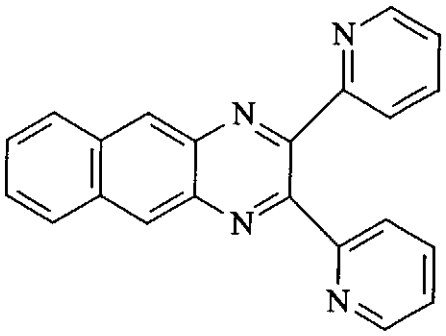

2,3-bis(2-pyridyl)benzoquinoxaline

(dpb)

Table of contents

Declaration *ii*

Acknowledgements *iii*

Abstract *v*

Structure of Ligands and Abbreviations *vii*

Chapter 1 *1*

Introduction *1*

1.1 Background **2**

1.2 Electrochemical Reduction of Carbon Dioxide Catalyzed by Transition Metal Complexes **7**

***1.3 In-situ* FTIR Spectroelectrochemistry** **18**

1.4 Aims and Objectives **22**

Chapter 2

Synthesis, Characterization, X-ray Crystal Structure and Electrochemical Behavior of the Ruthenium Carbonyl Complexes *24*

2.1 Introduction **25**

2.2 Experimental Section **26**

2.3 Results and Discussion **34**

2.4 Conclusion **60**

Chapter 3

In-situ FTIR Spectroelectrochemical Study on the Reduction of CO_2 Catalyzed by the Ruthenium Complexes *61*

3.1 Introduction **62**

3.2 Experimental **63**

3.3 Results and Discussion **64**

3.4 Conclusion 114

Chapter 4

In-situ FTIR Spectroelectrochemical Study on the Reduction of CO_2 Catalyzed by an Iron Complex *115*

4.1 Introduction 116

4.2 Experimental Section 117

4.3 Results and Discussion 121

4.4 Conclusion 151

Chapter 5

Conclusions *152*

References *156*

Chapter 1

Introduction

1.1 Background

Carbon dioxide is the ultimate by-product of all the processes involving oxidization of carbon compounds; the content of CO_2 in the atmosphere has been increased since Industrial Revolution. Until the beginning of this decade, the total amount of CO_2 human have added to the atmosphere was approximately $7x10^9$ ton carbon [1]. Although green plants can remove a certain amount of carbon dioxide by converting it into energy-rich molecules via photosynthesis, heavy deforestation and interference by mankind greatly upset the equilibrium. The build-up of carbon dioxide causes the development of the "Green House" effect which leads to global warming with unpredictable but potentially catastrophic consequences. It has been speculated that global warming causes the melting of floating arctic ice and rise in the sea level. According to a forecast by climatologists, by the end of the century, the globally average temperature will increase by 1.5°C to 4.5°C for a doubling of CO_2 concentration [2]. In order to minimize the impact to the ecosystem, a change in energy policy to cut back the human-induced emission of CO_2 is essential. One effective way is to recycle the poor energy CO_2 into useful fuel and chemicals. This is an attractive solution because of the vast supply of CO_2, its low cost and its use as a possible source for C_1 feedstock [3].

However, to recycle CO_2 is not a simple task because it is a very inert and thermodynamically stable molecule (the free energy of formation of CO_2, ΔG_f=-394 kJ/mol [4], is so negative that a very high-energy reductant is required for its reduction). Besides, the high-energy gap between the HOMO and LUMO of the CO_2 molecule induces a large kinetic barrier [4, 5]. The E°' value for the $CO_2/CO_2^{\bullet-}$ redox couple was

estimated to be beyond –2.21 V vs. saturated calomel electrode (SCE) [5-7]. Hence, the development of low-overpotential methods for activating CO_2 would have profound consequences on the economics of C_1 chemical industry. Although there are many successful applications of CO_2 based on its special physical properties, e.g. its use as protective gas in steel industry, a refrigerant in the form of "dry ice", a fire extinguishing agent and a propellant gas, only a few of these applications actually use CO_2 as raw materials. The representative examples include the production of urea, salicylic acid and terephthalic acid [3, 8]. Recent research on carbon dioxide reactions has been extended to various fields of chemistry and a number of potentially useful reactions of carbon dioxide have been studied: electrochemical [4-7, 9-111], photochemical activation of carbon dioxide [2, 112-132] and biomimetic fixation of carbon dioxide [3]. Among various approaches, the electrochemical method is a promising approach. When coupled with a photoelectrochemical device, it is possible to use the energy from sunlight for CO_2 fixation. In principle, useful products like methane and methanol can be afforded through multi-electron reduction of carbon dioxide with redox potential becoming less and less negative, i.e. thermodynamically more favorable. The thermodynamic reduction of CO_2 to various products in a pH 7.0 aqueous buffer solution is given as follows (eqs. 1-5) [133]:

			E°' vs. NHE
$CO_2 + 2H^+ + 2e^-$	$\rightarrow$	$CO + H_2O$	-0.52 V (1)
$CO_2 + 2H^+ + 2e^-$	$\rightarrow$	$HCOOH$	-0.61 V (2)
$CO_2 + 4H^+ + 4e^-$	$\rightarrow$	$HCOH + H_2O$	-0.48 V (3)
$CO_2 + 6H^+ + 6e^-$	$\rightarrow$	$CH_3OH + H_2O$	-0.38 V (4)
$CO_2 + 8H^+ + 8e^-$	$\rightarrow$	$CH_4 + H_2O$	-0.24 V (5)

Investigations on the direct electrochemical reduction of carbon dioxide have been carried out for many years. In the early stage, studies were focused on the electrocatalytic reduction of CO_2 at semi-conductor and metal electrodes in both aqueous and non-aqueous media [1, 10, 27, 28, 33-35, 52, 59, 65, 78-85, 107, 126]. Hori et al. [80, 107] have reported the formation of CH_3OH, CO and HCOOH in the electrochemical reduction of CO_2 by various metal electrodes (Cd, Sn, Pb, In, Zn, Ag, Cu, Ni and Fe). Among them, Au and Ag electrodes gave CO as the main product. Jermann et al. [86] also reported the changes in product distribution (CH_4, C_2H_4, C_2H_5OH) as a function of electrolysis time for the cathodic reduction of CO_2 at a Cu electrode. Anodic activation of the copper electrode also resulted in a change in the product distribution favoring the formation of ethylene. Hori and Takahashi have performed experiments on the reduction of CO_2 using a Cu electrode in an aqueous medium [10]. Their results indicated that CO_2 was electrochemically reduced to CH_4, C_2H_4 and alcohol in $KHCO_3$ solution with high current densities. Apart from Cu electrodes, other electrode materials can also give rise to hydrocarbon production. Azuma et al. reported that Pd electrodes could be used for the reduction of CO_2 to hydrocarbons in an aqueous solution. However, they exhibit lower current efficiencies and higher overvoltages. Interestingly, Frese and Leach [87] reported the formation of CH_4, CO and CH_3OH at Ru electrodes. Moreover, molybdenum [88] was shown to be a useful cathodic material for generating methanol from CO_2 after the electrodes had been pretreated by cycling in a CO_2-saturated solution.

Since the solubility of CO_2 in aqueous solutions is low and in order to increase the concentration of CO_2, high pressure or low temperature conditions have been employed for the reduction process. Ito et al. [81] studied the electrochemical reduction

of CO_2 at 20 atm using In, Pb, Sn and Pb-Hg electrodes. All electrodes gave formate together with a small amount of carboxylic acids. Kaneco et al. [59] also investigated the electrochemical reduction of CO_2 in tetraethylammonium perchlorate/methanol electrolyte at -30°C. Carbon monoxide, methane, ethylene and formic acid were the major products. In addition, Kaneco et al. have studied the electrochemical reduction of CO_2 in 0.1 M KOH-methanol electrolyte with a Ag electrode [82] at low temperature and CsOH-methanol electrolyte with a Cu electrode [83]. The main products of the former case were carbon monoxide and formic acid while methane, ethylene, carbon monoxide and formic acid were afforded in the latter case. Semiconductors are of special interest in the electrochemical reduction of carbon dioxide because of the opportunity in fabricating photoelectrochemical devices based on these materials [1, 78, 79, 126]. Pi-Si, p-Cd Te, p-Ip P, p-Ga As have all been used [1, 126]. The current efficiency of CO could be achieved up to 90% while H_2 production was suppressed to a low level.

In general, the electrochemical reduction of CO_2 on metallic electrodes require a relatively negative potential (typically beyond –2.2 V vs. SCE). Moreover, the distribution of products critically depends on reaction conditions such as electrode materials, solvent systems and operational parameters including current density and CO_2 concentration [1]. In order to reduce the energy consumption and optimize the product selectivity, the use of molecular electrocatalysts in conjunction with cathode mediated electroreduction is an appealing approach. Besides, subtle variation in the structure of the molecular catalyst and fine tuning of the transition metal center environment can be achieved through synthetic techniques. Hence, much effort has

been devoted to search for an effective molecular system for the reduction and fixation of CO_2.

1.2 Electrochemical Reduction of Carbon Dioxide Catalyzed by Transition Metal Complexes

It is known that CO_2 can bind to a transition metal center or insert into a metal ligand bond. The major binding modes of CO_2 on a metal center include "end on" through the oxygen atom (η^1-O-C-O) or via the central C atom (η^1-CO_2) and "side on" to a C-O bond (η^2-CO_2) [134]. Insertion of CO_2 to a metal-ligand bond (where the ligand can have H, C, N or O ligating atom) has been extensively studied [23, 60]. For instance, insertion of CO_2 into a M-H bond to give a metalloformate complex of the form M-OC(O)H is kinetically favoured over the formation of a metal carboxylate species [23, 60].

A large variety of transition metal complexes have been shown to catalyze CO_2 reduction. The following is a brief review of the major classes of transition metal complexes that have been reported to be electrocatalysts for CO_2 reduction.

1.2.1 Porphyrins and Phthalocyanines

In 1974, Meshitsuka et al. [70] first reported that cobalt or nickel phthalocyanine deposited on electrode surface can catalyse the electrochemical reduction of CO_2 to oxalic and glycolic acid, although there is considerable controversy over the nature of products being reported by two independent groups [71, 72]. Extensive investigations on electrode materials [73] including mechanistic studies [74, 75] have been carried out. In 1977, Hiratsuka et al. [76] reported the use of water-soluble tetrasulfonated Co and

Ni phthalocyanines as catalysts for CO_2 reduction. Later, the investigation was extended to water-soluble porphyrins in aqueous and non-aqueous media [77].

Savéant et al. [66, 68, 89, 135] reported that iron porphyrins catalyzed the electrochemical reduction of CO_2 to CO. The catalytic activity of Fe(0) tetraphenylporphyrin was dramatically increased upon the addition of Lewis acid such as Mg^{2+} or Brönsted acids like CF_3CH_2OH [66, 68, 89] while the degradation rate of the catalysts was suppressed. Gisselbrecht et al. [136] also investigated the electrochemical behavior of iron porphycenes (a class of porphyrin analogue) in various aprotic solvents. The iron porphycenes also displayed catalytic activity towards CO_2 reduction.

Besides iron porphyrins, Tezuka et al. [92] also investigated the electrocatalytic reduction of CO_2 with cobalt tetraphenylporphyrin in DMF. Based on kinetic studies, the rate constant for electron transfer from catalyst to CO_2 was determined and the activation energy of the reaction was also estimated. Furthermore, Atoguchi et al. [93] reported that cobalt tetraphenylporphyrin adsorbed on glassy carbon electrode in the presence of pyridine is an active catalyst for the electroreduction of CO_2. Recently, Behar et al. [11] reported the catalytic formation of CO and $HCOO^-$ in the photochemical reduction of CO_2 catalyzed by cobalt porphyrins in acetonitrile solutions containing triethylamine as a reductive quencher.

1.2.2 Tetraazamacrocyclic complexes

Fisher and Eisenberg [90] were the first to demonstrate the catalytic activity of various Ni(I) tetraazamacrocyclic complexes in the electrochemical reduction of CO_2 in aqueous medium or acetonitrile/water mixture. CO and H_2 were the major reduction products. The tetraazamacrocyclic complexes are stable over a long period of electrolysis with minimal loss of catalytic activity in the presence of a protic source. Tinnemans et al. [91] also reported a number of cobalt and nickel tetraazamacrocyclic complexes of cobalt and nickel that are active electrocatalysts for CO_2 reduction. Schbioh et al. [109] have studied the electrochemical reduction of CO_2 catalyzed by $[NiL]^{2+}$ (L= 1,3,6,9,11,14-hexaazacychexadecane) which produced CO, H_2 and HCOOH. Blinn et al. [9] demonstrated that electrolysis of $[Ni(Me_2[12]aneN_4)(H_2O)]^{2+}$ in the presence of carbon dioxide and various electrolytes resulted in the quantitative formation of formic acid. High yield of formic acid was obtained using a mercury pool electrode in 0.1 M $NaClO_4$, whereas lower yield was obtained in 0.1 M NaCl solution.

1,4,8,11-tetraazacyclotetradecane, usually known as cyclam, is one of the most popular macrocyclic ligands in coordination chemistry. It forms highly stable complexes with a large variety of transition metals [137, 138]. Sauvage et al. [94-96] reported that nickel cyclam and dimetallic $[Ni_2(biscyclam)]^{4+}$ complexes are efficient and selective catalysts for electroreduction of CO_2 to CO at Hg electrode even in aqueous medium. Mochizuki et al. [112] also reported that the bimarcocyclic complex [6,6'-bi(5,7-dimethyl-1,4,8,11-tetraazacyclotetradecane)] dinickel (II) acts as a more efficient catalyst to generate CO than the monomacrocyclic complex.

Recently, Bujno et al. [63] reported that systemic increase of N-methyl substitutions in $[Ni(cyclam)]^{2+}$ would suppress its catalytic activity towards CO_2 reduction. Anson et al. [101] proposed that the origin of the decrease in catalytic activity of nickel cyclam was due to the presence of an insoluble Ni(cyclam)(CO) complex. While CO is the product of CO_2 reduction, the formation of Ni(cyclam)(CO) limits the long-term effectiveness of the nickel cyclam catalyst. The size of the cyclam ligand and the presence of secondary amine group are important in tuning the activity of the catalyst: the former imparts high kinetic and thermodynamic stability to the nickel cyclam complex, whereas the latter favors CO_2 binding by hydrogen bonding in addition to the carbon-to-Ni(I) bond.

1.2.3 Metal clusters

Hidai et al. [100] reported that tetranuclear iron-sulfur clusters of the type $[Fe_4S_4(SR)_4]^{2-}$ (R = $CH_2C_6H_5$, C_6H_5) can function as electrocatalysts of CO_2 reduction in DMF with formate as the major product. Tanaka et al. also [97, 98] investigated the electrochemical reduction of CO_2 with metal clusters like $[\{Rh(C_5Me_5)\}_3(\mu_3\text{-}S)_2]^{2+}$, $[\{Ir(C_5Me_5)\}_3(\mu_3\text{-}S)_2]^{2+}$ and $[\{CoC_5H_4Me)\}_3(\mu_3\text{-}S)_2]^{2+}$. The rhodium cluster reduced CO_2 to formate and oxalate whereas the iridium and cobalt clusters produced oxalate exclusively. A coupling reaction of two CO_2 molecules bonded on adjacent μ_3-S and Ir in the iridium clusters was proposed for the generation of $C_2O_4^{2-}$ without accompanying CO evolution [58]. In addition, Kubiak et al. [99] reported that the trinuclear nickel complex $[Ni_3(\mu\text{-}CNMe)(\mu_3\text{-}I)(dppm)_3]^+$ is an electrocatalyst of CO_2 reduction. The reduction products corresponded to the reductive disproportionation of CO_2 to CO and

CO_3^{2-}. Mann et al. [51] have studied the eletrocatalytic reduction of CO_2 by $[Ir_2(dimen)_4]^{2-}$ (dimen = 1,8-diisocyanomenthane). Bicarbonate and formate were identified as the reduction products by infrared spectroelectrochemistry.

1.2.4 Phosphine complexes

Wagenknecht and Slater [104] reported the electrocatalytic reduction of CO_2 by $Rh(diphos)_2Cl$ (diphos = 1,2-bis(diphenylphosphine)ethane) in anhydrous CH_3CN. Formate was obtained with a current efficiency of 22-42% depending on electrolysis time. Since a small amount of cyanoacetate ($CN\text{-}CH_2\text{-}COO^-$) was detected, CH_3CN is suspected to be the proton source for formate formation. Dubois et al. [102, 103] have investigated a series of palladium complexes of the type $[Pd(triphos)L]^{2+}$ (triphos = bis (2-diphenylphosphinoethyl)phenylphosphine); L = CH_3CN, PEt_3, $P(OMe)_3$, $P(OCH_2OH)_3$) as catalysts for the electrochemical reduction of CO_2 to CO in acidic acetonitrile solution. Mechanistic studies indicated that the rate-determining step in the catalytic cycle at high acid concentration is the reaction of Pd(I) complex with CO_2. The catalysts were deactivated by the formation of Pd(I) dimers but the deactivation could be reversed by electrochemical oxidation. The same group also [64] reported that $[Pd(Me_2P^+etpE)(CH_3CN)]^{3+}$ (Me_2P^+etpE = $[(Me_2PCH_2CH_2)P(CH_2CH_2PEt_2)_2]^+$) is an active catalyst for the electrochemical reduction of CO_2 to CO in acidic dimethylformamide solution. Recently, Ogura et al. [105] reported that $[M(PPh_3)_2L]X$ (M = Pd, Co; L = 2-methyl-8-hydroxyquinoline, 2-quinoxalinol, 1-hydroxyisoquinoline, 3-hydroxyisoquinoline, 4,4'-dimethyl-2,2'-bipyridine or 4-methyl-1,10-phenanthroline; X = Cl, Br or ClO_4) work as catalysts for CO_2 reduction in anhydrous acetonitrile at an

applied potential of -1.3 V vs. Ag/Ag^+ to give CO with high current efficiency. In acetonitrile-water mixture, the reduction products were HCOOH and H_2 to addition to CO.

The binuclear copper complex, $[Cu_2(\mu\text{-}PPh_2bipy)_2(MeCN)_2][PF_6]_2$ (PPh_2bipy = 6-(diphenylphosphino)-2,2'-bipyridine) and its pyridine analogue $[Cu_2(\mu\text{-}PPh_2bipy)_2(py)_2][PF_6]_2$ (py = pyridine) have been shown to be electrocatalysts for the reduction of CO_2 [56]. Based on kinetic and spectroscopic results, a mechanism involving substitution of a solvent molecule by a CO_2 molecule followed by two sequential heterogeneous electron transfers was proposed. The rate-determining step is the reaction between the doubly-reduced dimer and CO_2 which is first order in both dimer and CO_2. Christensen et al. [54] have shown that CO_2 is selectively reduced to oxalate at potentials < -1.1 V vs. SCE at a $[Ni(dppm)_2Cl_2]$/polyvinylalcohol (dppm = $Ph_2PCH_2PPh_2$) modified Pt electrode in acetonitrile. The consumption rate of CO_2 was maximum at –1.8 V; about 70-90% of the CO_2 was converted to oxalate. When $[Ni(dppm)_2Cl_2]$ was employed as a homogeneous catalyst in acetonitrile, only CO was produced.

1.2.5 Polypyridyl complexes

Polypyridyl complexes are of much interest among the catalysts being discussed. Ligands like 2,2'-bipyridine (bpy) or 1,10-phenanothroline (phen) can stabilize transition metal in a large number of oxidization states and they serve as an "electron reservoirs" by utilizing vacant π^* orbitals to store electrons. A large number of these metal complexes have been reported to be active in the electrocatalytic reduction of CO_2.

Hawecker et al. first reported that $[Re(bpy)(CO)_3Cl]$ is a catalyst for the photochemical reduction of CO_2 to CO [111]. Subsequently, it was shown that the same complex can catalyze the selective electroreduction of CO_2 to CO in DMF-water mixture (9:1 v/v) [49]. Under suitable conditions, high faradaic yields (98%) with large catalytic turnovers could be achieved. Meyer et al. [29] studied the mechanism of CO_2 reduction by $[Re(bpy)(CO)_3Cl]$ in acetonitrile. Electrolysis at –1.55 V vs. SCE produced both CO and CO_3^{2-} whereas electrolysis at –1.8 V would lead to the formation of CO only. Two different electrocatalytic pathways are proposed: initial one-electron reduction of the catalyst at ca. –1.5 V followed by the reduction of CO_2 to give CO and CO_3^{2-}, or an initial two-electron reduction of the catalyst at ca. –1.8 V to give CO only. Complexes of the type $[Re(bpy)(CO)_3X]$ (X = H, HCO_2^- or OCO_2^-) have been isolated and characterized. Recently, Hori et al. [129] have investigated the photochemical reduction of CO_2 using [*fac*-$Re(bpy)(CO)_3$(4-Xbpy)] (X = t-butyl, methyl, H, CH_3CO, CN) in a triethanolamine (TEOA) - DMF solution. The system was able to produce CO catalytically.

Several groups have fabricated chemically modified electrodes for CO_2 reduction based on derivatives of $[Re(bpy)(CO)_3Cl]$. Meyer et al. [108] used a vinyl derivative of the rhenium complex $[Re(vbpy)(CO)_3Cl]$ (vbpy = 4-vinyl-4'-methyl-2,2'-bipyridine) to form a rhenium polymeric film on Pt electrode surface. The modified electrode was able to catalyze the electrochemical reduction of CO_2 to CO. Deronzier et al. [41, 44] also investigated the polymeric film produced by electropolymerization of $[fac\text{-}Re^{I}(L)(CO)_3Cl]$ (L = pyrrole containing 2,2-bipyridine ligand). The stability of the catalyst was greatly enhanced in the polymeric film compared with that in homogeneous solution. Recently, Parimal et al. [12] studied the electrochemical reduction of CO_2 catalyzed by $[Rh(tptz)Cl_3].2H_2O$, $[Rh(tptz)_2][ClO_4]_2.2H_2O$ and $[Rh(tpy)Cl_3]$ (tptz = 2,4,6-tris(2-pyridyl)-1,3,5-triazine). Formic acid was obtained as the major product in the electrolysis in DMF containing 2.5% water saturated with CO_2.

Polypyridyl complexes of ruthenium have been used as catalysts in the photochemical [113-118] and electrochemical reduction [5, 6, 17-25, 38-40, 47, 48, 69] of CO_2. Collomb-Dunand-Sauthier et al. [38-40, 47, 48] demonstrated that the mono(bipyridyl) complex trans-(Cl)-$[Ru^{II}(bpy)(CO)_2Cl_2]$ is a selective and efficient catalyst in solution. The electrocatalytic activity is due to the formation of a polymeric $[\{Ru^0(bpy)(CO)_2\}_n]$ film on the electrode surface. The electrogenerated $[\{Ru^0(bpy)(CO)_2\}_n]^{n-}$ is proposed to be the key species in the electrocatalytic reduction. The bis(bipyridyl) complex cis-$[Ru(bpy)_2(CO)_2]^{2+}$ was found to exhibit similar catalytic activities as the mono(bipyridyl) complexes [69]. Electroreduction of this complex in CH_3CN can also lead to the formation of a polymeric film $[Ru^0(bpy)(CO)_2]_n$ on electrode surface. In aqueous solution, films containing bipyridine ligand or 4,4'-substituted bipyridine with electron donating groups gave CO as the main. With films

containing bipyridine with electron-withdrawing substituents like esters, $HCOO^-$ was obtained quantitatively [69].

Apart from the mono(bipyridyl) ruthenium complexes, Tanaka et al. [5, 22] reported the reduction of CO_2 catalyzed by $[Ru(bpy)_2(CO)_2]^{2+}$ at –1.5 V vs. (SCE) in a DMF–H_2O (1:9 v/v) solution buffered at pH 9.5. Formic acid and CO as well as H_2 were formed in alkaline condition, whereas only CO and H_2 were evolved in acidic medium. A mechanism in which the reaction occurred via the formation of a stable pentacoordinated Ru(0) complex $[Ru(bpy)_2(CO)]^0$ generated by two-electron reduction of $[Ru(bpy)_2(CO)_2]^{2+}$ or $[Ru(bpy)(CO)(Cl)]^+$ was suggested. Besides mono bipyridine complexes, Tanaka et al. [17] also investigated the electrocatalytic reduction of CO_2 catalyzed by $[RuL_1(L_2)(CO)_2]^{2+}$ (L_1, L_2= $(bipy)_2$, (bipy)(dmbipy), $(dmbipy)_2$ or $(phen)_2$] in acetonitrile which gave HCOOH and $C_2O_4^{2-}$ in the presence and absence of proton source respectively. Moreover, study on the multi-step CO_2 reduction catalyzed by $[Ru(bpy)_2(qu)CO]^{2+}$ (qu=quinoline) was carried out [21]. The work is the first example of catalytic formation of $CH_3C(O)CH_3$ and $CH_3C(O)CH_2COO^-$ by double methylation of the carbonyl moiety resulting from the reductive disproportionation of CO_2 followed by subsequent carboxylation. $[Ru(bpy)(trpy)CO]^{2+}$ is also known to be an effective electrocatalyst for CO_2 reduction [20]. Electrolysis of this complex at –1.75 V vs. Ag/Ag^+ in CO_2-saturated C_2H_5OH/H_2O (8:2 v/v) mixture at -20°C leads to a variety of products including HCOH, CH_3OH, HCOCOOH, $HCOCH_2COOH$, CO and HCOOH. Under aprotic conditions, CO and CO_3^{2-} are produced due to an oxide transfer reaction from the Ru-η^1-CO_2 intermediate to CO_2. Tanaka et al. proposed that the formyl complex $[Ru(bpy)(trpy)(CHO)]^+$ is a possible intermediate in the multi-electron reduction of CO_2 [19].

Recently, Tanaka et al. [25] reported the electrocatalytic reduction of CO_2 by $[Ru(L_2)(dmbbbpy)][PF_6]_2$ and $[L_2Ru(dmbbbpy)RuL_2][PF_6]_4$ (L = bpy, dmbbbpy = 2,2'-bis(1-methyl-benzimidazol-2-yl)-4,4'-bipyridine) in acetonitrile which gave HCOOH and $C_2O_4^{2-}$ in the presence and absence of H_2O respectively. The two-electron reduction of the mono- or di-nuclear ruthenium complexes caused dechelation of dmbbbpy from the Ru center which may provide binding sites for 2 molecules of CO_2 thus facilitating the coupling reaction of CO_2 to give oxalate. Moreover, they reported the first selective production of acetone in the electrochemical reduction of CO_2 catalyzed by $[Ru(bpy)(napy)_2(CO)_2][PF_6]_2$ [24] in the presence of $(CH_3)_4NBF_4$. It was suggested that $(CH_3)_4N^+$ works not only as an electrolyte, but also as a methylation reagent for the catalytic generation of acetone.

Osmium, iridium and rhodium polypyridyl complexes have also been studied as catalysts for CO_2 reduction in acetonitrile solution to give CO as the major product [16, 26, 46, 110]. Addition of water resulted in the formation of formate with current efficiency up to 22%. Brewer et al. [110] showed that $[Rh(L)_2Br_2]^+$ and $[Ir(L)_2Cl_2]^+$ (L = 2,2'-bipyrimidine (bpm), 2,3-bis(2-pyridyl)pyrazine (dpp), 2,3-bis(2-pyridyl)quinoxaline (dpq) or 2,3-bis(2-pyridyl)benzoquinoxaline (dpb)) can catalyze the electrochemical reduction of CO_2 to formate in acetonitrile. As these bridging ligands are easier to reduce than bipyridine, the complexes prepared are easier to reduce and exhibit electron transitions at lower energies. Meyer et al. [26] also investigated the cis-$[M(bpy)_2X_2]^+$ complexes (M = Rh^{III} or Ir^{III}, X = Cl or trifluoromethanesulfonate) as electrocatalysts for the reduction of CO_2. Electrolysis performed in acetonitrile at –1.55 V vs. SCE lead to the production of formate. The source of formate proton is apparently the tetraalkylammonium salt. In addition, Deronizier et al. [57] showed that

$[\eta^5\text{-}(Me_5C_5)M(L)Cl]^+$ (L = 2,2'-bipyridine; M = Rh(III) and Ir(III)) can act as electrocatalysts for CO_2 reduction. It appears that the Rh(III) complex is a better catalyst than the Ir(III) and current efficiency up to 50% for formate production could be reached.

Most of the systems reported so far lead to either CO or HCOOH or a mixture of both. Therefore, a better understanding of the reduction mechanism is essential in order to determine the factors influencing the product selectivity and efficiency. Although the mechanism for the formation of CO is generally believed to occur via a M-COOH intermediate, the reaction mechanism for the formation of $HCOO^-$ still remains controversial. All metal-OC(O)H [23, 50, 57, 60, 139-142], -C(O)OH [5, 143] and –C(O)H [19] have been postulated as the reaction intermediates. Different approaches have been used by researchers to identify the intermediates involved in the formation of formate. One of the approaches is to prepare model complexes whose properties might enhance the understanding of steps in the catalytic cycles [19, 23, 144]. Gibson et al. [145] and Meyer et al. [23] suggested that formate can be afforded in the catalytic reactions via CO_2 insertion into a M-H bond. Perutz et al. also showed that the η^1-formate hydride complex, cis-$Ru(PMe_3)_4$-(η^1-OCHO)H was afforded through bubbling CO_2 to a solution of $Ru(PMe_3)_4H_2$ and proposed that the formato complex was most likely formed by the insertion of CO_2 into the Ru-H bond.

1.3 *In-situ* FTIR spectroelectrochemistry

As mentioned before, most electrocatalysts for CO_2 reduction give a mixture of carbon monoxide and formate as products. Many attempts, not all with concordant results, have been made to elucidate the nature of the intermediate species involved in the reduction process in order to have a better understanding of the mechanism. Most of the mechanistic studies were restricted to bulk electrolysis, cyclic voltammetry and synthesis of model complexes. Most recently, a number of research groups [4, 50, 54, 140, 146, 147] employed the *in-situ* FTIR spectroelectrochemical technique to investigate the mechanism of CO_2 reduction. FTIR spectroelectrochemical technique is particularly useful in these studies because many plausible intermediates in CO_2 reduction such as M-(η^1-OCO), M-(η^2-OCO), M-(η^1-CO_2^-) and M-CO species all absorb strongly in the IR region.

In our study, the IR spectra collected are presented in the form of difference spectra. A reference spectrum, S_1, was first collected at a reference potential E_1 which is usually in the electro-inactive region. The potential of the working electrode was then stepped to a potential E_2 and a second spectrum S_2 was collected at successive time intervals. A certain number of co-added and averaged scans were taken to give the desired S/N ratio. The spectra were therefore presented as:

$$\Delta R/R = (S_2-S_1)/S_1 \text{ versus } \nu \text{ (cm}^{-1}\text{)}$$

It follows that both positive and negative peaks can appear in the difference spectrum. A positive peak, i.e.. $+\Delta R/R$ represents absorption from species that decrease in concentration in the thin layer on stepping the potential from E_1 to E_2. A negative peak,

i.e. $-\Delta R/R$ represents a gain in the concentration of that particular species in the thin layer.

1.3.1 Experimental set-up

In our study, the FTIR spectroelectrochemistry experiments were performed on a Nicolet Avatar 360 FTIR Spectrometer in the reflectance mode equipped with a wide band mercury cadmium tellueride (MCT) detector. The cell was a standard three-electrode thin layer design [4, 148, 149] with a CaF_2 window, a platinum foil counter electrode, a glassy carbon working electrode (o.d. = 6 mm) and an $Ag/AgNO_3$ (0.1 M) reference electrode. The potential of the spectroelectrochemical cell was controlled by a Princeton Applied Research model 362 potentiostat. The FTIR spectrometer was coupled with a Spectra-Tech Series 500 variable angle specular reflectance accessory which allowed the spectral reflectance measurement to be carried out at incident angles between 30°-80°; the optimum angle for maximum reflectance was determined before each experiment and was usually around 55°. The distance between the working electrode and the CaF_2 window can be adjusted to accommodate a thin layer of electrolyte (ca. 1 mm thick) for spectroelectrochemical measurement. All the spectra were collected at 8 cm^{-1} resolution and consisted of 100 co-added and averaged scans. The sample compartment of the FTIR spectrometer was purged by N_2 prior to the measurement to ensure the removal of CO_2 and water vapor. The temperature of the electrolyte was maintained at –0.5°C by circulating a coolant through the jacket wall of the electrochemical cell when performing low-temperature *in-situ* FTIR spectroelectrochemistry experiments.

1.3.2 Previous FTIR spectroelectrochemical studies on CO_2 reduction

Stor et al. [50, 146, 147] have performed a detailed study on the mechanism of CO_2 reduction catalyzed by $[Re(bpy)(CO)_3L]^n$ (bpy = bipyridine; L = CH_3CN, $P(OEt)_3$) by *in-situ* FTIR spectroelectrochemistry. The results showed that the complex goes through a either a $1e^-$ or $2e^-$ catalytic pathways involving $[Ru(bpy)(CO)_3]^{\bullet}$ or $[Ru(bpy)(CO)_3]^-$ as intermediates depending on the electronic properties of the ligand L. The main products of CO_2 reduction were CO, $HCOO^-$ and CO_3^{2-}. Christensen et al. [54, 140] also carried out the spectroelectrochemical investigations on the CO_2 reduction mechanism catalyzed by nickel-4,4'-dimethyl-2,2'-bipyridine, nickel-1,10-phenanthroline complexes and $[Ni(dppm)_2]Cl_2$ complexes. Spectroscopic evidence for the transient formation of $[Ni(phen^{\bullet-})(CO)_2]$ and $[Ni(Me_2bipy^{\bullet-})(CO)_2]$ were reported. They also investigated the reduction of CO_2 catalyzed by rhenium tricarbonyl complex [4]; *fac*-$[Re(dmbipy^{\bullet-})(CO)_3Cl]$ was reported as one of the intermediates involved in the reduction process.

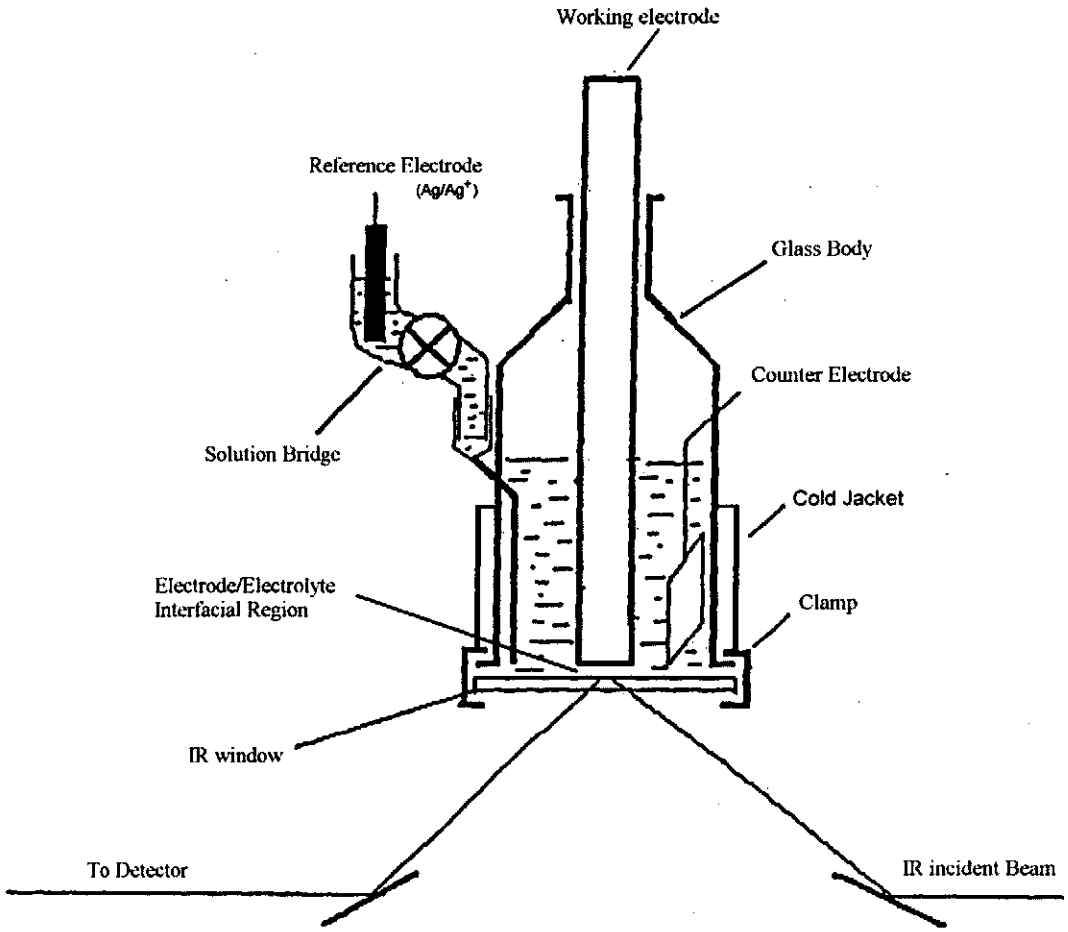

Figure 1.1 *In-situ* FTIR spectroelectrochemistry set-up

1.4 Aims and Objectives

Most of the systems on CO_2 reduction studied so far usually lead to two-electron reduction products such as CO, $HCOO^-$ or $C_2O_4^{2-}$ or a mixture of them. A better understanding on the mechanism and factors influencing the product selectivity and efficiency is essential for the design of efficient systems for CO_2 reduction. It has been shown that CO could be afforded exclusively in acidic medium by adding H_2O as proton source in the electroreduction of CO_2 catalyzed by $[Ru(bpy)_2(CO)_2]^{2+}$ whereas formic acid was produced when electrolysis was carried out in alkaline medium [5]. Tanaka et al. [22] also addressed that addition of protonated alkyl amine salts could enhance the yield of formic acid in the ruthenium system. It has been reported that the presence of weak Brönsted acids such as CF_3CH_2OH and H_2O in the iron porphyrin [66] and $[Re(bpy)(py)(CO)_3]^+$ [106] systems can promote the formation of CO.

Comprehensive work has been done to probe the mechanism in the formation of CO in iron porphyrin and $[Re(bpy)(py)(CO)_3]^+$ systems by cyclic voltammetry [66, 106] and in the $[Re(bpy)(CO)_3Cl]$ system by *in-situ* FTIR spectrelectrochemistry [4]. It is generally accepted that formation of CO occurred via a M-η^1-CO_2 species. However, not much study have been performed on the mechanism of $HCOO^-$ formation. There have been arguments concerning the precursors to $HCOO^-$, species such as M-OC(O)H [23, 57, 60, 113, 141, 150], M-C(O)OH [34, 151], M-C(O)H [19] all have been proposed as reaction intermediates. Therefore, it is our aim to further investigate the conditions influencing the product selectivity and the mechanisms of CO vs. $HCOO^-$ formation.

In this project, we have synthesized two new ruthenium carbonyl complexes – $[Ru(bdmpp)(bpy)CO][ClO_4]_2$ **[1]** and $[Ru(tpm)(bpy)CO][ClO_4]_2$ **[2]** (bdmpp = 2,6-bis(3,5'-dimethylpyrazoyl)pyridine, tpm = tris-(1-pyrazyl)methane, bpy = 2,2'-bipyridine) and investigated the catalytic CO_2 reduction process by cyclic voltammetry, constant potential electrolysis and specially *in-situ* FTIR spectroelectrochemistry. Experiments were carried out in the presence of different proton sources to study their effect on product distribution. We have also investigated the electrochemical behavior of an iron complex $[Fe(dophen)(N\text{-}MeIm)_2][ClO_4]$ **[3]** (H_2dophen = 2,9'-bis(2'-hydroxyphenyl)-1,10'-phenanthroline, N-MeIm = 1-methylimidazole) on the electrocatalytic reduction of CO_2 in the presence of weak Brönsted acids such as methanol and 2,2,2-trifluoroethanol. Monitoring of the CO_2 reduction process by *in-situ* FTIR spectroelectrochemistry was carried out to identify the intermediates involved in the reduction process. The results will be discussed in the subsequent chapters.

Chapter 2

Synthesis, Characterization, X-ray Crystal Structure and Electrochemical Behavior of Two Ruthenium Carbonyl Complexes

2.1 Introduction

Among the various classes of transition metal complexes that have been utilized as electrocatalysts, ruthenium and rhenium polypyridyl carbonyl complexes appear to be particularly promising. In order to exploit the reaction chemistry in more details, we have synthesized two new ruthenium carbonyl complexes with the tridentate ligands 2,6-bis(3,5-dimethyl-N-pyrazole)pyridine (bdmpp) and tris-(pyrazoyl)methane (tpm) which are analogues of 2,2':6',2"-terpyridine. We have conducted spectroscopic characterizations, electrochemical studies and X-ray crystal structural determinations on these carbonyl complexes. The results are presented in this chapter.

2.2 Experimental Section

2.2.1 Materials

All the chemicals and solvents used in synthesis and recrystallization were of analytical (A.R.) grade. $RuCl_3.xH_2O$ and 2,2'-bipyridine were purchased from Aldrich. All other chemicals and reagents were used as received unless otherwise noted. Chloroform and N,N'-dimethylformamide were distilled over calcium chloride under argon atmosphere before being used. Tetrahydrofuran was distilled over sodium under argon atmosphere.

2.2.2 Synthesis of Ligands

Tris(pyrazoly-1-ly)methane (tpm)

Under argon, a solution of pyrazole (10 g, 0.147 mol) in dry tetrahydrofuran was stirred with potassium metal (5.8 g, 0.148 mol) at about 70°C for about 4 hours. When all potassium metal had been dissolved, about 15 ml of dry chloroform was added. The resulting solution was refluxed for 30 h to give a brown viscous liquid. Silica gel (10 g) was added into the resulting mixture and removal of solvent from the viscous solution produced a brown powder. Unreacted pyrazole was removed by sublimation of the brown powder at about 110°C under vacuum. The desired product was collected as a white solid which sublimes at about 160°C under vacuum. (yield 44%)

2,6-Bis(3,5-dimethyl-N-pyrazoyl)pyridine (bdmpp)

The ligand was synthesized by a literature procedure with slight modification [152]. Under argon, the potassium salt of 3,5-dimethylpyrazole (7.8 g, 0.11 mol) was added to a stirred suspension of NaH (2.6 g, 0.11 mol) in dry N,N'-dimethylformamide (100 ml) at 60°C. After 2 hours, 2,6-bis(chloromethyl)pyridine (9.3 g, 0.055 mol) was added, the mixture was then stirred for 48 h. The solution was then evaporated to dryness at reduced pressure and the residue was extracted with chloroform (3 x 25 ml). The organic portions were combined and washed with water (2 x 25 ml) and dried with anhydrous Na_2SO_4 before filtration. Evaporation of chloroform under reduced pressure yielded the product as a brown oily liquid (Yield > 75%).

2.2.3 Synthesis of Ruthenium Complexes

$Ru(L)Cl_3$ (L = bdmpp, tpm) [154]

$RuCl_3.xH_2O$ (0.2 g, 0.77 mmol) and L (0.77 mmol) and LiCl (0.5 g) were added into ethanol (30 ml). The mixture was refluxed for 4 h. The brownish red precipitate was filtered, washed with ether and dried in vacuo. The isolated yield was about 80%.

[Ru(bdmpp)(bpy)Cl]ClO_4

To a solution of Ru(bdmpp)Cl_3 (0.5 g, 1.1 mmol) in ethanol (30 ml), solid bpy (0.16 g, 1.1 mmol), 8-9 drops of triethylammine (as reducing agent) and LiCl (0.5 g) were added. The mixture was then refluxed for 10 h. A saturated $LiClO_4$ solution was added into the resulting mixture. The product was obtained as a reddish orange precipitate (0.57 g, yield ~ 80%). Anal. for [Ru(bdmpp)(bpy)Cl]ClO_4. Calcd: C, 45.42; H, 3.79; N, 14.87 %. Found: C, 35.56; H, 4.53; N, 9.83 %. ^{1}H NMR in CD_3CN [δ/ppm]: 1.59 (6H, s, pyrazoyl Me), 2.99 (6H, s, pyrazoyl Me), 6.25 (2H, s, pyrazoyl H), 7.09 (2H, dd, pyrazoyl H, J = 1.72), 7.53 (2H, dd, bipyridinyl H, J = 5.52), 7.77-7.79 (2H, d, bipyridinyl H, J = 8.04), 8.15-8.35 (2H, m, bipyridinyl H, J = 8.12, 7.68), 8.58-8.60 (2H, d, bipyridinyl H, J = 7.92), 10.47-10.49 (1H, dd, pyrazoyl H, J = 5.6, 5.4). UV/VIS in CH_3CN [λ_{max}/nm(ε/ $mol^{-1}dm^3cm^{-1}$)]: 466(10418), 291(54753), 266(41217), 236(31280). The ^{1}H NMR and UV/VIS spectra are shown in Figure 2.1 and 2.5 respectively.

[Ru(tpm)(bpy)Cl]ClO_4

To a solution of Ru(tpm)Cl_3 (0.5 g, 1.2 mmol) in ethanol (30 ml), solid bpy (0.2 g, 1.2 mmol), 8-9 drops of triethylammine (as reducing agent), LiCl (0.5 g) were added. The mixture was then refluxed for 10 h. A saturated $LiClO_4$ solution was added into the resulting mixture. The product was obtained as a reddish orange precipitate (0.58 g, yield ~ 80 %). Anal. For [Ru(tpm)(bpy)Cl]ClO_4. Calcd: C, 39.60; H, 2.97; N, 18.48 %. Found: C, 37.26; H, 3.18; N, 15.51 %. ^{1}H NMR in CD_3CN [δ/ppm]: 6.24-6.57 (2H, d,

pyrazoyl H, J = 2.28), 6.67 (2H, pyrazoyl H, J = 2.55), 7.45-7.48 (2H, dd, bipyridinyl H, J = 7.52, 6.49), 7.99-8.03 (2H, dd, bipyridinyl H, J = 7.66, 1.47), 8.25-8.35 (3H, m, pyrazoyl H, J = 2.75), 8.45-8.46 (2H, d, pyrazoyl H, J = 2.76), 8.48-8.50 (2H, d, bipyridinyl H, J = 8.16), 8.69-8.70 (2H, d, bipyridinyl H, J = 5.55), 9.36 (1H, s, pyrazoyl H). UV/VIS in CH_3CN [λ_{max}/nm(ε/ $mol^{-1}dm^3cm^{-1}$)]: 475(3893), 343(6993), 293(24918). The ^1H NMR and UV/VIS spectra are shown in Figure 2.2 and 2.6 respectively.

[Ru(bdmpp)(bpy)CO][ClO_4]$_2$ [1]

[Ru(bdmpp)(bpy)Cl]ClO_4 (0.5 g, 0.8 mmol) was dissolved in a water:acetone (9:1 v/v) mixture (10 ml). Silver p-toulenesulfonate (0.5 g) was added into the solution which was then heated for 45 minutes. The white AgCl precipitate was filtered off. The clear reddish orange solution was then heated at 120°C under 10 atm CO in a high pressure reactor for 24 h. The clear yellow solution was cooled to room temperature and filtered to remove any insoluble materials. An aqueous solution of $LiClO_4$ was then added into filtrate. The pale yellow [Ru(bdmpp)(bpy)CO][ClO_4]$_2$ formed was collected by filtration, washed with water and ether and dried in vacuo (0.48 g, 80%). Anal. For [Ru(bdmpp)(bpy)CO][ClO_4]$_2$. Calcd: C, 41.54; H, 3.33; N, 13.05 %. Found: C, 40.54; H, 3.17; N, 11.88 %. ^1H NMR in CD_3CN [δ/ppm]: 1.57 (6H, s, pyrazoyl Me), 2.88 (6H, s, pyrazoyl Me), 6.34 (2H, s, pyrazoyl H), 7.40-7.55 (2H, dd, pyrazoyl H, J = 5.2), 7.95-8.10 (2H, dd, bipyridinyl H, J = 7.42, 1.21), 8.25 (2H, d, bipyridinyl H, J = 1.45), 8.42-8.60 (2H, m, bipyridinyl H, J = 7.64, 0.56), 8.69 (2H, d, bipyridinyl H, J = 0.57), 9.81 (1H, dd, pyrazoyl H, J = 0.76). UV/VIS in CH_3CN [λ_{max}/nm(ε/ $mol^{-1}dm^3cm^{-1}$)]:

370(sh), 315(15476), 305(sh), 265(27166). The ^{1}H NMR and UV/VIS spectra are shown in Figure 2.3 and 2.7 respectively. Crystals suitable for X-ray structural analysis were obtained by dissolving the pale yellow solid in acetonitrile followed by vapor diffusion of diethyl ether to the solution.

[Ru(tpm)(bpy)CO][ClO_4]$_2$ [2]

[Ru(tpm)(bpy)Cl]ClO_4 (0.5 g, 0.8 mmol) was dissolved in a water:acetone (9:1 v/v) mixture (10 ml). Silver p-toluene sulfonate (0.5 g) was added into the resulting solution which was then heated for 45 minutes. The white AgCl precipitate was filtered off. The clear reddish orange solution was then heated at 120°C under 10 atm CO in a high pressure reactor for 24 h. The clear yellow solution was cooled to room temperature and filtered to remove any insoluble materials. An aqueous solution of $LiClO_4$ was added into filtrate. The yellowish orange [Ru(tpm)(bpy)CO][ClO_4]$_2$ precipitate was collected by filtration, washed with water and ether and dried in vacuo. Yield ~ 80% (0.45 g). Anal. For [Ru(tpm)(bpy)CO][ClO_4]$_2$. Calcd: C, 36.10; H, 2.57; N, 16.04 %. Found: C, 36.49; H, 2.63; N, 14.52 %. ^{1}H NMR in CD_3CN [δ/ppm]: 6.22-6.23 (2H, d, pyrazoyl H, J = 2.81), 6.67-6.68 (2H, d, pyrazoyl H, J = 2.02), 7.48-7.49 (2H, dd, bipyridinyl H, J = 4.51, 1.56), 8.12-8.14 (2H, dd, bipyridinyl H, J = 6.50, 1.18), 8.23-8.25 (3H, m, pyrazyol H, J = 2.74, 1.94), 8.29 (2H, d, pyrazoyl H, J = 2.88), 8.33-8.34 (2H, d, bipyridinyl H, J = 5.32), 8.38-8.40 (2H, d, bipyridinyl H, J = 8.12), 8.97 (1H, s, pyrazoyl H). UV/VIS in CH_3CN [λ_{max}/nm(ε/ $mol^{-1}dm^3cm^{-1}$)]: 375(sh), 313(14501), 302(sh), 257(20581), 211(sh). The ^{1}H NMR and UV/VIS spectra are shown in Figure 2.4 and 2.8 respectively. Crystals suitable for X-ray structural analysis

were obtained by dissolving the yellowish orange solid in acetonitrile followed by vapor diffusion of diethyl ether to the solution.

2.2.4 Physical Measurements

Cyclic voltammetry was performed with a Bioanalytical Systems (BAS) model 100 W electrochemical analyzer interfaced to a microcomputer. A conventional two-compartment electrochemical cell was used. The glassy carbon working electrode was treated by polishing with 0.05 μm alumina on a microcloth and then sonicated for 5 minutes in deionized water followed by rinsing with the solvent used in the electrochemical studies. An $Ag/AgNO_3$ (0.1 M) electrode was used as reference electrode. The $E_{1/2}$ values are the average of the cathodic and anodic peak potentials for the oxidative and reductive wave. The $E_{1/2}$ of ferrocenium/ferrocene couple ($Cp_2Fe^{+/0}$) was used as internal reference in non-aqueous medium ($E_{1/2}$ of $Cp_2Fe^{+/0}$ in CH_3CN = +0.307 vs. SCE [153]) and all potentials reported are quoted with respect to $Cp_2Fe^{+/0}$.

UV/visible spectra were recorded on a Milton Roy Spectronic 3000 photodiode array spectrophotometer. Infrared spectra were obtained as KBr pellets in the 3200-900 cm^{-1} region on a Nicolet Magna-IR 750 FTIR spectrometer. ^1H NMR spectra were recorded on a Brucker 400 MHz DPX 400 spectrometer.

2.2.5 X-ray Crystallographic Data Collection and Refinement of the Structures

All measurements were made on a Brucker SMART CCD diffractometer with graphite monochromated MoK_α radiation (λ=0.71073) operated at 50 kV, 30 mA condition. Intensity data were collected in the range of 2θ = 3 to 55 degree and were

corrected for Lorentz polarization and absorption effects; empirical absorption correction based on azimuthal scans of several reflections was applied. Computations were performed on a SHELXTL software package obtained from Brucker. Analytical expression of neutral-atom scattering factors were employed, and anomalous dispersion corrections were incorporated.

2.3 Results and discussion

2.3.1 UV-visible Spectra

The UV/VIS spectra of the ruthenium complexes are shown in Figures 2.5-2.8. For [Ru(bdmpp)(bpy)Cl]ClO_4 (Figure 2.5) the transition at 466 nm can be assigned to the $d_\pi(Ru) \rightarrow \pi^*$ (bdmpp) metal-to-ligand charge transfer (MLCT) based on previous studies [154]. The lower-wavelength transitions (<300 nm) are assigned as $\pi \rightarrow \pi^*$ ligand-localized transitions [155]. Similar transitions can be observed for the free ligands. For [Ru(tpm)(bpy)Cl]ClO_4, (Figure 2.6) the visible region is dominated by a single $d_\pi(Ru) \rightarrow \pi^*$ (tpm) metal-to-ligand charge transfer (MLCT) band at 343 nm and 475 nm [154]. The transitions in the region < 300 nm can be assigned to the ligand-localized $\pi \rightarrow \pi^*$ transitions [155].

Upon replacement of the Cl^- ligand by the CO ligand in the Ru complexes, all of the MLCT transitions shift to shorter wavelengths. This is due to the fact that CO is a weaker σ-donor than Cl^-. For [Ru(bdmpp)(bpy)CO][ClO_4]$_2$ (Figure 2.7) the band at 370 nm can be assigned to a MLCT transition; transitions at wavelenghts <350 nm are assigned to $\pi \rightarrow \pi^*$ ligand-localized transitions in analogy to the [Ru(bdmpp)Cl_2(PMe_3)] complex [154]. For [Ru(tpm)(bpy)CO][ClO_4]$_2$ (Figure 2.8) the MLCT transition is shifted to 375 nm. The transitions at <320 nm are assigned to a $\pi \rightarrow \pi^*$ (bpy) ligand-localized transition.

2.3.2 Infrared Spectra

Figures 2.9 and 2.10 show the infrared spectra of $[Ru(bdmpp)(bpy)Cl]^+$ and $[Ru(tpm)(bpy)Cl]^+$ respectively. For complex $[Ru(bdmpp)(bpy)Cl]ClO_4$, the peak at 1386 cm^{-1} is assigned as the ring-stretching and bending (C=C and C=N) of the pyrazoles of the bdmpp ligand [157]. Peaks in the region 1400-1600 cm^{-1} are attributed to the stretching of both the bpy and bdmpp ligands. For $[Ru(tpm)(bpy)Cl]ClO_4$, bands attributed to the bpy stretching overlap with those of tpm in the region 1120-1450 cm^{-1}.

Figures 2.11 and 2.12 depict the infrared spectra of $[Ru(bdmpp)(bpy)CO][ClO_4]_2$ **[1]** and $[Ru(tpm)(bpy)CO][ClO_4]_2$ **[2]**. The spectra bear resemblance to those of the chloro complexes, showing the characteristic bands of the bpy, bdmpp and tpm ligands. The characteristic peak of the carbonyl ligand (νCO) is located at 2006 cm^{-1} for complex **[1]** and at 2010 cm^{-1} for complex **[2]**.

2.3.3 X-ray Structural Determination of the Ruthenium Complexes

The ORTEP plots of $[Ru(bdmpp)(bpy)CO]^{2+}$ **[1]** and $[Ru(tpm)(bpy)CO]^{2+}$ **[2]** are depicted in Figures 2.13 and 2.14 respectively. The crystallographic data are summarized in Table 2.1. Selected bond distances and angles are tabulated in Tables 2.2 and 2.3.

[Ru(bdmpp)(bpy)CO]$^{2+}$ [1]

Figure 2.13 depicts the ORTEP plot of [Ru(bdmpp)(bpy)CO]$^{2+}$ with atom numbering. The ruthenium ion is ligated to five nitrogen atoms and one carbon atom. The tridentate ligand (bdmpp) is coordinated meridonally to the ruthenium center and the carbonyl ligand is bound opposite to the bpy ligand. The structure bears close resemblance to that of [Ru(terpy)(bpy)CO]$^{2+}$ (terpy = 2,2':6,2"-terpyridine) [20]. The distances Ru(1)-C(26), C(26)-O(1) of 1.861(3) and 1.133(4) Å are close to that of 1.844(4) and 1.160(4) Å in [Ru(terpy)(bpy)CO]$^{2+}$. The Ru(1)-C(26)-O(1) bond angle of 176.5(3) is close to that of 175.2(3)° in [Ru(terpy)(bpy)CO][PF_6] It has been shown that bpp (2,6-bis(pyrazoyl)pyridine) is a weaker π-acceptor and σ-donor than terpy [155]. Thus, the introduction of electron donating methyl group onto the pyrazoyl-containing ligand increases the σ-donating ability of bdmpp. Therefore, the bond distances and angles of [Ru(bdmpp)(bpy)CO][ClO_4]$_2$ are similar to those of [Ru(terpy)(bpy)CO][PF_6]$_2$.

[Ru(tpm)(bpy)CO]$^{2+}$ [2]

The ORTEP plot of [Ru(tpm)(bpy)CO]$^{2+}$ with atom numbering is shown in Figure 2.14. The ruthenium atom is coordinated to 5 nitrogen atoms and one carbon atom. The tridentate ligand (tpm) is ligated in a facial manner to the ruthenium ion. The monodentate carbonyl ligand is bound opposite to the tpm ligand. The Ru(1)-C(13) and O(1)-C(13) distances of 1.848(4) and 1.143(4) Å are close to that of 1.844(4) and

1.160(4) Å in $[Ru(terpy)(bpy)CO]^{2+}$. The Ru(1)-C(13)-O(1) bond angle of 175.4(3) is also close to that of 175.2(3)° in $[Ru(terpy)(bpy)CO]^{2+}$.

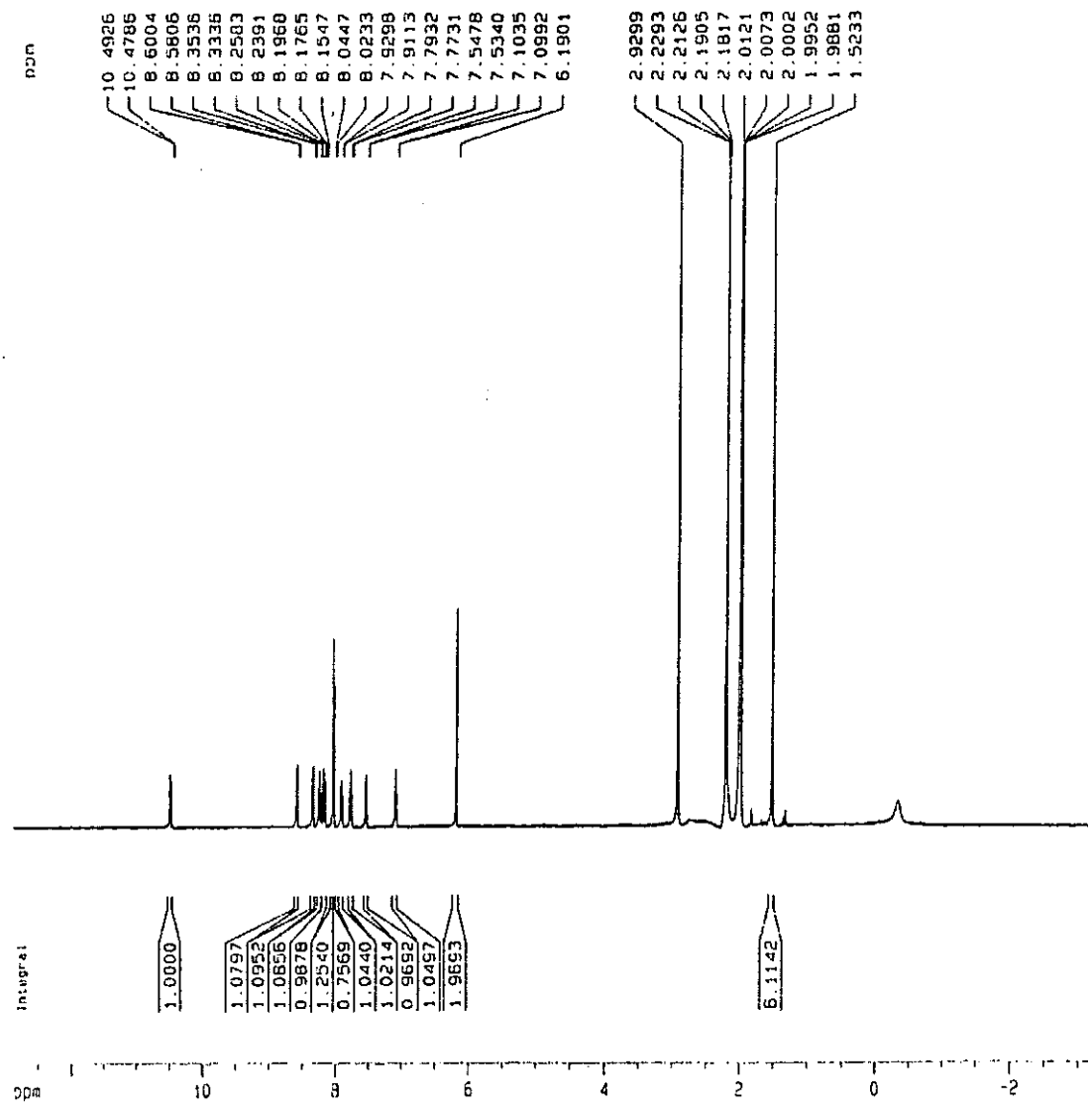

Figure 2.1 ^{1}H NMR spectrum of $[Ru(bdmpp)(bpy)Cl]ClO_4$ in CD_3CN

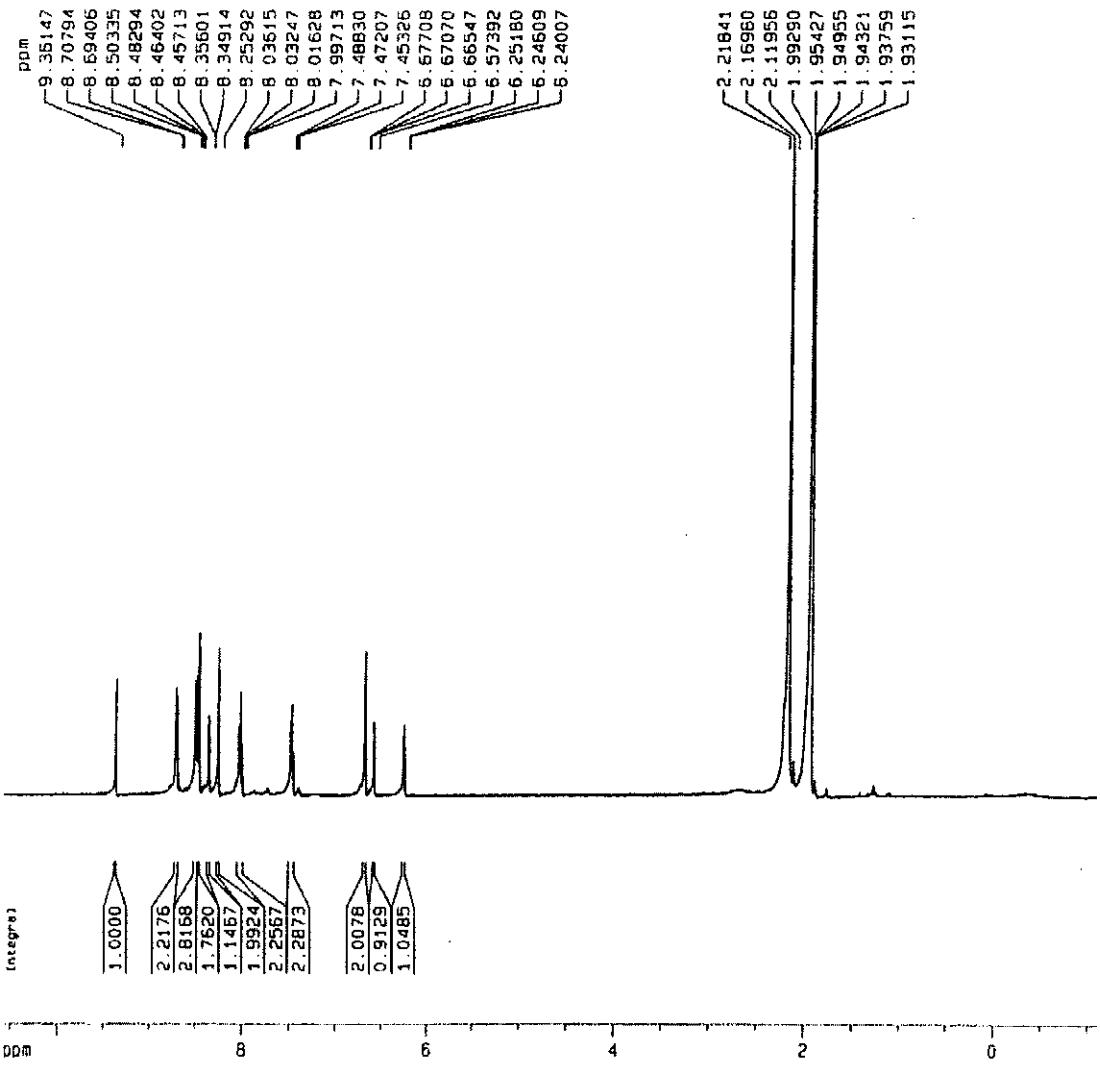

Figure 2.2 ^{1}H NMR spectrum of $[Ru(tpm)(bpy)Cl]ClO_4$ in CD_3CN

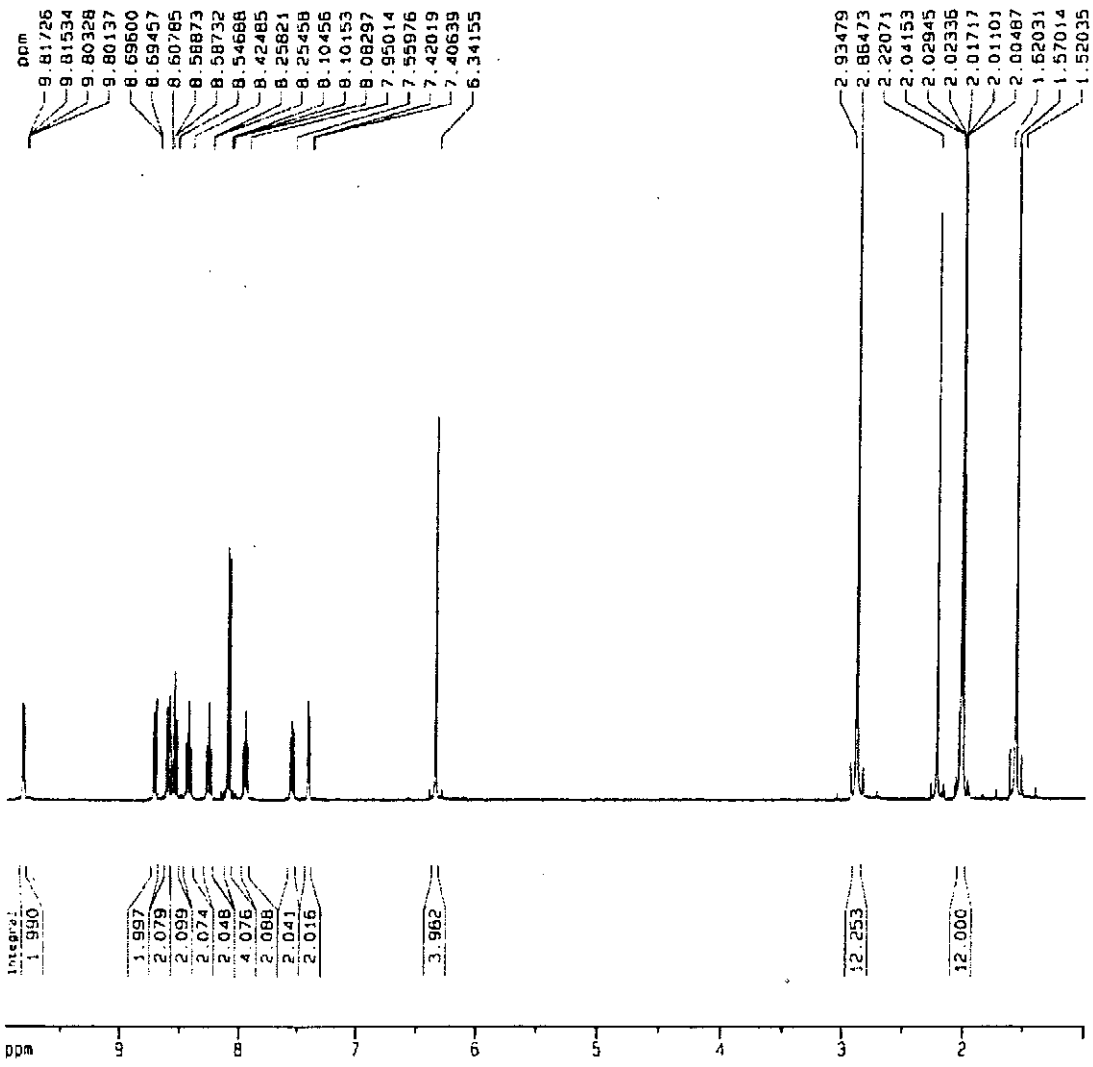

Figure 2.3 ^{1}H NMR spectrum of $[Ru(bdmpp)(bpy)CO][ClO_4]_2$ in CD_3CN

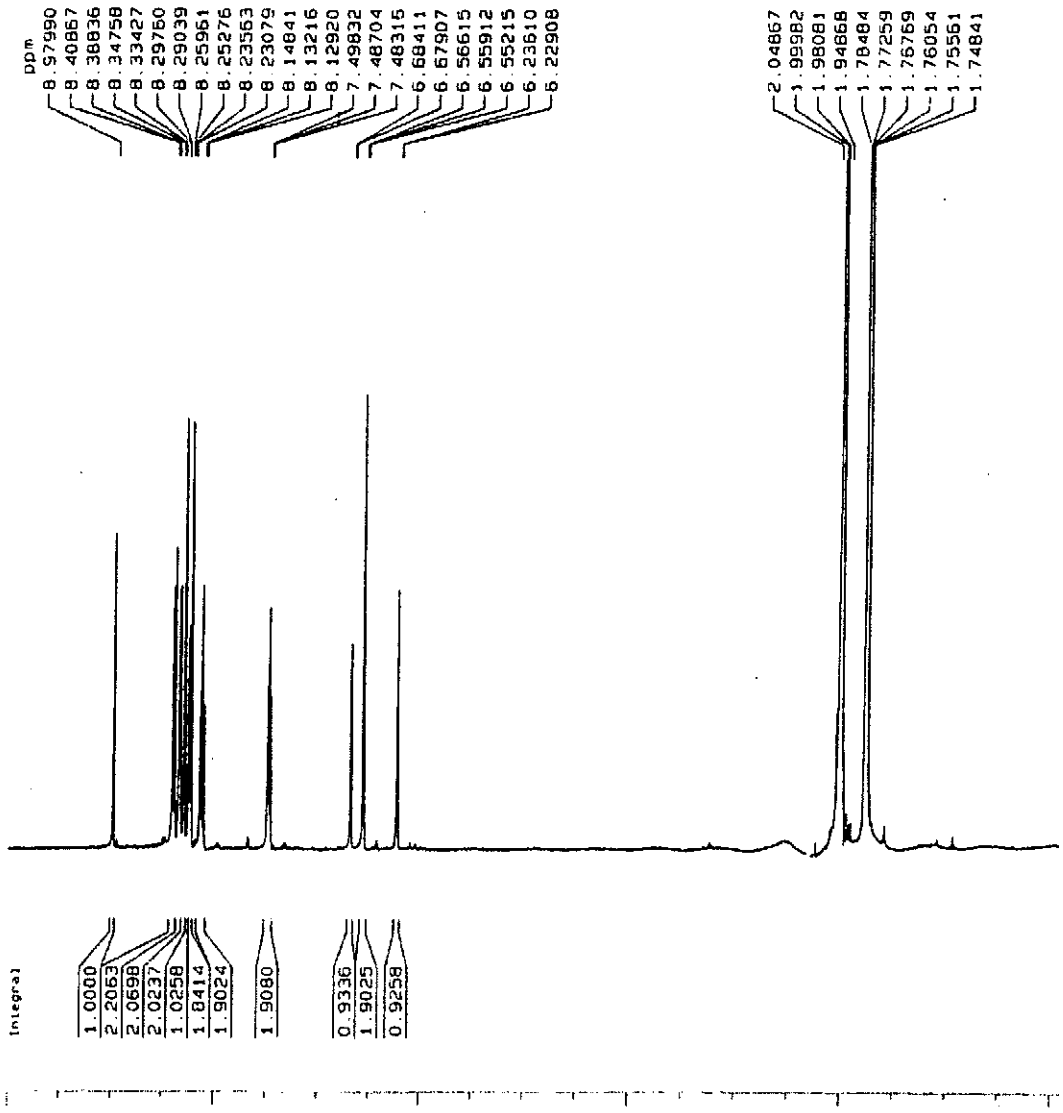

Figure 2.4 ^{1}H NMR spectrum of $[Ru(tpm)(bpy)CO][ClO_4]_2$ in CD_3CN

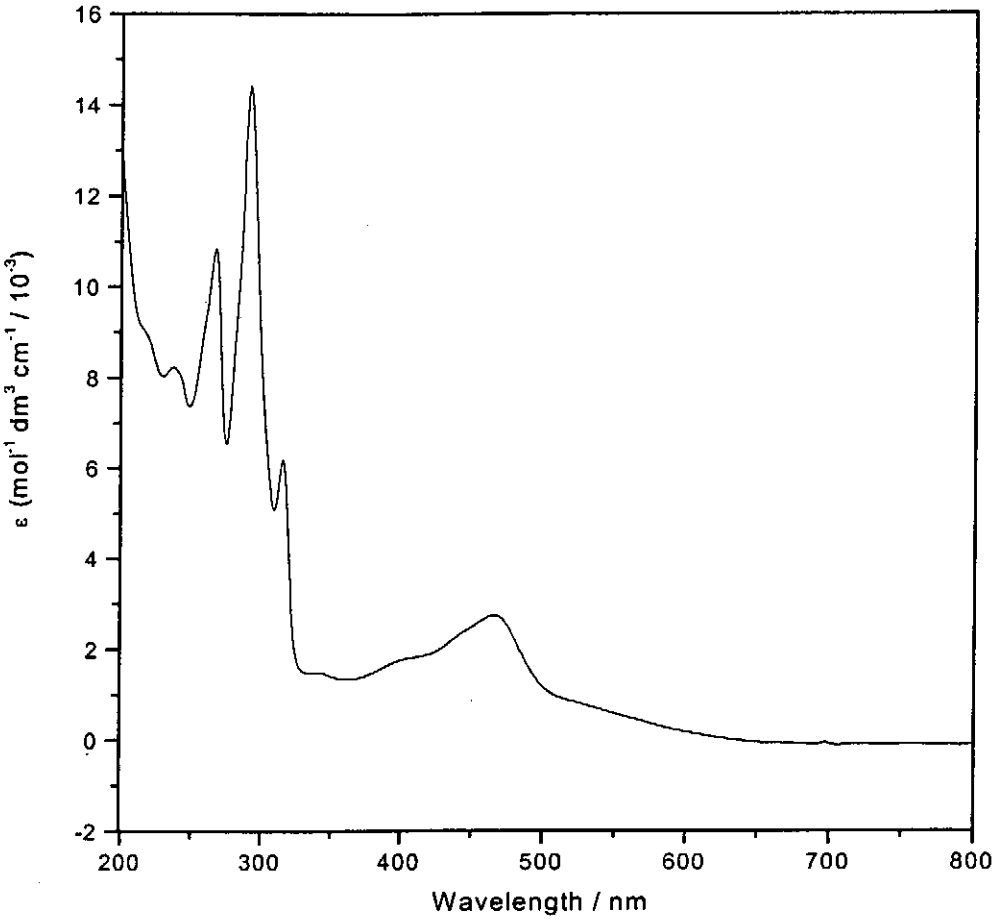

Figure 2.5 UV/VIS spectrum of [Ru(bdmpp)(bpy)Cl]ClO_4 in CH_3CN

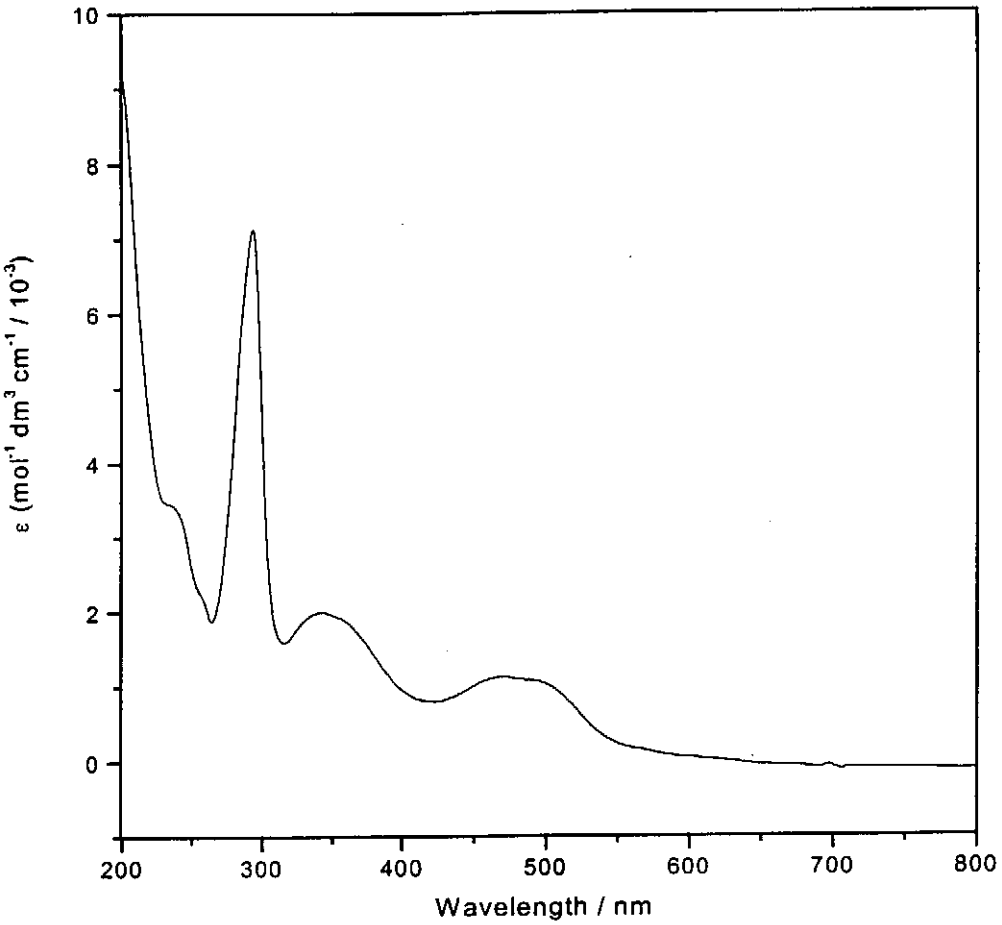

Figure 2.6 UV/VIS spectrum of $[Ru(tpm)(bpy)Cl]ClO_4$ in CH_3CN

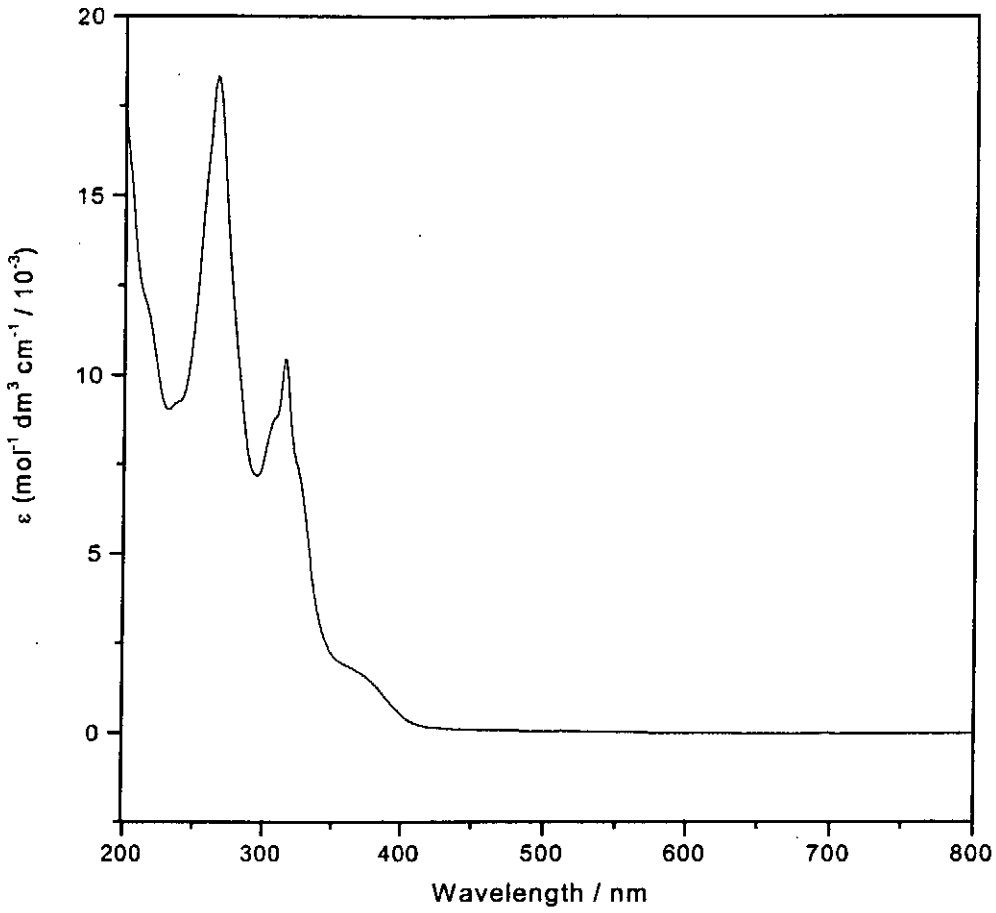

Figure 2.7 UV/VIS spectrum of $[Ru(bdmpp)(bpy)CO][ClO_4]_2$ in CH_3CN

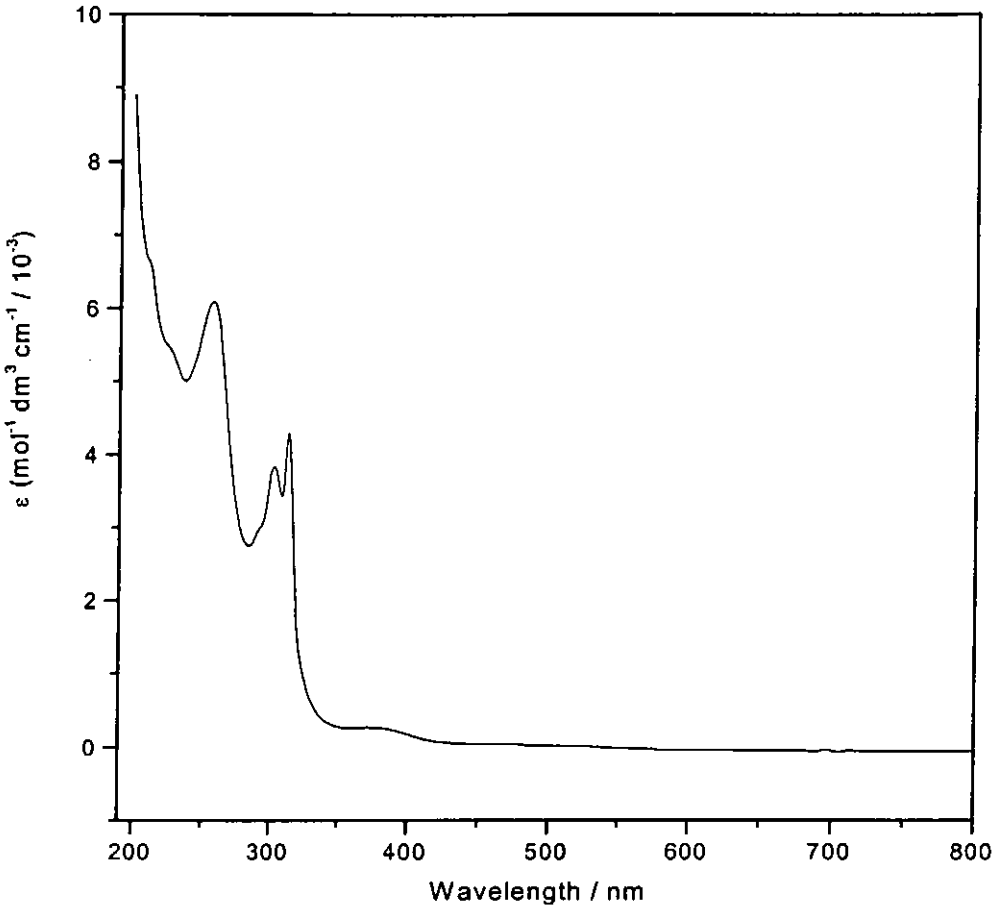

Figure 2.8 UV/VIS spectrum of $[Ru(tpm)(bpy)CO][ClO_4]_2$ in CH_3CN

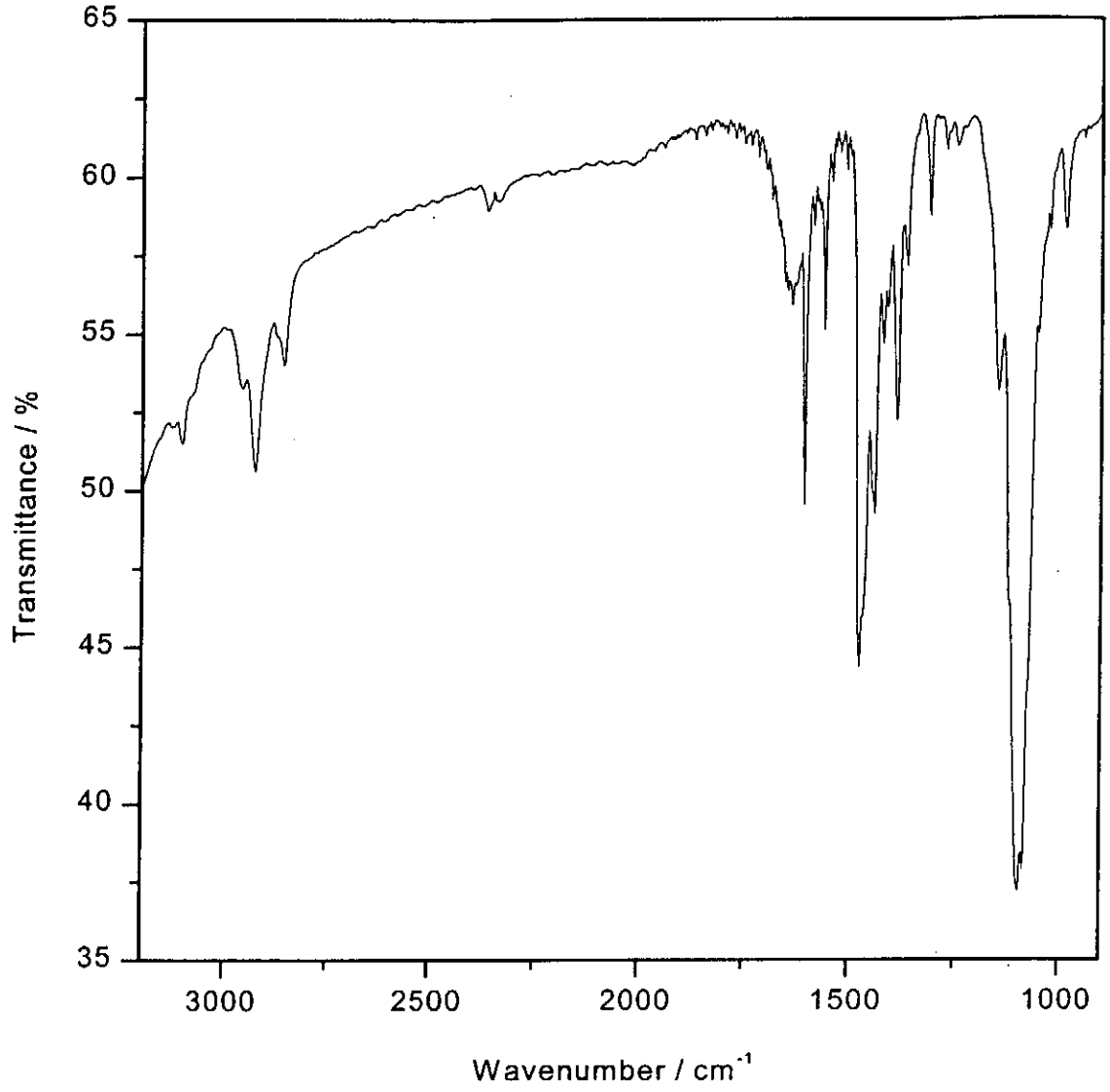

Figure 2.9 Infrared spectrum of $[Ru(bdmpp)(bpy)Cl]ClO_4$ as KBr pellet

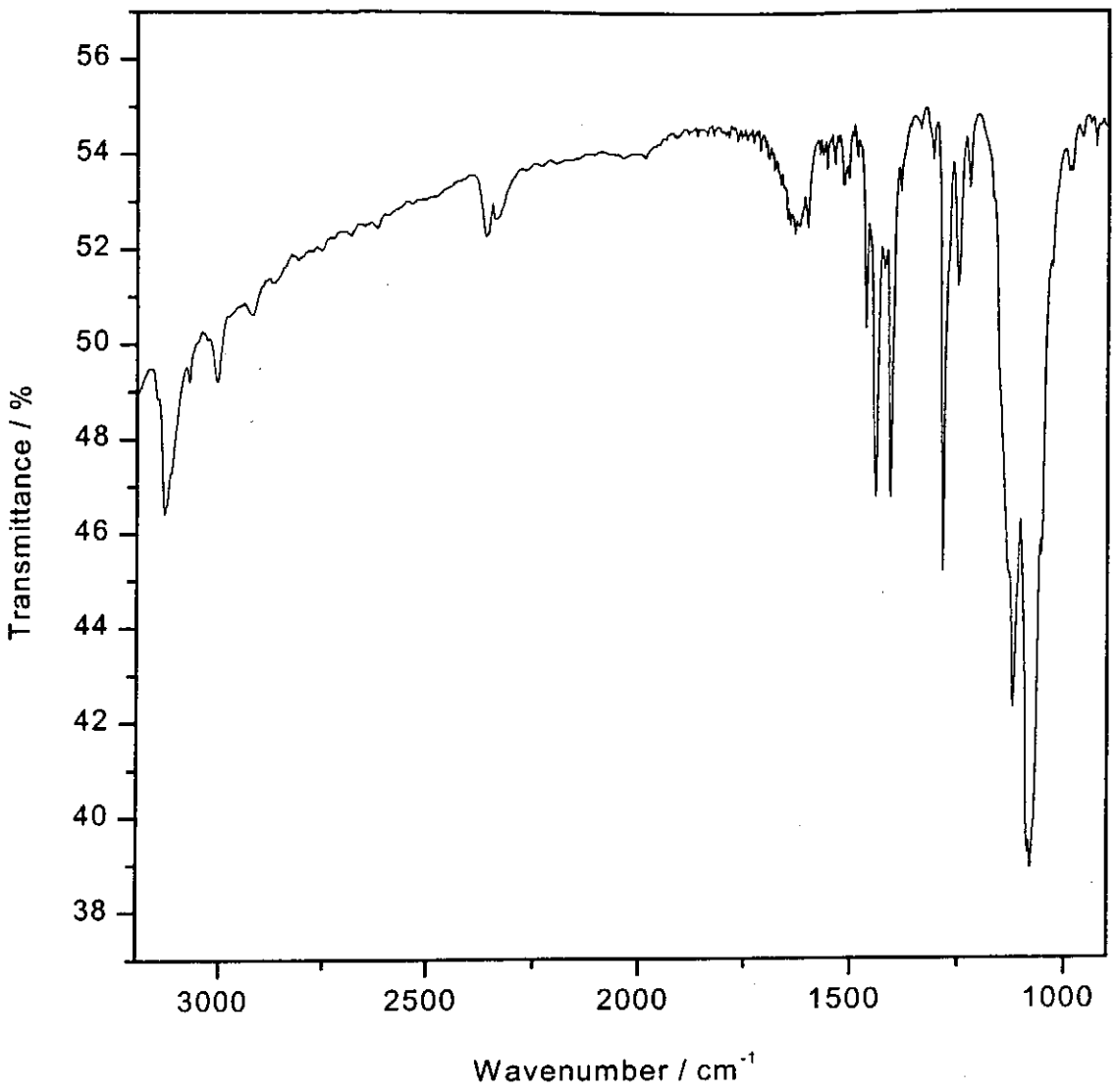

Figure 2.10 Infrared spectrum of $[Ru(tpm)(bpy)Cl]ClO_4$ as KBr pellet

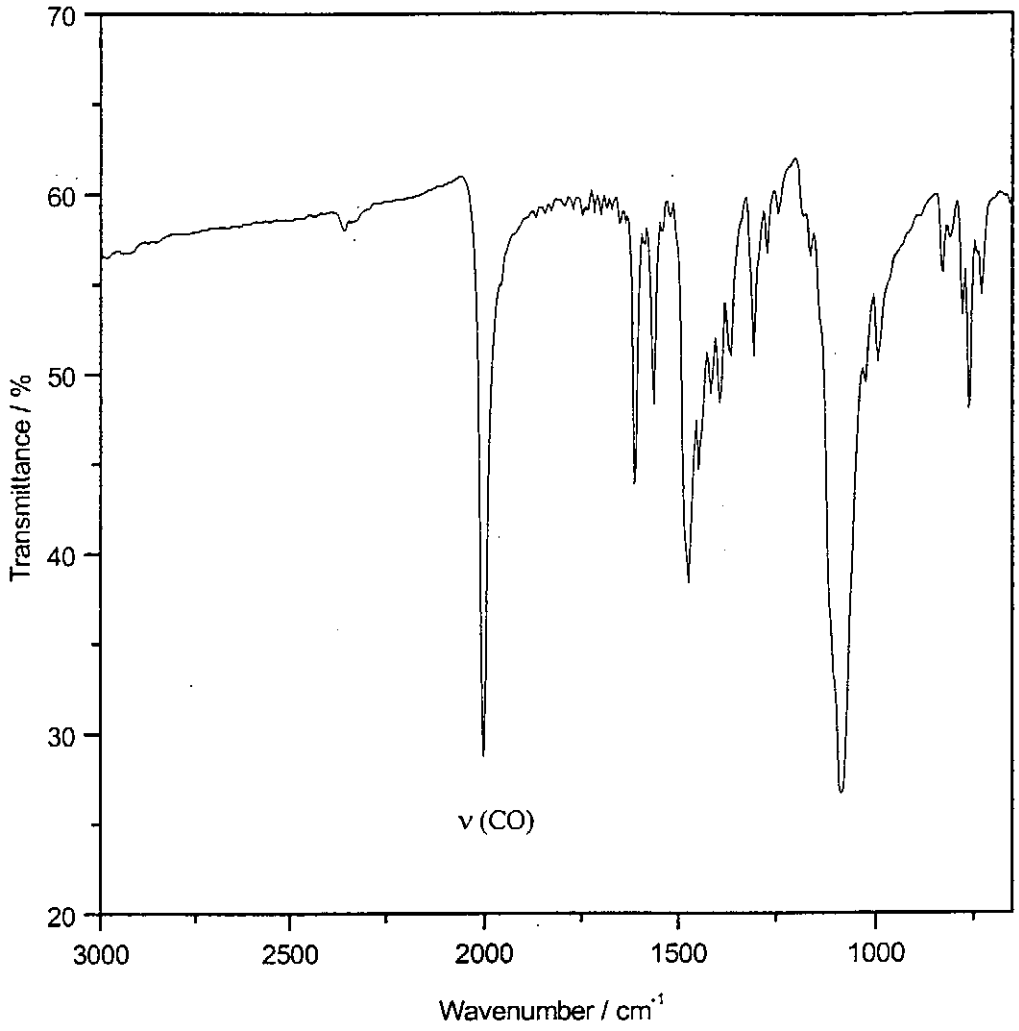

Figure 2.11 Infrared spectrum of $[Ru(bdmpp)(bpy)CO][ClO_4]_2$ as KBr pellet

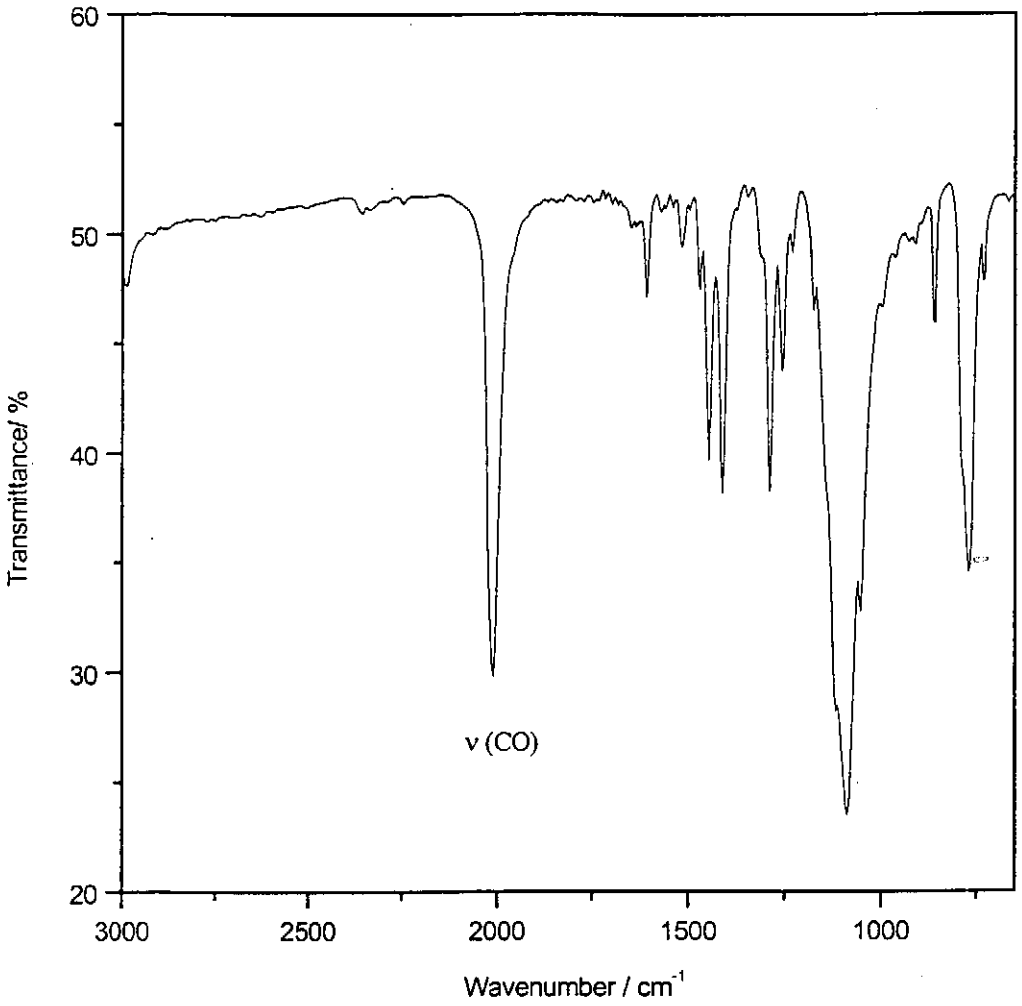

Figure 2.12 Infrared spectrum of $[Ru(tpm)(bpy)CO][ClO_4]_2$ as KBr pellet

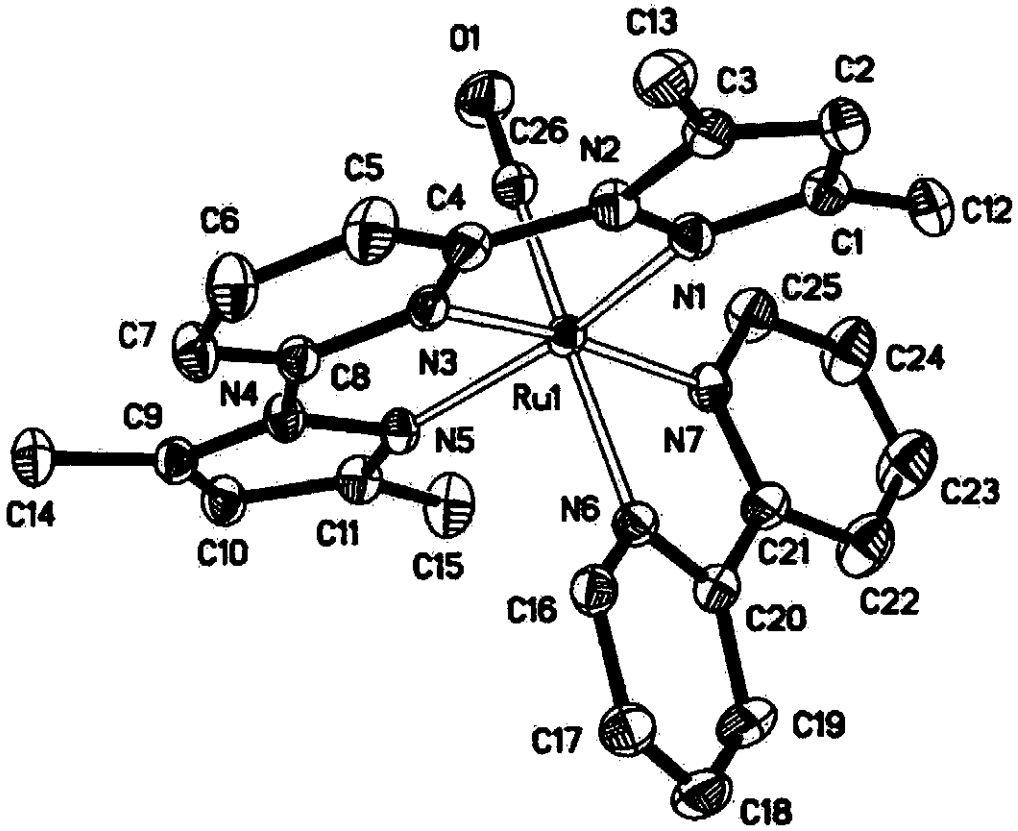

Figure 2.13 An ORTEP plot of $[Ru(bdmpp)(bpy)CO]^{2+}$ with atom numbering

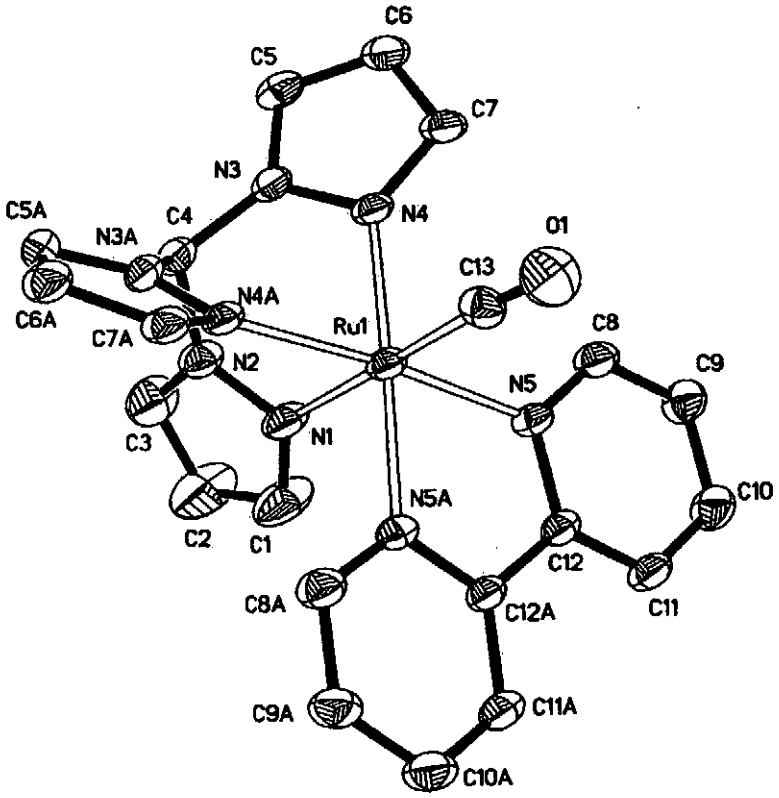

Figure 2.14 An ORTEP plot of $[Ru(tpm)(bpy)CO]^{2+}$ with atom numbering

Table 2.1 Crystal Data and Conditions for Crystallographic Data Collection and Structure Refinement of the ruthenium complexes

Complex	$[Ru(bdmpp)(bpy)CO][ClO_4]_2$	$[Ru(tpm)(bpy)CO][ClO_4]_2$
Space group	Monoclinic $P2_1/n$	Orthorhombic $P2_1/n$
a (Å)	8.1958 (7)	10.7519(14)
b (Å)	17.083(2)	21.681(3)
c (Å)	10.7240(9)	11.8784(15)
β (deg.)	98.044(2)°	90°
U ($Å^3$)	1486.2(2)	2769.0(6)
λ (Å)	0.71703	0.71073
Z	2	2
D_c (gcm^{-3})	1.679	1.744
Crystal dimensions (mm)	0.18 X 0.14 X 0.14	0.14 X 0.08 X 0.06
μ(Mo-K_α) (mm^{-1})	0.722	0.830
F(000)	760	1488
Scan mode	θ-2θ	θ-2θ
no. of reflection	10108	17921
2θ range	1.92°-27.49°	1.89°-27.56°
R1; wR2	0.0465; 0.1059	0.0935; 0.1719

Table 2.2 Selected bond distances (Å) and angles (°) for [Ru(bdmpp)(bpy)CO][ClO_4]$_2$ **[1]**

Ru(1)-C(26)	1.861(3)	Ru(1)-N(3)	2.001(2)
Ru(1)-N(1)	2.067(3)	Ru(1)-N(5)	2.071(2)
Ru(1)-N(7)	2.077(2)	Ru(1)-N(6)	2.125(2)
N(1)-N(2)	1.410(3)	N(2)-C(3)	1.397(4)
N(3)-C(4)	1.332(4)	N(4)-N(5)	1.404(3)
N(5)-C(11)	1.317(4)	N(6)-C(16)	1.342(4)
N(7)-C(25)	1.338(4)	O(1)-C(26)	1.133(4)

C(26)-Ru(1)-N(3)	92.80(12)	C(26)-Ru(1)-N(1)	95.09(12)
N(3)-Ru(1)-N(1)	78.65(10)	C(26)-Ru(1)-N(5)	89.28(12)
N(3)-Ru(1)-N(5)	78.99(9)	N(1)- Ru(1)-N(5)	157.39(9)
N(1)-Ru(1)-N(7)	100.71(10)	N(5)-Ru(1)-N(7)	100.92(10)
C(26)-Ru(1)-N(6)	172.79(12)	N(5)-Ru(1)-N(6)	88.85(9)
N(1)-Ru(1)-N(6)	89.30(10)	O(1)-C(26)-Ru(1)	176.5(3)

Table 2.3 Selected bond distances (Å) and angles (°) for [Ru(tpm)(bpy)CO][ClO_4]$_2$ **[2]**

Ru(1)-C(13)	1.848(4)	Ru(1)-N(5A)	2.0658(18)
Ru(1)-N(5)	2.0658(18)	Ru(1)-N(4)	2.0911(18)
Ru(1)-N(4A)	2.0911(18)	Ru(1)-N(1)	2.134(3)
N(3)-N(4)	1.357(2)	N(3)-C(4)	1.447(3)
N(2)-C(4)	1.464(4)	N(1)-N(2)	1.359(4)
C(13)-O(1)	1.143(4)		

C(13)-Ru(1)-N(5A)	91.20(10)	C(13)-Ru(1)-N(5)	91.20(10)
N(5A)-Ru(1)-N(5)	78.17(10)	C(13)-Ru(1)-N(4)	94.54(10)
N(5A)-Ru(1)-N(4)	173.69(7)	N(5)-Ru(1)-N(4A)	99.04(7)
C(13)-Ru(1)-N(4A)	94.54(10)	N(5A)-Ru(1)-N(4A)	99.04(7)
N(5)-Ru(1)-N(4A)	173.69(7)	N(4)-Ru(1)-N(4A)	83.16(10)
C(13)-Ru(1)-N(1)	178.98(13)	N(5A)-Ru(1)-N(1)	89.59(7)
N(5)-Ru(1)-N(1)	89.59(7)	N(4A)-Ru(1)-N(1)	84.70(7)
O(1)-C(13)-Ru(1)	175.4(3)		

2.3.4 Electrochemical Behavior of the ruthenium complexes

Figure 2.15 shows the cyclic voltammograms of $[Ru(bdmpp)(bpy)CO]^{2+}$ **[1]** in CH_3CN under argon atmosphere. Upon reductive scan, two successive redox couples with $E_{1/2}$ = -1.56 V and –1.80 V vs. $Cp_2Fe^{+/0}$ appeared (labeled couple I and II respectively). When the potential ramp is reversed before the commencement of the second wave, couple I is reversible on the CV time scale with anodic to cathodic current close to 1.0 for scan rate 50-500 mV s^{-1} (Figure 2.15). Constant potential coulometry at –1.76 V vs. $Cp_2Fe^{+/0}$ established couple I as a one-electron wave. Tanaka et al. [20] have reported that the first reduction process ($E_{1/2}$ = -1.52 V vs. $Cp_2Fe^{+/0}$) in $[Ru(terpy)(bpy)CO]^{2+}$ is a bipyridine based reduction. Since complex **[1]** is structurally similar to $[Ru(terpy)(bpy)CO]^{2+}$ and the $E_{1/2}$ of couple I is close to that of $[Ru(terpy)(bpy)CO]^{2+}$, we can assign the first reduction as a ligand based reduction process:

Couple I:

$$[Ru(bdmpp)(bpy)CO]^{2+} + e^- \rightarrow [Ru(bdmpp)(bpy^{\bullet})CO]^{+}$$

Couple II is irreversible at room temperature. Constant potential coulometry at –1.86 V vs. $Cp_2Fe^{+/0}$ revealed that couple II is also a one-electron wave. A small hump appeared at –0.4 V in the reverse scan which can be assigned to the oxidiation of CO released upon reduction of $[Ru(bdmpp)(bpy)CO]^{2+}$ [20].

Couple II:

$$[Ru(bdmpp)(bpy^{\bullet})CO]^{+} + e^- \rightarrow [Ru(bdmpp)(bpy^{\bullet -})CO]^{0}$$

$$[Ru(bdmpp)(bpy^{\bullet -})CO]^{0} \rightarrow [Ru(bdmpp)(bpy^{\bullet -})]^{0} + CO$$

When the experiment was conducted at -20°C by cooling the electrochemical cell with acetone/dry ice mixture (Figure 2.16), the small hump at –0.4 V disappeared and the $[Ru(bdmpp)(bpy)CO]^{+/0}$ couple became more reversible. The appearance of the $[Ru(bdmpp)(bpy)CO]^{+/0}$ couple indicates that the Ru-CO bond of $[Ru(bdmpp)(bpy)CO]^{0}$ is maintained at least in the CV time scale [20].

Figure 2.17 shows a typical cyclic voltammogram of $[Ru(tpm)(bpy)CO]^{2+}$ **[2]** under Ar atmosphere. It exhibits two sequential waves at $E_{1/2}$ = -1.55 V and –1.95 V vs. $Cp_2Fe^{+/0}$ (labeled couple I' and II' respectively). When the potential ramp is reversed before the second wave, couple I' at –1.55 V is reversible on the CV time scale with the anodic and cathodic peak current close to 1.0 for scan rate 50-500 mV s^{-1} (Figure 2.17). Constant potential coulometry at –1.66 V vs. $Cp_2Fe^{+/0}$ showed that couple I' is a one-electron wave that is believed to be a bipyridine based reduction wave. Since the cyclic voltammogram of complex **[2]** is very similar to that of complex **[1]**, therefore couple I' and II' are assigned according as follows:

Couple I':

$$[Ru(tpm)(bpy)CO]^{2+} + e^{-} \rightarrow [Ru(tpm)(bpy^{\bullet})CO]^{+}$$

Couple II':

$$[Ru(tpm)(bpy^{\bullet})CO]^{+} + e^{-} \rightarrow [Ru(tpm)(bpy^{\bullet-})CO]^{0}$$

$$[Ru(tpm)(bpy^{\bullet-})CO]^{0} \rightarrow [Ru(tpm)(bpy^{\bullet-})]^{0} + CO$$

As tpm is a stronger σ-donor than bdmpp ligand [155], a shift of the second reduction potential in $[Ru(tpm)(bpy)CO]^{2+}$ (couple II vs. couple II') to the cathodic side is expected.

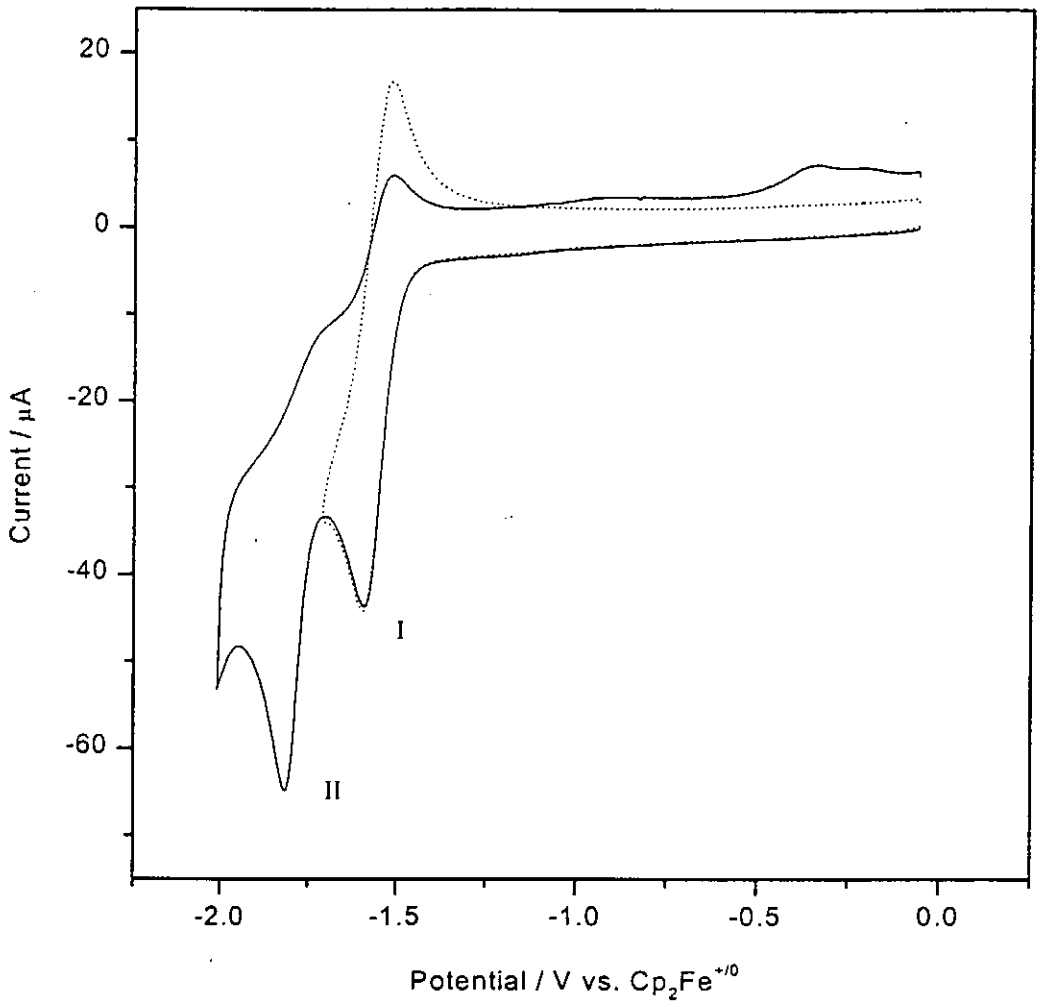

Figure 2.15 Cyclic voltammograms of 0.3 mM $[Ru(bdmpp)(bpy)CO]^{2+}$ in acetonitrile under 1 atm argon (—); potential ramp is reversed before the second wave (----). Working electrode: glassy carbon (0.2 cm^2). Supporting electrolyte: 0.1 M TBAH. Scan rate: 100 mV s^{-1}.

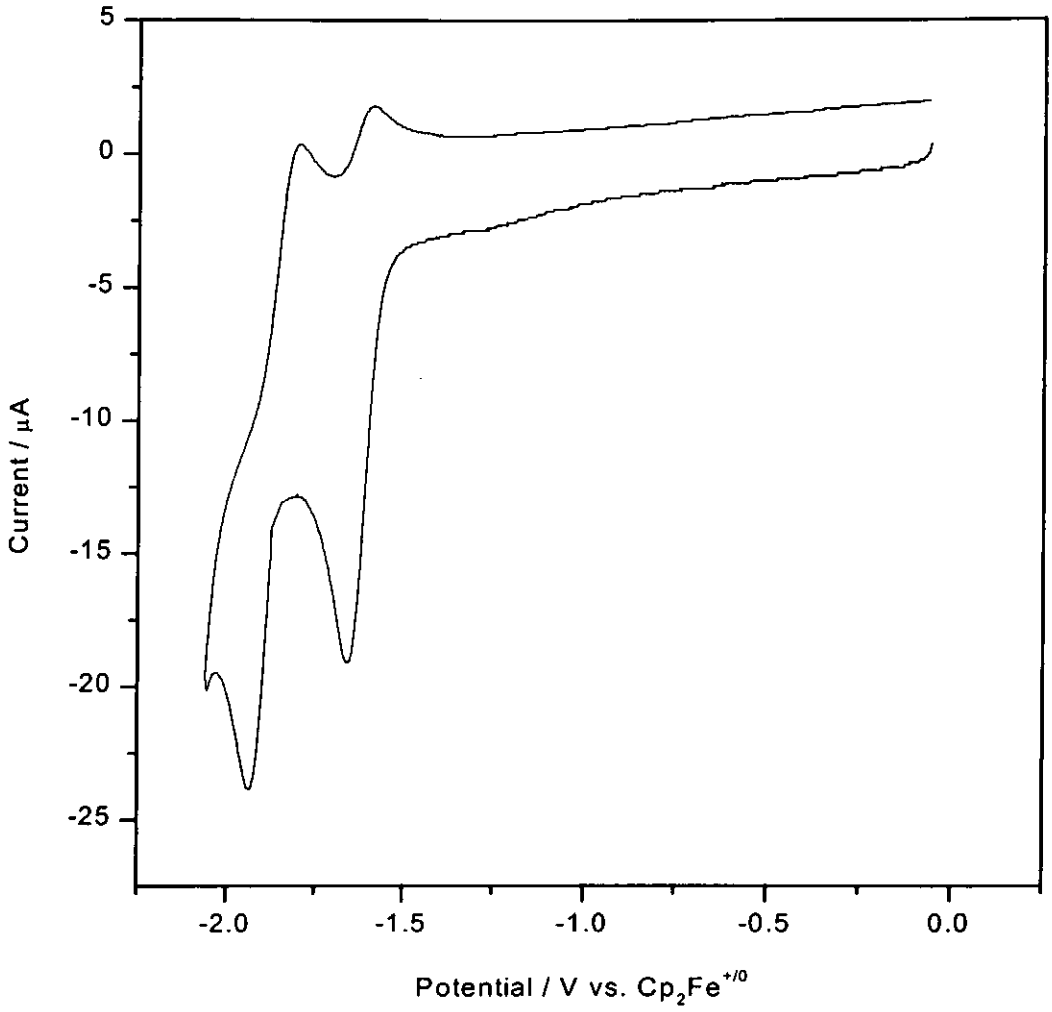

Figure 2.16 Cyclic voltammogram of 0.25 mM $[Ru(bdmpp)(bpy)CO]^{2+}$ in acetonitrile under 1 atm argon at -20°C. Working electrode: glassy carbon (0.2 cm^2). Supporting electrolyte: 0.1 M TBAH. Scan rate: 100 mV s^{-1}.

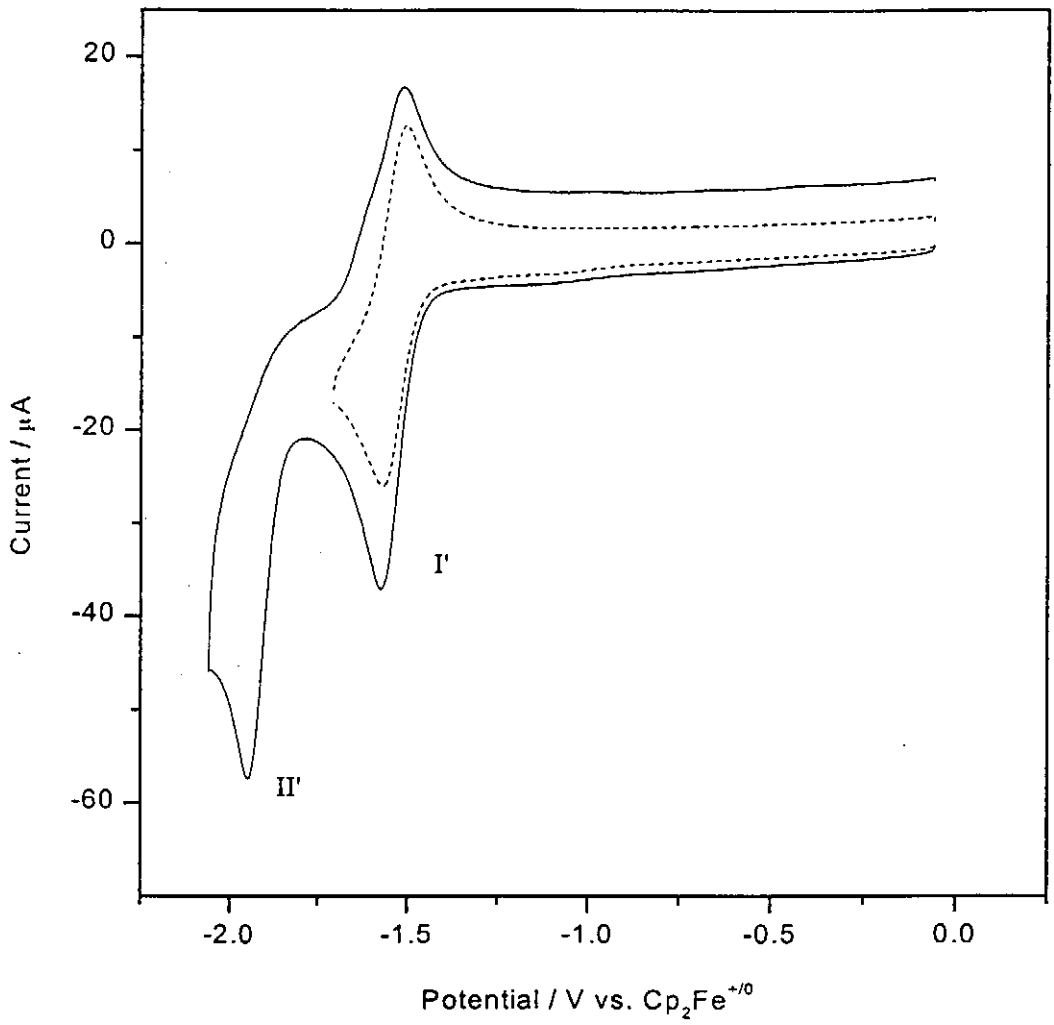

Figure 2.17 Cyclic voltammograms of 0.4 mM $[Ru(tpm)(bpy)CO]^{2+}$ in acetonitrile under 1 atm argon (—); the potential ramp is reversed before the second wave (----). Working electrode: glassy carbon (0.2 cm^2). Supporting electrolyte: 0.1 M TBAH. Scan rate: 100 mV s^{-1}.

2.4 Conclusion

Two new ruthenium carbonyl complexes – $[Ru(bdmpp)(bpy)CO][ClO_4]_2$ **[1]** and $[Ru(tpm)(bpy)CO][ClO_4]_2$ **[2]** have been synthesized and characterized. X-ray crystallographic study indicated that the bdmpp ligand is bounded meridonally to the ruthenium center and the tpm ligand is coordinated facially to the ruthenium center. The carbonyl ligand is bound opposite to the bpy ligand in complex **[1]** and the tpm ligand in complex **[2]**. Electrochemical studies showed that both complex **[1]** and **[2]** exhibit two one-electron reduction processes in acetonitrile which can be assigned to a ligand-based and a metal-based redox process respectively.

Chapter 3

In-situ FTIR Spectroelectrochemical Study of the Reduction of CO_2 Catalyzed by the Ruthenium Complexes

3.1 Introduction

In this chapter, we will describe the electrochemical reduction of CO_2 catalyzed by two ruthenium carbonyl complexes – $[Ru(bdmpp)(bpy)CO][ClO_4]_2$ **[1]** and $[Ru(tpm)(bpy)CO][ClO_4]_2$ **[2]** that have been synthesized in our laboratory. While bdmpp (2,6'-bis(3,5-dimethylpyrazol)pyridine) is a meridonal tridentate ligand similar to terpy (2,2':6,2"-terpyridine), tpm (tris(1-pyrazoyl)methane) is a facial analogue of these tridentate N-donor ligands. The effect of different proton sources on the product distribution was investigated. *In-situ* FTIR spectroelectrochemistry was used to probe the different mechanistic pathways that lead to the production of CO and $HCOO^-$ respectively.

3.2 Experimental

3.2.1 Physical Measurement

Cyclic voltammetry was performed by procedures as described in Chapter 2. Constant potential electrolysis was performed in a gas-tight three-compartment cell. Reticulated vitreous carbon obtained from the Electrosynthesis Co. was used as the working electrode. A control experiment was always performed by electrolysing a blank solution saturated with argon. After completion of an electrolysis, gas samples were taken through the septum from the head-space above the solution in the working electrode compartment and analyzed for CO (g) and H_2 (g) by a Hewlett-Packard model 5890 gas chromatography equipped with a thermal conductivity detector. A 6 ft x 1/8 in stainless steel column packed with 5 Å molecular sieves was employed in the analysis with helium as the carrier gas. Formate and oxalate ions in the solution were analyzed by HPLC with Waters Associate model 510 liquid chromatography equipped with a Supergel C-610H column. The supported electrolyte tetra-n-butylammonium hexafluorophosphate was removed from the reaction solution prior to formate analysis by the following procedure: the solvent (CH_3CN) was removed from the reaction solution under reduced pressure. Distilled water was added to the residue in a 1:1 (v/v) ratio (H_2O / total original reaction volume). Analysis was conducted on the aqueous filtrate obtained after removal of the precipitated tetra-n-butylammonium hexafluorophosphate by filtration. *In-situ* FTIR spectroelectrochemistry was performed as described in previous chapters.

3.3 Results and discussion

3.3.1 Electrochemical behavior of complex [1] and [2] in CO_2-saturated acetonitrile

The electrochemical behavior of $[Ru(bdmpp)(bpy)CO][ClO_4]_2$ **[1]** and $[Ru(tpm)(bpy)CO][ClO_4]_2$ **[2]** in acetonitrile under argon atmosphere has been described in Chapter 2. Upon introduction of CO_2 into the CH_3CN solution of **[1]**, an increase in cathodic current was observed at couple II (Figure 3.1) indicating that the two-electron reduced form of **[1]** is an active catalyst towards CO_2 reduction. Controlled potential electrolysis of **[1]** ($1x10^{-3}$ M) at -1.86 V vs. $Cp_2Fe^{+/0}$ in CO_2-saturated acetonitrile using TBAH (0.1M) as electrolyte at room temperature produced a mixture of carbon monoxide and formate. Figure 3.2 depicts the cyclic voltammograms of $[Ru(tpm)(bpy)CO][ClO_4]_2$ **[2]** in CO_2-saturated CH_3CN, a sharp increase in cathodic current at couple II' is observed indicating that the two-electron reduced form of **[2]** is also an electrocatalyst for CO_2 reduction. Controlled potential electrolysis of **[2]** at – 2.01 V vs. $Cp_2Fe^{+/0}$ in CO_2-saturated acetonitrile using TBAH as electrolyte at room temperature produced primarily carbon monoxide with a small amount of formate (Table 3.1).

When a small amount of H_2O was added to the electrolyte, an increase in the catalytic current was observed for both complex **[1]** and **[2]** in the presence of CO_2 (Figures 3.3 and 3.4). No increase in cathodic current was observed in an argon-saturated electrolyte containing the same amount of of H_2O but without CO_2, indicating that the increase in current was not due to the catalytic reduction of H_2O. The peak

current i_p is normalized to the peak current i_p^o corresponding to the one electron reduction wave as obtained from the $[1]^+/[1]^0$ and $[2]^+/[2]^0$ couples in the absence of CO_2 and H_2O. The i_p/i_p^o reaches its limiting value at relatively high H_2O concentration (5.0 M) for complex **[1]** (Figure 3.5). Similar trend can be observed for the i_p/i_p^o of complex **[2]** except that the i_p/i_p^o reaches its limiting value at only about 0.6 M H_2O (Figure 3.6). A decrease in the i_p/i_p^o value at higher H_2O concentration for both complex **[1]** and **[2]** was observed. This may be due to the fact that the solubility of CO_2 is lowered when the concentration of water in the electrolyte is increased. Moreover, the ruthenium complexes will precipitate out at high H_2O concentration. Tanaka et al. [22] have reported that the addition of protonated alkyl amine salts could enhance the rate of electrocatalytic reduction of CO_2 and lead to the selective formation of $HCOO^-$. Figures 3.7 and 3.8 show the cyclic voltammograms of complex **[1]** and **[2]** in CO_2-saturated acetonitrile and in the presence of triethylammine hydrochloric acid salt as proton source. The catalytic current increased at couple II for complex **[1]** and at couple II' for complex **[2]**. There is a sharp increase in cathodic current at potential beyond couple II and II' which is due to the catalytic reduction of the alkyl amine salt. Enhancement in catalytic current can also be observed for other proton sources such as $Me_3NH^+Cl^-$ and $Me_2NH_2^+Cl^-$ (Figures 3.9-3.12). For complex **[1]**, the magnitude of i_p/i_p^o does not have a strong dependence on the $Et_3NH^+Cl^-$ concentration (Figure 3.13). For complex **[2]**, only a slight increase in i_p/i_p^o was observed with the concentration of protonated alkyl amine salts (Figure 3.14). The i_p/i_p^o levels off at high $Et_3NH^+Cl^-$ concentration.

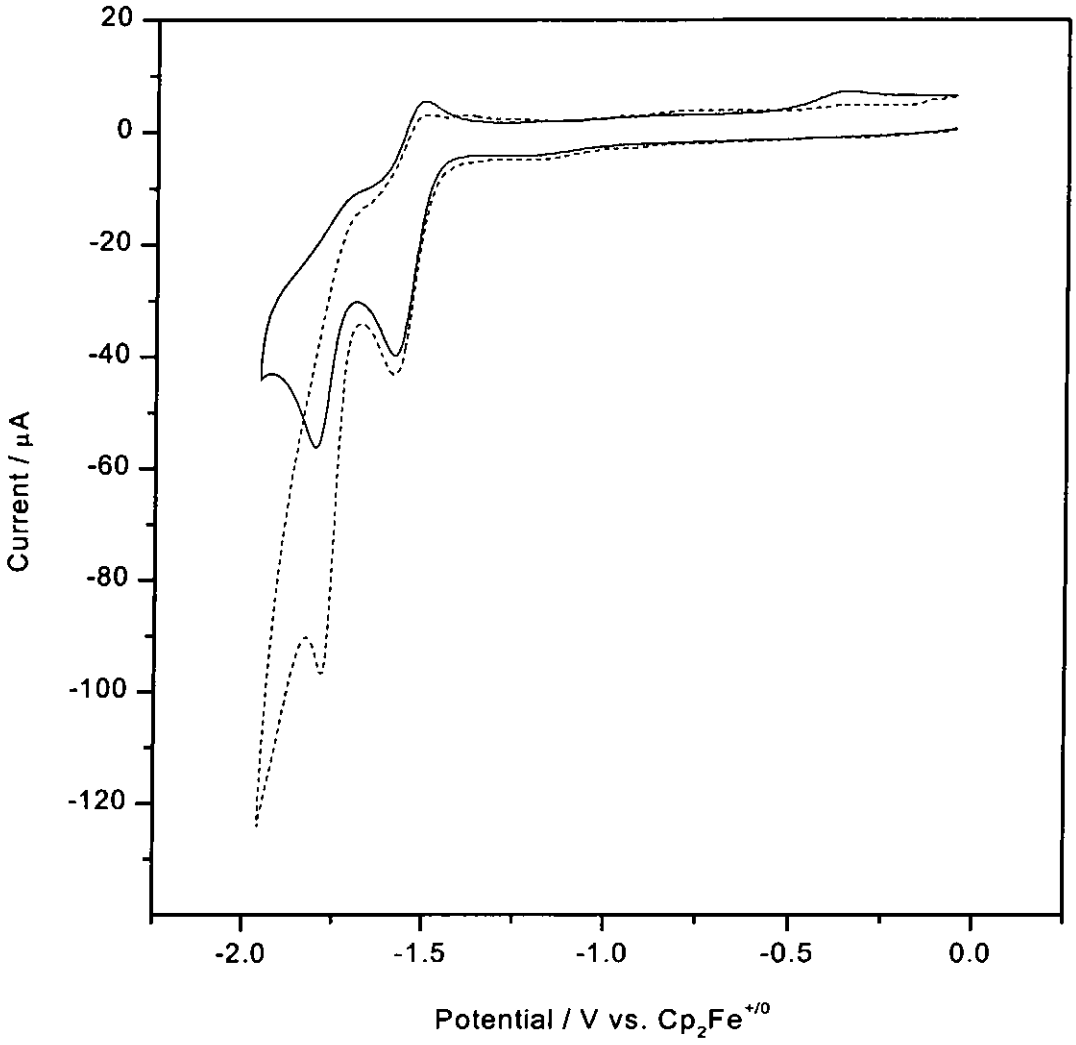

Figure 3.1 Cyclic voltammogram of 0.5 M $[Ru(bdmpp)(bpy)CO]^{2+}$ in acetonitrile under argon atmosphere (—); under CO_2 atmosphere (----). Working electrode: 0.2 cm^2. Supporting electrolyte: 0.1 M tetra-n-butylammonium hexafluorophosphate (TBAH). Scan rate: 100 mV s^{-1}.

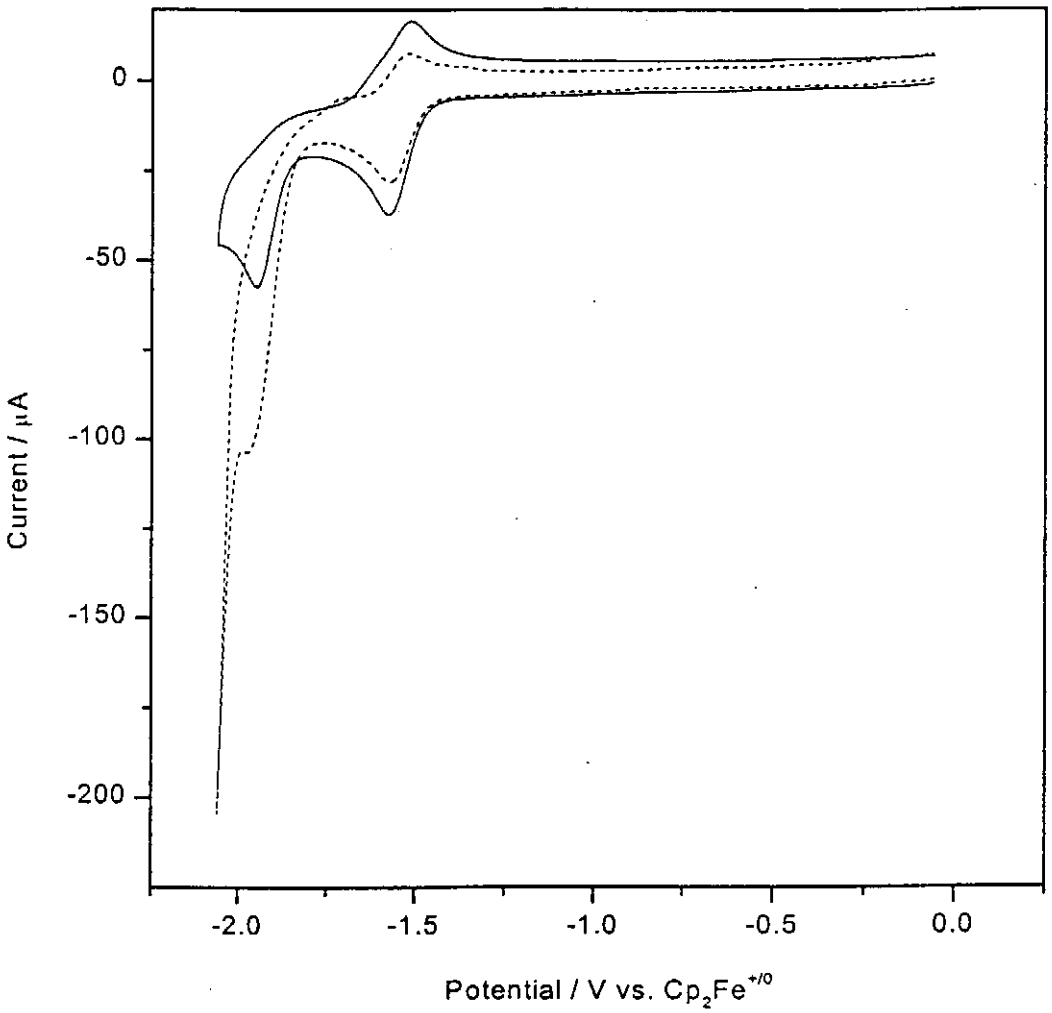

Figure 3.2 Cyclic voltammogram of 0.5 M $[Ru(tpm)(bpy)CO]^{2+}$ in acetonitrile under argon atmosphere (—); under CO_2 atmosphere (----). Working electrode: 0.2 cm^2. Supporting electrolyte: 0.1 M tetra-n-butylammonium hexafluorophosphate (TBAH). Scan rate: 100 mV s^{-1}.

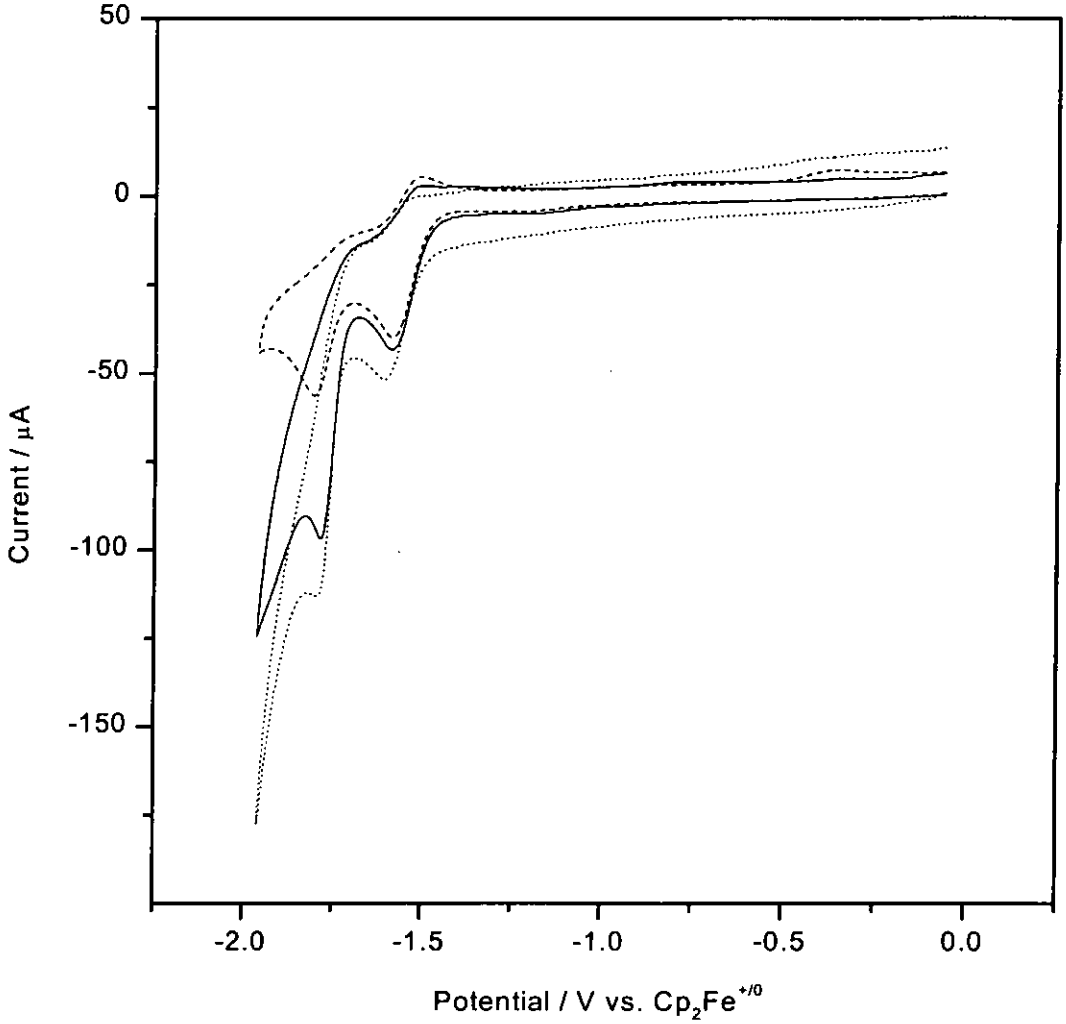

Figure 3.3 Cyclic voltammogram of 0.5 M $[Ru(bdmpp)(bpy)CO]^{2+}$ in acetonitrile under argon atmosphere (----); under CO_2 atmosphere (—) and in the presence of 0.05 M H_2O (....). Working electrode: 0.2 cm^2. Supporting electrolyte: 0.1 M tetra-n-butylammonium hexafluorophosphate (TBAH). Scan rate: 100 mV s^{-1}.

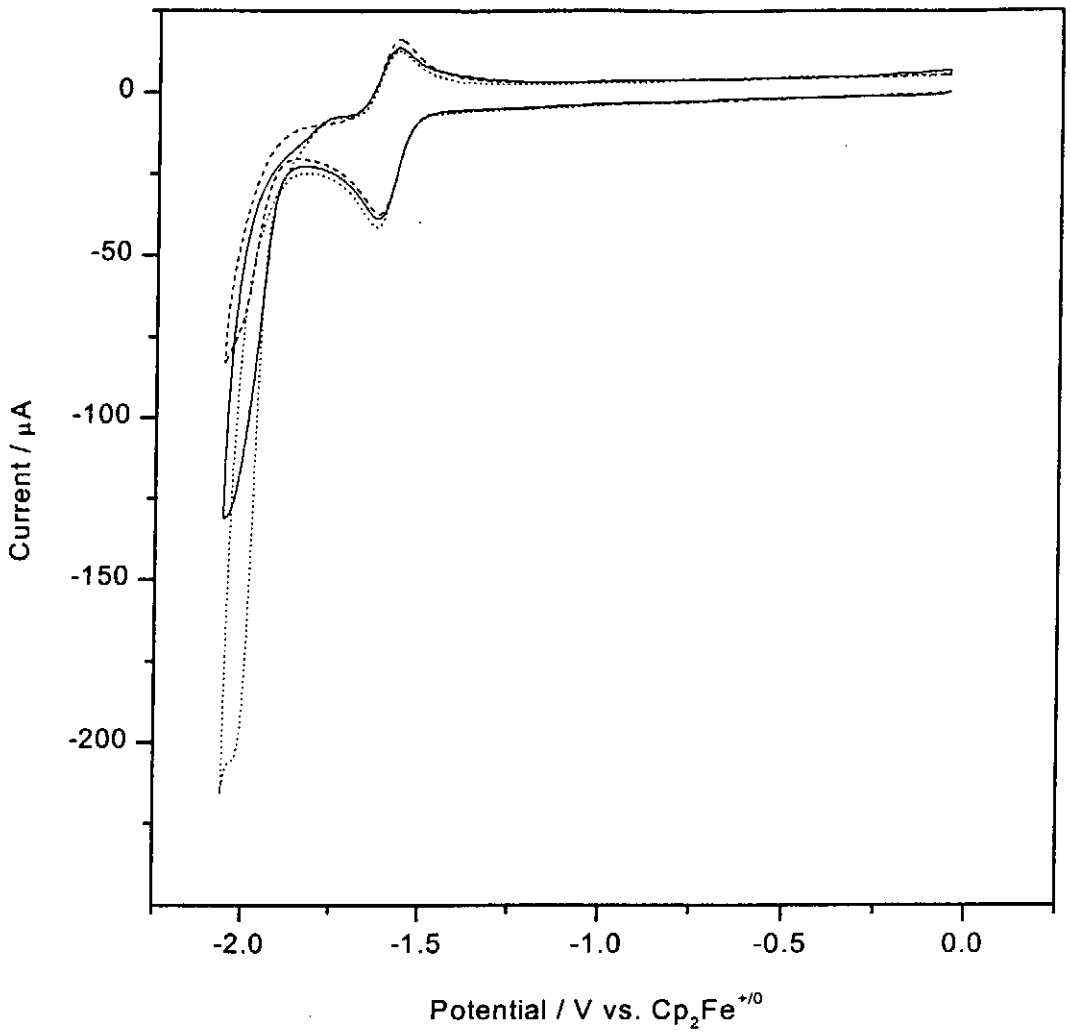

Figure 3.4 Cyclic voltammogram of 0.5 M $[Ru(tpm)(bpy)CO]^{2+}$ in acetonitrile under argon atmosphere (----); under CO_2 atmosphere (—) and in the presence of 0.05 M H_2O (....). Working electrode: 0.2 cm^2. Supporting electrolyte: 0.1 M tetra-n-butylammonium hexafluorophosphate (TBAH). Scan rate: 100 mV s^{-1}.

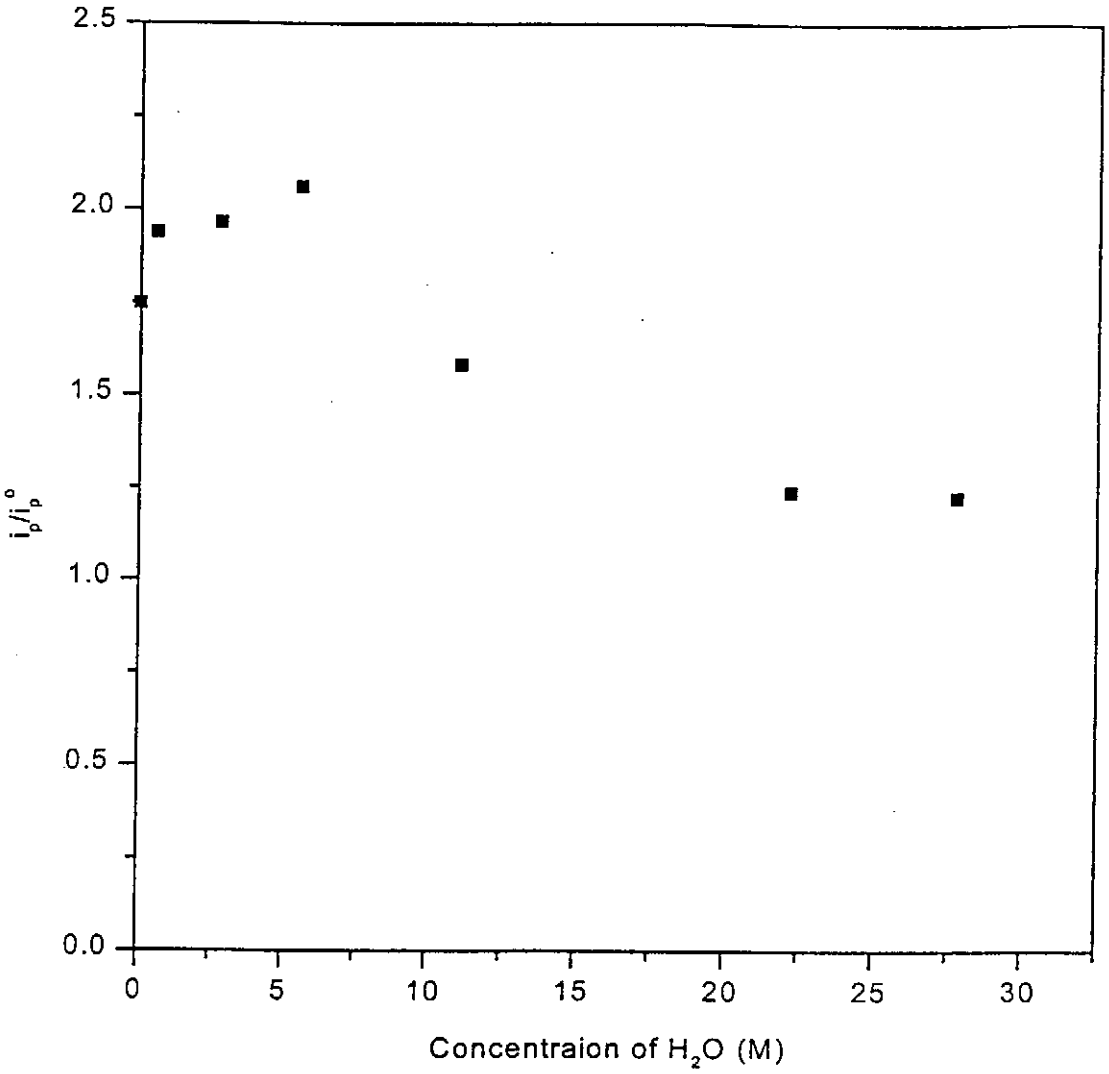

Figure 3.5 Plot of the change of plateau current as a function of H_2O concentration in the presence of $[Ru(bdmpp)(bpy)CO]^{2+}$ in CO_2-saturated acetonitrile.

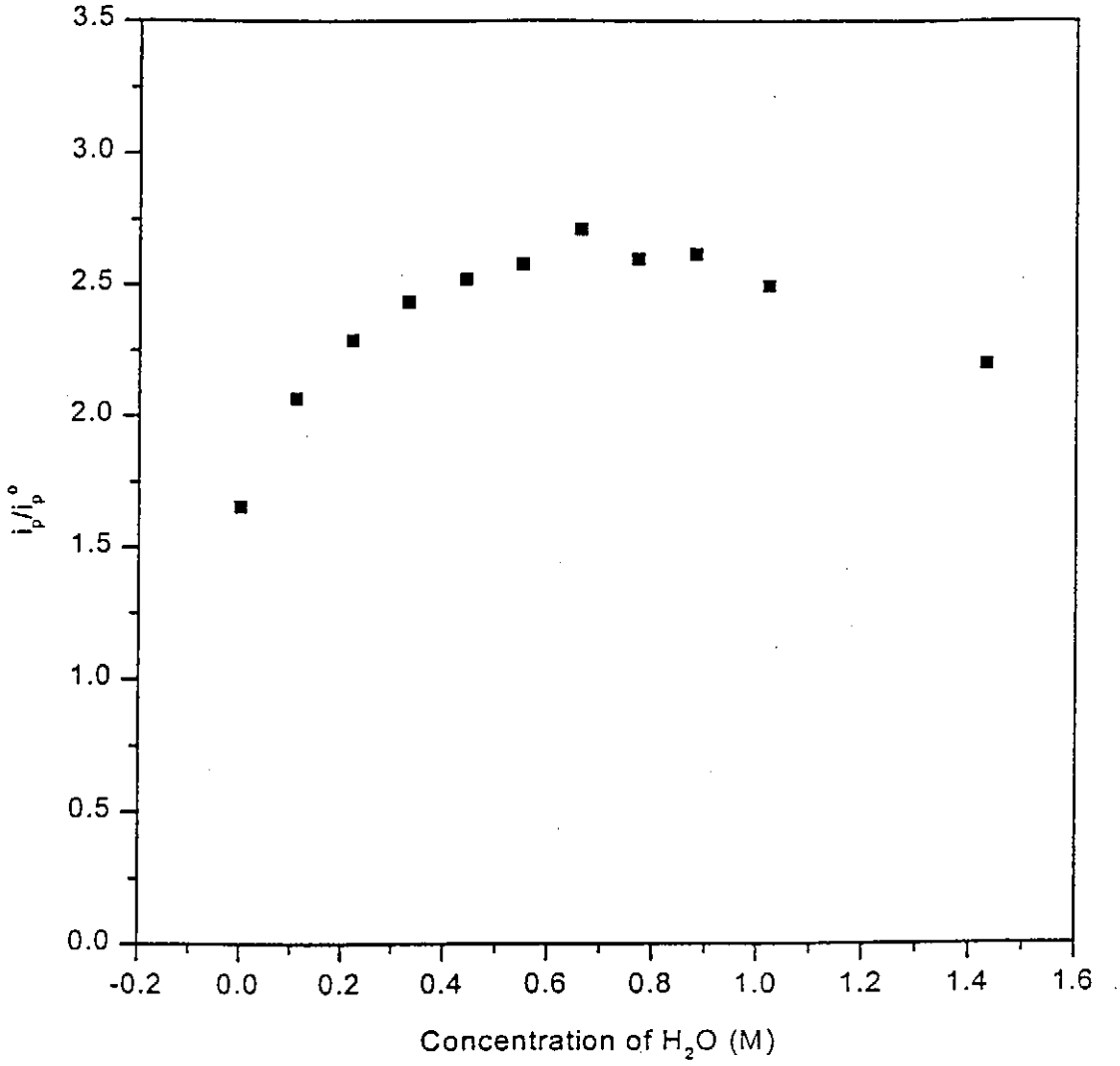

Figure 3.6 Plot of the change of plateau current as a function of H_2O concentration in the presence of $[Ru(tpm)(bpy)CO]^{2+}$ in CO_2-saturated acetonitrile.

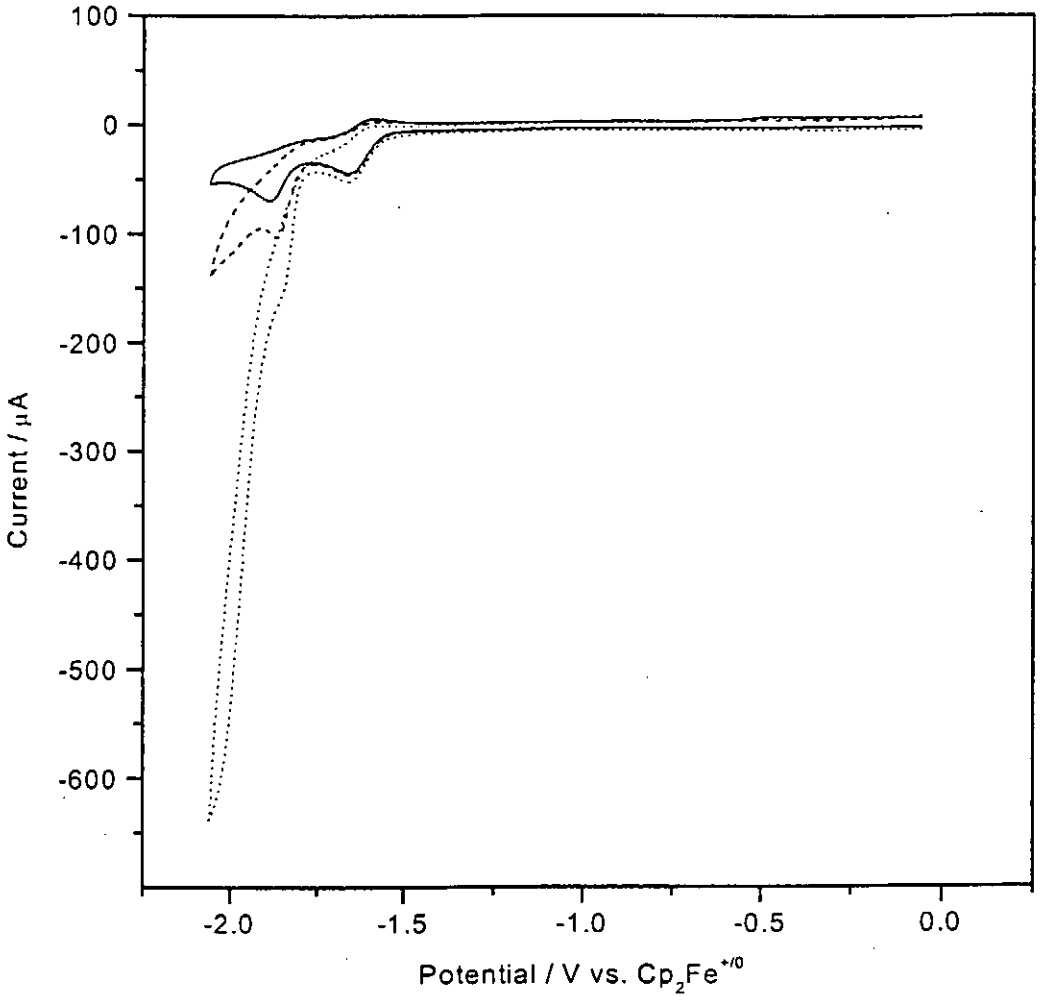

Figure 3.7 Cyclic voltammogram of 0.5 M $[Ru(bdmpp)(bpy)CO]^{2+}$ in acetonitrile under argon atmosphere (—); under CO_2 atmosphere (----) and in the presence of 0.05 M $Et_3NH^+Cl^-$ (....). Working electrode: 0.2 cm^2. Supporting electrolyte: 0.1 M tetra-n-butylammonium hexafluorophosphate (TBAH). Scan rate: 100 mV s^{-1}.

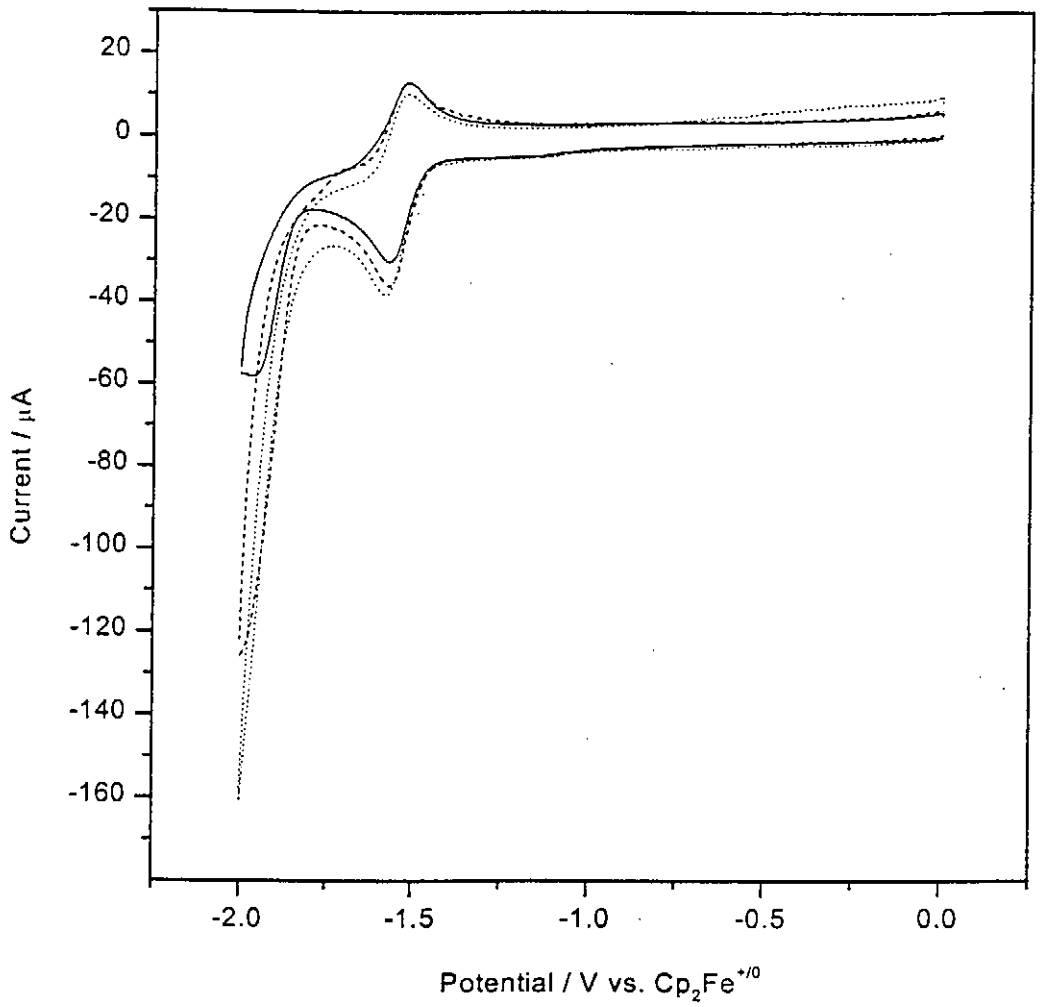

Figure 3.8 Cyclic voltammogram of 0.5 M $[Ru(tpm)(bpy)CO]^{2+}$ in acetonitrile under argon atmosphere (—); under CO_2 atmosphere (----) and in the presence of 0.05 M $Et_3NH^+Cl^-$ (....). Working electrode: 0.2 cm^2. Supporting electrolyte: 0.1 M tetra-n-butylammonium hexafluorophosphate (TBAH). Scan rate: 100 mV s^{-1}.

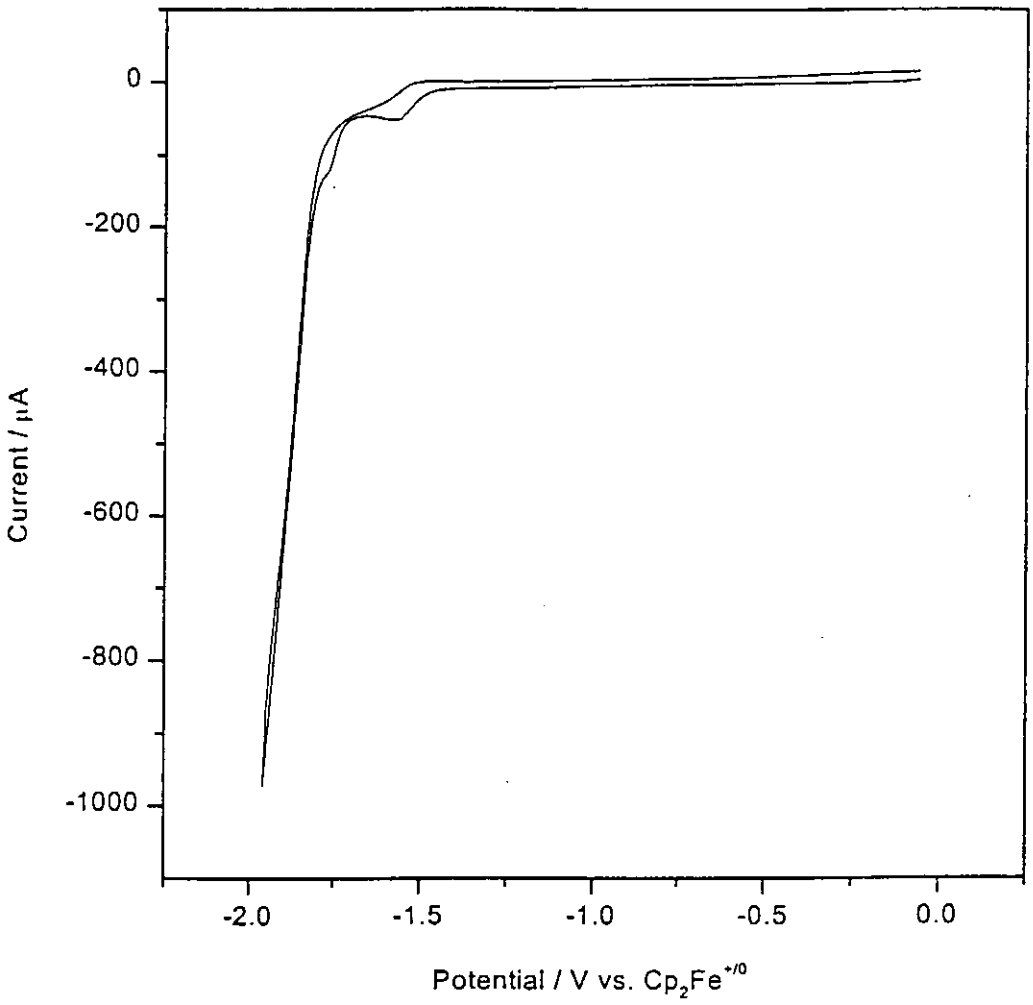

Figure 3.9 Cyclic voltammogram of 0.5 mM $[Ru(bdmpp)(bpy)CO]^{2+}$ in CO_2-saturated acetonitrile and in the presence of 0.05 M $Me_2NH_2^+Cl^-$. Working electrode: glassy carbon (0.2 cm^2). Supporting electrolyte: 0.1 M tetra-n-butylammonium hexafluorophosphate (TBAH). Scan rate: 100 mV s^{-1}.

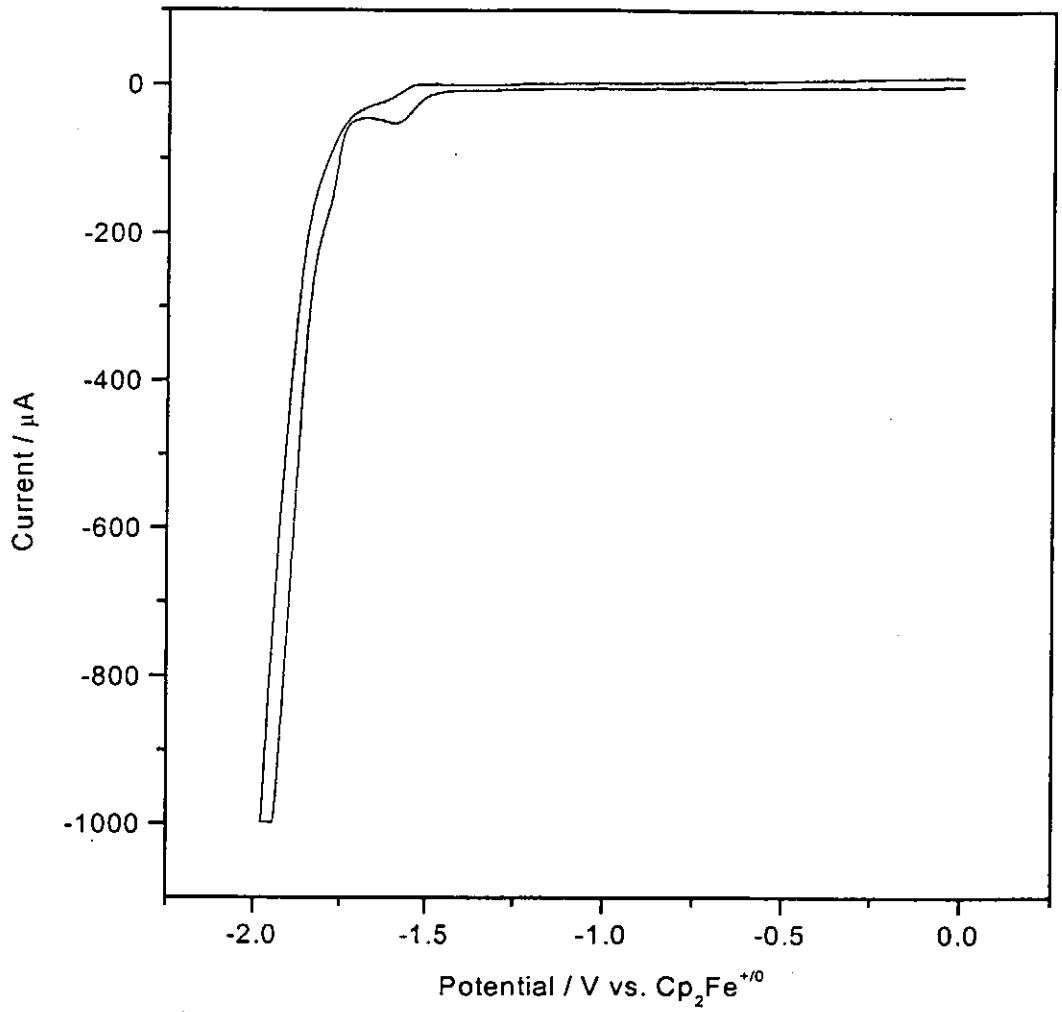

Figure 3.10 Cyclic voltammogram of 0.5 mM $[Ru(bdmpp)(bpy)CO]^{2+}$ in CO_2-saturated acetonitrile and in the presence of 0.05 M $Me_3NH^+Cl^-$. Working electrode: glassy carbon (0.2 cm^2). Supporting electrolyte: 0.1 M tetra-n-butylammonium hexafluorophosphate (TBAH). Scan rate: 100 mV s^{-1}

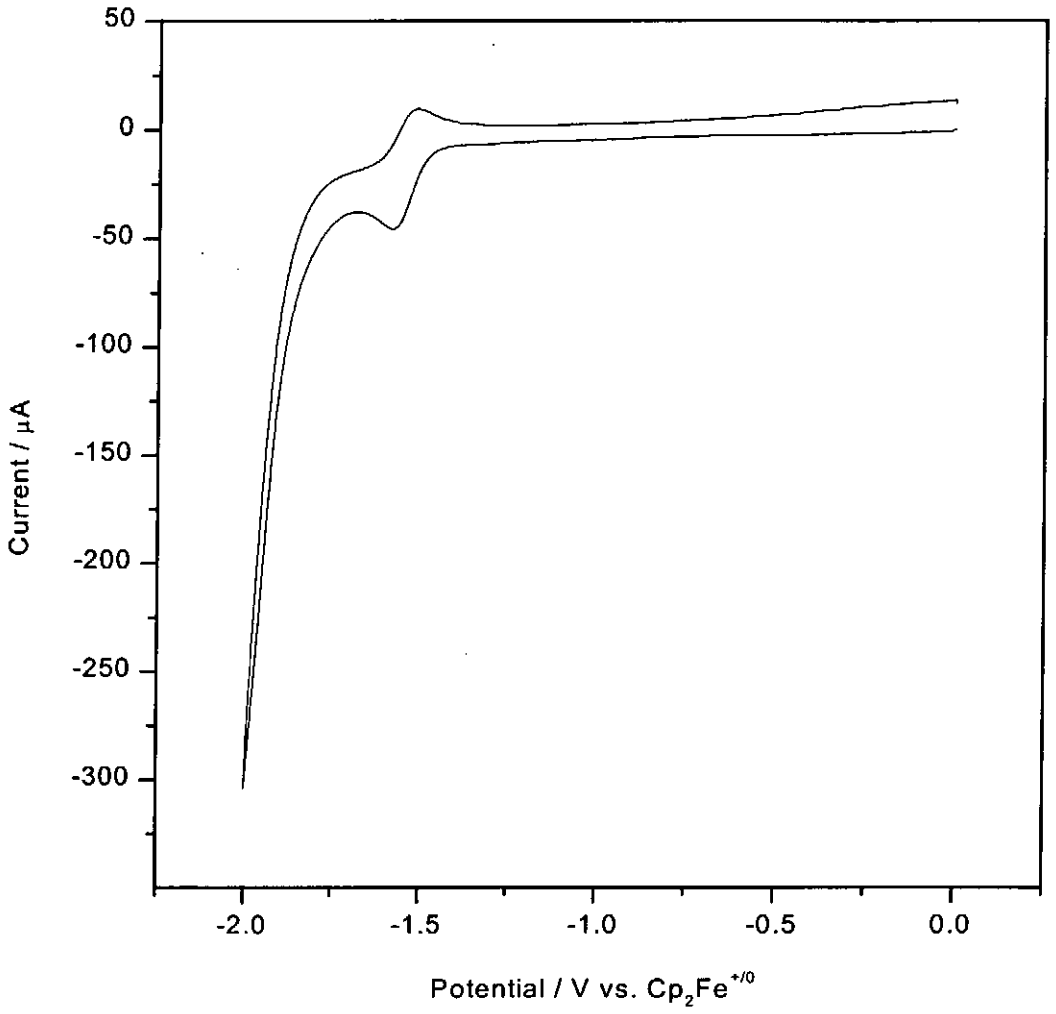

Figure 3.11 Cyclic voltammogram of 0.5 mM $[Ru(tpm)(bpy)CO]^{2+}$ in CO_2-saturated acetonitrile and in the presence of 0.05 M $Me_3NH^+Cl^-$. Working electrode: glassy carbon (0.2 cm^2). Supporting electrolyte: 0.1 M tetra-n-butylammonium hexafluorophosphate (TBAH). Scan rate: 100 mV s^{-1}.

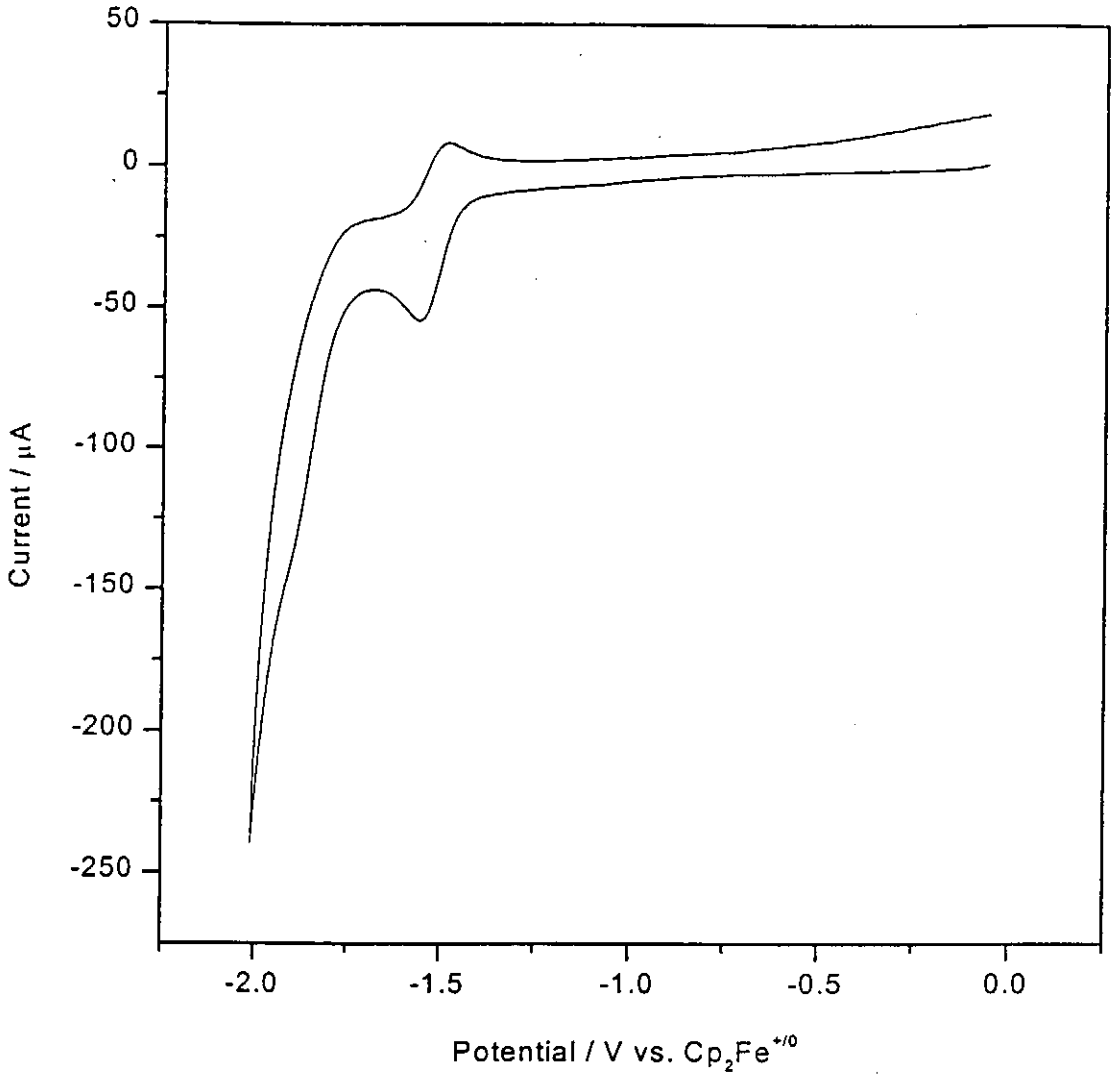

Figure 3.12 Cyclic voltammogram of 0.5 mM $[Ru(tpm)(bpy)CO]^{2+}$ in CO_2-saturated acetonitrile and in the presence of 0.05 M $Me_2NH_2^+Cl^-$. Working electrode: glassy carbon (0.2 cm^2). Supporting electrolyte: 0.1 M tetra-n-butylammonium hexafluorophosphate (TBAH). Scan rate: 100 mV s^{-1}.

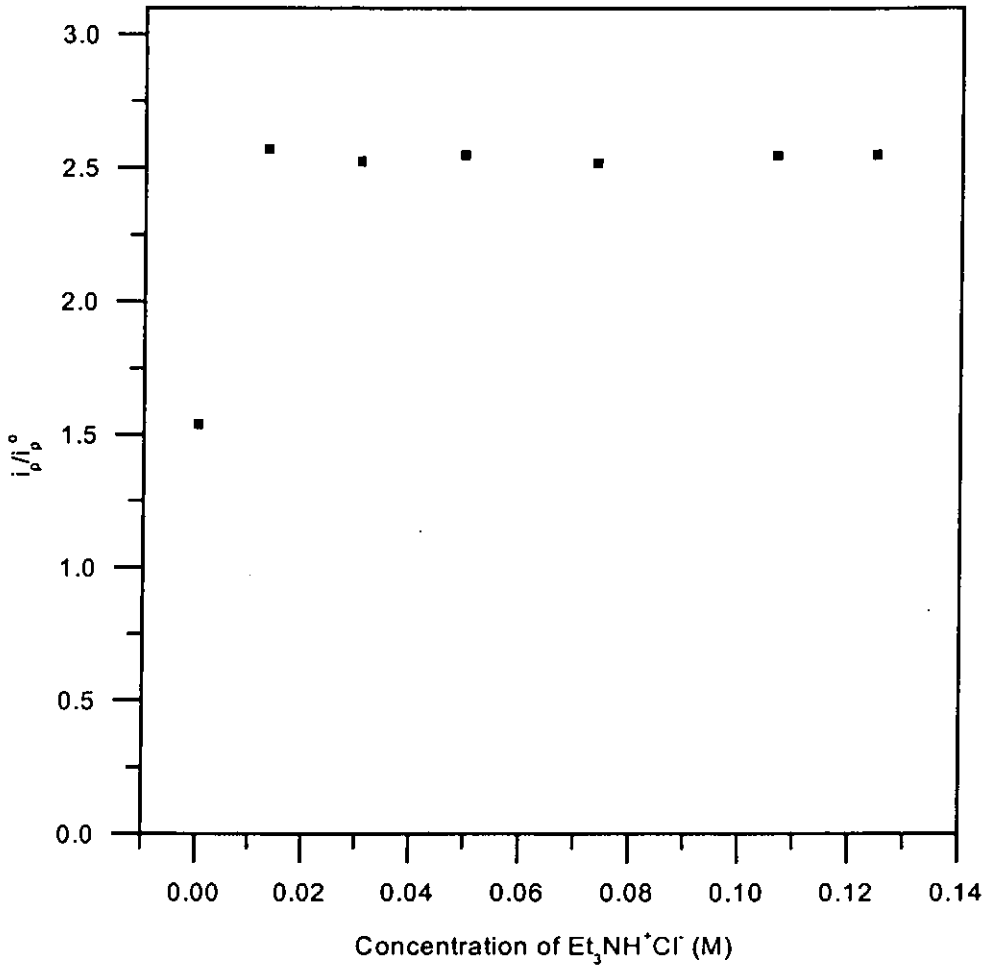

Figure 3.13 Plot of the change of plateau current as a function of $Et_3NH^+Cl^-$ concentration in the presence of $[Ru(bdmpp)(bpy)CO]^{2+}$ in CO_2-saturated acetonitrile.

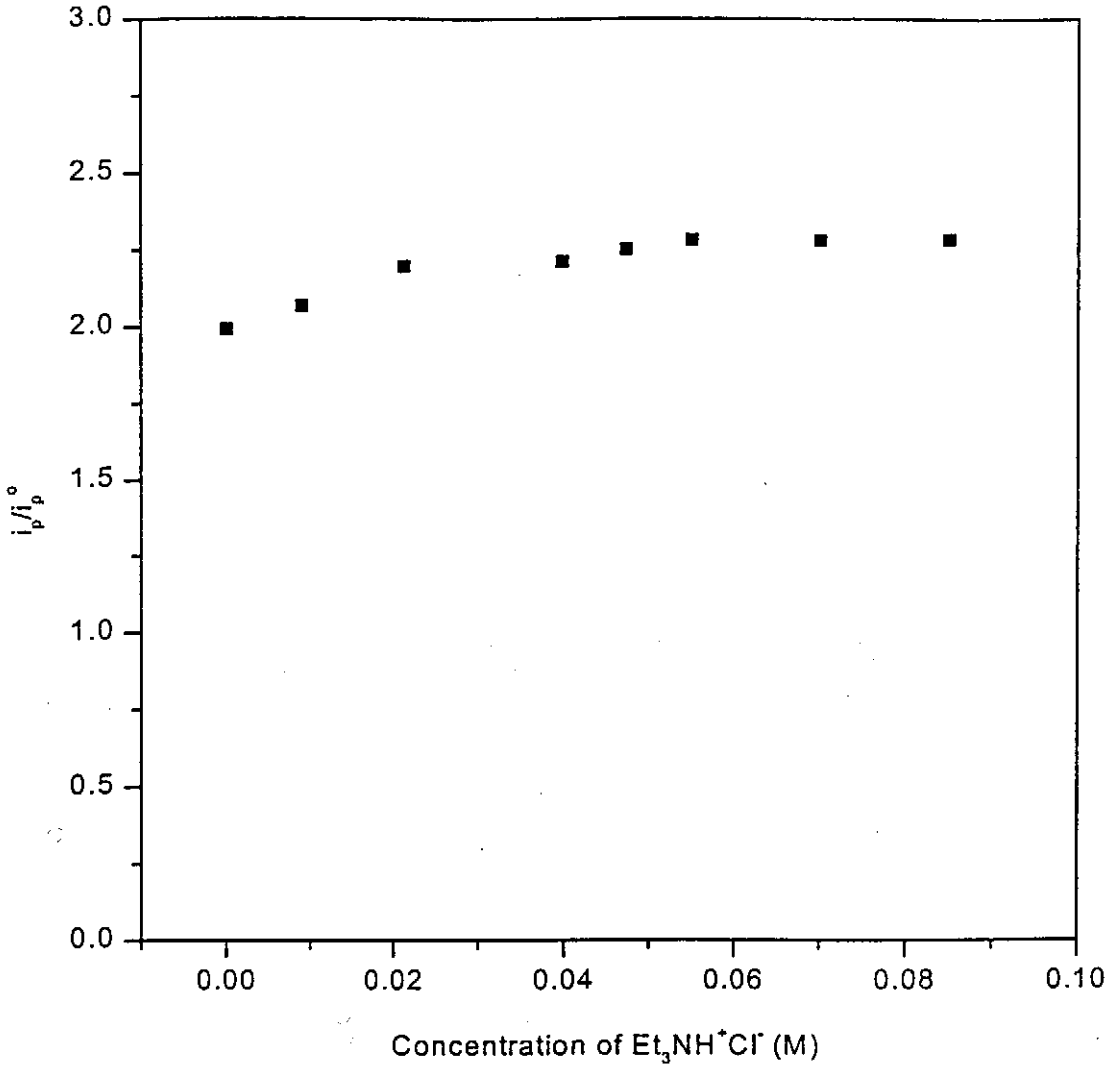

Figure 3.14 Plot of the change of plateau current as a function of $Et_3NH^+Cl^-$ concentration in the presence of $[Ru(tpm)(bpy)CO]^{2+}$ in CO_2-saturated acetonitrile.

3.3.2 Preparative Scale Electrolysis

Table 3.1 summarizes the results obtained from the constant potential electrolysis of CO_2 with the ruthenium catalysts at a reticulated vitreous carbon working electrode. Controlled potential electrolysis of complex **[1]** and **[2]** in CO_2-saturated acetonitrile and in the absence of a proton source produced a mixture of carbon monoxide and formate, although the relative amount of formate produced by complex **[2]** is much lower than that of complex **[1]**. Addition of proton source increases the rate of catalysis. The electrolyses were performed at proton source concentrations corresponding to the maximum i_p/i_p^o values as determined in the cyclic voltammograms. It is noted that CO was produced exclusively with high current efficiencies when H_2O was added, whereas the formation of formate was promoted in the presence of protonated amine salts. The pK_a of H_2O in acetonitrile is 2.2-2.35 which is subsubstantially lower than that of $Et_3NH^+Cl^-$ (pK_a = 16.8) [156]. For the three protonated amine salts employed in the study, the yield of formate decreases in the order $Et_3NH^+Cl^-$ (pK_a = 16.8) > $Me_2NH_2^+Cl^-$ (pK_a = 15.8 [22]) > $Me_3NH^+Cl^-$ (pK_a = 14.8 [22]). Significant amount of H_2 gas was produced with $Me_3NH^+Cl^-$ as proton source. The current efficiency of formate formation reaches 90% and 76% with $[Ru(bdmpp)(bpy)CO]^{2+}$ and $[Ru(tpm)(bpy)CO]^{2+}$ respectively when $Et_3NH^+Cl^-$ was utilized as the proton source. On the other hand, CO was produced with current efficiencies of 98% and 88% for complex **[1]** and **[2]** respectively in the presence of H_2O.

Table 3.1. A summary on the electrolysis of CO_2 in the presence of ruthenium catalysts [a]

Catalysts	Proton source	Potential held / V vs. $Cp_2Fe^{+/0}$ [d]	Charge consumed / C	Current efficiency of CO produced / %	Current efficiency of $HCOO^-$ produced / %	Current efficiency of H_2 produced / %
$[Ru(bdmpp)(bpy)CO]^{2+}$	----	-1.86	23.36 (14.26)[c]	60.6 (56.4)[c]	35.3 (37.6)[c]	---- (----)[c]
$[Ru(bdmpp)(bpy)CO]^{2+}$	0.05M $Me_3NH^+Cl^-$	-1.86	43.31	9.6	51.8	38.6
$[Ru(bdmpp)(bpy)CO]^{2+}$	0.05M $Me_2NH_2^+Cl^-$	-1.86	13.68	17.3	75.9	5.8
$[Ru(bdmpp)(bpy)CO]^{2+}$	0.05M $Et_3NH^+Cl^-$	-1.86	47.95 (21.42)[c]	7.7 (6.5)[c]	90.2 (87.8)[c]	2.2 (1.9)[c]
$[Ru(bdmpp)(bpy)CO]^{2+}$	5.0M H_2O	-1.86	58.00 (30.25)[c]	98.0 (96.0)[c]	---- (----)[c]	---- (----)[c]
$[Ru(tpm)(bpy)CO]^{2+}$	----	-2.01	11.40 (6.80)[c]	88.8 (86.2)[c]	8.7 (6.9)[c]	---- (----)[c]
$[Ru(tpm)(bpy)CO]^{2+}$	0.05M $Me_3NH^+Cl^-$	-2.01	44.02	7.5	63.4	28.7
$[Ru(tpm)(bpy)CO]^{2+}$	0.05M $Me_2NH_2^+Cl$	-2.01	33.96	13.8	73.5	7.2
$[Ru(tpm)(bpy)CO]^{2+}$	0.05M $Et_3NH^+Cl^-$	-2.01	29.98 (13.85)[c]	20.8 (15.4)[c]	76.6 (79.5)[c]	1.6 (1.8)[c]
$[Ru(tpm)(bpy)CO]^{2+}$	0.66M H_2O	-2.01	13.46 (8.52)[c]	79.7 (82.1)[c]	---- (----)[c]	---- (----)[c]

[a]Amount of catalyst in solution = 1 x 10^{-3} M; Time of electrolysis = 1h; Solvent: CH_3CN

[b]TBAH = tetra-n-butylammonium hexafluorophosphate

[c]Temperature of the electrolyte = -0.5°C

[d]The $E_{1/2}$ of $Cp_2Fe^{+/0}$ in CH_3CN = +0.307 vs. SCE [153]

3.3.3 *In-situ* FTIR spectroelectrochemistry

All the *In-situ* FTIR spectroelectrochemical experiments were performed at – 0.5°C to enable the detection of unstable intermediates during the course of reaction.

(1) Reduction of $[Ru(bdmpp)(bpy)CO]^{2+}$ and $[Ru(tpm)(bpy)CO]^{2+}$in N_2-saturated acetonitrile

Figures 3.15a-b show the normalized time resolved spectra collected from a solution of $[Ru(bdmpp)(bpy)CO]^{2+}$ and $[Ru(tpm)(bpy)CO]^{2+}$ in N_2-saturated acetonitrile respectively with the potential held beyond the $E_{1/2}$ of couple II and II'.

The ν(CO) of complex **[1]** and **[2]** are located at 2006 cm^{-1} and 2010 cm^{-1} respectively. The positive ΔR/R reflectance of the band at 2006 cm^{-1} can be assigned to the cleavage of the Ru-CO moiety upon two-electron reduction of complex **[1]** (Figure 3.10a). Based on previous studies [4], the gain in absorbance at 2273 cm^{-1} can be assigned to a modified C≡N stretch of acetonitrile. The absorbance of acetonitrile is shifted from its 'free' value of 2253 cm^{-1} to 2273 cm^{-1}, suggesting that it undergoes coordination. The lone pair on the sp-hybridized nitrogen MeCN is slightly antibonding and so donation to the metal center will increase the C≡N stretching frequency [4]. Similar changes in the IR spectra were observed for complex **[2]** (Figure 3.15b).

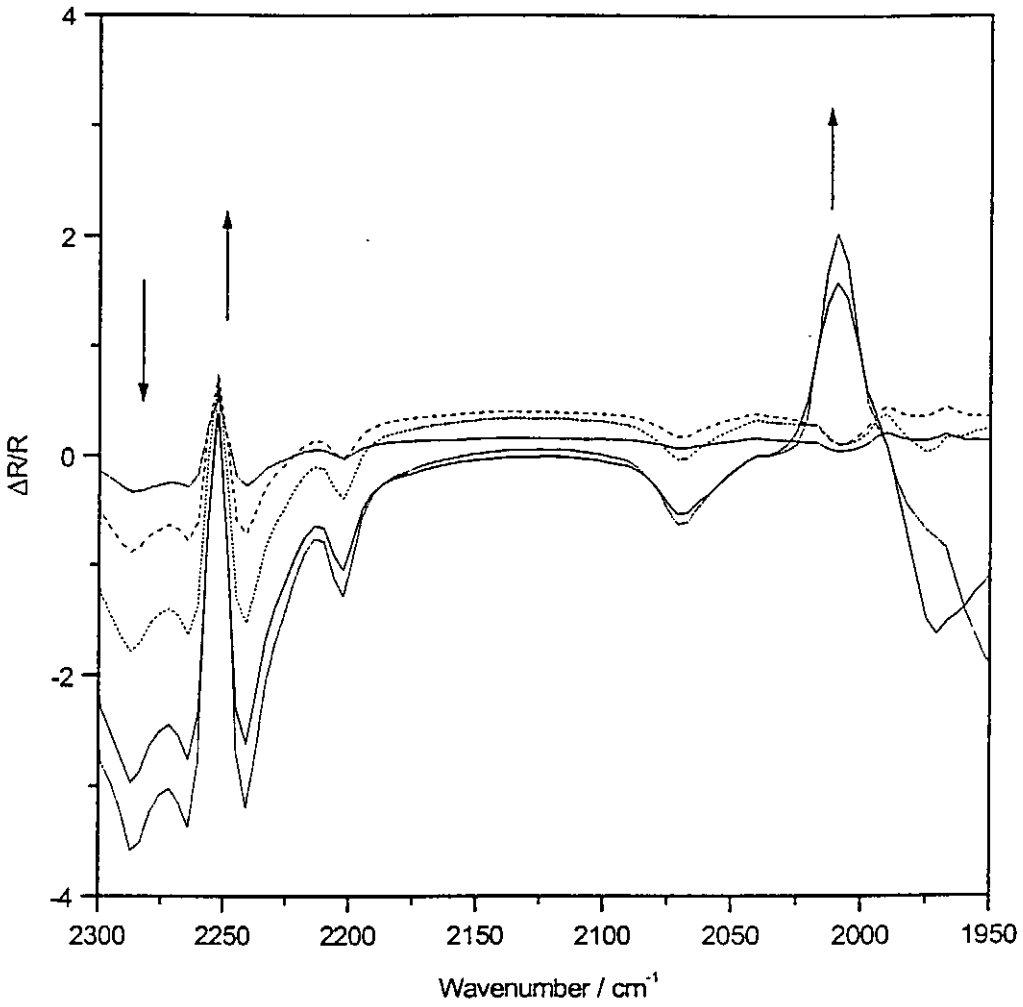

Figure 3.15a A series of normalized time resolved FTIR spectra in the region 2300-1950 cm^{-1} (8 cm^{-1} resolution, 100 scans) collected from a glassy carbon electrode immersed in a solution of $[Ru(bdmpp)(bpy)CO]^{2+}$ (5 mM) in N_2-saturated acetonitrile. E_1 = -0.46 V and E_2 = -1.86 V vs. $Cp_2Fe^{+/0}$. Supporting electrolyte: 0.1 M tetra-n-butylammonium hexafluorophosphate. The temperature of the electrolyte was kept at -0.5°C.

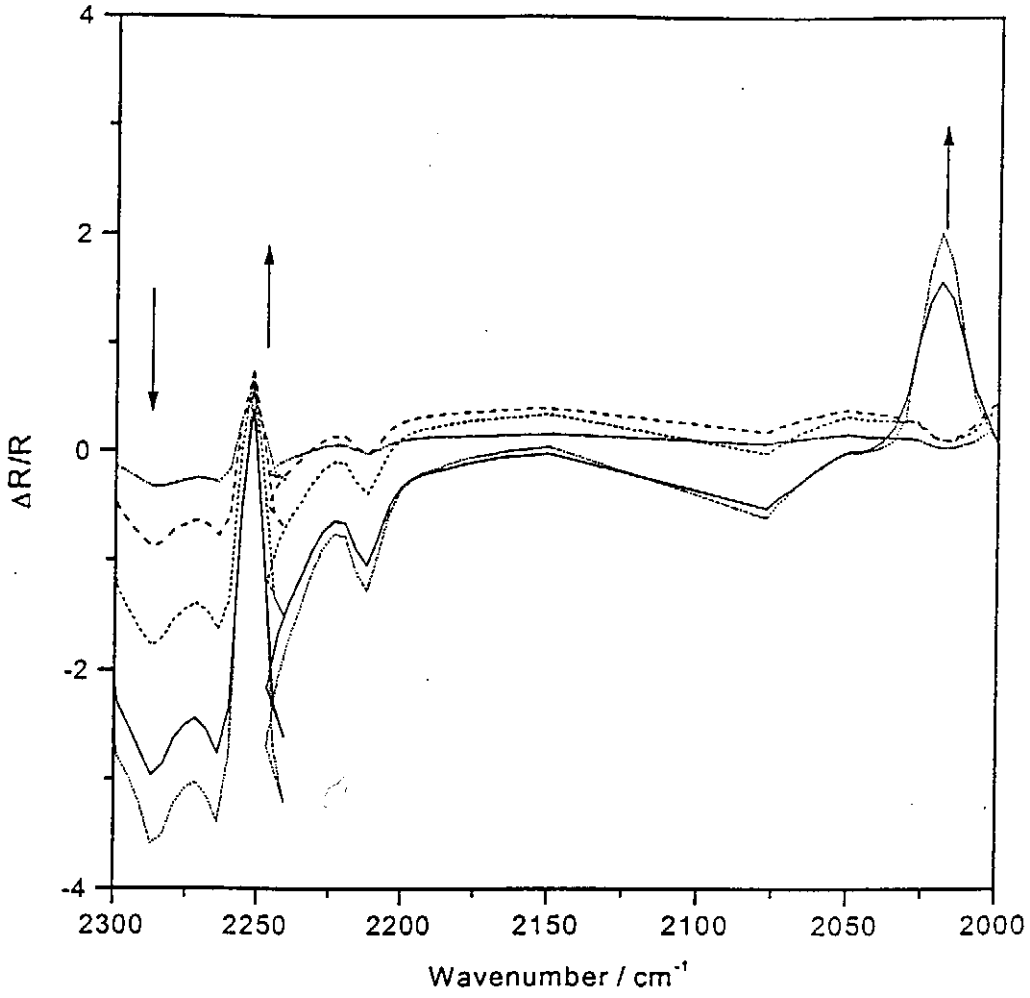

Figure 3.15b A series of normalized time resolved FTIR spectra in the region 2300-2000 cm^{-1} (8 cm^{-1} resolution, 100 scans) collected from a glassy carbon electrode immersed in a solution of $[Ru(tpm)(bpy)CO]^{2+}$ (5 mM) in N_2-saturated acetonitrile. E_1= -0.46 V and E_2 = -2.01 V vs. $Cp_2Fe^{+/0}$. Supporting electrolyte: 0.1 M tetra-n-butylammonium hexafluorophosphate. The temperature of the electrolyte was kept at -0.5°C.

(2) Reduction of $[Ru(bdmpp)(bpy)CO]^{2+}$ and $[Ru(tpm)(bpy)CO]^{2+}$ in CO_2-saturated acetonitrile

The normalized time resolved spectra in the region 3200-1000 cm^{-1} collected from a solution of $[Ru(bdmpp)(bpy)CO]^{2+}$ in CO_2-saturated acetonitrile are shown in Figure 3.16.

The results showed an intense negative band at 3100-3000 cm^{-1}. According to previous studies [4, 140, 146], these bands can be assigned to the absorptions caused by the increase in the concentration of TBA^+ ions in the thin layer as the electrode surface became more negatively charged. The carbonyl ligand was dissociated from the ruthenium metal center which is supported by the positive reflectance of the band at 2006 cm^{-1}. There is little change in absorption intensity in the carbonyl region (1800-1000 cm^{-1}). A weak absorption band at 1605 cm^{-1} can be observed which can be assigned to the presence of free formate. There is also a small increase in the absorption intensity at 2140 cm^{-1} which is most suitably assigned to the presence of CO [4]. The intensity of CO absorption observed in the IR spectra is relatively small which is due to the comparatively low oscillator strength for IR absorption by CO as compared to CO_2 (a factor of eight) as well as the low concentration of CO [4]. Similar observations were obtained for complex **[2]** except that the intensity of the peak at 1605 cm^{-1} is much smaller than that of complex **[1]** due to the much lower concentration of formate afforded in the electrolysis. This is consistent with the results of constant potential electrolysis (Table 3.1) which indicated that in the absence of any proton source, complex **[2]** gave a relatively smaller proportion of $HCOO^-$ than complex **[1]**. The $E_{1/2}$ of the metal-centered reduction (couple II') of complex **[2]** is more negative than that

(couple II) of complex **[1]**. Hence complex **[2]** should be a more powerful reductant. It is also noted that the ligand opposite to the binding site for CO_2 in complex [1] is a pyridine, whereas that in complex **[2]** is a pyrazole. As pyrazole is a stronger π-acid than pyridine, the electron density should be more localized in the Ru center in the reduced form of complex **[2]** than complex **[1]**. The very nucleophilic ruthenium center of complex **[2]** can therefore interact more favorably with the weakly electrophilic carbon center in CO_2 giving rise to a Ru-η^1-CO_2 intermediate which is commonly believed to be the precursor for CO formation.

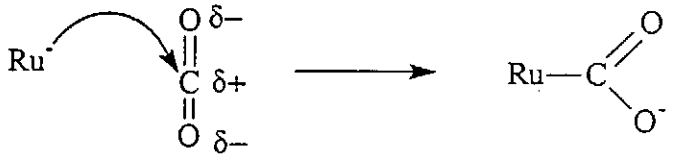

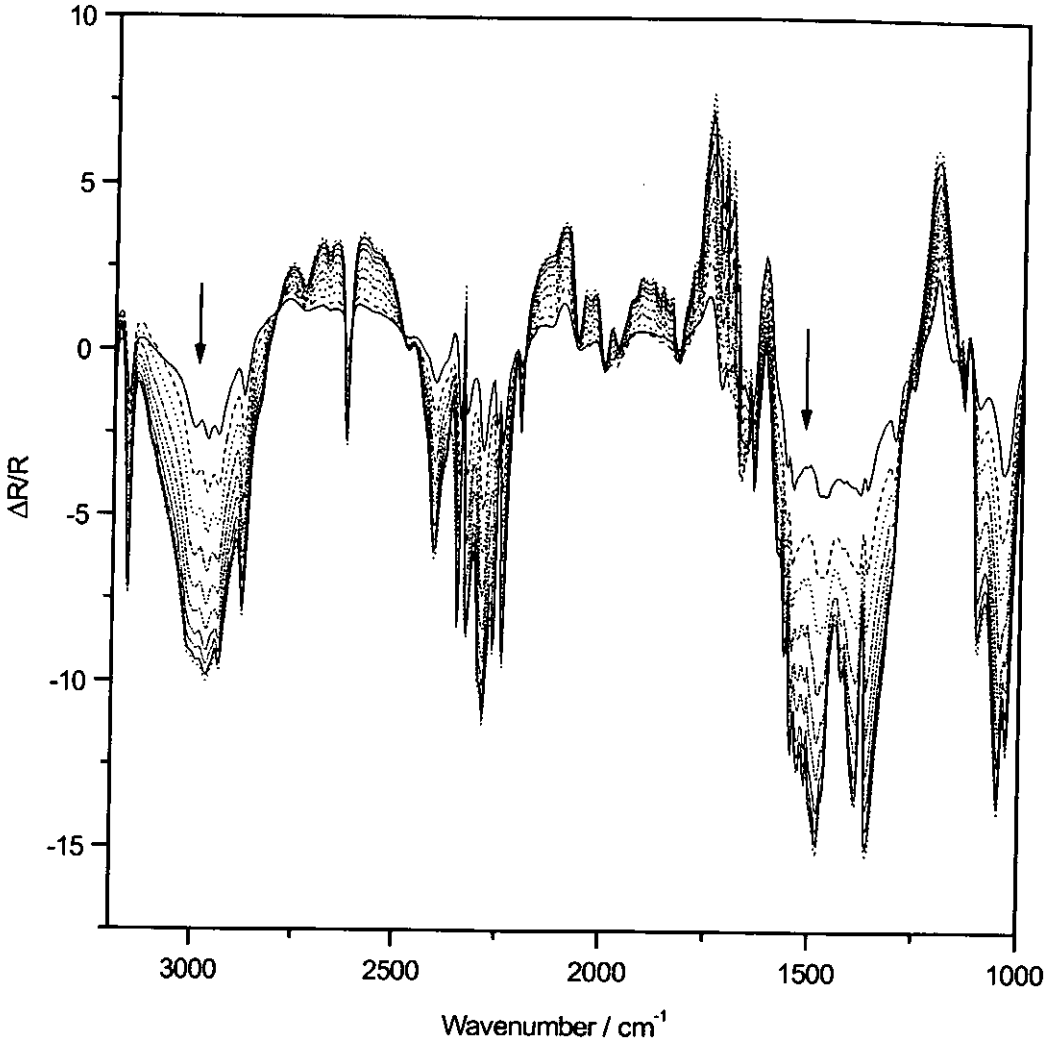

Figure 3.16 A series of normalized time resolved FTIR spectra in the region 3200-1000 cm^{-1} (8 cm^{-1} resolution, 100 scans) collected from a glassy carbon electrode immersed in a solution of $[Ru(bdmpp)(bpy)CO]^{2+}$ (5 mM) in CO_2-saturated acetonitrile. E_1= -0.46 V and E_2 = -1.86 V vs. $Cp_2Fe^{+/0}$. Supporting electrolyte: 0.1 M tetra-n-butylammonium hexafluorophosphate. The temperature of the electrolyte was kept at -0.5°C.

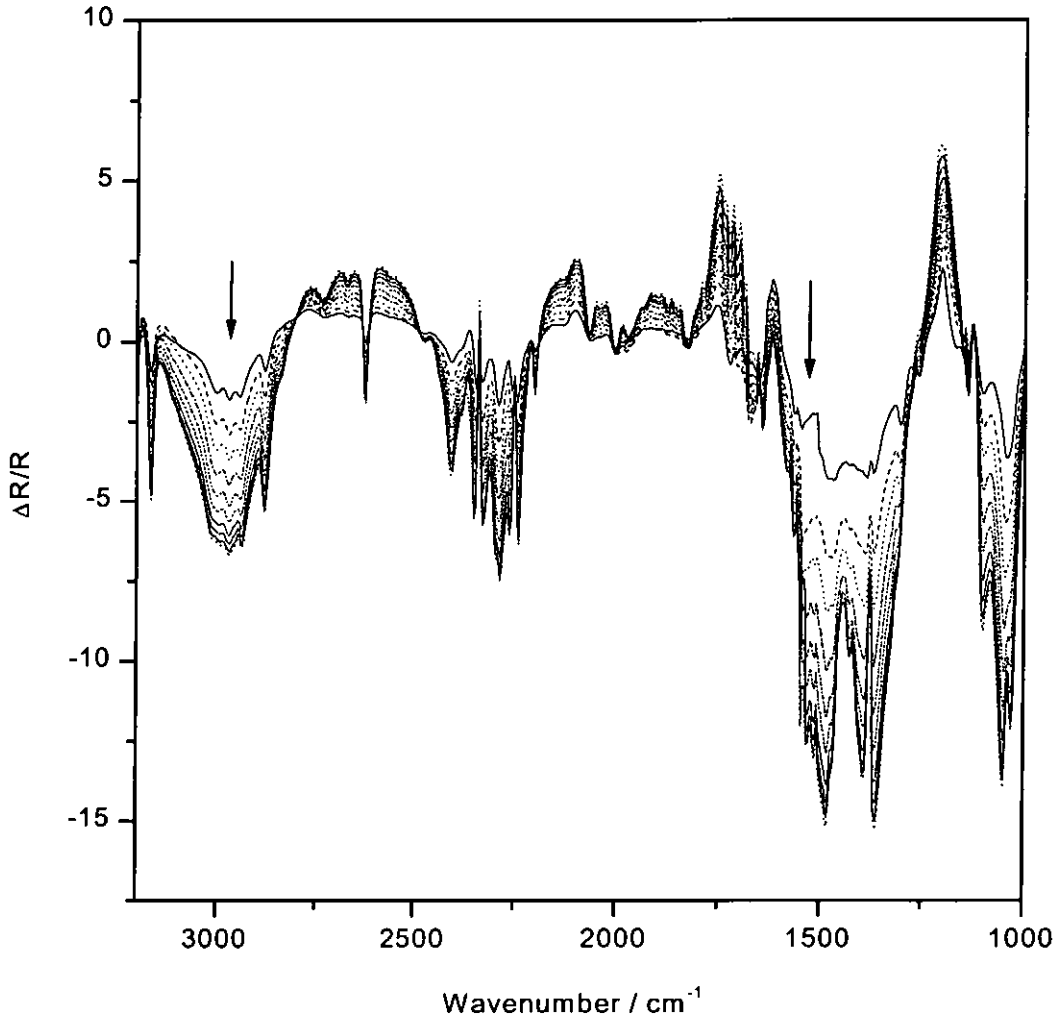

Figure 3.17 A series of normalized time resolved FTIR spectra in the region 3200-1000 cm^{-1} (8 cm^{-1} resolution, 100 scans) collected from a glassy carbon electrode immersed in a solution of $[Ru(tpm)(bpy)CO]^{2+}$ (5 mM) in CO_2-saturated acetonitrile. E_1= -0.46 V and E_2 = -2.01 V vs. $Cp_2Fe^{+/0}$. Supporting electrolyte: 0.1 M tetra-n-butylammonium hexafluorophosphate. The temperature of the electrolyte was kept at -0.5°C.

(3) Reduction of $[Ru(bdmpp)(bpy)CO]^{2+}$ and $[Ru(tpm)(bpy)CO]^{2+}$ in CO_2-saturated acetonitrile and in the presence of H_2O

Figure 3.18 shows the time resolved FTIR spectra obtained at –1.86 V vs. $Cp_2Fe^{+/0}$ in the absorption region ranging 3200-1000 cm^{-1} for complex **[1]** in CO_2 saturated acetonitrile in the presence of H_2O. The negative bands at 3100-3000 cm^{-1} are caused by the absorption of the positively charged TBA^+ ions that were attracted to the thin layer [4, 140]. The positive band at 2343 cm^{-1} is attributed to the consumption of CO_2 during the reduction reaction. Furthermore, the reflectance at 2006 cm^{-1} (characteristic of Ru-CO absorption) showed an initial increment in the early stage of the electrolysis, but then the absorption intensity became constant afterwards. This suggests a continual formation and consumption of the Ru-CO moiety during the course of electrolysis. Similar results were also obtained for complex **[2]** in CO_2 saturated acetonitrile in the presence of H_2O (Figure 3.19).

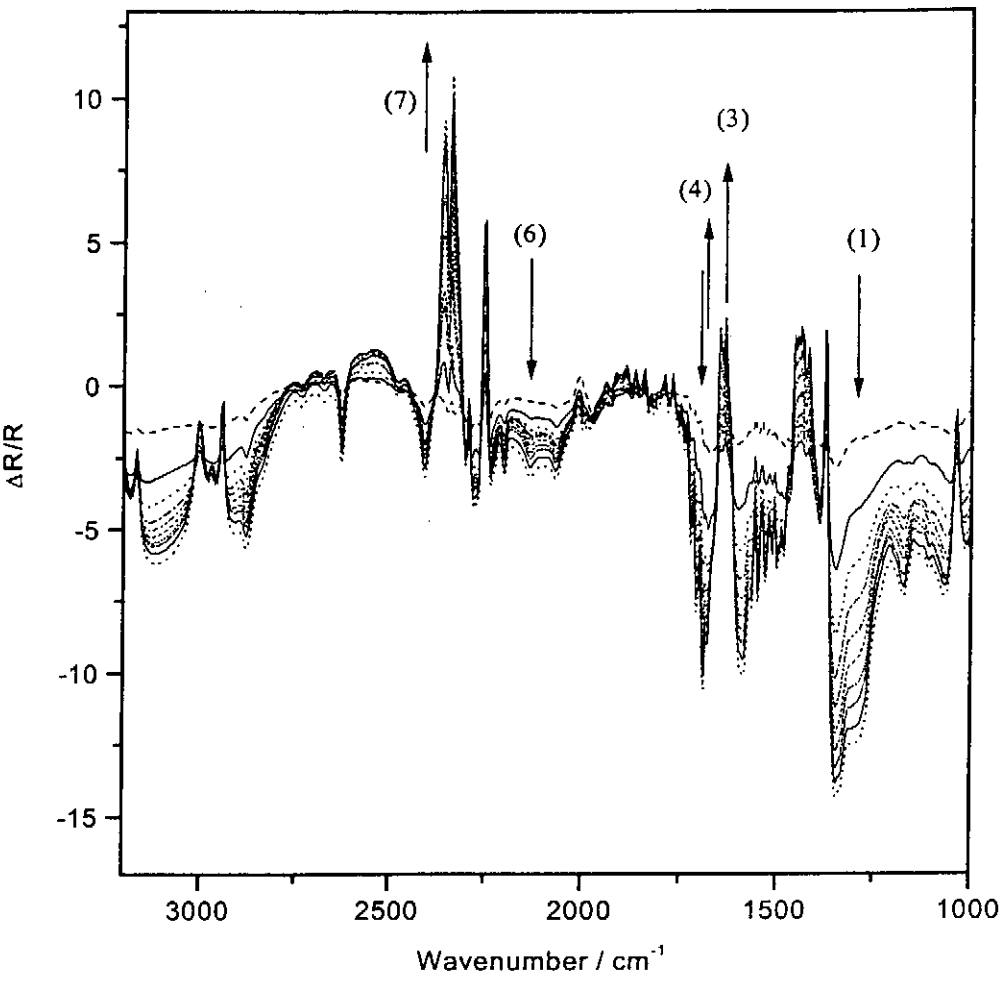

Figure 3.18a A series of normalized time resolved FTIR spectra in the region 3200-1000 cm^{-1} (8 cm^{-1} resolution, 100 scans) collected from a glassy carbon electrode immersed in a solution of $[Ru(bdmpp)(bpy)CO]^{2+}$ (5 mM) in CO_2-saturated acetonitrile and in the presence of H_2O (5.0 M). E_1 = -0.46 V and E_2 = -1.86 V vs. $Cp_2Fe^{+/0}$. Supporting electrolyte: 0.1 M tetra-n-butylammonium hexafluorophosphate. The temperature of the electrolyte was kept at -0.5°C. A summary of the assignment of the bands 1, 3-7 is given in Table 3.2.

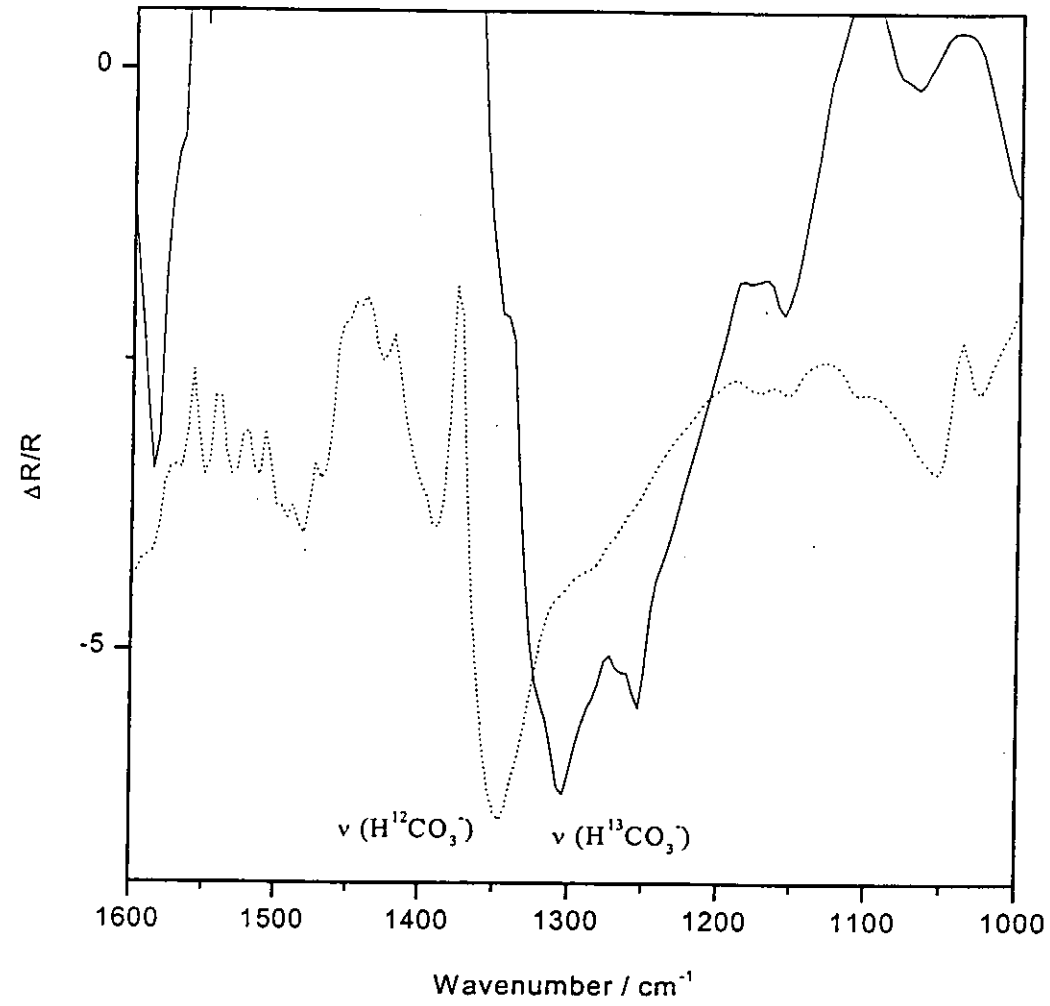

Figure 3.18b A series of normalized time resolved FTIR spectra in the region 3200-1000 cm^{-1} (8 cm^{-1} resolution, 100 scans) collected from a glassy carbon electrode immersed in a solution of $[Ru(bdmpp)(bpy)CO]^{2+}$ (5 mM) in $^{13}CO_2$-saturated acetonitrile and in the presence of H_2O (5.0 M). E_1 = -0.46 V and E_2 = -1.86 V vs. $Cp_2Fe^{+/0}$. Supporting electrolyte: 0.1 M tetra-n-butylammonium hexafluorophosphate. The temperature of the electrolyte was kept at -0.5°C.

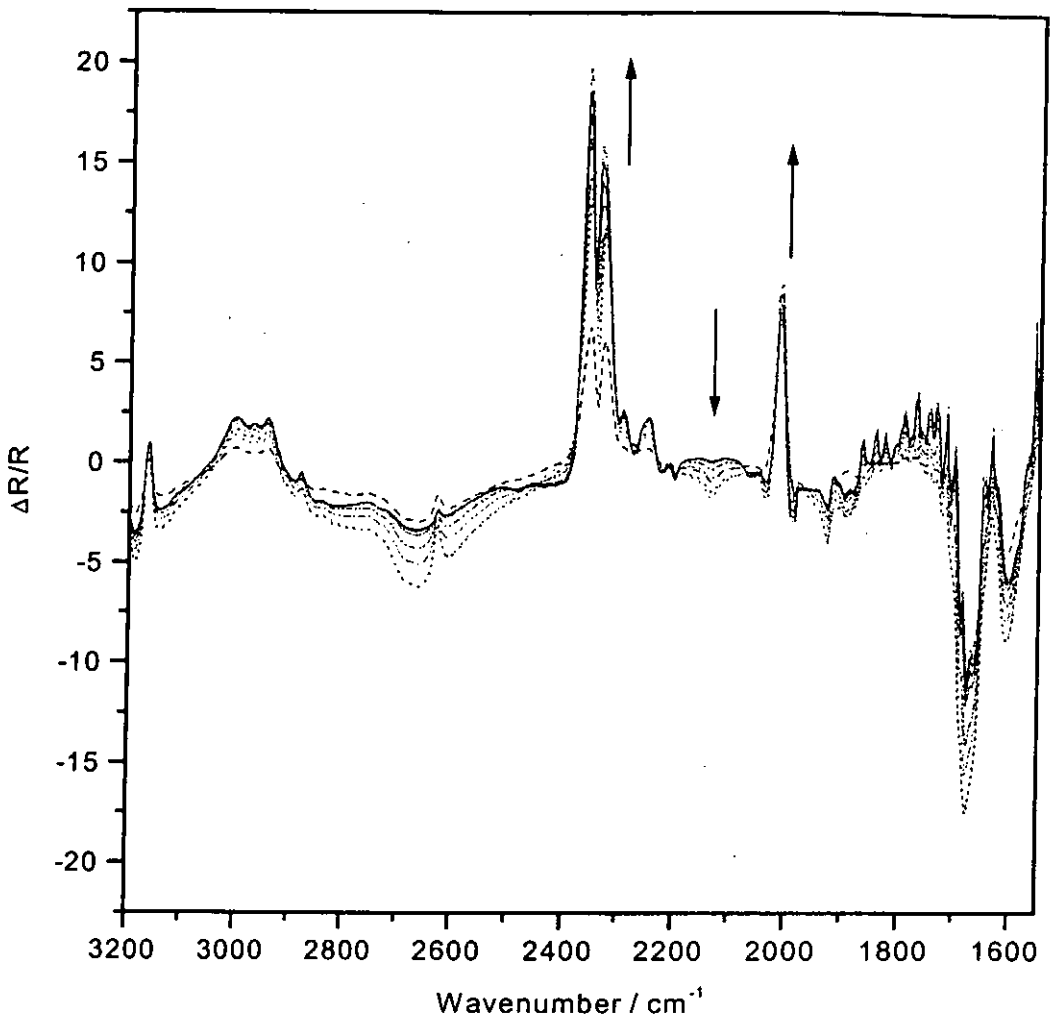

Figure 3.19 A series of normalized time resolved FTIR spectra in the region 3200-1500 cm^{-1} (8 cm^{-1} resolution, 100 scans) collected from a glassy carbon electrode immersed in a solution of $[Ru(tpm)(bpy)CO]^{2+}$ (5 mM) in CO_2-saturated acetonitrile and in the presence of H_2O (0.66 M). E_1 = -0.46 V and E_2 = -2.01 V vs. $Cp_2Fe^{+/0}$. Supporting electrolyte: 0.1 M tetra-n-butylammonium hexafluorophosphate. The temperature of the electrolyte was kept at -0.5°C.

Figure 3.20 shows the expanded normalized time resolved spectra in the region 2200-2100 cm^{-1} for complex **[1]**. An increase in the absorption intensity at 2140 cm^{-1} is observed. Figure 3.21 shows the results obtained in the same region when complex **[2]** was electrolyzed under the same conditions. The band at 2140 cm^{-1} is most suitably assigned to the gain in CO concentration during the reduction process [4].

Significant changes were also observed in the carbonyl absorption region during the course of CO_2 reduction; the expanded spectra of which are shown in Figure 3.22. Negative bands appeared at 1587 cm^{-1} and 1171 cm^{-1}. It is known that the IR bands of coordinated CO_2 do not resemble those of free linear molecules (ν_{asym} 2349 cm^{-1}, ν_{asy} 1388 cm^{-1} or 1285 cm^{-1} (one of these is due to Fermi resonance)) but are more closely related to certain types of metal-bound CO_2^- or the radical anion itself [134]. Mascetti et al. has studied the interaction of a series of metal atoms with CO_2 (M-η^1-CO_2) by FTIR. The ν_{OCO} bands in the M-η^1-CO_2 compounds were found at 1750-1690 cm^{-1} and 1180-1090 cm^{-1} [58, 134]. Therefore, the features at 1587 cm^{-1} and 1171 cm^{-1} observed in our experiments can be assigned to the presence of Ru-η^1-CO_2 species. The growth in intensity at these features became less profound in the latter course of electrolysis indicating its concentration had reached a steady state. The negative bands at 1276 cm^{-1} and 1345 cm^{-1} can be assigned to the formation of the ion pair $[CO_3^{2-}][TBA^+]_2$ [140, 157]. Another feature is the positive band at 1642 cm^{-1}, which can be attributed to the ν_3 absorption of CO_3^{2-}. As proton is consumed in the electrolysis, the pH around the electrode surface will increase as the reduction of CO_2 proceeds. An alkaline medium would favor the formation of CO_3^{2-} which can form ion pair with TBA^+ ion on the electrode surface. Any free CO_3^{2-} would be repelled from the highly negatively charged

electrode surface. The existence of the band at 1333 cm^{-1} can be assigned to the symmetric stretch of C-O-H in hydrogencarbonate.

It was noted that no bands assignable to species like M-CHO or M-OCOH could be observed in the IR spectra. All the above assignments are supported by isotopic labeling using $^{13}CO_2$ instead of $^{12}CO_2$. Under $^{13}CO_2$ atmosphere, a positive band at 2278 cm^{-1} corresponding to the consumption of $^{13}CO_2$ was observed during the reduction process. Bands assignable to ^{13}CO at 2110 cm^{-1} and $H^{13}CO_3^{2-}$ at 1313 cm^{-1} could also be observed (Figure 3.18b).

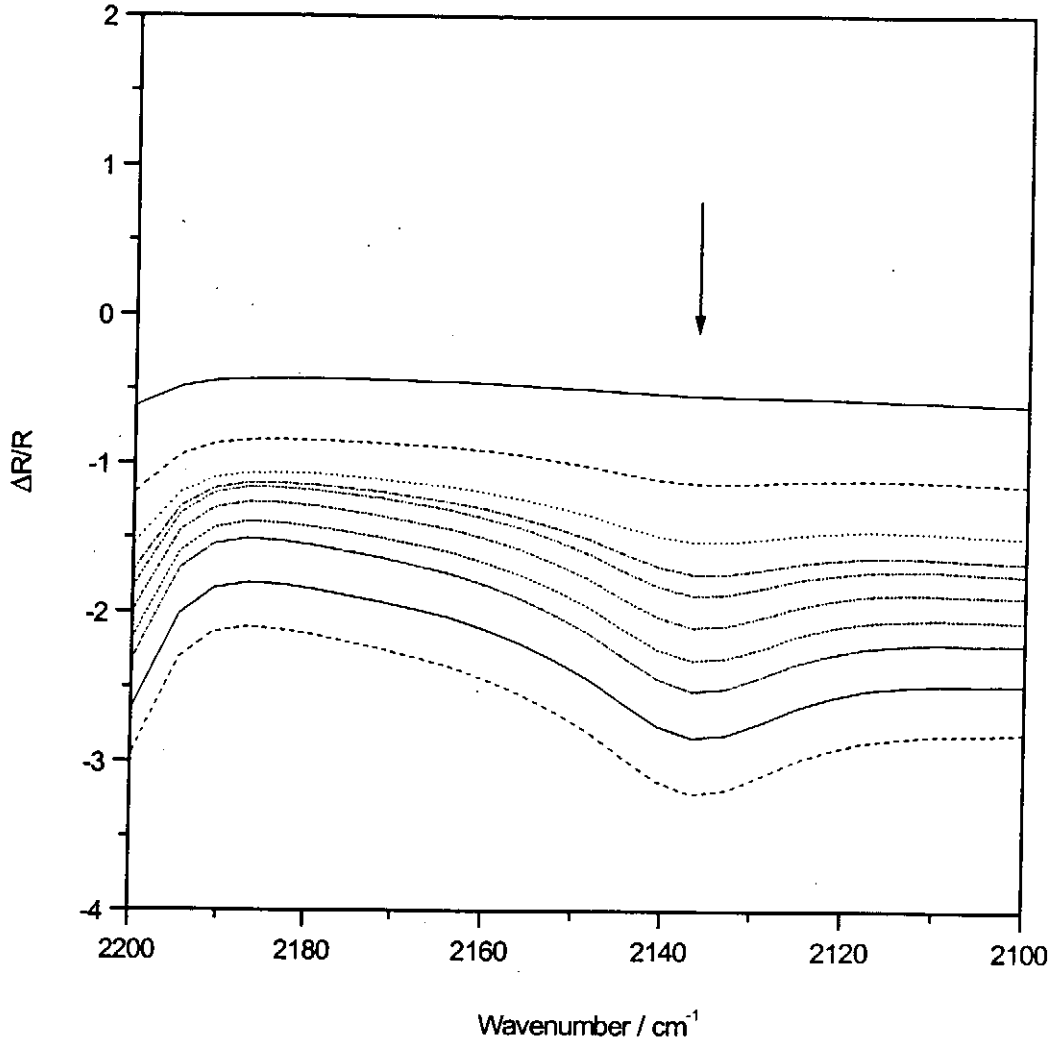

Figure 3.20 A series of normalized time resolved spectra in the region 2200-2100 cm^{-1} (8 cm^{-1} resolution, 100 scans) collected from a glassy carbon electrode immersed in a solution of $[Ru(bdmpp)(bpy)CO]^{2+}$ (5 mM) in CO_2-saturated acetonitrile and in the presence of H_2O (5.0 M). E_1 = -0.46 V and E_2 = -1.86 V vs. $Cp_2Fe^{+/0}$. Supporting electrolyte: 0.1 M tetra-n-butylammonium hexafluorophate. The temperature of the electrolyte was kept at -0.5°C.

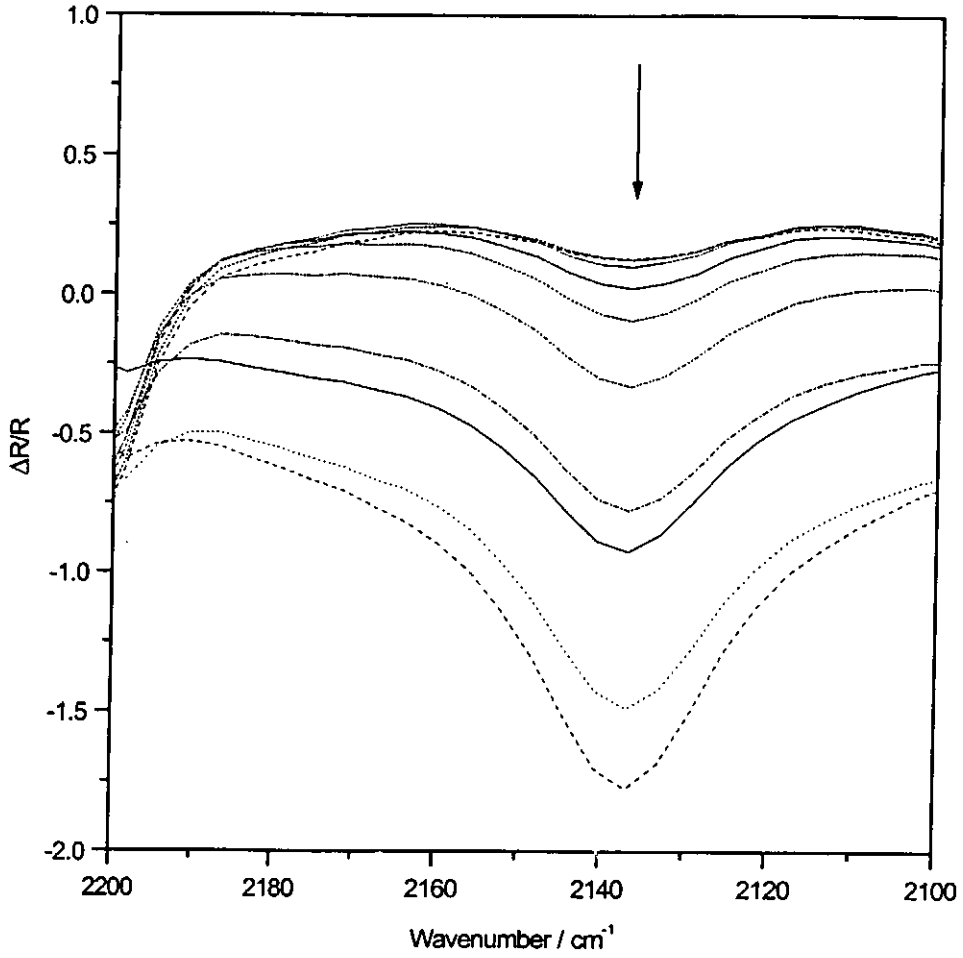

Figure 3.21 A series of normalized time resolved spectra in the region 2200-2100 cm^{-1} (8 cm^{-1} resolution, 100 scans) collected from a glassy carbon electrode immersed in a solution of $[Ru(tpm)(bpy)CO]^{2+}$ (5 mM) in CO_2-saturated acetonitrile and in the presence of H_2O (0.66 M). E_1 = -0.46 V and E_2 = -2.01 V vs. $Cp_2Fe^{+/0}$. Supporting electrolyte: 0.1 M tetra-n-butylammonium hexafluorophate. The temperature of the electrolyte was kept at -0.5°C.

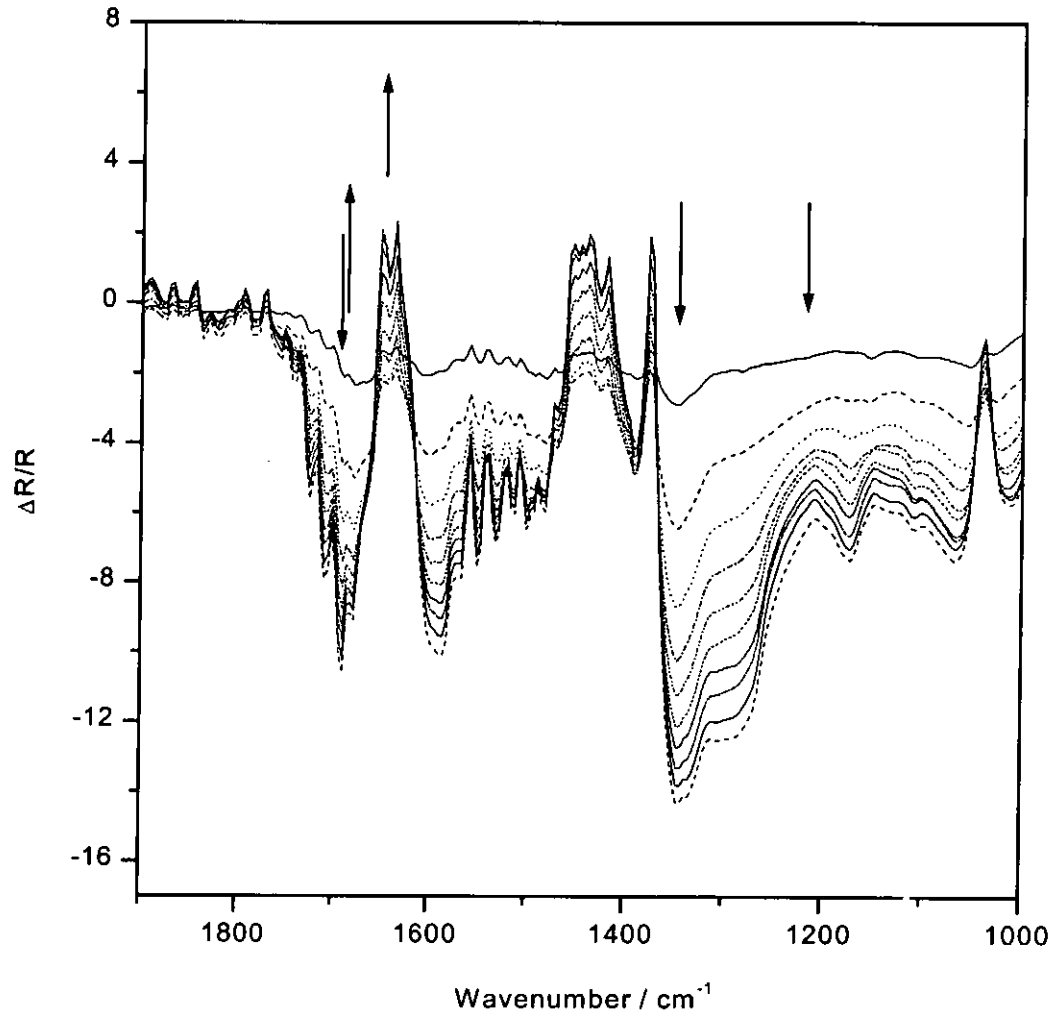

Figure 3.22 A series of normalized time resolved FTIR spectra in the region 1900-1000 cm^{-1} (8 cm^{-1} resolution, 100 scans) collected from a glassy carbon electrode immersed in a solution of $[Ru(bdmpp)(bpy)CO]^{2+}$ (5 mM) in CO_2-saturated acetonitrile and in the presence of H_2O (5.0 M). E_1 = -0.46 V and E_2 = -1.86 V vs. $Cp_2Fe^{+/0}$. Supporting electrolyte: 0.1 M tetra-n-butylammonium hexafluorophosphate. The temperature of the electrolyte was kept at -0.5°C.

We can interpret the spectroelectrochemical results as follows: $[Ru(L)(bpy)CO]^{2+}$ first undergoes an irreversible reduction to give $[Ru(L)(bpy^{\bullet-})S]^{0}$ (where S is the solvent molecule). In the presence of H_2O, hydration of CO_2 is expected to occur as H_2O is a relatively strong proton source in acetonitrile (pK_a = 2.2-2.35) [156]. The CO_2 molecule is expected to form hydrogen bonding in the solution with the H_2O molecule.

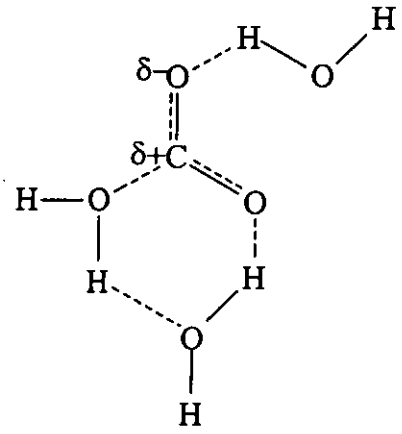

The drainage of electron density to the oxygen atom through hydrogen bonding would make the carbon center in the CO_2 molecule more electrophilic. Therefore, the nucleophilic Ru center can attack the CO_2 molecule favorably to produce the Ru-CO_2 adduct - $[Ru(L)(bpy)(COO^{-})]^{+}$. The presence of proton source can stabilize the Ru-CO_2 adduct by hydrogen bonding and triggers the cleavage of one of the two C-O bonds resulting in the formation of CO [66, 68]. This can explain why CO was produced exclusively in the presence of a relatively strong proton source such as H_2O. The proposed mechanistic pathway is summarized in Scheme I.

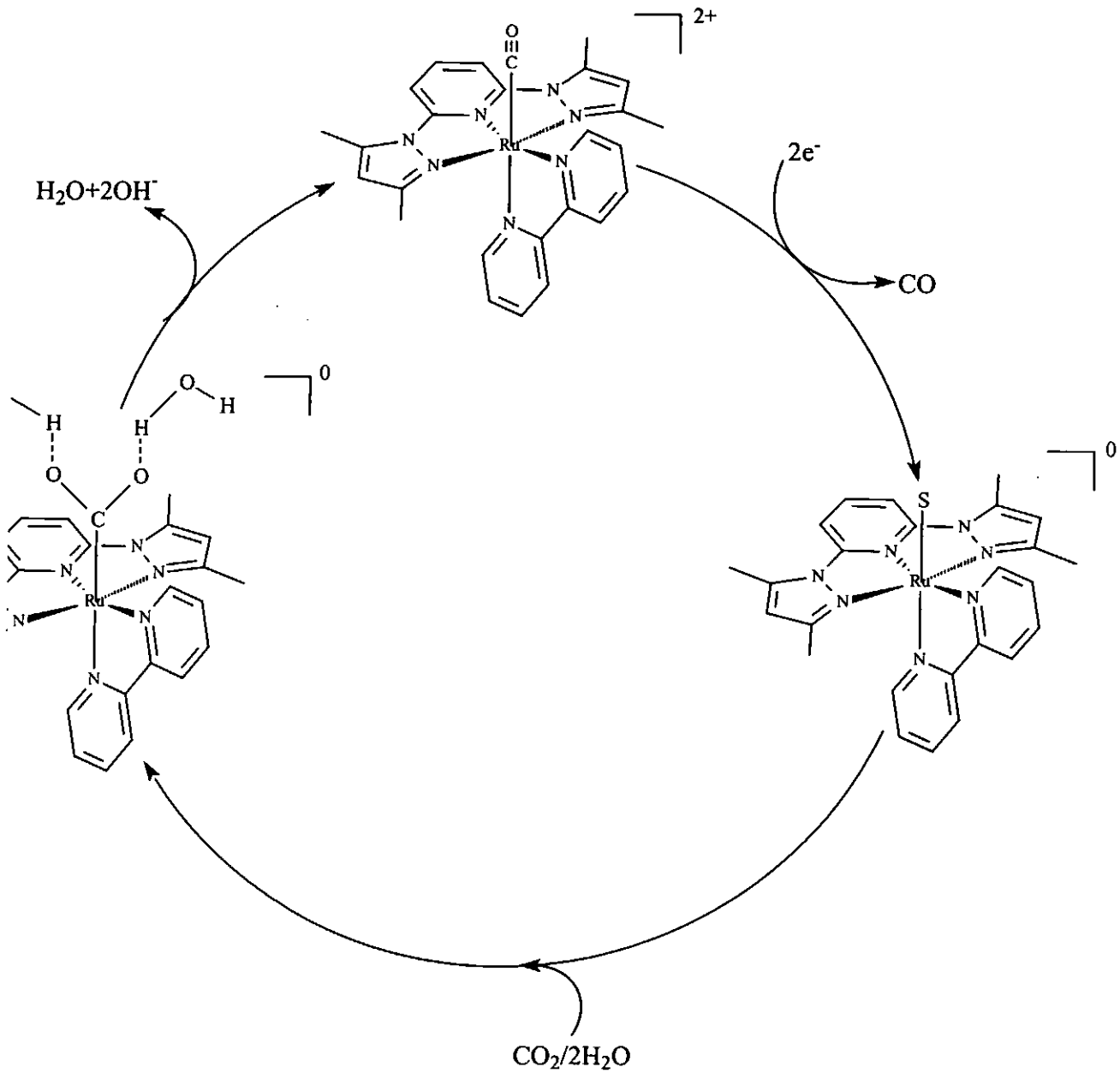

Scheme I

Where S is a solvent molecule

(4) Reduction of $[Ru(bdmpp)(bpy)CO]^{2+}$ and $[Ru(tpm)(bpy)CO]^{2+}$ in CO_2-saturated acetonitrile in the presence of $Et_3NH^+Cl^-$

Figure 3.23a shows the time resolved FTIR spectra of complex **[1]** in the region 3200-1000 cm^{-1} in the presence of $Et_3NH^+Cl^-$ as proton source. The intense negative bands at 2971-2874 cm^{-1} can be assigned to the absorption attributed to TBA^+ [140]. The consumption of CO_2 can be monitored by the positive band at 2340 cm^{-1}. The positive reflectance band at 2006 cm^{-1} indicates that the CO ligand is detached from the ruthenium center (Figure 3.23a). The loss of the carbonyl ligand leads to the formation of $[Ru(bdmpp)(bpy)S]^0$ (S = CH_3CN) with a vacant site available for the coordination of CO_2. Similar results were obtained for complex **[2]** (Figure 3.26).

A growth in the absorption at 1977 cm^{-1} was observed at the expense of the absorption intensity of the Ru-CO species at 2006 cm^{-1} (Figure 3.24). This band showed a negative trend in the difference spectrum in the initial stage of the electrolysis indicating an increase in concentration of this absorbing species. The change in $\Delta R/R$ then leveled off which may imply the steady formation and consumption of this species. In order to have better understanding of this intermediate species, *in-situ* FTIR spectroelectrochemical monitoring of an acetonitrile solution containing 5 mM of complex **[1]** and 0.05M $Et_3NH^+Cl^-$ under nitrogen was conducted. It revealed a board absorption at 1977 cm^{-1} (Figure 3.25a). It is known that metal-hydride species strongly absorb in the IR spectrum in the region 1850-2000 cm^{-1} [116, 158, 159]. It is also noted that hydrogen gas was produced in the electroreduction of CO_2 in the presence of $Et_3NH^+Cl^-$ besides $HCOO^-$. As a metal-hydride intermediate is usually involved in the production of gaseous hydrogen, the species at 1977 cm^{-1} is most probably due to a

metal-hydride complex. When deuterium labeled $Et_3ND^+Cl^-$ was used, an isotopic shift is observed in the negative band corresponding to the Ru-D complex at 1410cm^{-1} (Figure 3.25b). Complex **[2]** also showed a similar band at 1971 cm^{-1} assignable to the formation of metal-hydride bond in the presence of $Et_3NH^+Cl^-$ in N_2-saturated acetonitrile (Figure 3.27a). An isotopic shift was also observed when $Et_3NHD^+Cl^-$ was used (Figure 3.27b).

Figure 3.24 shows the expanded IR spectra in the carbonyl-stretching region (2200-1000 cm^{-1}) for complex **[1]**. A feature appeared at 1377 cm^{-1} in phase with another band at 1580 cm^{-1} which suggests that the two bands might be attributable to the same species. These bands were formed at the expense of the Ru-H peak at 1977 cm^{-1}. The absorption intensity of these bands increased at the beginning of the reduction process and then became constant in the latter course of reduction. The available formato complexes data permit the possible assignments of these bands to be either (1) a Ru formato complex (i.e. M-η^1-OCO^- complex ν_{CO}= 1500-1700 cm^{-1} and 1200-1400 cm^{-1}), or (2) a Ru carbonato complex (ν_{CO}= 1590-1610 cm^{-1} and 1260-1300 cm^{-1}) [60, 140]. As this species was produced at a potential at which ruthenium metal would almost certainly favor the Ru(0) oxidization state and the difference in stretching frequency $\Delta\nu$ (212 cm^{-1}) between the $\nu(CO_2)_{assym}$ and $\nu(CO_2)_{sym}$ is typical of a monodentate formato species [60], it is unlikely that this species is a ruthenium carbonate complex. Therefore, the bands at 1377 cm^{-1} and 1580 cm^{-1} can be most suitably assigned as a ruthenium formate species with the formato ligand bound in a terminal, monodentate fashion. The formation of the formato complex is most likely caused by the insertion of CO_2 into the Ru-H bond [60, 160-162].

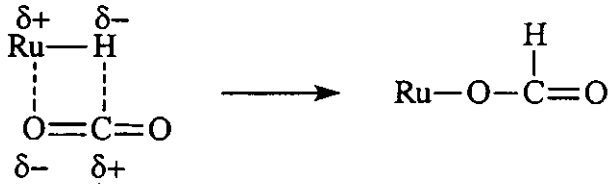

Another important feature is the growth in absorption at 1605 cm^{-1}, 1207 cm^{-1} and 1151 cm^{-1} (Figure 3.24). These bands can be assigned to the C-O-C stretching of formate based on previous studies [110, 157, 163]. The ruthenium formato species is the precursor of the free formate. This is supported by the observation that the ruthenium formate species is detected in significant concentration prior to the production of appreciable quantities of free formate (Figure 3.24). Moreover, it can be seen that the peak intensity at 1605 cm^{-1} continues to grow during electrolysis, while that at 1377 cm^{-1} and 1580 cm^{-1} became less profound afterwards and the reflectance of the band at these wavenumbers switch to a positive trend (Figure 3.24). There is also a weak negative band at 1642 cm^{-1} that is assigned to CO_3^{2-}. The formation of CO_3^{2-} is probably due to the increase in pH around the electrode surface during electrolysis. When the electrocatalytic reduction of $^{13}CO_2$ was conducted under similar conditions, there was growth in absorbance at 1148 cm^{-1} that is due to the presence of $H^{13}COO^-$ and observation of $^{13}CO_3^{2-}$ at 1604 cm^{-1} (Figure 3.23b). Table 3.2 summarized the assignments of the bands in Figure 3.15-3.27.

Several key experimental observations for the catalytic reduction of CO_2 in the presence of $Et_3NH^+Cl^-$ are as follows: (1) No absorption bands assignable to Ru-η^1-CO_2 species could be detected when $Et_3NH^+Cl^-$ was used as proton source. As $Et_3NH^+Cl^-$ is a much weaker proton source (pK_a = 16.8) compared to H_2O (pK_a = 2.2-2.35) in

acetonitrile, the degree of the formation of hydrogen bonding between Et_3NH^+ and CO_2 is of a much lesser extent, if not impossible. As the electrophilicity of the carbon center in CO_2 is not enhanced by hydrogen bonding, the attack by the electron rich ruthenium metal is not that kinetically favored as compared to the formation of a Ru-H species. Instead, the electron rich ruthenium center tends to react with Et_3NH^+ to give a Ru-H species. (2) The ruthenium hydride complex was formed at the expense of the Ru-CO species whereas the ruthenium formato complex was formed in the expense of the hydride complex. The formation of the ruthenium formato complex is generally believed to occur via the insertion of CO_2 into the Ru-H bond. The mechanism proposed for the formation of formate is summarized in Scheme II.

The $[Ru(L)(bpy)CO]^{2+}$ first undergoes two-electron reduction accompanied with the loss of CO to generate the five-coordinated species (where S is the solvent moleucle). The electron rich species tends to react with the H^+ originate from $Et_3NH^+Cl^-$ affording the hydride complex. Subsequent CO_2 insertion into the Ru-H bond gives the formato intermediate. Since the metalloformate species can be detected in significant concentration prior to the production of appreciable quantities of free formate, it is believed that the elimination of the $HCOO^-$ from the $[Ru(bdmpp)(bpy)(OCOH^-)]$ is a slow step. From the results obtained from the bulk electrolysis experiment, a small amount of hydrogen gas was generated in the presence of $Et_3NH^+Cl^-$. The formation of a Ru-H intermediate species can also account for the formation of H_2.

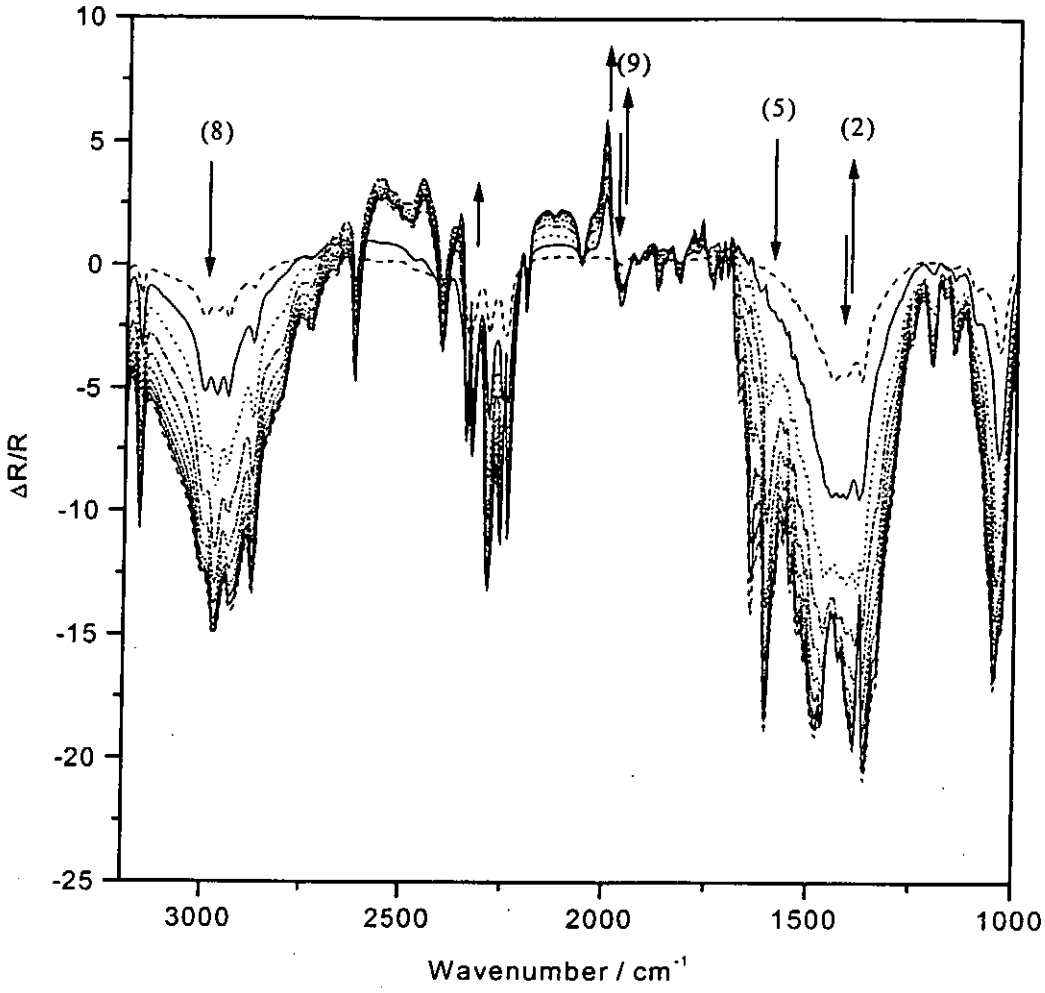

Figure 3.23a A series of normalized time resolved FTIR spectra in the region 3200-1000 cm^{-1} (8 cm^{-1} resolution, 100 scans) collected from a glassy carbon electrode immersed in a solution of $[Ru(bdmpp)(bpy)CO]^{2+}$ (5 mM) in CO_2-saturated acetonitrile and in the presence of $Et_3NH^+Cl^-$ (0.05 M). E_1 = -0.46 V and E_2 = -1.86 V vs. $Cp_2Fe^{+/0}$. Supporting electrolyte: 0.1 M tetra-n-butylammonium hexafluorophosphate. The temperature of the electrolyte was kept at -0.5 °C. A summary of the assignment of the bands 2,5,8,9 is given in Table 3.2.

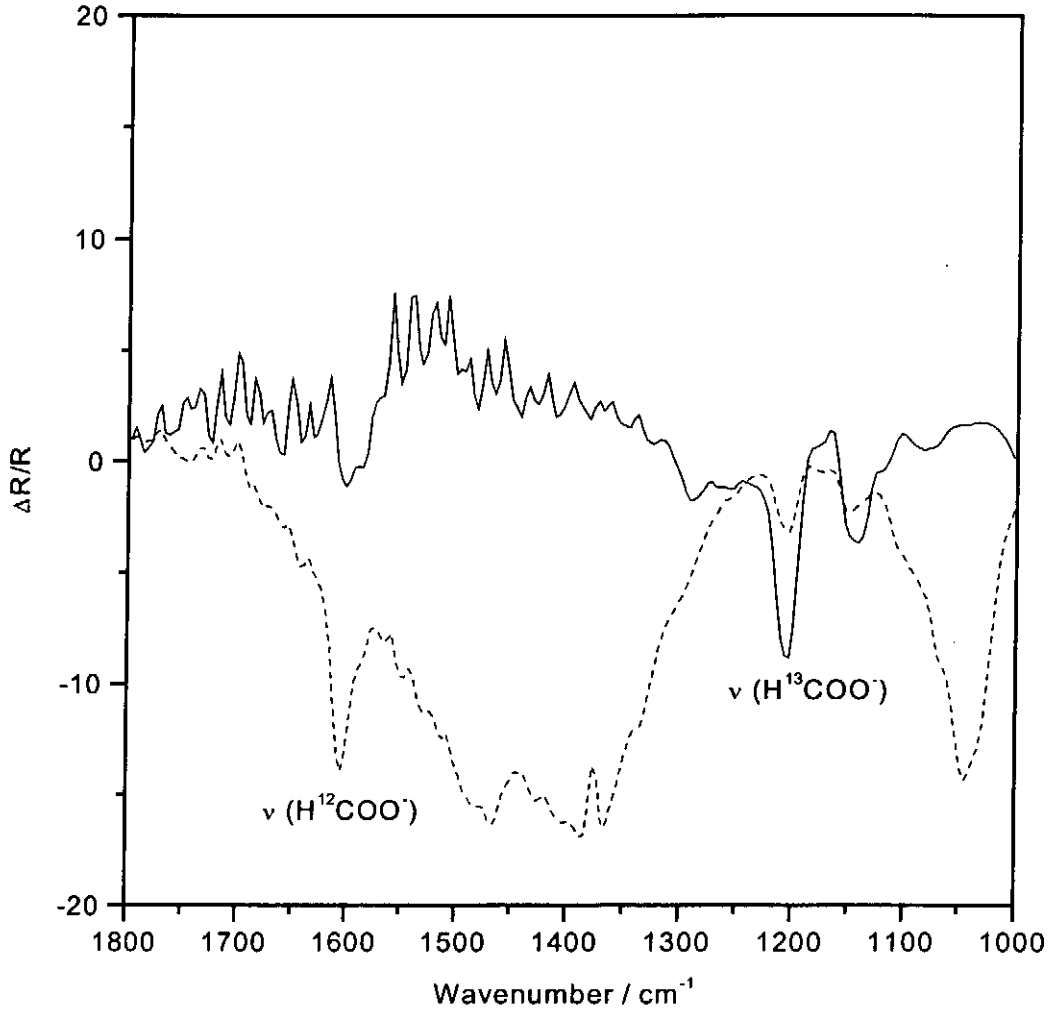

Figure 3.23b A series of normalized time resolved FTIR spectra in the region 3200-1000 cm^{-1} (8 cm^{-1} resolution, 100 scans) collected from a glassy carbon electrode immersed in a solution of $[Ru(bdmpp)(bpy)CO]^{2+}$ (5 mM) in $^{13}CO_2$-saturated acetonitrile and in the presence of $Et_3NH^+Cl^-$ (0.05 M). E_1 = -0.46 V and E_2 = -1.86 V vs. $Cp_2Fe^{+/0}$. Supporting electrolyte: 0.1 M tetra-n-butylammonium hexafluorophosphate. The temperature of the electrolyte was kept at -0.5 °C.

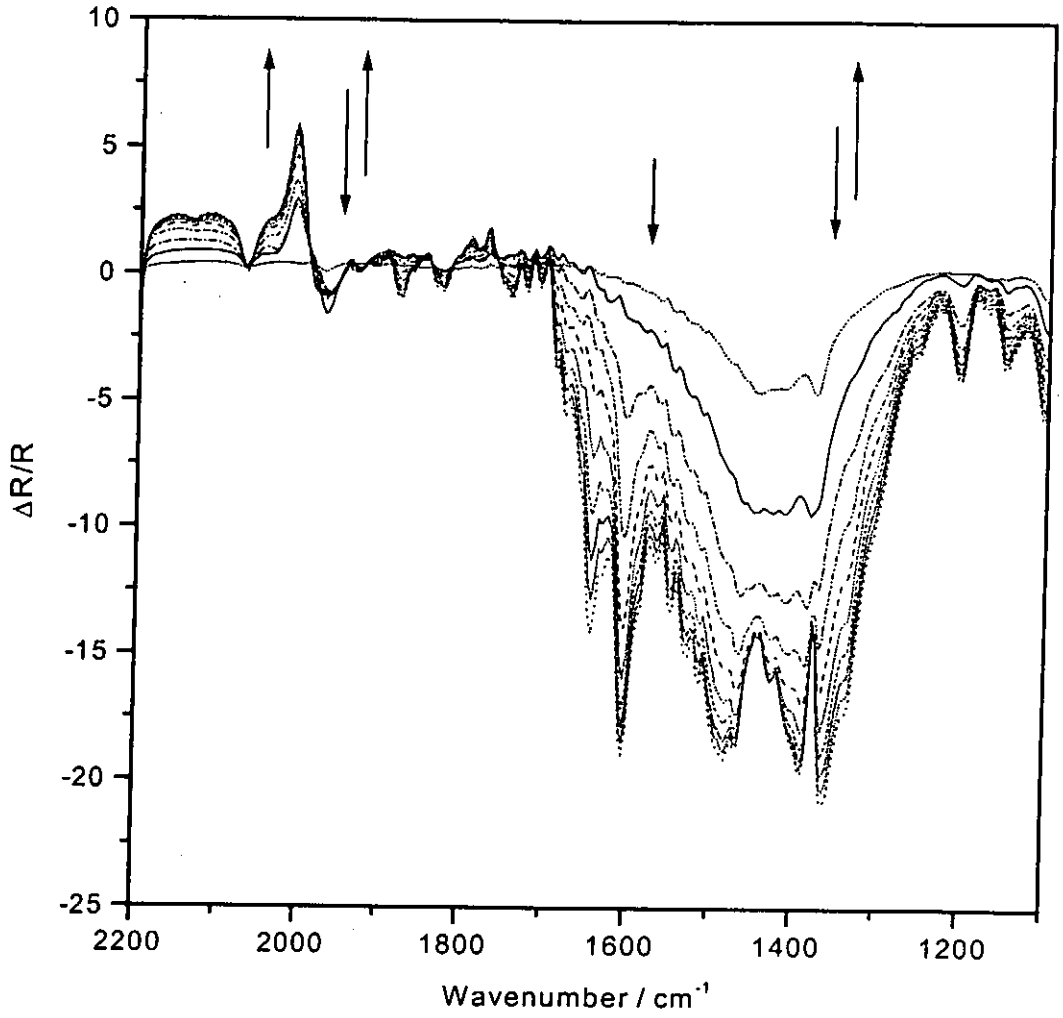

Figure 3.24 A series of normalized time resolved FTIR spectra in the region 2200-1100 cm^{-1} (8 cm^{-1} resolution, 100 scans) collected from a glassy carbon electrode immersed in a solution of $[Ru(bdmpp)(bpy)CO]^{2+}$ (5 mM) in CO_2-saturated acetonitrile and in the presence of $Et_3NH^+Cl^-$ (0.05 M). E_1 = -0.46 V and E_2 = -1.86 V vs. $Cp_2Fe^{+/0}$. Supporting electrolyte: 0.1 M tetra-n-butylammonium hexafluorophosphate. The temperature of the electrolyte was kept at -0.5 °C.

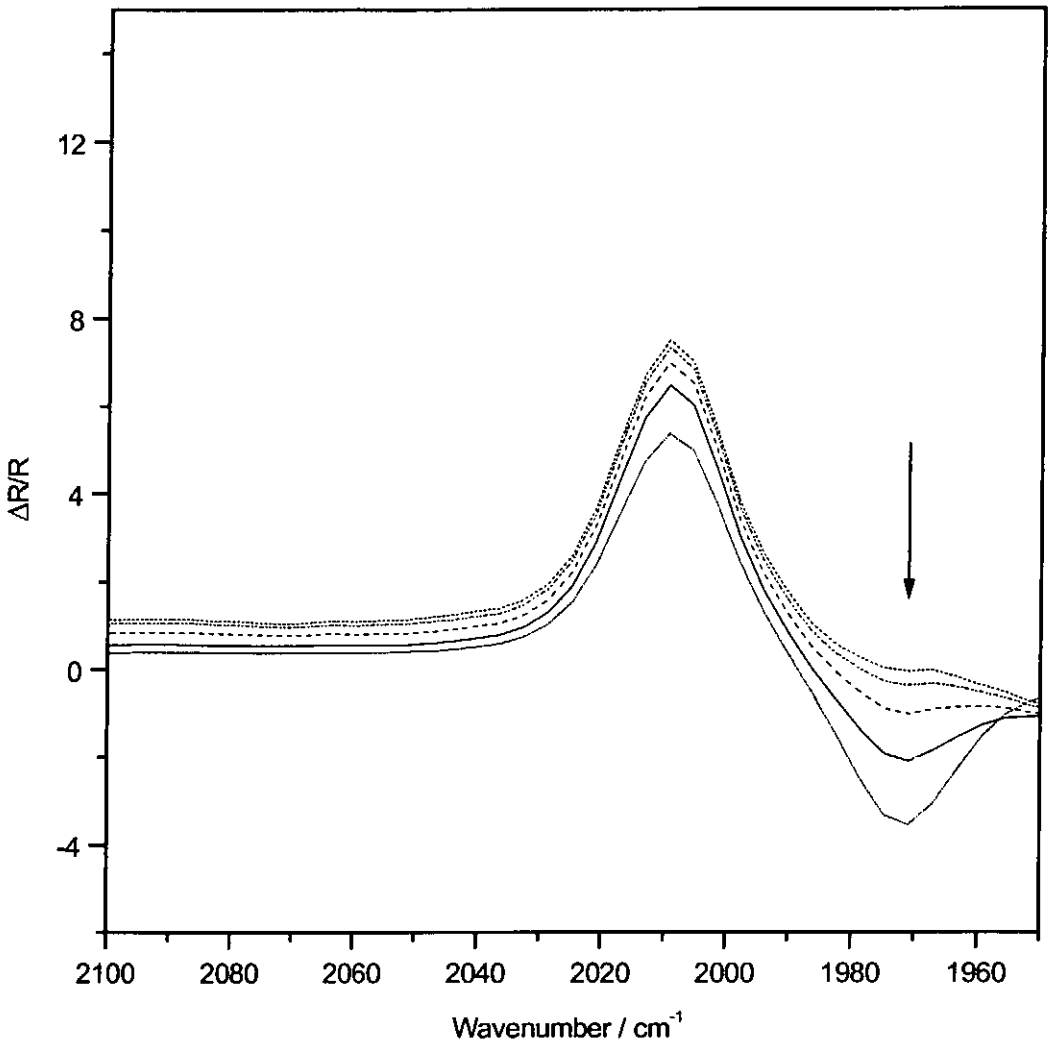

Figure 3.25a A series of normalized time resolved FTIR spectra in the region 2100-1950 cm^{-1} (8 cm^{-1} resolution, 100 scans) collected from a glassy carbon electrode immersed in a solution of $[Ru(bdmpp)(bpy)CO]^{2+}$ (5 mM) in N_2-saturated acetonitrile and in the presence of $Et_3NH^+Cl^-$ (0.05 M). E_1 = -0.46 V and E_2 = -1.86 V vs. $Cp_2Fe^{+/0}$. Supporting electrolyte: 0.1 M tetra-n-butylammonium hexafluorophosphate. The temperature of the electrolyte was kept at -0.5 °C.

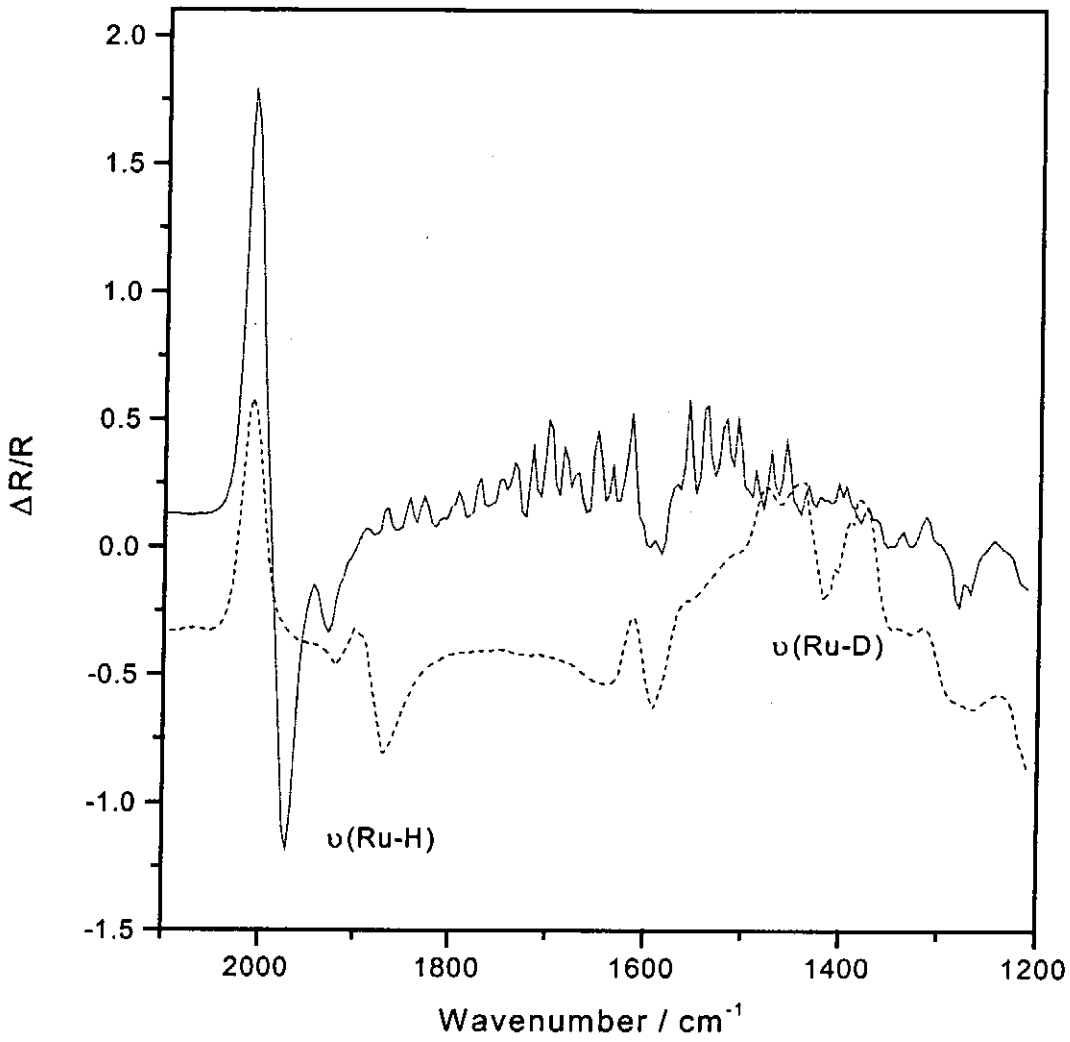

Figure 3.25b *In-situ* FTIR spectra obtained from $[Ru(bdmpp)(bpy)CO]^{2+}$ in N_2 saturated acetonitrile in the presence of 0.05 M $Et_3NH^+Cl^-$ (—) and 0.05 M $Et_3ND^+Cl^-$ (----). E_1: -0.46 V and E_2 = -1.86 V vs. $Cp_2Fe^{+/0}$. Supporting electrolyte: 0.1 M tetra-n-butylammonium hexafluorophosphate. The temperature of the electrolyte was kept at -0.5 °C.

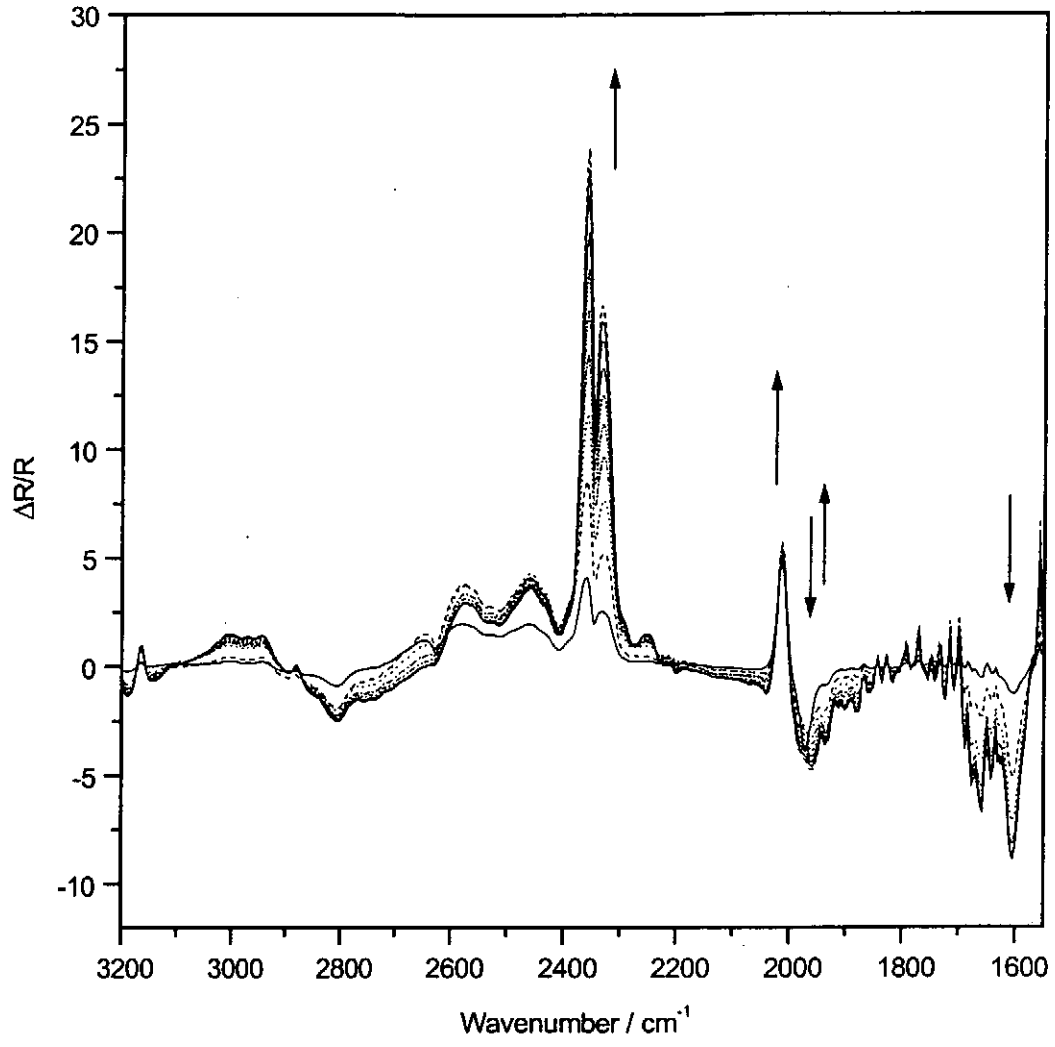

Figure 3.26 A series of normalized time resolved FTIR spectra in the region 2200-1550 cm^{-1} (8 cm^{-1} resolution, 100 scans) collected from a glassy carbon electrode immersed in a solution of $[Ru(tpm)(bpy)CO]^{2+}$ (5 mM) in CO_2-saturated acetonitrile and in the presence of $Et_3NH^+Cl^-$ (0.05 M). E_1 = -0.46 V and E_2 = -2.01 V vs. $Cp_2Fe^{+/0}$. Supporting electrolyte: 0.1 M tetra-n-butylammonium hexafluorophosphate. The temperature of the electrolyte was kept at -0.5 °C.

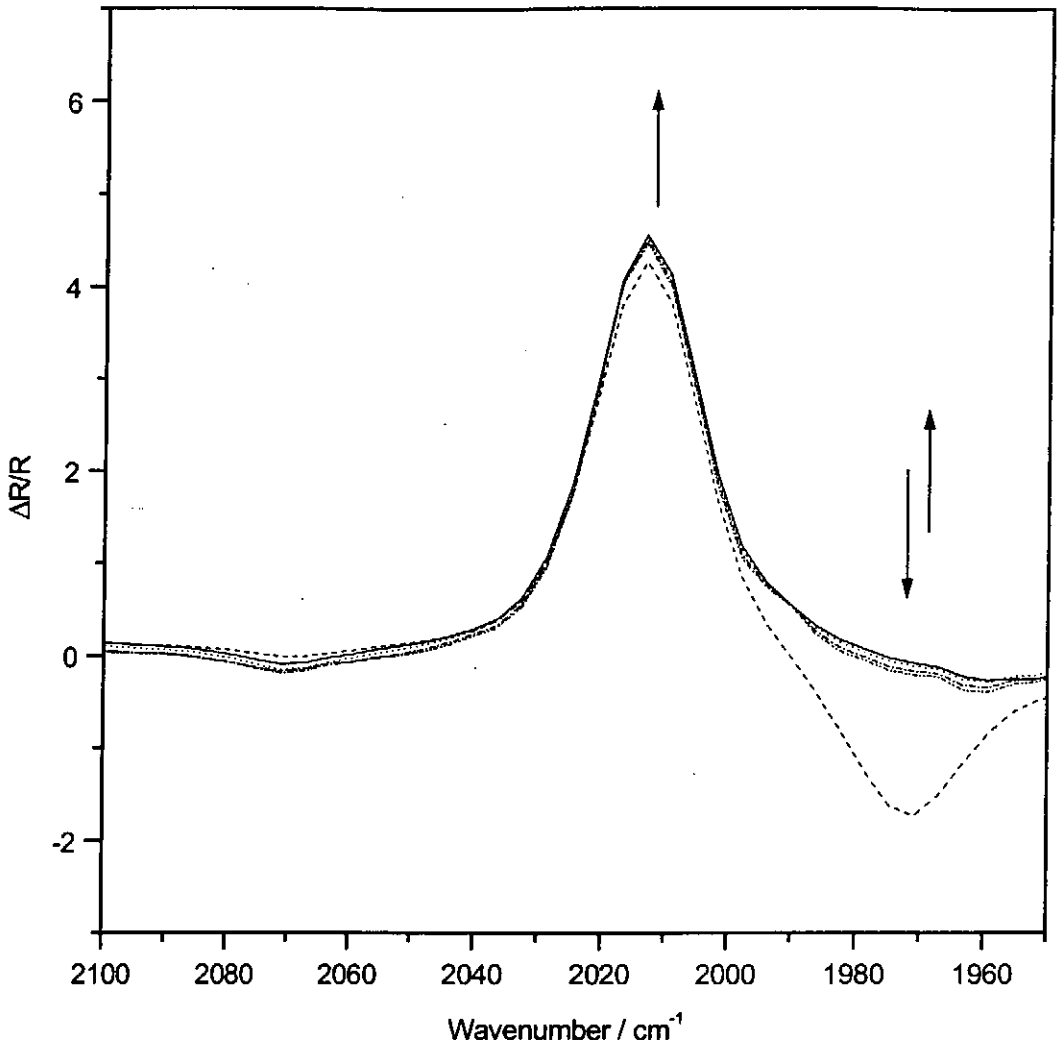

Figure 3.27a A series of normalized time resolved FTIR spectra in the region 2100-1950 cm^{-1} (8 cm^{-1} resolution, 100 scans) collected from a glassy carbon electrode immersed in a solution of $[Ru(tpm)(bpy)CO]^{2+}$ (5 mM) in N_2-saturated acetonitrile and in the presence of $Et_3NH^+Cl^-$(0.05 M). E_1 = -0.46 V and E_2 = -2.01 V vs. $Cp_2Fe^{+/0}$. Supporting electrolyte: 0.1 M tetra-n-butylammonium hexafluorophosphate. The temperature of the electrolyte was kept at -0.5 °C.

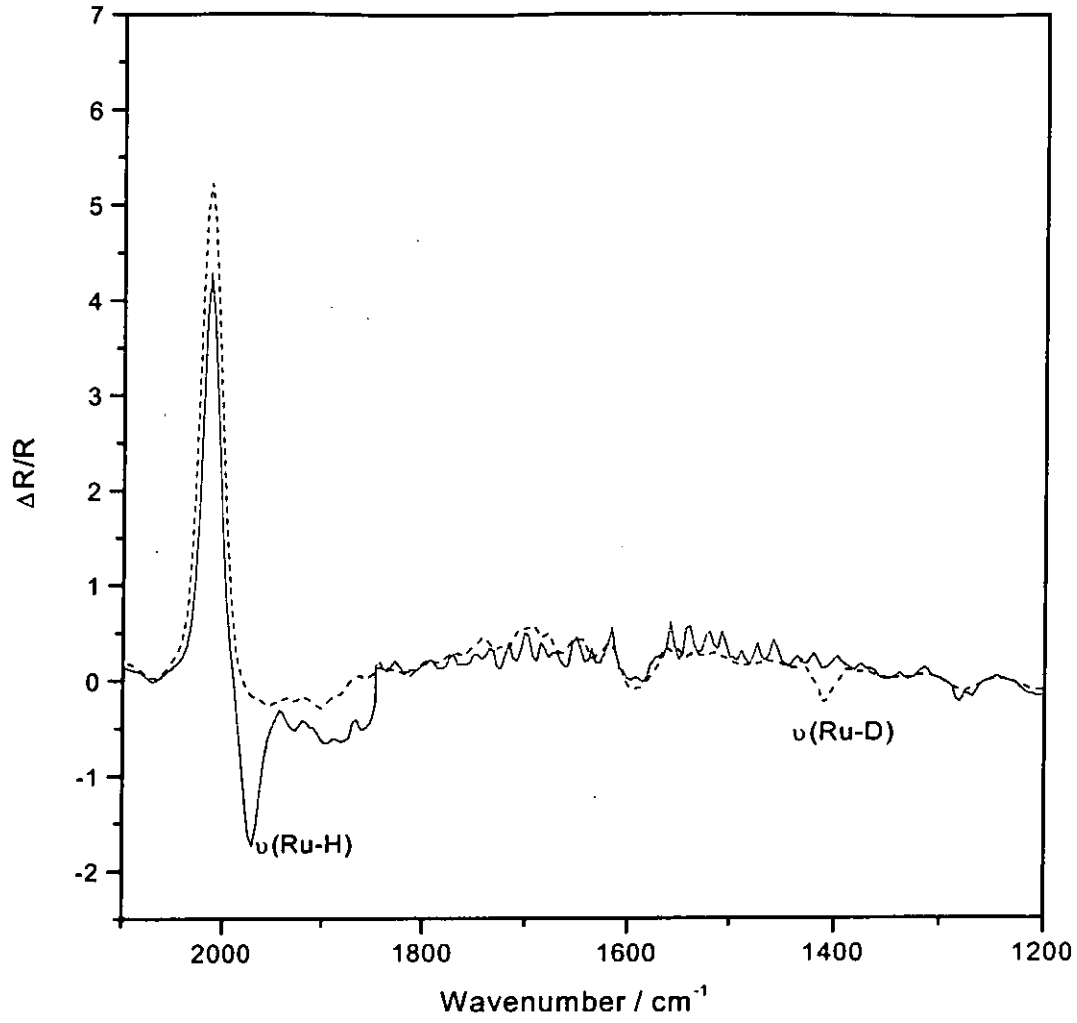

Figure 3.27b *In-situ* FTIR spectra obtained from $[Ru(tpm)(bpy)CO]^{2+}$ in N_2 saturated acetonitrile in the presence of 0.05 M $Et_3NH^+Cl^-$ (—) and 0.05 M $Et_3ND^+Cl^-$ (----). E_1 = -0.46 V and E_2 = -2.01 V vs. $Cp_2Fe^{+/0}$. Supporting electrolyte: 0.1 M tetra-n-butylammonium hexafluorophosphate. The temperature of the electrolyte was kept at -0.5 °C.

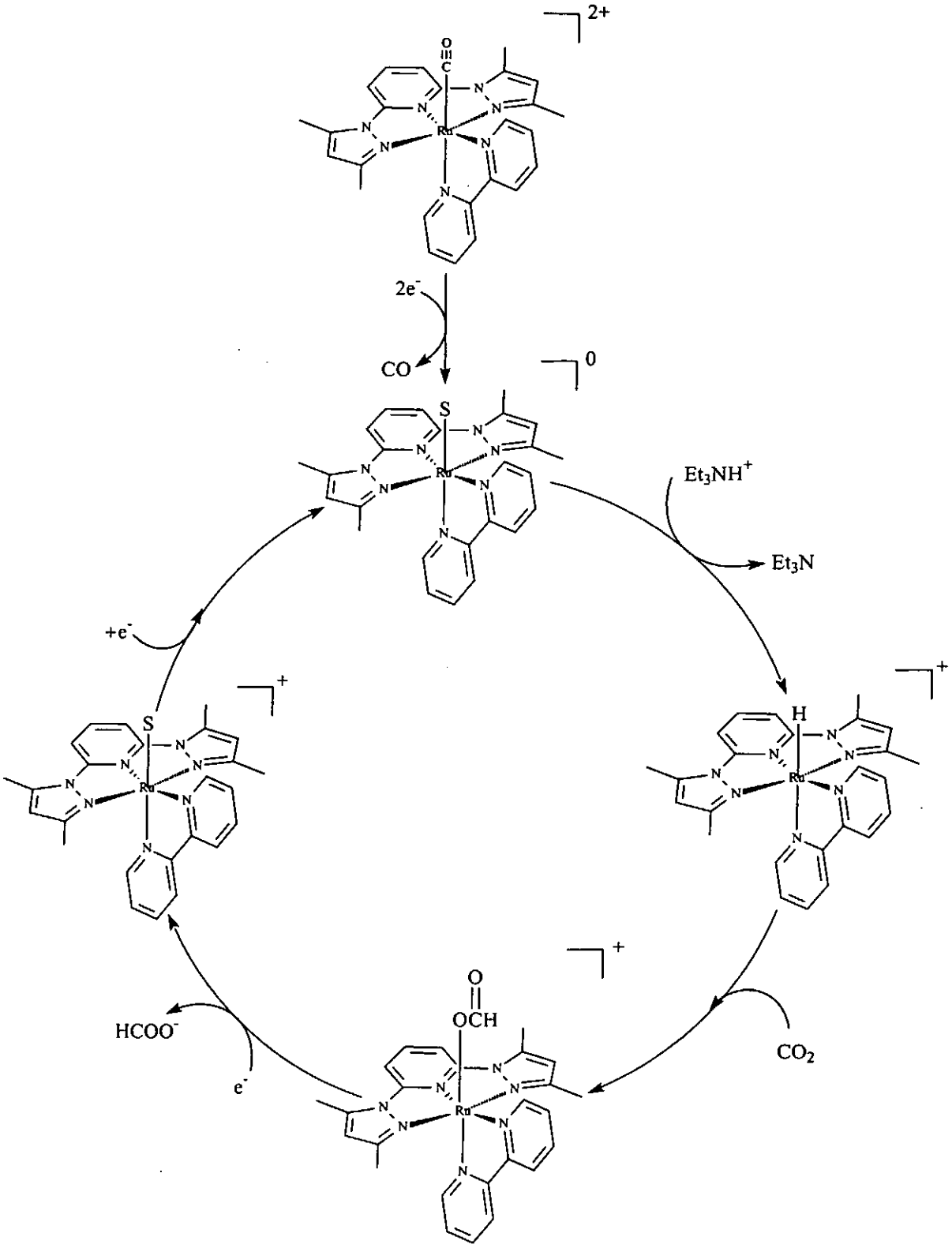

Scheme II

Where S is a solvent molecule

Table 3.2. Assignments of features in Figures 3.15-3.27

Peak in the figure	Position ν / cm^{-1}	Assignment
(1)	1270 cm^{-1} 1345 cm^{-1}	$[CO_3^{2-}][TBA^+]_2$
(2)	1377 cm^{-1} 1580 cm^{-1}	M-OCOH (metalloformate complex)
(3)	1642 cm^{-1}	CO_3^{2-}
(4)	1587 cm^{-1} 1171 cm^{-1}	M-η^1-CO_2
(5)	1027 cm^{-1} 1151 cm^{-1} 1605 cm^{-1}	Free $HCOO^-$
(6)	2140 cm^{-1}	Free CO
(7)	2340 cm^{-1}	CO_2
(8)	2971 cm^{-1}	TBA^+
(9)	1977 cm^{-1}	Ru-H

3.4 Conclusion

Both complex [1] and [2] are active towards the electrocatalytic reduction of CO_2. Only CO was produced in the presence of H_2O in the electrocatalytic reaction. The presence of protonated amine salts shifts the reaction towards the formation of formate. *In-situ* FTIR spectroelectrochemical studies revealed the existence of Ru-η^1-CO_2 species in the presece of H_2O in the electrocatalytic reduction of CO_2. On the contrary, a ruthenium hydride species was detected in the presence of $Et_3NH^+Cl^-$. It is interesting to note that although H_2O is a stronger Brönsted acid than Et_3NH^+ in acetonitrile, a ruthenium hydride species was formed between the reduced ruthenium center and Et_3NH^+ but not H_2O in the presence of CO_2. We argue that the formation of hydrogen bonding between H_2O and CO_2 can enhance the electrophilicity of the carbon center in the CO_2 molecule thus facilitating the attack by the electron rich Ru to give a Ru-CO_2 species which would lead to the subsequent formation of CO. On the contrary, Et_3NH^+ is not acidic enough to form hydrogen bonding with CO_2. When the very electron rich ruthenium is generated, it will react with Et_3NH^+ in a kinetically favorable manner to give a Ru-H species which will allow the subsequent insertion of CO_2 to produce formate as the major product.

Chapter 4

In-situ FTIR Spectroelectrochemical Study on the Reduction of CO_2 Catalyzed by an Iron Complex

4.1 Introduction

Although numerous reports on ruthenium catalysts for CO_2 reduction have appeared in literature [5, 6, 20-22], there are relatively few reports on iron catalysts despite the two elements belong to the same group. Iron porphyrins [66, 68, 89] and porphycenes [136] are the two classes of iron complexes that have been reported to be effective catalysts for the electrochemical reduction of carbon dioxide. Therefore, it would be interesting to investigate the electrocatalytic activity of non-porphyrin analogues of the iron complexes. Although iron schiff base (Fe(salen)) is an obvious candidate, the ease of hydrolysis of the iron imino bond in the salen ligand limits its applications. The ligands 6,6'-bis(2-hydroxy)-2,2'-bipyridine (H_2dobpy) and 2,9-bis(2'-hydroxyphenyl)-1,10-phenanothroline (H_2dophen) are structurally similar to N,N'-bis(salicylidene)ethylenediamine (H_2salen). However, the absence of free imino bonds in the dophen ligand makes it much more stable than the salen ligand [164]. Therefore, we have studied the catalytic properties of the iron complex of 2,9-bis(2'-hydroxyphenyl)-1,10'-phenanothroline (H_2dophen). Experiments were also conducted in the presence of various proton sources to study the effect of Brönsted acids on the Fe(dophen) system. *In-situ* FTIR spectroelectrochemistry was employed to probe the intermediates formed in the course of the reduction process.

4.2 Experimental Section

4.2.1 Materials

2,9'-Bis(2'-hydroxyphenyl)-1,10-phenanthroline (H_2dophen) was synthesized by literature reported method [164, 165]. Anhydrous iron (III) chloride was obtained from Janssen Chemical Co. Dimethylsulphoxide was distilled over anhydrous calcium sulphate under reduced pressure and stored over 4Å molecular sieves before used. Tetra-n-butylammonium hexaflouorophosphate (Aldrich) was recrystallized in ethanol and dried in vacuo at 80°C for 24 hr before used. Carbon dioxide (purity > 99.9%) was obtained from Hong Kong Oxygen Co. Other chemicals were obtained from Aldrich Chemical Co. were of reagent grade and were used as received.

4.2.2 Synthesis

The preparation of ligand and iron complexes followed a previously reported procedure [166].

2,9-Bis(2'-hydroxyphenyl)-1,10-phenanthroline (H_2dophen)

A solution of ortho-methoxyphenyl lithium, prepared from ortho-bromoanisole (37.4 g, 0.2 mol) and lithium (3.0 g, 0.4 mol) in 50 ml anhydrous ether, was rapidly added to a solution of 1,10-phenanthroline (0.05 mol, 9.0 g) in 100 ml anhydrous toluene. The mixture was stirred for 48 h at room temperature under argon atmosphere.

After this period, 100 ml water was added and the aqueous layer was extracted with dichloromethane (3 x 100 ml). The organic portions were combined and dried over anhydrous Na_2SO_4. After removing the organic solvent under reduced pressure, 17 g of the crude product was redissolved in dichloromethane and 100 g of activated MnO_2 powder was added in small portions. The resulting mixture was stirred at room temperature for 4 h. 50 g of anhydrous Na_2SO_4 was then added and stirred for another one hour. After filtration, the solvent was removed and 15 g of brown oily material was obtained. The brown oily material was chromatographed on a silica-gel column with ethyl acetate and hexane mixture (1:3 v/v) as eluent. Pale yellow 2,9-bis(o-methoxyphenyl)-1,10-phenanthroline crystals were obtained. Then 0.75 g of the pale yellow crystals (1.9 mmol), 48% aqueous HBr (3 ml) and acetic acid (3 ml) were heated at 120°C for 20 h under argon atmosphere. A yellow precipitate formed during the process. The cooled mixture was added to ice (40 g) and neutralized to pH 6 by the addition of Na_2CO_3. The product was extracted with dichloromethane (2 x 50 ml), dried over Na_2SO_4 and the solvent was distilled under reduced pressure. The resulting yellow crystals of H_2dophen were washed with diethyl ether and dried in vacuo (0.54 g, 80% yield). ^{1}H NMR in d-DMSO [δ/ppm]: 8.70 (2H, d), 8.60 (2H, d), 8.27 (2H, dd), 8.08 (2H, s), 7.41 (2H, m), 7.09 (2H, d), 7.03 (2H, m).

$[Fe^{III}(dophen)Cl]_2$

The H_2dophen ligand (0.15 g) was dissolved in warm methanol (50 ml). Anhydrous $FeCl_3$ (0.1 g) was added to the solution. This led to an immediate color

change from pale yellow to dark green and the precipitation of a dark green microcrystalline solid. The dark green solid was filtered and washed with methanol (yield ~70%). Anal. for [Fe(dophen)Cl]CH_3OH.: Calcd. C, 61.41; H, 3.68; N, 5.73%. Found C, 61.17; H, 3.45; N, 5.78%. UV/VIS in DMSO [λ_{max}/nm (ε/dm^3 mol^{-1} cm^{-1})]: 402 (11400), 314 (27500). The complex exists as a dimer in solid state and the structure has been confirmed by X-ray crystallography [166].

$[Fe^{III}(dophen)(N\text{-}MeIm)_2]ClO_4$ (N-MeIm = 1-methylimidazole)

$[Fe(dophen)Cl]_2$ (0.15 g) was dissolved in methanol (30 ml). Excess 1-methylimidazole was added to the solution, which was heated to ca 60°C for 15 min. The solution was then concentrated to ca. 15 ml and excess $LiClO_4$ was added to the concentrate. Dark green precipitate of $[Fe^{III}(dophen)(N\text{-}MeIm)_2]ClO_4$ appeared upon cooling in a refrigerator. The crude product was filtered and recrystallized by vapor diffusion of diethyl ether into a methanol solution of the complex. (Yield ~80%). Anal. for $[Fe(dophen)(N\text{-}MeIm)_2]ClO_4$,: Calcd. C, 56.35; H, 3.82; N, 12.33%. Found: C, 56.28; H, 3.68; N, 12.26%. UV/VIS in CH_3CN [λ_{max}/nm (ε/cm^3 mol^{-1} cm^{-1})]: 396 (7900), 312 sh (21400), 282 (29500), 262 (29500). The structure of the complex has been confirmed by X-ray crystallography [166].

4.2.3 Physical Measurements

UV/VIS spectra were recorded on a Milton Roy Spectronic 3000 diode array spectrophotometer. Cyclic voltammetry was performed by a Bioanalytical Systems (BAS) model 100W electrochemical analyzer as described in previous chapters. Thin layer UV/VIS spectroelectrochemistry was performed by the Milton Roy spectrophotometer together with a Princeton Applied Research Mode 273 A potentiostat. The electrolysis cell was a thin layer quartz cell of path length 0.5 mm with a platinum gauze working electrode, a platinum wire counter electrode and an $Ag/AgNO_3$ (0.1 M) reference electrode. The electrolyte was thoroughly degassed with pre-purified argon before measurement. *In-situ* FTIR spectroelectrochemistry was performed according to the procedures described in previous chapters.

Constant potential electrolysis was performed in a gas-tight three-compartment cell. Reticulated vitreous carbon obtained from The Electrosynthesis Co. was used as working electrode. A control experiment was always performed by electrolysing a blank solution saturated with argon. After completion of an electrolysis, gas samples were taken through a septum from the head-space above the solution in the working electrode compartment and analyzed for CO and H_2 by a Hewlett-Packard model 5890 gas chromatography equipped with a thermal conductivity detector. A 6 ft x 1/8 in stainless steel column packed with 5 Å molecular sieves was employed in the analysis with helium as the carrier gas. Formate and oxalate ions in the solution were analyzed by HPLC with a Waters Associate model 510 liquid chromatograph equipped with a Supelcogel C-610H column. The supporting electrolyte tetra-n-buytlammonium

hexafluorophosphate was removed from the reaction solutions prior to formate analysis by the following procedures: the solvent (dimethylsulphoxide) was removed from the reaction solutions under reduced pressure. Distilled water was added to the residue in a 2:1 (v/v) ratio (H_2O/total original reaction volume). Analysis was conducted on the aqueous filtrate obtained after removal of the precipitated tetra-n-butylammonium hexafluorophosphate by filtration.

4.3 Results and Discussion

4.3.1 Electrochemical Behavior of $[Fe(dophen)(N\text{-}MeIm)_2]^+$ in DMSO

As the iron complex is only soluble in polar solvents, investigations on the electrochemistry of the complex were conducted in N,N-dimethylformamide (DMF) and dimethylsulphoxide (DMSO). The voltammetric behavior of the complex in DMSO and DMF is very similar. The cyclic voltammograms of $[Fe^{III}(dophen)(N\text{-}MeIm)_2]^+$ in DMSO and DMF are shown in Figures 4.1a and 4.1b respectively. Upon reductive scan, three reversible couples of similar size appear at $E_{1/2}$ = -0.75, -2.03 and –2.45 V vs. $Cp_2Fe^{+/0}$ in DMF which are labeled couple I, II and III respectively ($E_{1/2}$ = -0.74, -2.02, -2.46 V vs. $Cp_2Fe^{+/0}$ in DMSO). Constant potential coulometry at –1.3 V and –2.3 V established that couples I and II are one-electron redox couples. Attempts to establish the stoichiometry of couple III by constant potential coulometry at –2.50 V, however, did not result in the decay of the current back to background level. As the size

of all three couples are similar, it is reasonable to assign couple III as one-electron couple.

Couple I is undoubtedly a metal-based Fe(III)/Fe(II) reduction as the free H_2dophen ligand can only be reduced at a much more negative potential (-2.05 V) (Figure 4.2). This is supported by the observation that addition of excess amount of the hard Lewis base diethylamine to the electrolyte would cause a significant shift in the $E_{1/2}$ of couple I accompanied by a large peak-to-peak separation of the couple (Figure 4.3). As the $E_{1/2}$ of couple II and III are very close to that of H_2dophen, it is difficult to assign couple II and III as metal- or ligand-based processes. However, in the presence of the soft base CO, a significant shift in the $E_{1/2}$ of couple II was observed (Figure 4.5). As CO is a strong π-acid ligand, our observation is consistent with the ligation of CO to the electron rich Fe^{II} center [167] and cathodic wave IIa can be assigned to the reduction of Fe^{II}-CO species. Addition of excess pyridine also caused a shift in the $E_{1/2}$ of both couple I and II (Figure 4.4). The $E_{1/2}$ of couple III remains unchanged in the presence of hard or soft Lewis bases. These results support the assignment of couple I and II to metal-based redox processes and couple III is a ligand-based redox reaction.

In order to get more insight into the nature of these reduction processes, we have conducted the *in-situ* UV thin layer spectroelectrochemical studies. The UV-visible spectrum of $[Fe^{III}(dophen)(N\text{-}MeIm)_2]^+$ shows an intense intraligand transition at 396 nm (Figure 4.6) which can also be observed in the spectrum of the free H_2dopnen ligand (Figure 4.7). Reduction of the free H_2dophen ligand at –2.05 V results in a significant decrease in intensity of this absorption band accompanied by a red shift of peak wavelength by over 60 nm as shown in Figure 3.7. We would expect similar spectral

change if the reduction process of the metal complex is primarily a ligand-based reduction. Stepping the potential of the iron complex from -0.7 V to -0.88 V causes a slight shift of this absorption peak from 396 nm to 402 nm with a small increase in the absorption intensity (Figure 4.6). This is consistent with the assignment of couple I to a metal-based process; the small change in peak maximum and intensity can be explained by perturbation of the intraligand transition upon coordination to the metal ion. Stepping the potential from -1.85 V to 2.2 V only causes a small decrease in the intensity in the intraligand transition band. This indicates that couple II is unlikely to be a ligand-based reduction process. Further reduction of the complex by stepping the potential to 2.52 V, however, causes a significant decrease in the intensity of the intraligand transition with a new hump arises to around 440 mm. The spectral change accompanying the reduction of the iron complex at this potential is similar to that of free H_2dophen ligand, suggesting that couple III is primarily a ligand-based reduction. We therefore assign couple II to the reduction of Fe(II) to Fe(I) and couple III to the reduction of $[Fe^{I}(dophen)]^{-}$ to $[Fe^{I}(dophen)^{\bullet}]^{2-}$ respectively.

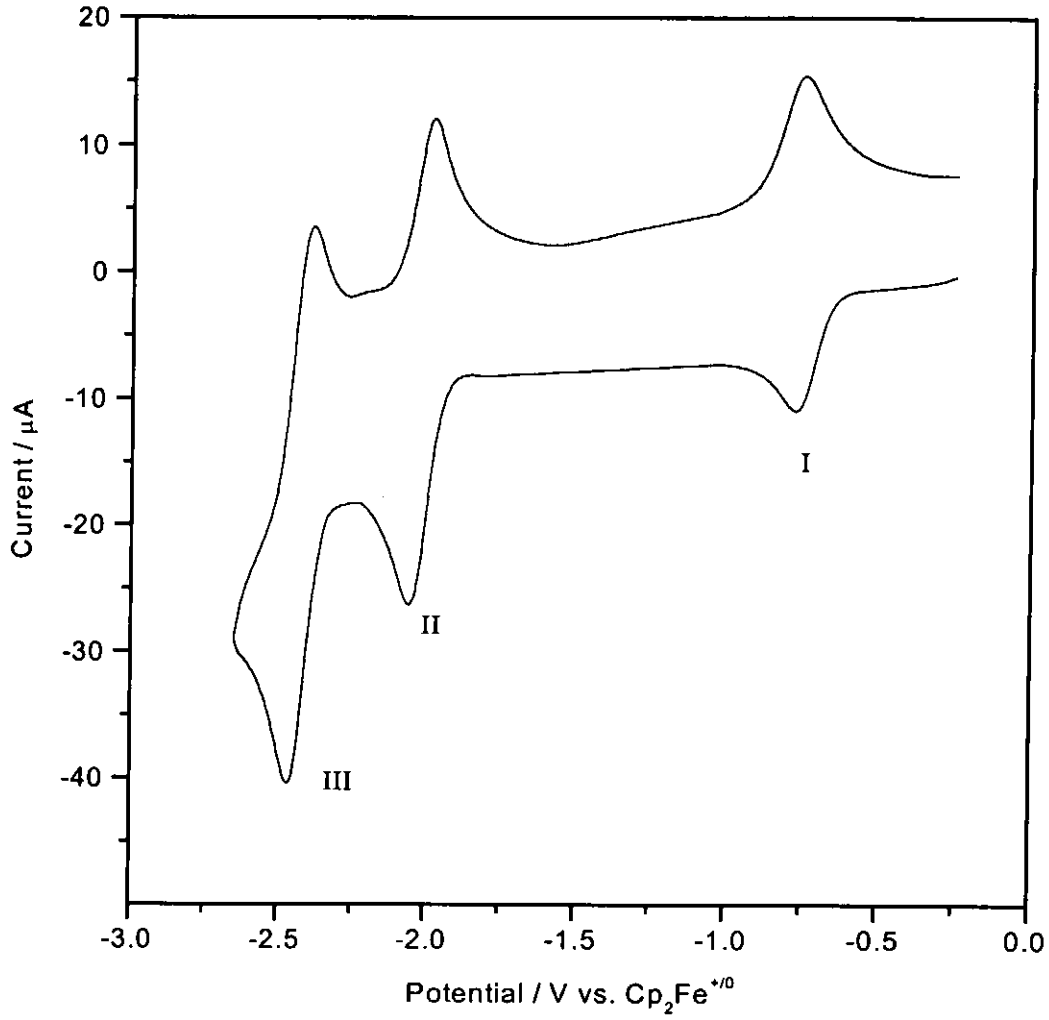

Figure 4.1a Cyclic voltammogram of 0.4 mM $[Fe(dophen)(N\text{-}MeIm)_2]^+$ in dimethylsulphfoxide under 1 atm argon. Working electrode: glassy carbon (0.2 cm^2). Supporting electrolyte: 0.1 M tetra-n-butylammonium hexafluorophosphate. Scan rate: 100 mV s^{-1}.

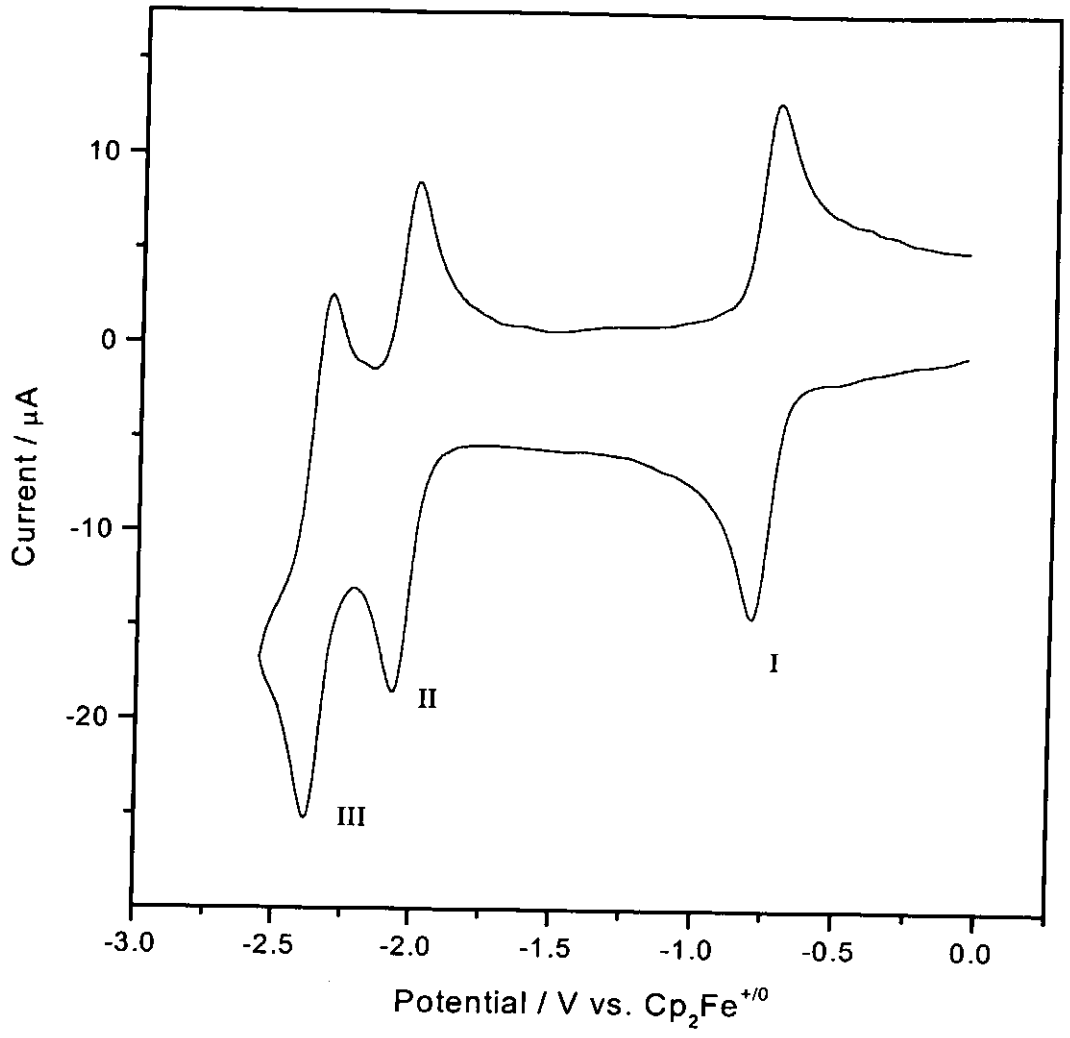

Figure 4.1b Cyclic voltammogram of 0.4 mM $[Fe(dophen)(N\text{-}MeIm)_2]^+$ in dimethylformamide under 1 atm argon. Working electrode: glassy carbon (0.2 cm^2). Supporting electrolyte: 0.1 M tetra-n-butylammonium hexafluorophosphate. Scan rate: 100 mV s^{-1}.

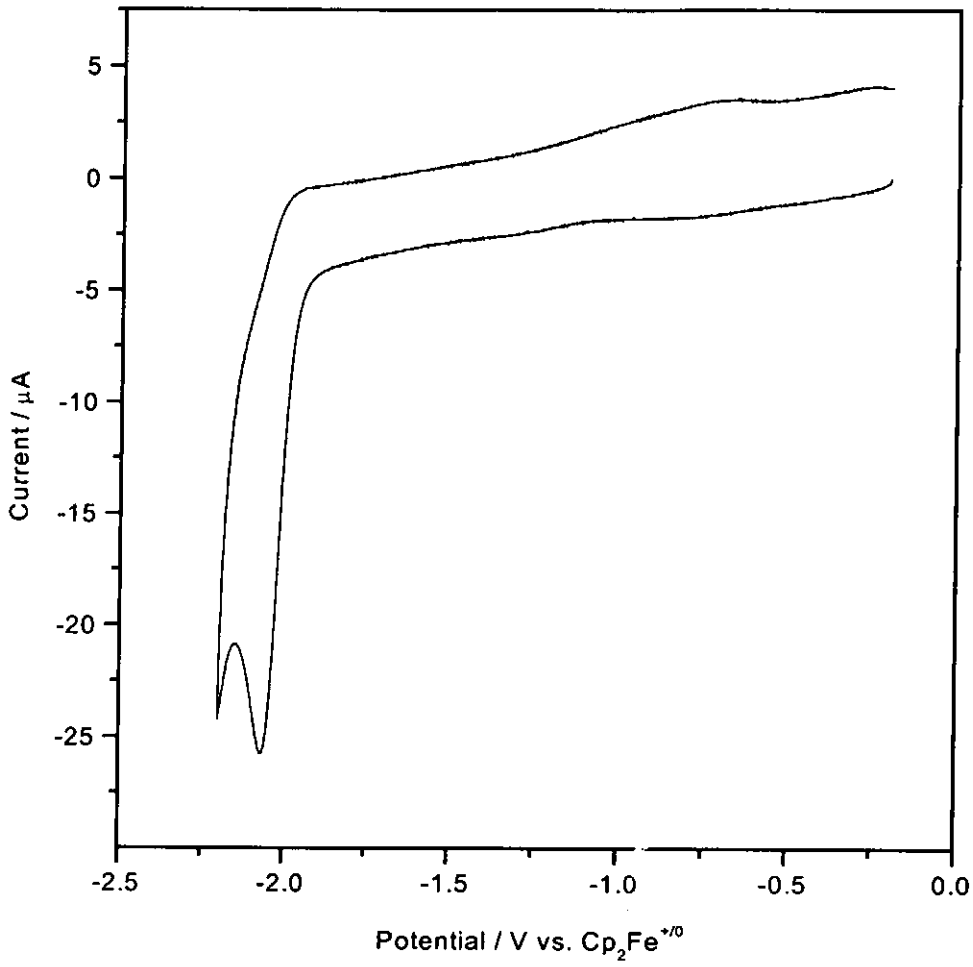

Figure 4.2 Cyclic voltammogram of 0.6 mM H_2dophen in dimethylsulphoxide under 1 atm argon. Working electrode: glassy carbon (0.2 cm^2). Supporting electrolyte: 0.1 M tetra-n-butylammonium hexafluorophosphate. Scan rate: 100 mV s^{-1}.

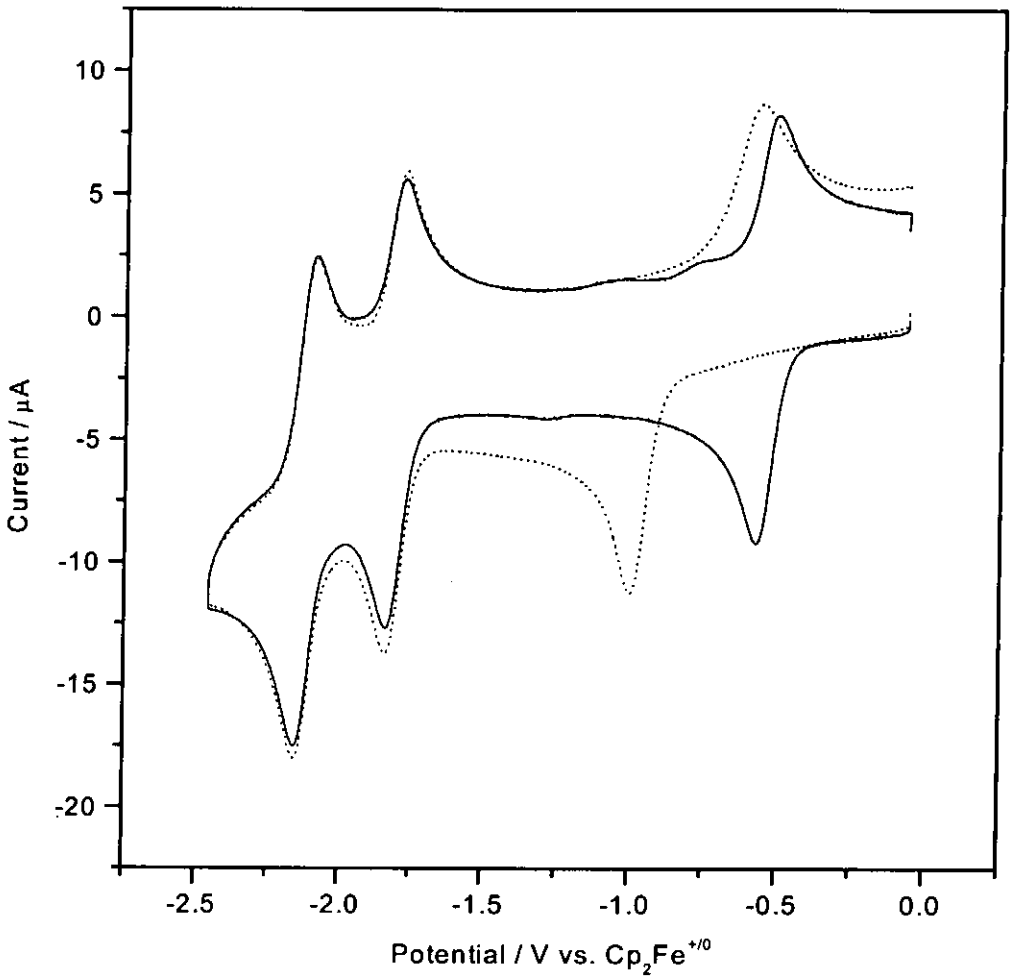

Figure 4.3 Cyclic voltammograms of 0.35 mM $[Fe(dophen)(N\text{-}MeIm)_2]^+$ under 1 atm argon (—) and in the presence of 3.0 mM of diethylamine (....) in dimethylsulphoxide. Working electrode: glassy carbon (0.2 cm^2). Supporting electrolyte: 0.1 M tetra-n-butylammonium hexafluorophosphate. Scan rate: 100 mV s^{-1}.

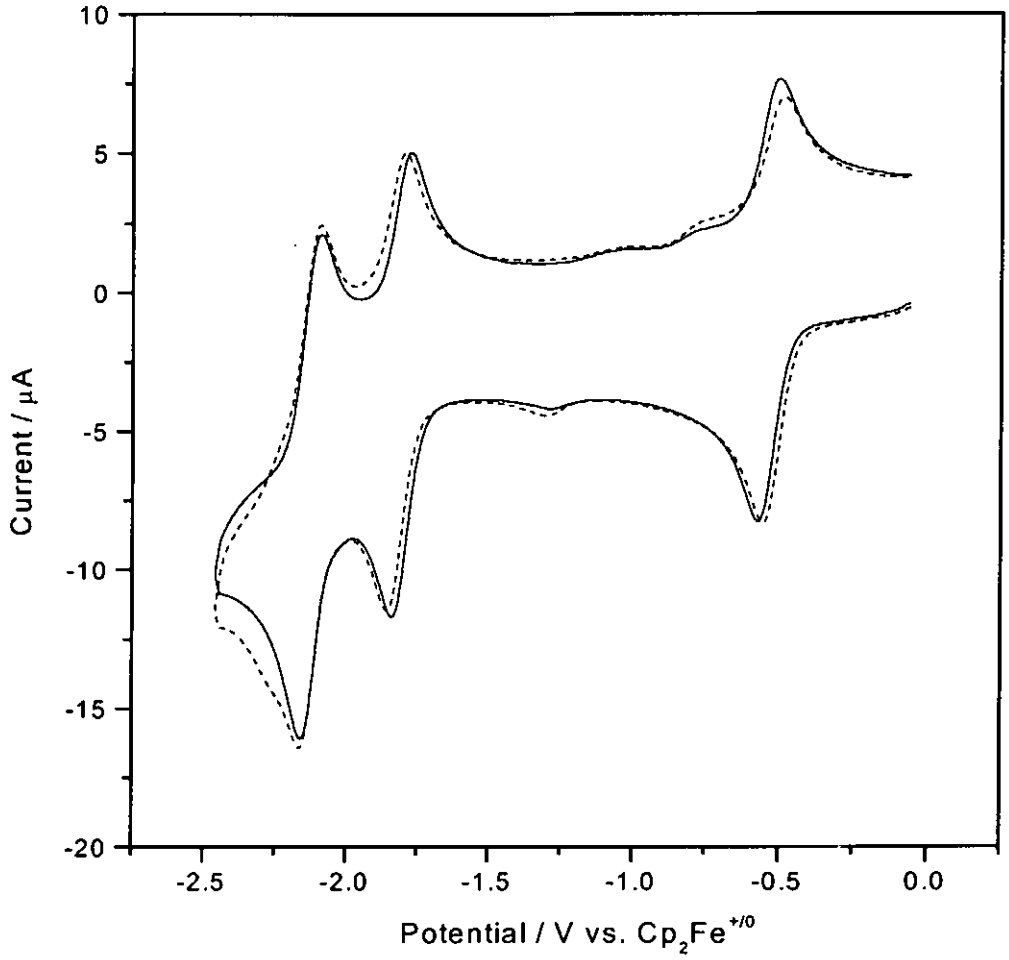

Figure 4.4 Cyclic voltammograms of 0.4 mM $[Fe(dophen)(N\text{-}MeIm)_2]^+$ (—) and in the presence of 0.25 M pyridine (----) in dimethylsulphoxide under 1 atm argon. Working electrode: glassy carbon (0.2 cm^2). Supporting electrolyte: 0.1 M tetra-n-butylammonium hexafluorophosphate. Scan rate: 100 mV s^{-1}.

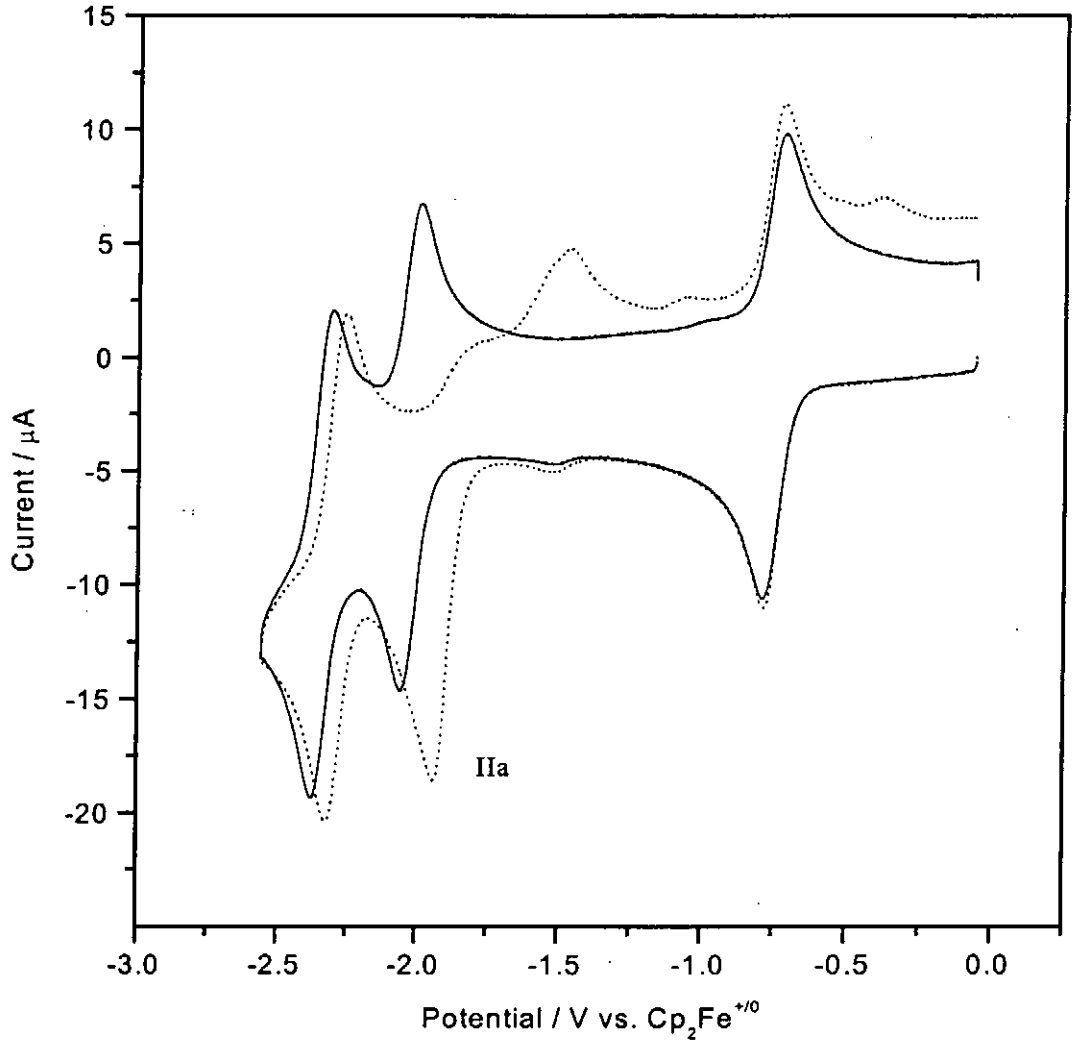

Figure 4.5 Cyclic voltammograms of 0.4 mM $[Fe(dophen)(N\text{-}MeIm)_2]^+$ in dimethylsulphoxide under 1 atm argon (—); under 1 atm CO (....). Working electrode: glassy carbon (0.2 cm^2). Supporting electrolyte: 0.1 M tetra-n-butylammonium hexafluorophosphate. Scan rate: 100 mV s^{-1}.

The $E_{1/2}$ of couple I and II are dependent on the concentration of 1-methylimadizole in the solution whereas the $E_{1/2}$ of couple III remains unchanged (Figure 4.8). Increasing the concentration of 1-methylimadazole in the solution causes a cathodic shift of the reduction waves I and II. The plot of the $E_{1/2}$ verses log[N-MeIm] for both couple I (Figure 4.9) and II (Figure 4.10) gave a straight line with a slope of -55 mV. The observation is consistent with the loss of N-MeIm during each reduction step [67]:

Couple I : $[Fe^{III}(dophen)(N\text{-}MeIm)_2]^+ + e^- \leftrightharpoons [Fe^{II}(dophen)(N\text{-}MeIm)] + N\text{-}MeIm$

Couple II: $[Fe^{II}(dophen)(N\text{-}MeIm)] + e^- \leftrightharpoons [Fe^{I}(dophen)]^- + N\text{-}MeIm$

Couple III : $[Fe^{I}(dophen)]^- + e^- \leftrightharpoons [Fe^{I}(dophen)^{\bullet}]^{2-}$

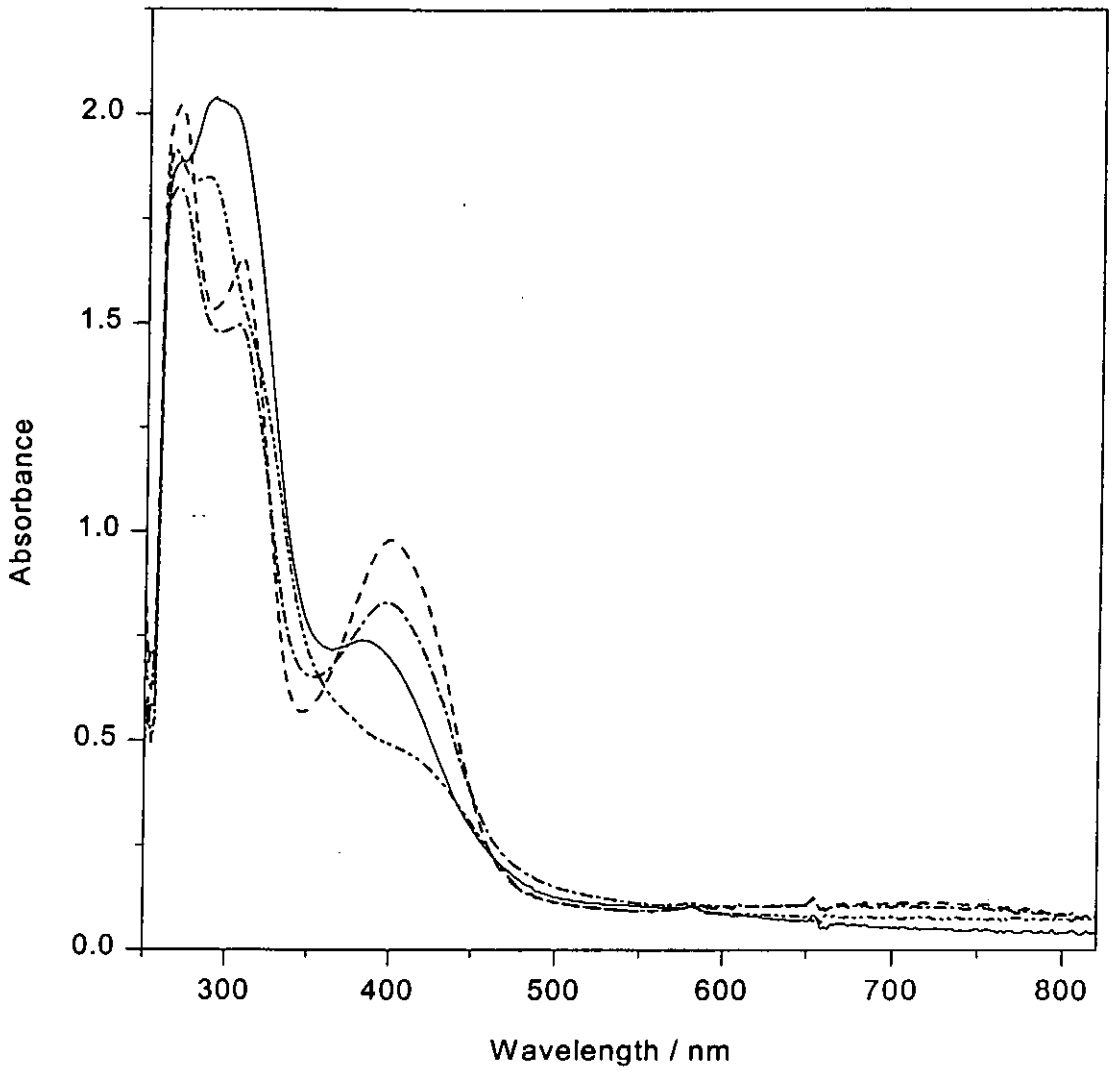

Figure 4.6 The reduction of $[Fe(dophen)(N\text{-}MeIm)_2]^+$ in dimethylformamide as monitored by thin-layer UV-visible spectroelectrochemistry. Spectra of $[Fe(dophen)(N\text{-}MeIm)_2]^+$ (—); after electrolysis at –1.75 V (----); after electrolysis at –2.2 V (.-.-.-) and after electrolysis at –2.63 V (-..-..). Supporting electrolyte: 0.1 M tetra-n-butylammonium hexafluorophosphate.

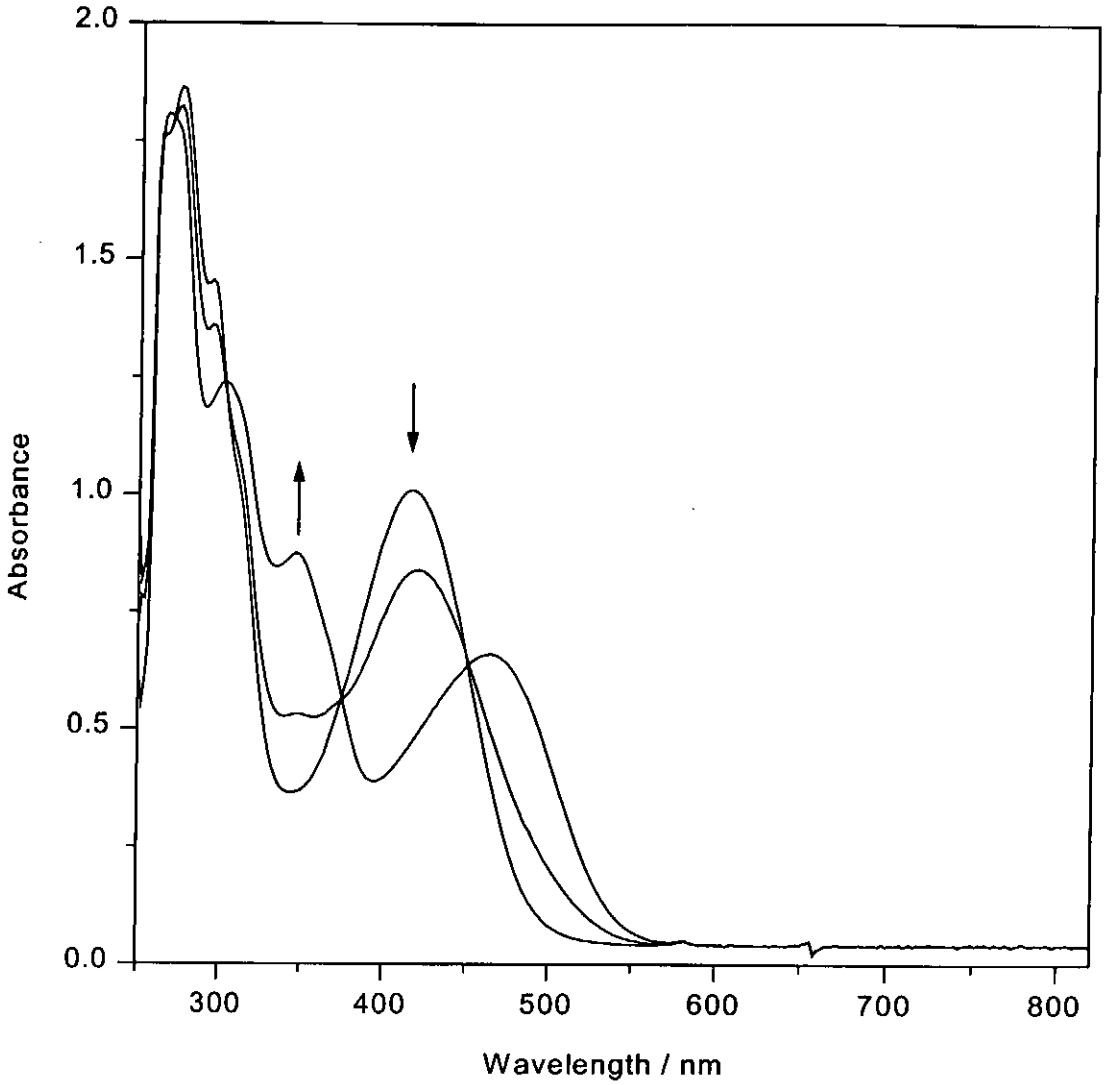

igure 4.7 The reduction of H_2dophen in dimethylformamide as monitored by thin-layer UV-visible spectroelectrochemistry. The reduction potential was stepped from –1.92 V to –2.05 V. Supporting electrolyte: 0.1 M tetra-n-butylammonium hexafluorophosphate.

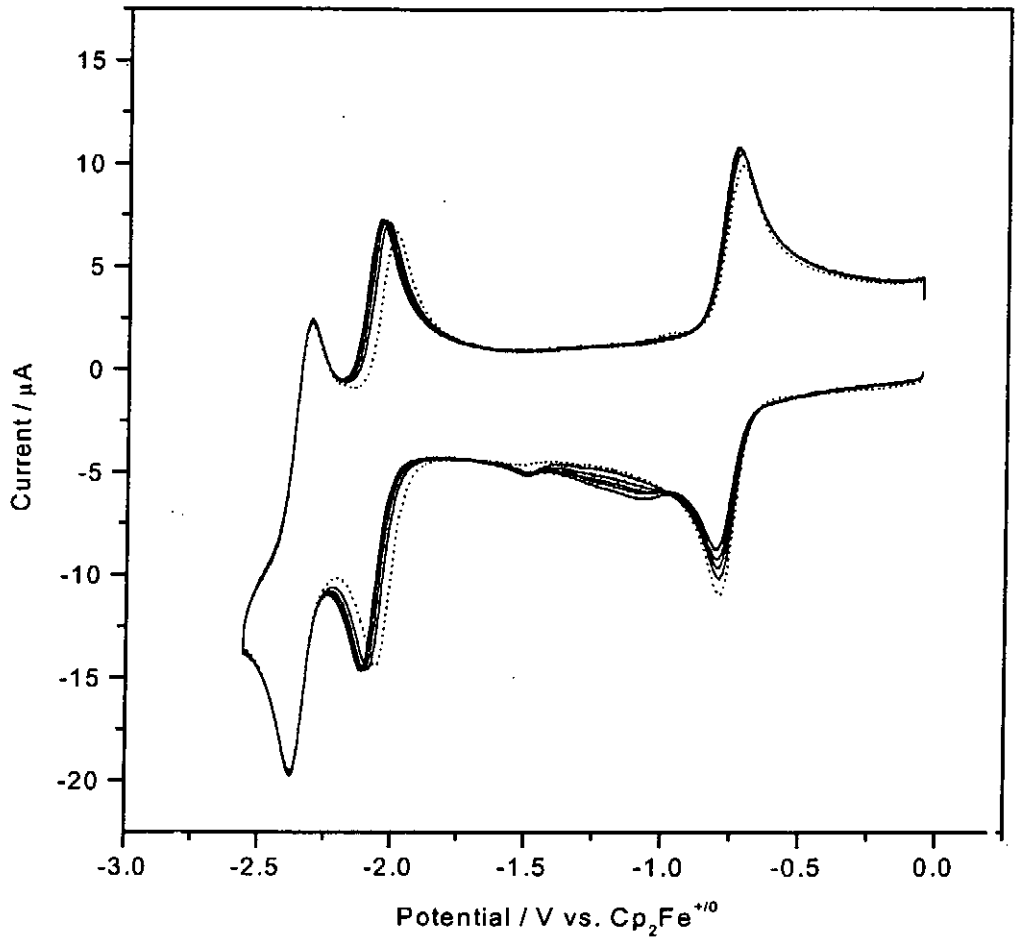

Figure 4.8 Cyclic voltammograms of 0.4 mM $[Fe(dophen)(N\text{-}MeIm)_2]^+$ (----) with increasing amount of 1-methylimidazole (—) in dimethylsulphoxide under 1 atm argon. Working electrode: glassy carbon (0.2 cm^2). Supporting electrolyte: 0.1 M tetra-n-butylammonium hexafluorophosphate. Scan rate: 100 mV s^{-1}.

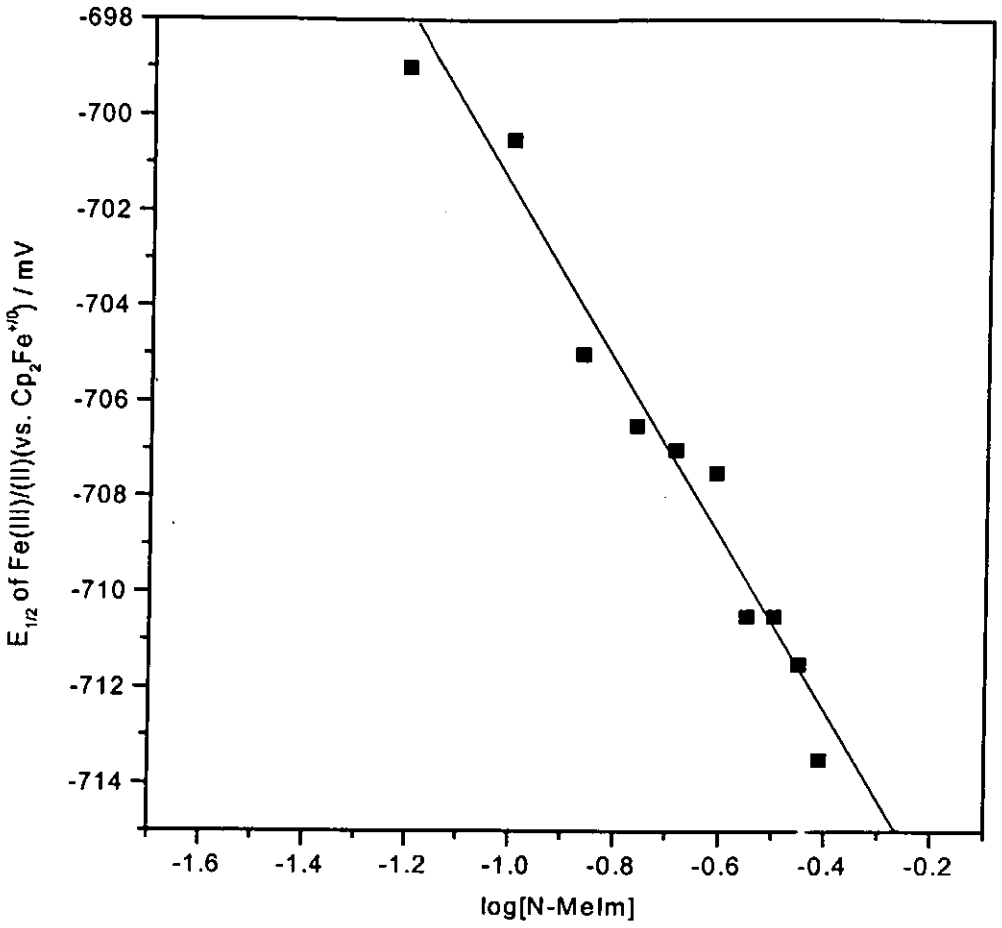

Figure 4.9 A plot of the half-wave potential ($E_{1/2}$) for $[Fe^{III}(dophen)(N\text{-}MeIm)_2]^+/[Fe^{II}(dophen)(N\text{-}MeIm)]$ with log[N-MeIm]

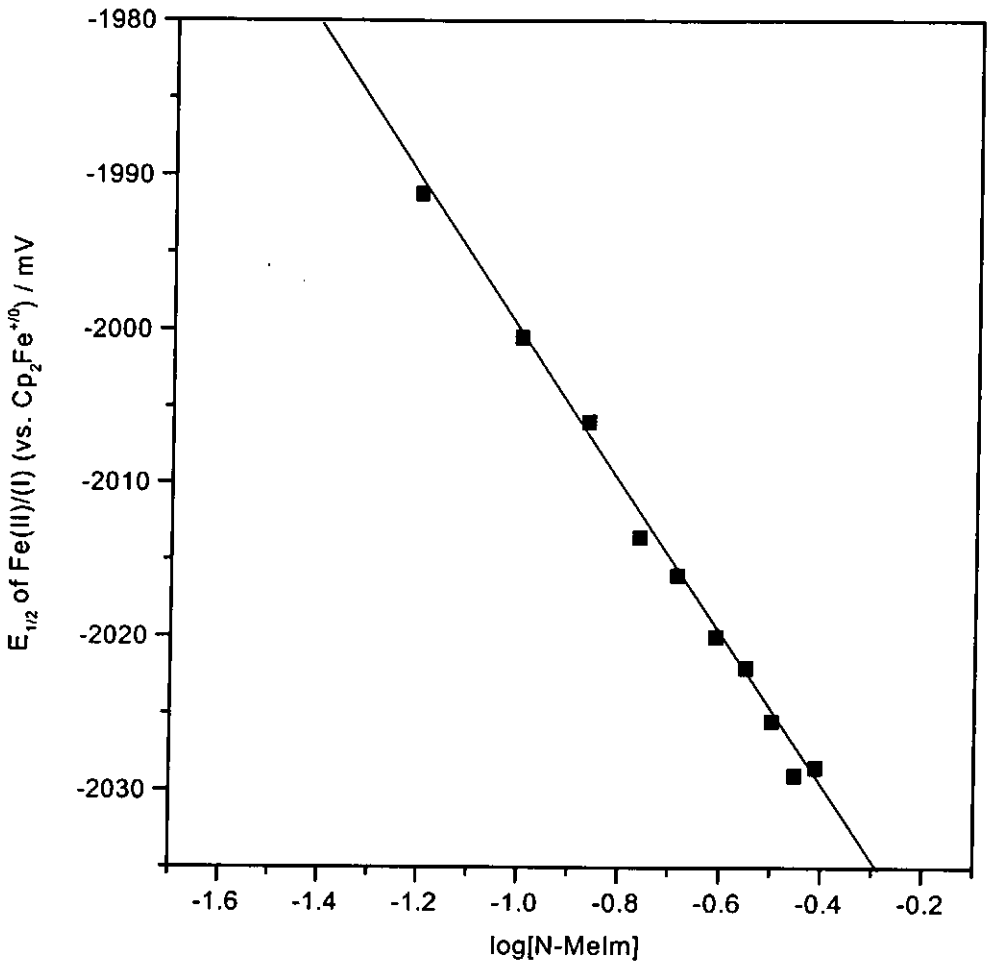

Figure 4.10 A plot of the half-wave potential ($E_{1/2}$) for $[Fe^{II}(dophen)(N\text{-}MeIm)]/[Fe^{I}(dophen)]^{-}$ with log[N-MeIm]

4.3.2 Electrocatalytic reduction of CO_2

Figure 4.11 shows the cyclic voltammograms of $[Fe^{III}(dophen)(N\text{-}MeIm)_2]^+$ in DMSO under argon and CO_2 atmospheres. In the presence of CO_2, the cathodic wave of the Fe(II)/Fe(I) couple is enhanced while the anodic wave is diminished. Constant potential electrolysis at –2.06 V vs. $Cp_2Fe^{+/0}$ in DMSO and DMF produced a mixture of carbon monoxide, formate and oxalate. When bulk electrolysis experiment was conducted in a DMSO-CO_2 saturated solution without electrocatalyst, no CO, $HCOO^-$ and $C_2O_4^{2-}$ could be detected, this confirmed that no catalysis was taken place at –2.06 V vs. $Cp_2Fe^{+/0}$ in the absence of the electrocatalyst.

Savéant and co-workers reported that addition of Brönsted acid can enhance the rate of electrocatalytic reduction of CO_2 by iron porphyrin [66]. Similar effect can also be observed for the iron dophen complex. Figure 4.11 shows the cyclic voltammograms of $[Fe(dophen)(N\text{-}MeIm)_2]^+$ in DMSO under CO_2 atmosphere and in the presence of the weak Brönsted acid CF_3CH_2OH. The catalytic current rises sharply beyond –2.0 V indicating the presence of CF_3CH_2OH would enhance the catalytic activation of Fe(I) complex towards CO_2 reduction. Enhancement in catalytic current can also be observed for the weaker acid methanol but the magnitude is smaller (pK_a of CF_3CH_2OH and CH_3OH in DMSO = 23.6 and 29.0 respectively [168]). This is consistent with previous study [66] that the synergistic efficiency of weak Brönsted acid is related to its acidity: the lower the pK_a, the higher the synergistic effect. The addition of H_2O did not cause a significant enhancement of the catalytic current for CO_2 reduction in the iron dophen system but the precipitation of the complex. The addition of protonated alkyl amine salts such as $Et_3NH^+Cl^-$, on the other hand, caused an enhancement of the reduction

current at the potential beyond the catalytic CO_2 reduction peak (Figure 4.12) which is due to the catalytic reduction of the amine salt itself.

The results of constant potential electrolysis of CO_2 with iron catalyst at a reticulated vitreous carbon as working electrode in the presence of different proton sources are summarized in Table 4.1. The product distributions obtained from the bulk electrolyses in DMSO and DMF are very similar. It is interesting to note that formate was always produced in the absence and presence of alcohols. When anhydrous $LiClO_4$ was used as supporting electrolyte instead of TBAH, the same relative amount of formate was also afforded. Therefore, the origin of proton source for the formation of formate in the absence of alcohol could have originated from the solvent or traces of water present in the electrolyte. From the results, it can be seen that the addition of CF_3CH_2OH or CH_3OH increases both the rate of catalysis and the relative amount of carbon monoxide produced. However, the dominant product was always $HCOO^-$ although a small amount of $C_2O_4^{2-}$ was also detected. When protonated alkyl amine salts were added as the proton source, the major product was H_2 together with a small amount of CO.

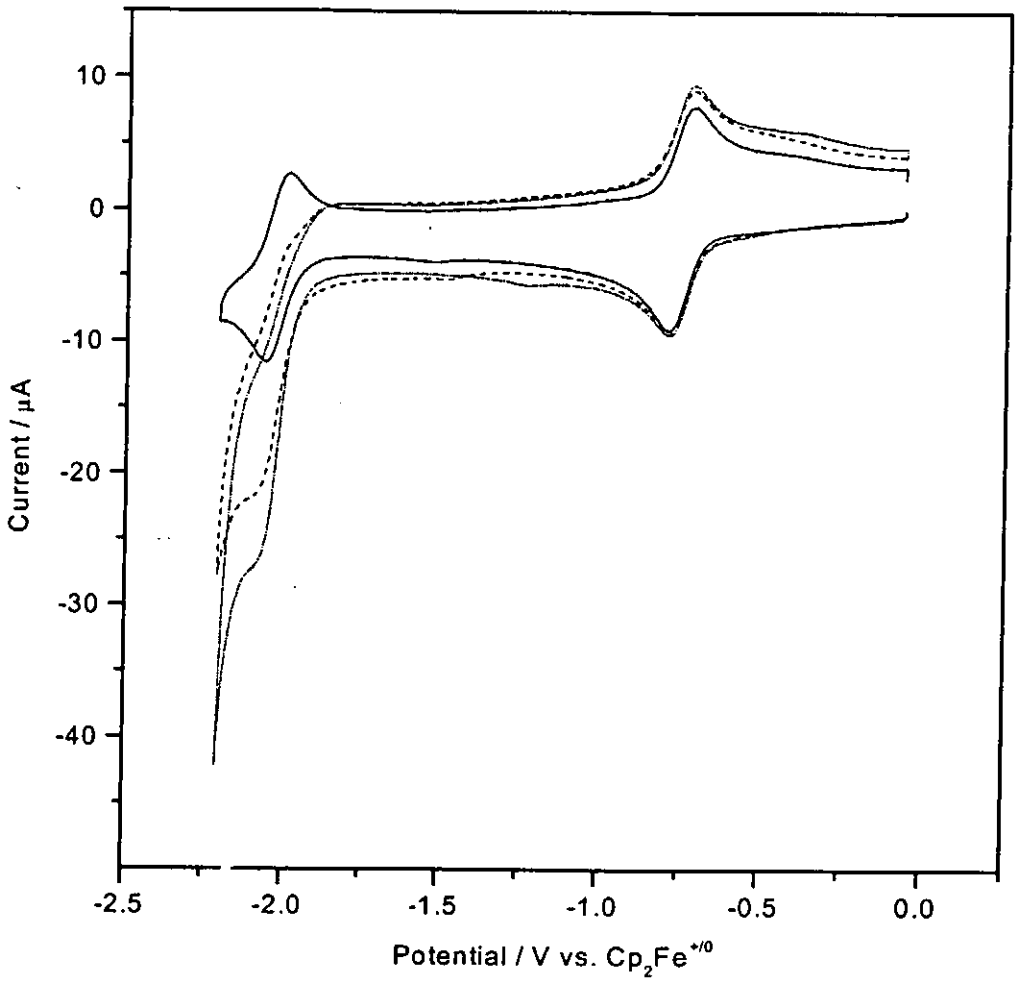

Figure 4.11 Cyclic voltammograms of 0.4 mM $[Fe(dophen)(N\text{-}MeIm)_2]^+$ in dimethylsulphoxide under 1 atm argon (—); under 1 atm CO_2 (----); and in the presence of 0.319 M 2,2,2-trifluoroethanol and under 1 atm CO_2 (....). Working electrode: glassy carbon (0.2 cm^2). Supporting electrolyte: 0.1 M tetra-n-butylammonium hexafluorophosphate. Scan rate: 100 mV s^{-1}.

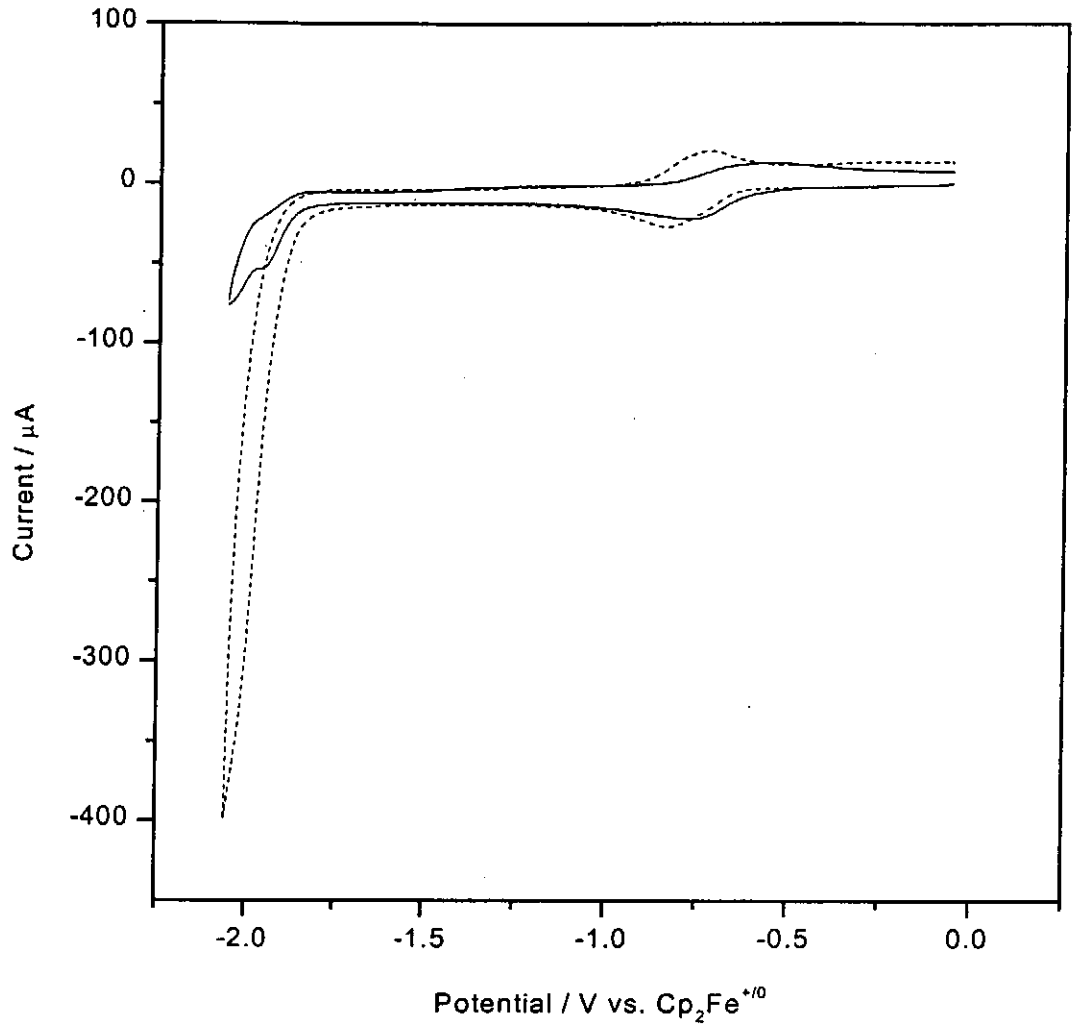

Figure 4.12 Cyclic voltammograms of 0.4 mM $[Fe(dophen)(N\text{-}MeIm)_2]^+$ in dimethylsulphoxide under 1 atm CO_2 (—)and in the presence of 0.16 M $Et_3NH^+Cl^-$ (----). Working electrode: glassy carbon (0.2 cm^2). Supporting electrolyte: 0.1 M tetra-n-butylammonium hexafluorophosphate. Scan rate: 100 mV s^{-1}.

Table 4.1 A summary on the electrolysis of CO_2 in the presence of [Fe(dophen)(N-MeIm)$_2$]$^{+a}$

Solvent	Proton source	Charge consumed / C	Current efficiency of CO produced / %	Current efficiency of $HCOO^-$ produced / %	Current efficiency of $C_2O_4^{2-}$ produced / %	Current efficiency of H_2 produced / %
DMSO	----	3.29 (3.08)[b]	18.5 (23.9)[b]	67.2 (66.8)[b]	9.8 (7.8)[b]	---- ----
DMSO	1.23 M CF_3CH_2OH	10.47	29.5	65.4	2.9	----
DMSO	1.23 M CH_3OH	8.01 (5.90)[c]	25.8 (----)[c]	66.4 (----)[c]	6.4 (----)[c]	---- (40.6)[c]
DMSO	0.16 M $Me_3NH^+Cl^-$	14.71	10.5	----	----	69.5
DMSO	0.16M $Me_2NH_2^+Cl^-$	13.31	9.8	----	----	78.5
DMSO	0.16 M $Et_3NH^+Cl^-$	15.81	11.4	----	----	72.1
DMF	----	9.98	22.5	57.2	13.4	----
DMF	1.23 M CH_3OH	7.63	29.8	51.5	10.6	----
DMF	1.23 M CF_3CH_2OH	8.73 (7.83)[d]	31.2 (----)[d]	52.6 (----)[d]	8.5 (----)[d]	---- (47.6)[d]

[a]Amount of catalyst in solution = 1 x 10^{-3} M; Time of electrolysis = 1h; Potential held: -2.06 V vs. $Cp_2Fe^{+/0}$; Supporting electrolyte: TBAH (tetra-n-butylammonium hexafluorophosphate)

[b]$LiClO_4$ was used as supporting electrolyte instead of TBAH

[c]Electrolysis was performed in N_2-saturated DMSO

[d]Electrolysis was performed in N_2-saturated DMF

4.3.3 *In-situ* FTIR spectroelectrochemical studies

It has been shown that the electrochemical behavior of the iron dophen complex and the products obtained from the bulk electrolysis experiments are very similar in dimethylsulphoxide (DMSO) and dimethylformamide (DMF). DMSO was chosen as the solvent in performing *in-situ* FTIR spectroelectrochemistry because DMF itself absorbs strongly in 1600-1400 cm^{-1} region of the infrared spectrum. However, the choice of DMSO also hindered us from conducting low temperature spectroelectrochemical experiments because DMSO solidifies at 18°C. Figure 4.13 reveals a series of normalized time-resolved FTIR spectra from the glassy carbon electrode immersed in CO_2-saturated dimethylsulphoxide in the presence of $[Fe(dophen)(N\text{-}MeIm)_2]^+$ at 23°C in the region 3500-1750 cm^{-1}. The reference potential (E_1) and the working potential (E_2) were held at –0.46 V and –2.16 V vs. $Cp_2Fe^{+/0}$ respectively. Spectra collected at E_2 at different time intervals were normalized to the reference spectrum taken at E_1.

The results revealed an intense growth features at 3200-3000 cm^{-1}. These bands can be assigned to the absorption of the positively charged TBA^+ ions in the thin layer [140, 169]. Positive reflectance at 2343 cm^{-1} is caused by the consumption of CO_2 during the course of reduction. In addition, there is a weak increase in absorption intensity at 2140 cm^{-1} that is most suitably assigned to the presence of CO [4].

The spectroscopic results also showed species with absorption peaks at 1934 cm^{-1} and 1881 cm^{-1} during the reduction process. This species was formed prior the observation of the CO peak. The intensity of these bands became constant in the later

course of the reduction which may be due to the steady formation and consumption of this species. Previous studies reported by Christensen et al. [140] indicated that the dicarbonyl species induced absorption at the same region. Thus, it is reasonable to assign these features as caused by the presence of $[Fe^{I}(dophen^{\bullet})CO]^{2-}$ or $[Fe^{I}(dophen^{\bullet})(CO)_2]^{2-}$. Moreover, negative band at 1328 cm^{-1} can be attributed to the formation of an iron formato species (Fe-OCOH) during the course of reduction (Figure 4.14). All the above assignments are supported by isotopic labeling using $^{13}CO_2$ instead of $^{12}CO_2$. Positive band at 2278 cm^{-1} corresponding to $^{13}CO_2$ was observed which is caused by the consumption of $^{13}CO_2$ during the reduction process. Bands due to ^{13}CO at 2110 cm^{-1} and iron formato (Fe-O^{13}COH) species at 1288 cm^{-1} were also observed (Figure 4.13b). When CF_3CH_2OH was added into the electrolyte (Figure 4.15), the spectra also showed the bands caused by the presence of the iron carbonyl species (ν = 1932 cm^{-1}, 1779 cm^{-1}) and the iron formato species (ν = 1326 cm^{-1}). The intensity of the band due to the presence the iron carbonyl species is larger than that in the absence of CF_3CH_2OH. This may be due to the higher concentration of CO afforded in the presence of CF_3CH_2OH.

4.3.4 Discussions on the Mechanism

For the iron dophen complex, the reaction mechanism is complicated as a mixture of CO, $HCOO^-$ and $C_2O_4^{2-}$ was produced by electrolysis. This also precludes the use of simple electrochemical kinetic models for mechanistic investigation. To date, the formation of CO is generally accepted to occur via a M-η^1-CO_2 intermediate [58,

170]. The formation of M-η^1-CO_2 complex is favored by an electron rich metal center with back bonding from the metal to the π^* orbital of CO_2 [171].

Scheme I

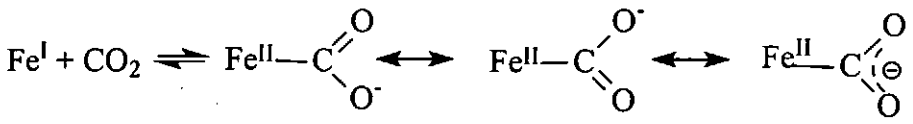

Brönsted acids can stabilize the M-η^1-CO_2 complex by protonation or hydrogen bonding with carbonyl oxygen [66]. Under such conditions, there is an intramolecular charge transfer from the metal center to the CO_2 moiety. Protonation of the coordinated CO_2 will facilitate the cleavage of one of the C-O (Scheme II) bonds leading to the formation of a M-CO intermediate which will subsequently release the reduced as CO. This is supported by the observation of bands assignable to the presence of iron-carbonyl species in the time resolved FTIR spectra and that CO was formed at the expense of the carbonyl complex.

Scheme II

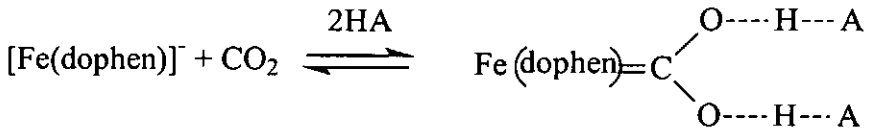

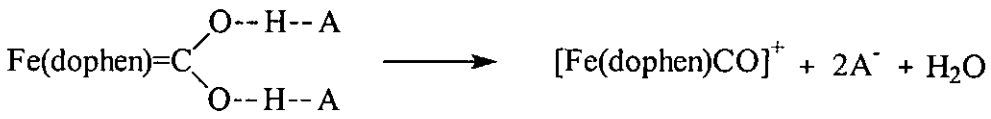

$$[Fe(dophen)CO]^{+} + e^{-} + S \quad \rightarrow \quad [Fe(dophen)S] + CO$$

where S is a solvent molecule

Early dissociation of the reduced CO_2 from the metal center would produce $CO_2^{\bullet-}$ which can dimerize to give oxalate. This would occur more easily in the first row transition metals which have much weaker metal-to-ligand back π bonding than the late transition metals. Hence it is not surprised to obtain oxalate in the reduction of CO_2 by $[Fe(dophen)]^{-}$.

$$[Fe(dophen)(CO_2)]^{-} + S \leftrightharpoons [Fe(dophen)S] + CO_2^{\bullet-}$$

$$2CO_2^{\bullet-} \rightarrow C_2O_4^{2-}$$

As formate was always produced in the absence or presence of alcohols, attempts were made to detect Fe-H species in the infrared spectrum. However, no signs of Fe-H could be traced from the spectroscopic data at room temperature. The Fe-H species is expected to be more reactive than Ru-H species; the late transition metal hydrides are usually thermodynamically more stable than the early transition metal hydrides [172]. Attempts to detect Fe-H or other reactive species at low temperatures were limited by the high melting point of DMSO (mp 18.4°C) which caused the electrolyte to solidify rapidly as the temperature was lowered. Since hydrogen was produced by electrolysis at –2.0 V vs. $Cp_2Fe^{+/0}$ in the presence of weak Brönsted acids under argon atmosphere and metal-hydride species are well known in the formation of hydrogen gas [159, 173-175], it is likely that an iron-hydride species was formed during

the course of CO_2 reduction in the presence of Brönsted acid. When alkyl amine salts were added as proton sources to the electrolyte, a substantial amount of hydrogen was produced. As our *in-situ* FTIR spectroelectrochemical study on the ruthenium carbonyl catalysts in the presence of $Et_3NH^+Cl^-$ indicated that a Ru-H species was produced, it is possible that a similar mechanism is also involved in the formation of formate.

$$[Fe(dophen)]^- + AH \leftrightharpoons [Fe(dophen)H] + A^-$$

$$[Fe(dophen)H] + CO_2 \leftrightharpoons [Fe(dophen)(OCOH)]$$

$$[Fe(dophen)(OCOH)] + e^- + S \leftrightharpoons [Fe(dophen)S] + HCOO^-$$

$$[Fe(dophen)S] + e^- \rightarrow [Fe(dophen)]^- + S$$

where S is a solvent molecule

If an Fe-H species is involved in the production of $HCOO^-$ in the Fe(dophen) system, then it appears that the iron system tends to form metal hydride kinetically faster than the ruthenium systems we described in Chapter 3. This is evidenced by the results of electrolysis in the presence of CF_3CH_2OH. Trifluoroethanol has a lower pK_a than H_2O in DMSO and should be able to form hydrogen bonding with CO_2. However, the addition of 1.23 M CF_3CH_2OH to the electrolyte only enhanced the percentage of CO production from 18.5 % to 29.5 %; formate was still the major product of CO_2 reduction. The $E_{1/2}$ of the Fe(II)/Fe(I) couple is more negative than the Ru(II)/Ru(I) couple in $[Ru(bdmpp)(bpy)CO]^{2+}$ but close to that of $[Ru(tpm)(bpy)CO]^{2+}$, thus the metal center in both the Fe and the Ru systems are sufficiently electron rich to attack the weakly electrophilic carbon in hydrogen-bonded CO_2. One should note, however, that we have used different solvent systems in the two studies due to the difference in

solubility of the two classes of metal complexes. Hence it is not known whether the DMSO or DMF solvent can promote the formation of metal-hydride species as the proton source can be the solvent itself.

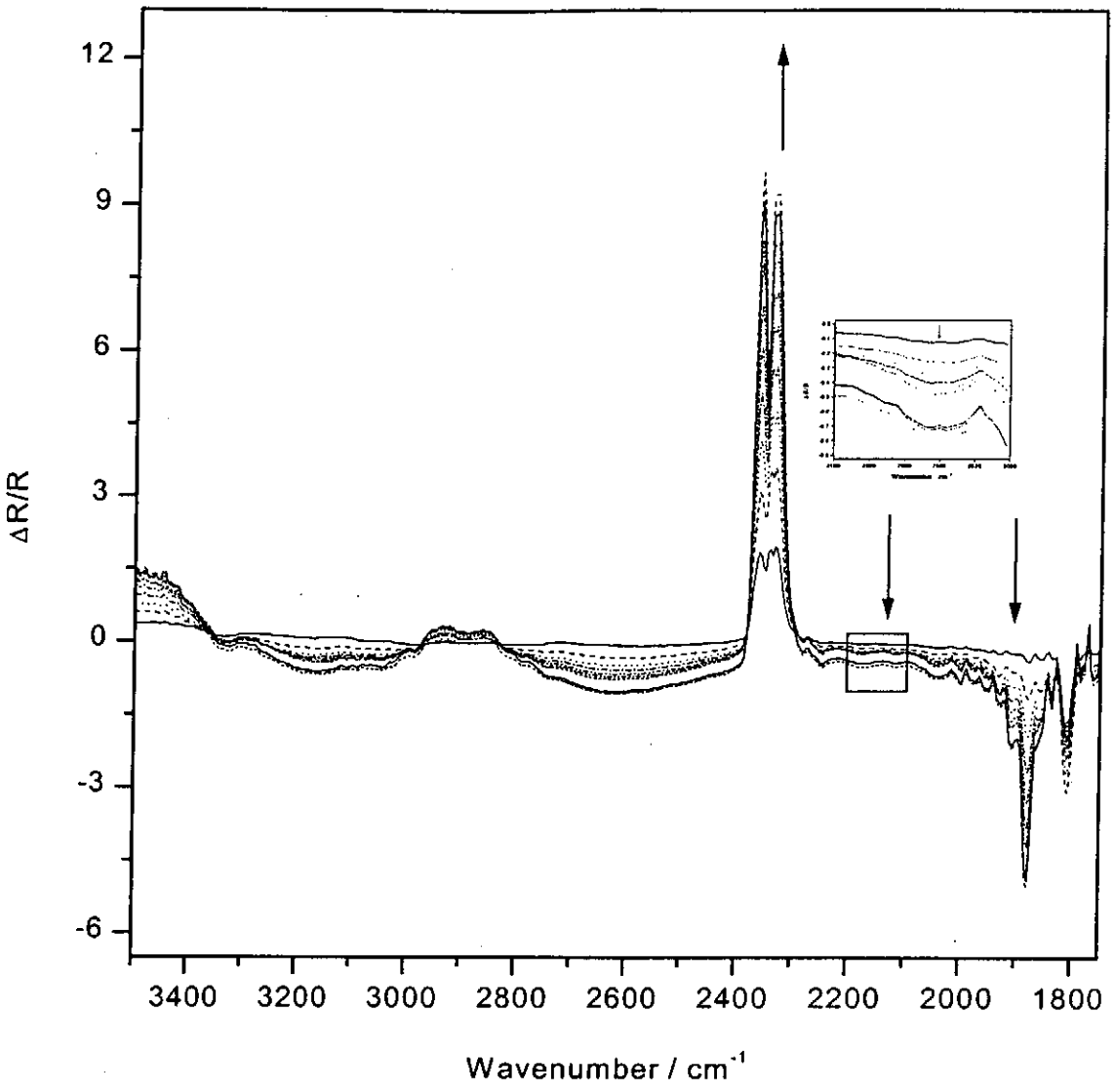

Figure 4.13a A series of normalized time resolved FTIR spectra in the region 3500-1750 cm^{-1} (8 cm^{-1} resolution, 100 scans) collected from a glassy carbon electrode immersed in a solution of $[Fe(dophen)(N\text{-}MeIm)_2]^+$ (5 mM) in CO_2-saturated DMSO at 23°C. E_1 = -0.46 V and E_2 = -2.16 V vs. $Cp_2Fe^{+/0}$. Supporting electrolyte: 0.1 M TBAH.

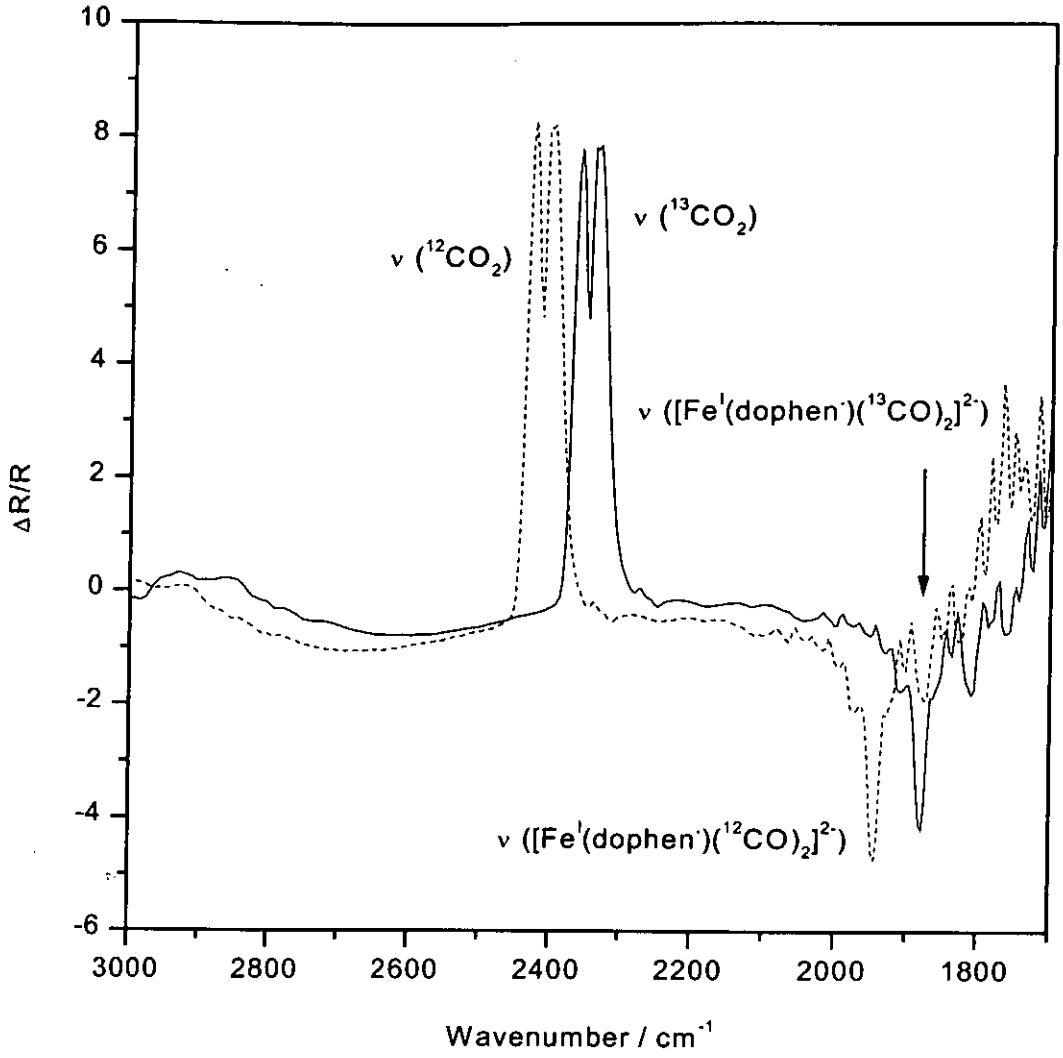

Figure 4.13b A series of normalized time resolved FTIR spectra in the region 3000-1750 cm^{-1} (8 cm^{-1} resolution, 100 scans) collected from a glassy carbon electrode immersed in a solution of $[Fe(dophen)(N\text{-}MeIm)_2]^+$ (5 mM) in $^{13}CO_2$-saturated DMSO at 23°C. E_1 = -0.46 V and E_2 = -0.46 V vs. $Cp_2Fe^{+/0}$. Supporting electrolyte: 0.1 M TBAH.

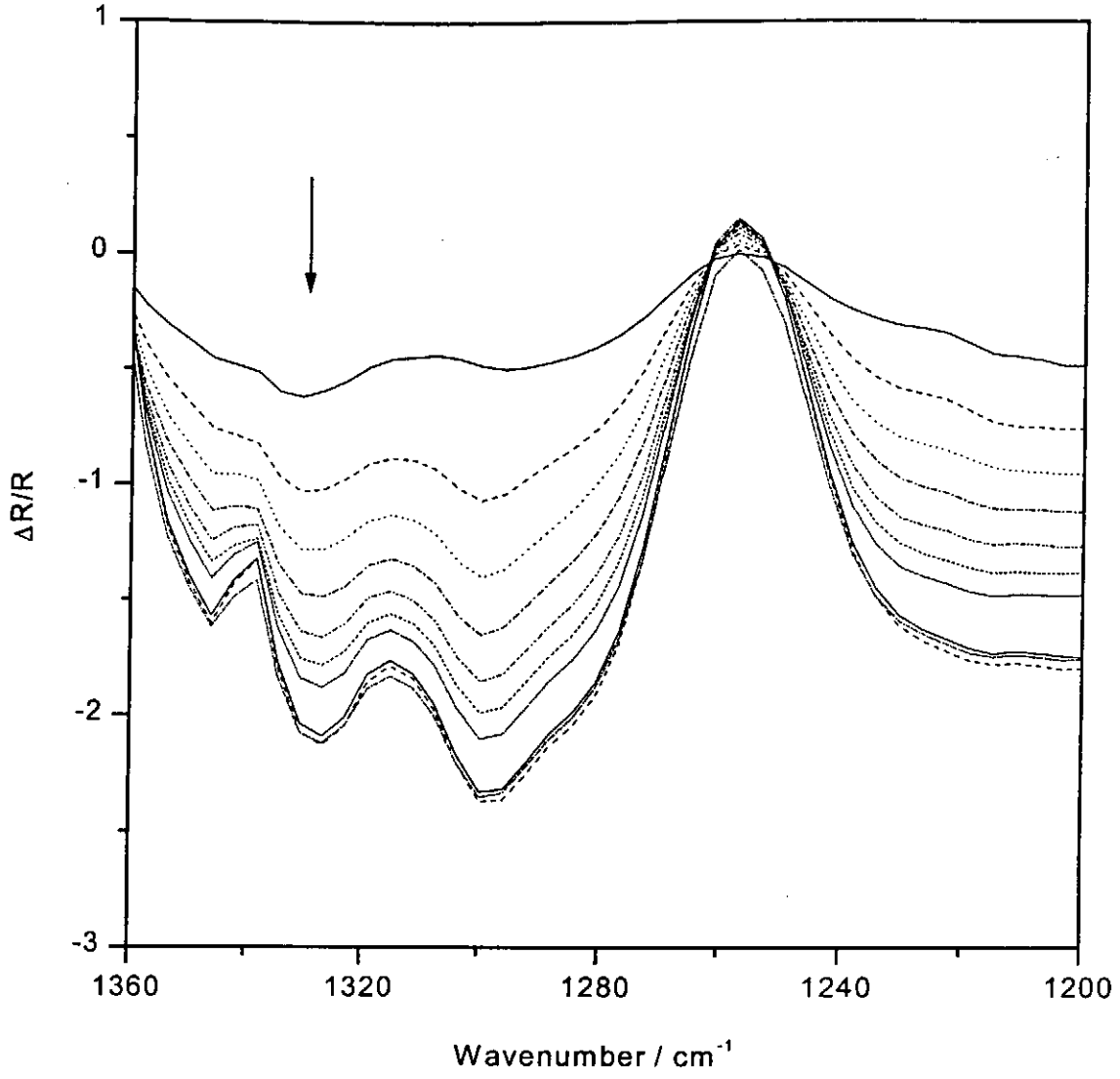

Figure 4.14 A series of normalized time resolved FTIR spectra in the region 1360-1200 cm^{-1} (8 cm^{-1} resolution, 100 scans) collected from a glassy carbon electrode immersed in a solution of $[Fe(dophen)(N\text{-}MeIm)_2]^+$ (5 mM) in CO_2-saturated DMSO at 23°C. E_1 = -0.46 V and E_2 = -2.16 V vs. $Cp_2Fe^{+/0}$. Supporting electrolyte: 0.1 M TBAH.

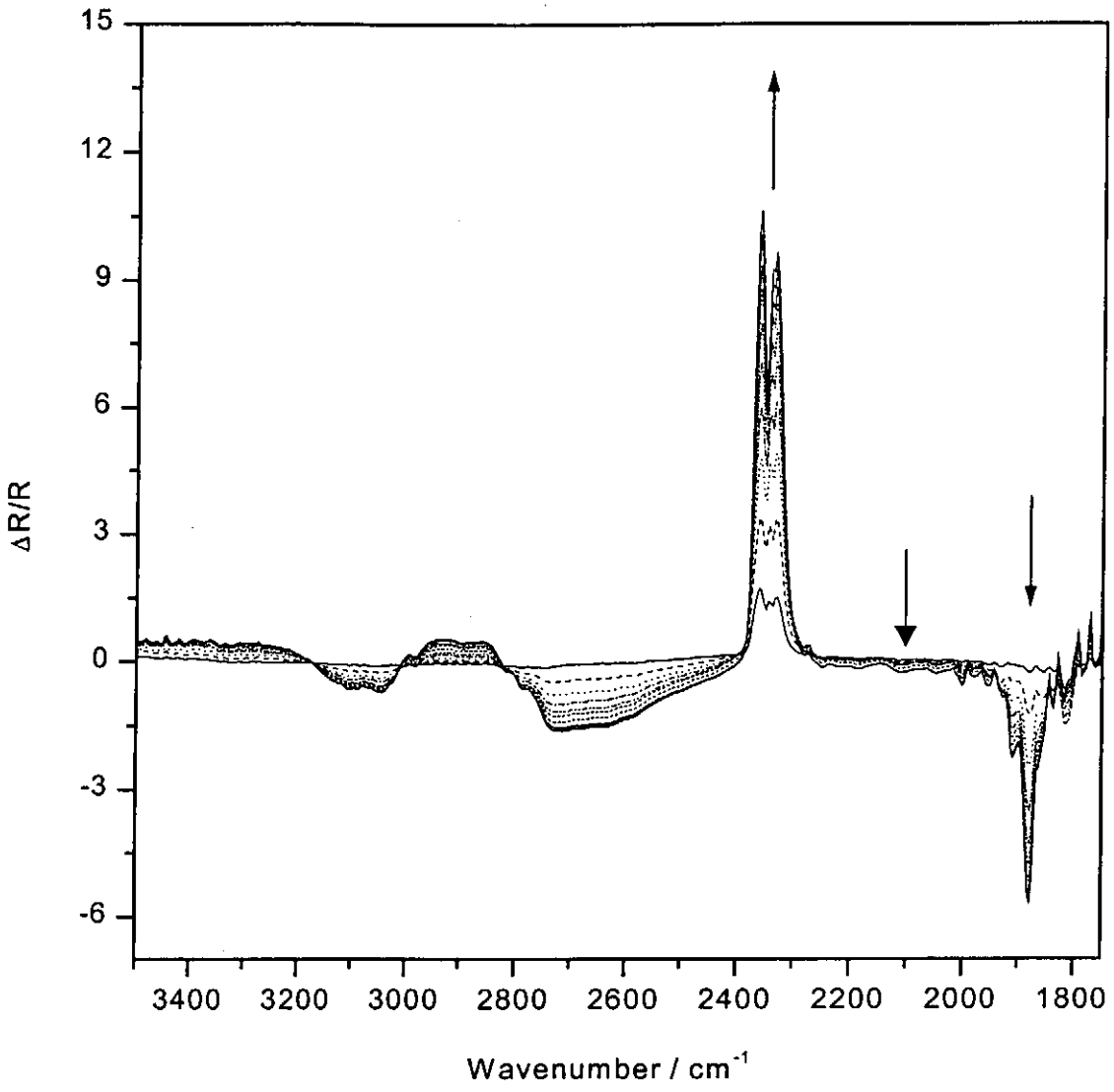

Figure 4.15 A series of normalized time resolved FTIR spectra in the region 3500-1750 cm^{-1} (8 cm^{-1} resolution, 100 scans) collected from a glassy carbon electrode immersed in a solution of $[Fe(dophen)(N\text{-}MeIm)_2]^+$ (5 mM) in CO_2-saturated DMSO and in the presence of CF_3CH_2OH (1.23 M) at 23°C. E_1 = -0.46 V and E_2 = -2.16 V vs. $Cp_2Fe^{+/0}$. Supporting electrolyte: 0.1 M TBAH.

4.4 Conclusion

$[Fe(dophen)(N\text{-}MeIm)_2]^+$ is an active catalyst for the electroreduction of CO_2 to carbon monoxide, formate and oxalate in DMSO and DMF. The rate of catalytic reduction is enhanced by weak Brönsted acids such as 2,2,2-trifluoroethanol and methanol. The presence of weak Brönsted acid also increase the relative amount of CO produced but the major product is still formate. *In-situ* FTIR studies revealed the presence of an iron carbonyl and an iron formato species during the course of reduction. The formation of CO and $HCOO^-$ probably occur via two different competing pathways

Chapter 5

Conclusions

The recycling of carbon dioxide for fuels and chemicals is a goal which can only be achieved with a thorough understanding of the catalytic processes, particularly electrocatalysis whereby redox transformation can be interfaced with solar or nuclear energy. In the studies so far, the reduction products in homogeneous catalytic reactions have been limited mostly to the two-electron reduction products CO and $HCOO^-$. It has been proposed that the formation of CO and $HCOO^-$ arise from different pathways.

In this project, we have investigated the electrochemical reduction of CO_2 catalyzed by two ruthenium carbonyl complexes namely $[Ru(bdmpp)(bpy)CO]^{2+}$ **[1]** and $[Ru(tpm)(bpy)CO]^{2+}$ **[2]** (bdmpp = 2,6'-bis(3,5-dimethylpyrazolyl)pyridine); tpm = tris(1-pyrazoyl)methane; bpy = 2,2'-bipyridine). In the presence of complex **[1]** and 5.0 M H_2O (pK_a = 2.2-2.35) as proton source, the electrocatalytic reduction of CO_2 produced exclusively CO with a current efficiency of 98%. In the presence of $Et_3NH^+Cl^-$ (pK_a = 16.8) selective production of formate could be achieved with a current efficiency close to 90% catalyzed by complexes **[1]**. For complex **[2]**, only CO was produced in the presence of H_2O while 76% of formate could be afforded in the presence of $Et_3NH^+Cl^-$. Our results revealed that product from electrolysis depends on the acidity of the weak proton sources in the electrolyte.

In-situ FTIR spectroelectrochemistry was used to probe the different mechanistic pathways that lead to the production of CO and $HCOO^-$ respectively. Bands assignable to the formation of the CO_2 adduct — $[Ru(bdmpp)(bpy)(CO_2)]^0$ (ν = 1587 cm^{-1}, 1171 cm^{-1}) were observed during the electrolysis in CO_2-saturated acetonitrile in the presence of H_2O. On the contrary, the IR spectra of **[1]** during the electrolysis in the presence of $Et_3NH^+Cl^-$ revealed the presence of the Ru-H species but

no sign of the CO_2 adduct. Furthermore, it was evidenced that ruthenium formato species (ν = 1377 cm^{-1}, 1580 cm^{-1}) was formed at the expense of the ruthenium hydrido intermediate. Formation of $HCOO^-$ could be observed by the growth in absorption intensity at 1605 cm^{-1}. Similar results were also afforded when complex **[2]** was used as electrocatalyst. On basis of the spectroscopic studies, mechanisms for the formation of formate and carbon monoxide in the electrocatalytic of CO_2 are proposed. We favored the opinion that the formation of a metal-hydride species followed by the insertion of CO_2 into M-H bond is the key step for the formation of formate.

We have also studied the electrochemical reduction of CO_2 catalyzed by $[Fe(dophen)(N\text{-}MeIm)_2]^+$ **[3]**. Addition of weak Brönsted acids such as trifluoroethanol or methanol enhance the rate of catalysis. When complex **[3]** was employed as the electrocatalyst, a mixture of carbon monoxide, formate and oxalate was produced. Monitoring the reduction process by *in-situ* FTIR spectroelectrochemistry showed the existence of both an iron carbonyl and an iron formato intermediates. We proposed CO was produced by successive protonation of the coordinated CO_2 by the Brönsted acids followed by the cleavage of one C-O bond and subsequently release of CO from the iron center of the iron carbonyl species. The homolytic cleavage of Fe-C bond of Fe-η^1-CO_2 will lead to the formation of $CO_2^{\bullet-}$ which will then dimerize to yield oxalate.

Our results showed that product selectivity could be adjusted by using different proton sources in the ruthenium system. Highly selective production of formate is favored by weak proton sources such as protonated alkyl amine that cannot form hydrogen bonding with CO_2 in the electrolyte. Detailed spectroelectrochemical study on the Fe(dophen) systems was limited by its poor solubility in CH_3CN. Based on the

results obtained in DMSO, it seems that the formation of a very reactive Fe-H species is kinetically fast. Hence formate was usually formed as the major product but hydrogen gas can also be obtained depending on the proton source available. Our results also revealed that no oxalate was formed during the electrolysis with the ruthenium complex **[1]** and **[2]** as catalysts. This may due to the stronger carbenoid character of the Ru-CO_2 than the Fe-CO_2 adduct, therefore suppressing the formation of free $CO_2^{\bullet-}$ in the iron system.

Our mechanistic investigations on the electrochemical reduction of CO_2 catalyzed by complex **[1]**, **[2]** and **[3]** indicate that CO is readily released from the reduced metal center. In order to obtain reduction products beyond the stage of CO and $HCOO^-$, the highly reduced metal-carbonyl intermediate must be stable enough to allow further protonation and reduction of the coordinated CO. One possible approach to achieve this is to employ metal catalysts which can form stronger metal-carbon bonds, i.e. the metal-carbonyl species should have a strong metal carbene character. This implies that the use of late transition metal catalysts is a promising approach. Another possible approach is to encapsulate the catalyst into a supporting matrix such as polymer or zeolite. Under such circumstances the displacement of the coordinated CO by solvent molecules is minimized and the metal-carbonyl intermediate should have a longer lifetime for further reaction.

References

References:

1. Scibioh, M. A. and Vijayaraghavan, V. R., "Electrocatalytic Reduction of Carbon Dioxide: Its Relevance and Importance", *Journal of Scientific and Industrial Research*, Vol. 57, pp. 111-123 (1998).

2. Fujita, E., "Photochemical Carbon Dioxide Reduction with Metal Complexes", *Coordination Chemistry Reviews*, Vol. 186, pp. 373-384 (1999).

3. Inoue, S. and Yamazaki, N. in "Organic and Bio-organic Chemistry of Carbon Dioxide", Kodansha, Tokyo (1981).

4. Christensen, P. A., Hamnett, A. and Timney, J. A., "An In Situ Infrared Study of CO_2 Reduction Catalyzed by Rhenium Tricarbonyl Bipyridyl Derivatives", *Journal of the Chemical Society, Dalton Transactions*, pp. 1455-1463 (1992).

5. Tanaka, T. and Tanaka, K., "Electrochemcial CO_2 Reduction Catalyzed by $[Ru(bpy)_2(CO)_2]^{2+}$ and $[Ru(bpy)_2(CO)Cl]^{+}$. The effect of pH on the Formation of CO and COO^{-}", *Organometallics*, Vol. 6, pp. 181-186 (1987).

6. Bolinger, C. M., Sullivan, B. P. and Meyer, T. -J., "Electrocatalytic Reduction of CO_2 Based on Polypyridyl Complexes of Rhodium and Ruthenium", *Chemical Communications*, pp. 796-797 (1985).

7. Collin, J. P. and Suvage, J. P., "Electrochemical Reduction of Carbon Dioxide Mediated by Molecular Catalysts", *Coordination Chemistry Reviews*, Vol. 93, pp. 245-268 (1989).

8. Sullivan, B. P., Krist, K. and Gruard, H. E., "Electrochemical and Electrocatalytic Reactions of Carbon Dioxide", *Elsevier, Amsterdam* (1993).

9. Blinn, E. L., Gundlach, E. M., Kelly, C. A., Koch, B., Luo, F. and Mejeritshaia, E., "The Reduction of Carbon Dioxide Employing 1,4,7,10-tetramethyl-

1,4,7,10tetraazacyclododecane nickel (II) as a Electron Relay Catalyst", *Inorganica Chimica Acta*, Vol. 246, pp. 295-299 (1996).

10. Hori, Y., Takahashi, R., Yoshinami, Y. and Murata, A., "Electrochemical Reduction of CO at a Copper Electrode", *Journal of Physical Chemistry B*, Vol. 101, pp. 7075-7081 (1997).

11. Behar, D., Dhanasekaran, T., Neta, P., Hosten, C. M., Ejeh, D., Hambright, P. and Fujita, E., "Cobalt Porphyrin Catalyzed Reduction of CO_2. Radiation Chemical, Photochemical, and Electrochemical Studies", *Journal of Physical Chemistry Part A*, Vol. 102, pp. 2870-2877 (1998).

12. Paul, P., Tyagi, B., Bilakhiya, A. K., Bhadbhade, M. M., Suresh, E. and Ramachandraiah, G., "Synthesis and Characterization of Rhodium Complexes Containing 2,4,6-Tris(2-pyridyl)-1,3,5-triazine and Its Metal-Promoted Hydrolytic Products: Potential Uses of the New Complexes in Electrocatalytic Reduction of Carbon Dioxide", *Inorganic Chemistry*, Vol. 37, pp. 5733-5742 (1998).

13. Arana, C. R., Casado, C., Cuadrado, I., Abruna, H. D. and Jr., G. C., "Electrocatalytic Reduction of Carbon Dioxide Mediated by Transition Metal Complexes with Terdentate Ligands Derived from Diacetylpyridine", *Inorganica Chimica Acta*, Vol. 300, pp. 32-4 (2000).

14. Bilewicz, R., Jarzebinkska, A., Rowinski, P., Zawisza, I., Siegfried, L. and Kaden, T., "Modified Electrode Surfaces for Catalytic Reduction of Carbon Dioxide", *Analytica Chimica Acta*, Vol. 396, pp. 1-12 (1999).

15. Szalda, D. J. and Fujita, E., "Crystallization and Structure of a Binuclear Species Containing the Co-C(OH)-O-Co Moiety", *Inorganica Chimica Acta*, Vol. 297, pp. 139-144 (2000).

16. Meyer, T. -J. and Downard, A., "Electrocatalytic Reduction of CO_2 by Associative Activation", *Organometallics*, Vol. 7, pp. 238-240 (1988).

17. Fujiki, K., Ohba, T. and Ohkubo, K., "Ligands Effects of Ruthenium 2,2'-Bipyridine and 1,10-Phenanothroline Complexes on the Electrochemical Reduction of CO_2", *Journal of the Chemical Society, Dalton Transactions*, pp. 2155-2160 (1990).

18. Ishida, H., Tanaka, K., Morimoto, M. and Tanaka, T., "Isolation of Intermediates in the Water Gas Shift Reactions Catalyzed by $[Ru(bpy)_2(CO)Cl]^+$ and $[Ru(bpy)_2(CO)_2]^{2+}$", *Organometallics*, Vol. 5, pp. 724-730 (1986).

19. Toyohara, K., Nagao, H., Mizukawa, T. and Tanaka, K., "Ruthenium Formyl Complexes as the Branch Point in Two- and Multi-Electron Reductions of CO_2", *Inorganic Chemistry*, Vol. 34, pp. 5399-5400 (1995).

20. Nagao, H., Mizukawa, T. and Tanaka, K., "Carbon-carbon Bond Formation in the Electrochemical Reduction of Carbon Dioxide Catalyzed by a Ruthenium Complex", *Inorganic Chemistry*, Vol. 33, pp. 3415-3420 (1994).

21. Nakajima, H., Kushi, Y., Nagao, H. and Tanaka, K., "Multistep CO_2 Reduction Catalyzed by $[Ru(bpy)_2(qu)(CO)]^{2+}$ (bpy = 2,2'-Bipyridine, qu = Quinoline). Double Methylation of the Carbonyl Moiety Resulting from Reductive Disproportionnation of CO_2", *Organometallics*, Vol. 14, pp. 5093-5098 (1995).

22. Ishida, H., Tanaka, H., Tanaka, K. and Tanaka, T., "Selective Formation of $HCOO^-$ in the Electrochemical CO_2 Reduction catalyzed by $[Ru(bpy)_2(CO)_2]^{2+}$ (bpy = 2,2'-bipyridine)", *Chemical Communications*, pp. 131-132 (1987).

23. Pugh, J. R., Bruce, M. R. M., Sullivan, P. B. and Meyer, T. -J., "Formation of Metal-Hydride Bond and the Insertion of CO_2. Key Steps in the Electrocatalytic

Reduction of Carbon Dioxide to Formate Anion", *Inorganic Chemistry*, Vol. 36, pp. 86-91 (1991).

24. Mizukawa, T., Tsuge, K., Nakajima, H. and Tanaka, K., "Selective Production of Acetone in the Electrochemical Reduction of CO_2 Catalyzed by a Ru-Naphthyridine Complex", *Chemical Communications*, Vol. 38, pp. 362-363 (1999).

25. Sato, H., Tsuge, K. and Tanaka, K., "Selective Formation of HCO_2^- and $C_2O_4^{2-}$ in Electrochemical Reduction of CO_2 Catalyzed by Mono- and Di-nuclear Ruthenium Complexes", *Chemical Communications*, pp. 249-250 (1998).

26. Bolinger, C. M., Meyer, T. -J. and Sullivan, B. P., "Electrocatalytic Reduction of Carbon Dioxide by 2,2'-Bipyridine Complexes of Rhodium and Iridium", *Inorganic Chemistry*, Vol. 27, pp. 4582-4587 (1988).

27. Hori, Y., Wakebe, H., Tsukamoto, T. and Koga, O., "Electrocatalytic Process of CO Selectivity in Electrochemical Reduction of CO_2 at Metal Electrode in Aqueous Media", *Electrochimica Acta*, Vol. 39, pp. 1833-1839 (1994).

28. Hori, Y., Murata, A., Takahashi, R. and Suzuki., S., "Electroreduction of CO to CH_4 and C_2H_4 at a Copper Electrode in Aqueous Solutions at Ambient Temperature and Pressure", *Journal of the American Chemical Society*, Vol. 109, pp. 5022-5023 (1987).

29. Sullivan, B. P., Bolinger, C. M. and Meyer, T. -J., "One- and Two-electron Pathways in the Electrocatalytic Reduction of CO_2 by *fac*-Re(bpy)$(CO)_3$Cl (bpy = 2,2'-bipyridine)", *Chemical Communications*, pp. 1414-1417 (1985).

30. Collin, J. P., Sauvage, J. P. and Beley, M., "Nickel(II)-Cyclam: an Extremely Selective Electrocatalysts for Reduction of CO_2 in Water", *Chemical Communications*, pp. 1315-1316 (1984).

31. Tominaga, K. I., Sasaki, Y. and Kawai, M., "Ruthenium Complex Catalyzed by Hydrogenation of Carbon Dioxide to Carbon Monoxide, Methanol and Methane", *Chemical Communications*, pp. 629-631 (1993).

32. Behr, A., *"Carbon Dioxide Activation by Metal Complexes"*, Weinheim, New York, pp. 1-8 (1998).

33. Hori, Y., Kikuchi, K. and Suzuki, S., "Production of CO and CH_4 in Electrochemical Reduction of CO_2 at Metal Electrodes in Aqueous Hydrogencarbonate Solution", *Chemistry Letters*, pp. 1695-1698 (1985).

34. Hori, Y., Kikuchi, K. and Murata, A., "Production of Methane and Ethylene in Electrochemical Reduction of Carbon Dioxide at Copper Electrode in Aqueous Hydrogencarbonoate Solution", *Chemistry Letters*, pp. 897-898 (1986).

35. Hori, Y., Murata, A. and Ito, S., "Enhanced Evolution of CO and Suppressed Formation of Hydrocarbons in Electroreduction of CO_2 at a Copper Electrode Modified with Cadmium", *Chemistry Letters*, pp. 1231-1234 (1990).

36. Nagaoka, T. and Ogura, K., "Electrocatalytic Reduction of Carbon Dioxide by Substituted Pyridine and Pyrazole Complexes of Palladium", *Electrochimica Acta*, Vol. 41, pp. 2773-2780 (1996).

37. Dubois, D. L., "Development of Transition Metal Phosphine Complexes as Electrocatalysts for CO_2 and CO Reduction", *Comments on Inorganic Chemistry*, Vol. 19, pp. 307-325 (1997).

38. Deronizer, A. and Zissel, R., "Electrocatalytic Reduction of Carbon Dioxide with Mono(bipyridine)carbonylruthenium Complexes in Solution or as Polymeric Thin Films", *Inorganic Chemistry*, Vol. 33, pp. 2961-2967 (1994).

39. Deronizer, A. and Ziessel, R., "Electrocatalytic Reduction of CO_2 in Water on Polymeric $[\{Ru^0(bpy)(CO)_2\}_n]$ (bpy = 2,2'-bipyridine) Complex Immobilized on Carbon Electrode", *Chemical Communications*, pp. 189-191 (1994).

40. Deronizer, A., Ziessel, R. and Zsoldos, D., "Formation of Polymeric $[\{Ru^0(bpy)(CO)_2\}_n]$ Films by Electrochemical Reduction of $[Ru(bpy)_2(CO)_2](PF_6)_2$: Its Implication in CO_2 Electrocatalytic Reduction", *Inorganic Chemistry*, Vol. 33, pp. 4410-4412 (1994).

41. Deronizer, A., Cosnier, S. and Moutet, J. -C., "Subsitution Effects on the Electrochemical Behavior of the (2,2'-bipyridine) Tricarbonylchlororhenium (I) Complex in Solution or in Polymeric Form and their Relation to the Catalytic Reduction of Carbon Dioxide", *New Journal of Chemistry*, Vol. 14, pp. 831-839 (1990).

42. Yoshida, T. and Iida, T., "Electrocatalytic Reduction of Carbon Dioxide in Aqueous Medium by Bis(2,2':6',2"-terpyridine)cobalt (II) Complex Incorporated into a Coated Polymer Membrane", *Journal of Electroanalytical Chemistry*, Vol. 344, pp. 355-362 (1993).

43. Arana, C., Keshavarz, M. and Potts, K. T., "Electrocatalytic Reduction of CO_2 and O_2 with Electropolymerized Films of Vinyl-terpyridine Complexes of Fe, Ni and Co", *Inorganica Chimica Acta*, Vol. 225, pp. 285-295 (1994).

44. Deronizer, A., Moutet, J. -C. and Cosnier, S., "Electrochemical Coating of a Platinum Electrode a Poly(pyrrole) Film containing the *fac*-Re(2,2'-

bipyridine)$(CO)_3Cl$ System", *Journal of Electroanalytical Chemistry*, Vol. 207, pp. 315-321 (1986).

45. Arana, C. R., Potts, K. T. and Sende, J. M. R., "Electrocatalysis of CO_2 Reduction in Aqueous Media at Electrodes Modified with Electropolymerized Films of Vinylterpyridine Complexes of Transition Metals", *Inorganic Chemistry*, Vol. 34, pp. 3339-3348 (1995).

46. Sullivan, B. P., Meyer, T. -J., Downard, A. and Megehee, E., "Electrocatalytic Reduction of Carbon Dioxide Based on 2,2'-Bipyridyl Complexes of Osmium", *Inorganic Chemistry*, Vol. 31, pp. 4864-4873 (1992).

47. Deronizer, A., Zsoldos, D. and Ziessel, R., "Selective Synthesis and Electrochemical Behavior of *trans*(Cl)- and *cis*(Cl)-$[Ru(bpy)(CO)_2Cl_2]$ Complexes (bpy= 2,2'-bipyridine). Comparative Studies of their Electrocatalytic Activity toward the Reduction of Carbon Dioxide", *Inorganic Chemistry*, Vol. 36, pp. 5384-5389 (1997).

48. Deronizer, A., Ziessel, R. and Zsoldos, D., "Electroreduction of CO_2 Catalyzed by Polymeric $[Ru(bpy)(CO)_2]_n$ Films in Aqueous Media: Parameters Influencing the Reaction Activity", *Journal of Electroanalytical Chemistry*, Vol. 444, pp. 253-260 (1998).

49. Lehn, J. -C., Ziessel, R. and Hawecker, J., "Electrocatalytic Reduction of Carbon Dioxide Mediated by $Re(bipy)(CO)_3Cl$(bipy = 2,2'-bipyridine)", *Chemical Communications*, pp. 328-330 (1984).

50. Johnson, F. P. A., George, M. W. and Hartl, F., "Electrocatalytic Reduction of CO_2 Using the Complexes $[Re(bpy)(CO)_3L]^n$ (n = +1, L = $P(OEt)_3$, CH_3CN; n = 0, L = Cl^-, Otf^-; bpy = 2,2'-bipyridine; Otf^- = CF_3SO_3) as Catalysts Precursors:

Infrared Spectroelectrocemical Investigation", *Organometallics*, Vol. 15, pp. 3374-3387 (1996).

51. Blaine, C. A., Hill, M. G., Mann, K. R. and Cheng, S. C., "Electrochemical and IR Spectroelectrochemical Studies of the Electrocatalytic Reduction of Carbon Dioxide by $[Ir_2(dimen)_4]^{2+}$ (dimen = 1,8-Diisocyanomenthane)", *Inorganic Chemistry*, Vol. 35, pp. 7704-7708 (1996).

52. Cabrera, C. R. and Abruna, H. D., "Electrocatalysis of CO_2 Reduction at Surface Modified Metallic and Semiconducting Electrode", *Journal of Electroanalytical Chemistry*, Vol. 209, pp. 101-107 (1986).

53. Dyson, P. J., Humphery, D. G., Clark, R. J. H. and Johnson, F. G., "In situ Infrared Spectroelectrochemical Studies of $[Ru_6C(CO)_{17}]$ and $[Ru_6C(CO)_{16}]^{2-}$: the Redox Induced Conversion of Carbon Monoxide to Carbon Dioxide", *Polyhedron*, Vol. 17, pp. 2985-2991 (1998).

54. Christensen, P. A. and Higgins, S. J., "The Electrochemical Reduction of CO_2 to Oxalate at a Pt Electrode Immersed in Acetonitrile and Coated with Polyvinylalcolol/$[Ni(dppm)_2Cl_2]$", *Journal of Electroanalytical Chemistry*, Vol. 387, pp. 127-132 (1995).

55. Savéant, J. M. and Amatore, C., "Mechanism and Kinetic Characteristics of the Electrochemical Reduction of Carbon Dioxide in Media of Low Proton Availability", *Journal of the American Chemical Society*, Vol. 103, pp. 5021-5023 (1981).

56. Haines, R. J., Wittrig, R. E. and Kubiak, C. P., "Electrocatalytic Reduction of Carbon Dioxide by the Binuclear Copper Complex $[Cu_2$(6-(diphenylphosphino)-

2,2'-bipyridyl)$_2$(MeCN)$_2$][PF$_6$]$_2$", *Inorganic Chemistry*, Vol. 33, pp. 4723-4728 (1994).

57. Deronizier, A., Caix, C. and Noblat, S. C., "Electrocatalytic Reduction of CO_2 into Formate with $[\eta^5\text{-}Me_5C_5)M(L)Cl]^+$ Complexes (L = 2,2'-bipyridine ligands; M= Rh(III) and Ir(III))", *Journal of Electroanalytical Chemistry*, Vol. 434, pp. 163-170 (1997).

58. Tanaka, K., Kushi, Y., Tsuge, K., Toyohara, K., Nishioka, T. and Isobe, K., "Catalytic Generation of Oxalate through a Coupling Reaction of Two CO_2 Molecules Activated on $[Ir(\eta^5\text{-}C_5Me_5))_2(Ir(\eta^4\text{-}C_5Me_5)CH_2CN)(\mu^3\text{-}S)_2]$", *Inorganic Chemistry*, Vol. 37, pp. 120-126 (1998).

59. Kaneco, S., Iiba, K., Ohta, K. and Mizuno, T., "Electrochemical CO_2 Reduction on a Copper Wire Electrode in Tetraethylammonium Perchlorate + Methanol at Extremely Low Temperature", *Energy Sources*, Vol. 21, pp. 643-648 (1999).

60. Nicholas, K. M. and Tsai, J. C., "Rhodium-Catalyzed Hydrogenation of Carbon Dioxide to Formic Acid", *Journal of the American Chemical Society*, Vol. 114, pp. 5117-5124 (1992).

61. Daniele, S. and Ugo, P., "An Electroanalytical Investigation on the Nickel-Promoted Electrochemical Conversion of CO_2 to CO", *Journal of Electroanalytical Chemistry*, Vol. 219, pp. 259-271 (1987).

62. Lewis, N. S., Miskelly, G. M. and Schmidt, M. H., "Effects of Redox Potential, Steric Configuration, Solvent, and Alkali Metal Cations on the Binding of Carbon Dioxide to Cobalt(I) and Nickel(I) Macrocycles", *Journal of the American Chemical Society*, Vol. 112, pp. 3420-3426 (1990).

63. Bilewicz, R., Bujno, K., Siegfried, L. and Kaden, T. A., "Effects of Ligand Structure on the Adsorption of Nickel Tetraazamarcocyclic Complexes and Electrocatalytic CO_2 Reduction", *Journal of Electroanalytical Chemistry*, pp. 47-53 (1998).

64. Dubois, D. K., Noll, B. C. and Miedaner, A., "Synthesis and Characterization of Palladium and Nickel Complexes with Positively Charged Triphosphine Ligands and Their Use as Electrochemical CO_2-Reduction Catalysts", *Organometallics*, Vol. 16, pp. 5779-5791 (1997).

65. Hori, Y., Murata, A., Takahashi, R. and Suzuki, S., "Enhanced Formation of Ethylene and Alcohols at Ambient Temperature and Pressure in Electrochemical Reduction of Carbon Dioxide at a Copper Electrode", *Chemical Communications*, pp. 17-19 (1988).

66. Savéant, J. M., Lexa, D. and Bhugun, I., "Catalysis of the Electrochemical Reduction of Carbon Dioxide by Iron(0) Porphyrins: Synergystic Effect of Weak Brönsted Acids", *Journal of the American Chemical Society*, Vol. 118, pp. 1769-1776 (1996).

67. Davis, D. G. and Constant, L. A., "Electrochemical Characterization of Iron Porphyrin Complexes in Aprotic Solvents", *Analytical Chemistry*, Vol. 47, pp. 2253-2260 (1975).

68. Lexa, D., Hammouche, M. and Momenteau, M., "Chemcial Catalysis of Electrochemical Reactions- Homogeneous Catalysis of the Electrochemical Reduction of Carbon Dioxide by Iron(0) Porphyrins - Role of the addition of Magnesium Cations", *Journal of the American Chemical Society*, Vol. 113, pp. 8455-8466 (1991).

69. Deronzier, A., Cecillon, C. C., Noblat, S. C., Haukka, M., Pakkanen, T. A. and Zsoldos, D., "Electrochemical Formation and Spectroelectrochemical Characterization of Organometallic $[Ru(L)(CO)_2]_n$ Polymers; L = disubstituted-2,2'-bipyridine", *Journal of Electroanalytical Chemistry*, Vol. 466, pp. 187-196 (1999).

70. Ichikawa, M., Tamaru, K. and Meshitsuka, S., "Electrocatalysis by Metal Phthalocyanines in the Reduction of Carbon Dioxide", *Chemical Communications*, pp. 158-159 (1974).

71. Kapusta, S. and Hackerman, N., "Carbon Dioxide Reduction at a Metal Phthalocyanine Catalyzed Carbon Electrode", *Journal of Electrochemical Society*, pp. 1511-1514 (1984).

72. Lewis, N. S. and Lieber, C. M., "Catalytic Reduction of CO_2 at Carbon Electrodes Modified with Cobalt Phthalocyanine", *Journal of the American Chemical Society*, Vol. 106, pp. 5033-5034 (1984).

73. Furuya, N. and Matsui, K., "Electroreduction of Carbon Dioxide on Gas-diffusion Electrodes Modified by Metal Phthalocyanines", *Journal of Electroanalytical Chemistry*, Vol. 1989, pp. 181-191 (1989).

74. Furuya, N. and Koide, S., "Electroreduction of Carbon Dioxide by Metal Phthalocyanines", *Electrochimica Acta*, Vol. 36, pp. 1309-1313 (1991).

75. Christensen, P. A., Hamnett, A. and Muir, A. V. G., "An In-Situ FTIR Study of the Electroreduction of CO_2 by CoPc-coated Edge Graphite Electrodes", *Journal of Electroanalytical Chemistry*, Vol. 241, pp. 361-371 (1988).

76. Hiratisuka, K., Takahashi, K., Sasaki, H. and Toshima, S., "Electrocatalytic Behavior of Tetrasulfonated Metal Phthalocyanines in the Reduction Of Carbon Dioxide", *Chemistry Letters*, pp. 1137-1140 (1977).

77. Takahashi, K., Hiratsuka, K., Sasaki, H. and Toshima, S., "Electrocatalytic Behavior of Metal Porphyrins in the Reduction of Carbon Dioxide", *Chemistry Letters*, pp. 305-308 (1979).

78. Ohkaoo, K., NOguchi, Y. and Nakayama, S., "Electrochemical Reduction of Carbon Dioxide on Hydrogen Storing Materials", *Journal of Electroanalytical Chemistry*, Vol. 348, pp. 459-464 (1993).

79. Nation, A., Ohta, K. and Mizune, T., "Electrochemical Reduction of Carbon Dioxide in Methanol at Low Temperature", *Electrochimica Acta*, Vol. 38, pp. 2177-2179 (1993).

80. Hori, Y., Kikuchi, K. and Suzuki, S., "Electrochemical Reduction of Carbon Dioxide to Carbon Monoxide at a Gold Electrode in Aqueous Potassium Hydrogen Carbonate", *Chemical Communications*, Vol. 10, pp. 728-729 (1987).

81. Ito, K., Ikeda, S. and Iida, T., "Electrochemical Reduction of Carbon Dioxide Dissolved under High-pressure. 2. In Aqueous-solutions of Tetraalkylammonium Salts", *Denki Kagaku*, Vol. 49, pp. 106-112 (1981).

82. Kaneco, S., Iiba, K., Ohta, K., Mizuno, T. and Saji, A., "Electrochemical Reduction of CO_2 at Ag Electrode in KOH-methanol at Low Temperature", *Electrochimica Acta*, Vol. 44, pp. 573-578 (1998).

83. Kaneco, S., Iiba, K., Hiei, K. H., Ohta, K., Mizuno, T. and Suzuki, T., "Electrochemical Reduction of Carbon Dioxide to Ethylene with High Faradaic Efficiency at a Cu Electrode in CsOH/methanol", *Electrochimica Acta*, Vol. 44, pp. 4701-4706 (1999).

84. Avramov-Ivic, M. L., Vukovic, N. B. and Popic, J. P., "Reduction of Carbon Dioxide on Ruthenium Oxide and Modified Ruthenium Oxide Electrodes in 0.5

M $NaHCO_3$", *Journal of Electroanalytical Chemistry*, Vol. 421, pp. 105-110 (1997).

85. Inui, T., Anpo, M., Izui, K., Yangida, S. and Yamaguchi, T., "Electrochemical Reduction of Carbon Dioxide at a Platinum Electrode in Acetonitrile-water Mixtures", *Studies in Surface Science and Catalysis*, Vol. 114, pp. 581-584 (1998).

86. Jermann, B. and Augustynski, J., "Long-term Activation of the Copper Cathode in the Course of CO_2 Reduction", *Electrochimica Acta*, Vol. 39, pp. 1891-1896 (1994).

87. Frese, K. W. and Leach, J. S., "Electrochemical Reduction of Carbon-dioxide to Methane, Methanol, and CO on Ru Electrodes", *Journal of Electrochemical Society*, Vol. 132, pp. 259-260 (1985).

88. Summers, D. P., Leach, S. and Frese, K. W., "The Electrochemical Reduction of Aqueous Carbon Dioxide to Methanol at Molybdenum Electrodes with Low Overpotentials", *Journal of Electrochemical Society*, Vol. 205, pp. 219-232 (1986).

89. Bhugun, I., Savéant, J. M. and Lexa, D., "Ultraefficient Selective Homogeneous Catalysis of the Electrochemical Reduction of Carbon Dioxide by an Iron("0") Porphyrin Associated with a Weak Brönsted Acid Catalyst", *Journal of the American Chemical Society*, Vol. 116, pp. 5015-5016 (1994).

90. Fisher, B. and Eisenberg, R., "Electrocatalytic Reduction of Carbon Dioxide by using Macrocycles of Nickel and Cobalt", *Journal of the American Chemical Society*, Vol. 131, pp. 7361-7363 (1980).

91. Thewissen, D. H. M. W., Tinnemans, A. H. A. and Vanderzouwenassink, E. A., "Photoelectrochemcial Properties of Alpha-Znp2 and Beta-Anp2 Electrodes and Powders", *Journal of Electrochemical Society*, Vol. 131, pp. 2048-2054 (1984).

92. Tezuka, M. and Iwasaki, M., "Voltammetric Study on CO_2 Reduction Electrocatalyzed by Cobalt Tetraphenylporphine in DMF", *Chemistry Letters*, Vol. 3, pp. 427-430 (1993).

93. Atoguchi, T., Aramata, A. and Kazusaka, A., "Cobalt (II) Tetraphenylporphyrin Pyridine Complex Fixed on a Glassy-carbon Electrode and Its Prominent Cataltyic Activity for Reduction of Carbon-dioxide", *Chemical Communications*, Vol. 3, pp. 156-157 (1991).

94. Beley, M., Collin, J. P. and Ruppert, R., "Nickel (II) Cyclam - an Extremely Selective Electrocatalysts for Reduction of CO_2 in Water", *Chemical Communications*, Vol. 19, pp. 1315-1316 (1984).

95. Beley, M., Collin, J. P. and Ruppert, R., "Electrocatalytic Reduction of CO_2 by $NiCyclam^{2+}$ in Water- Study of the Factors Affecting the Efficiency and the Selectivity of the Process", *Journal of the American Chemical Society*, Vol. 108, pp. 7461-7467 (1986).

96. Collin, J. P., Jouaiti, A. and Sauvage, J. P., "Electrocatalytic Properties of $Ni(Cyclam)^{2+}$ and $Ni_2(biscyclam)^{4+}$ with Respect to CO_2 and H_2O Reduction", *Inorganic Chemistry*, Vol. 27, pp. 1986-1990 (1988).

97. Kushi, Y., Nagao, H. and Nishioka, T., "Oxalate Formation in Electrochemical CO_2 Reduction Catalyzed by Rhodium-Sulfur Cluster", *Chemistry Letters*, Vol. 11, pp. 2175-2178 (1994).

98. Koshi, Y., Nagao, H. and Nishioka, T., "Remarkable Decrease in Overpotential of Oxalate Formation in Electrochemcial CO_2 Reduction by a Metal-Sulfide Cluster", *Chemical Communications*, Vol. 12, pp. 1223-1224 (1995).

99. Ratliff, K. S., Lentz, R. E. and Kubiak, C. P., "Carbon Dioxide Chemistry of the Trinuclear Complex $[Ni_3(Mu\text{-}CNME)(Mu\text{-}3\text{-}I)(Dppm)_3][PF_6]$ - Electrocatalytic Reduction of Carbon Dioxide", *Organometallics*, Vol. 11, pp. 1986-1988 (1992).

100. Tezuka, M., Yajima, T. and Tsuchiya, A., "Electroreduction of Carbon Dioxide Catalyzed by Iron Sulfur Clusters", *Journal of the American Chemical Society*, Vol. 104, pp. 6834-6836 (1982).

101. Balazs, G. B. and Anson, F. C., "The Adsorption of $Ni(cyclam)^+$ at Mercury-Electrodes and Its Relation to the Electrocatalytic Reduction of CO_2", *Journal of Electroanalytical Chemistry*, Vol. 322, pp. 325-345 (1992).

102. Dubois, D. L. and Miedaner, A., "Mediated Electrochemical Reduction of CO_2 - Preparation and Comparison of an Isoelectronic Series of Complexes", *Journal of the American Chemical Society*, Vol. 109, pp. 113-117 (1987).

103. Dubois, D. L., Miedaner, A. and Haltiwanger, R. C., "Electrochemical Reduction of CO_2 Catalyzed by $[Pd(triphosphine)(Solvent)](BF_4)_2$ Complexes - Synthetic and Mechanistic Studies", *Journal of the American Chemical Society*, Vol. 113, pp. 8753-8764 (1991).

104. Wagenknecht, J. H. and Slater, S., "Electrochemical Reduction of CO_2 Catalyzed by $Rh(diphos)_2Cl$", *Journal of the American Chemical Society*, Vol. 106, pp. 5367-5368 (1984).

105. Ogura, K., Nagaoka, T. and Hossain, A. G. M. M., "Palladium and Cobalt Complexes of Substituted Quinoline, Bipyridine and Phenanthroline as Catalysts

for Electrochemical Reduction of Carbon Dioxide", *Electrochimica Acta*, Vol. 42, pp. 2577-2585 (1997).

106. Wong, K. Y., Chung, W. H. and Lau, C. P., "The Effect of Weak Brönsted Acids on the Electrocatalytic Reduction of Carbon Dioxide by a Rhenium Biypyridyl Complex", *Journal of Electroanalytical Chemistry*, Vol. 453, pp. 161-170 (1998).

107. Hori, Y., Kikuchi, K. and Suzuki, S., "Production of CO and CH_4 in Electrochemical Reduction of Hydrogencarbonate Solution", *Chemistry Letters*, Vol. 11, pp. 1695-1698 (1985).

108. Meyer, T. -J., Murray, R. W. and Margerum, L. D., "Electrocatalytic Reduction of CO_2 at a Chemically Modified Electrode", *Chemical Communications*, pp. 1416-1417 (1985).

109. Vijayaraghavan, V. R. and Scibioh, M. A., "Electrochemical Reduction of Carbon Dioxide using Nickel(II) Marrocyclic Complex of 1,3,6,9,11,14-Hexaazacyclohexadecane as Catalyst in Water at HMDE", *Bulletin of Electrochemistry*, Vol. 13, pp. 275-279 (1997).

110. Brewer, K. J., Place, H., Yi, E., Richter, M. M. and Rasmussen, S. C., "Synthesis and Characterization of a Series of Novel Rhodium and Iridium Complexes Containing Polypyridyl Bridging Ligands: Potential Uses in the Development of Multimetal Catalysts for Carbon Dioxide Reduction", *Inorganic Chemistry*, Vol. 29, pp. 3926-3932 (1990).

111. Hawecker, J., Lehn, J. M. and Zissel, R., "Efficient Photochemical Reduction of CO_2 to CO by Visible-Light Irradiation of Systems Containing $Re(bipy)(CO)_3X$ or $Ru(bipy)_3^{2+}$ - CO_2 + Combination as Homogeneous Catalysts", *Chemical Communications*, Vol. 9, pp. 536-538 (1983).

112. Mochizuki, K., Manaka, S., Takeda, I. and Kondo, T., "Synthesis and Structure of [6,6'-Bis(5,7-dimethyl-1,4,8,11-tetraazacyclotetradecane)]dinickel(II) Triflate and Its Catalytic Activity for Photochemical CO_2 Reduction", *Inorganic Chemistry*, Vol. 35, pp. 5132-5136 (1996).

113. Tanaka, K., Tanaka, T., Terada, T. and Ishida, H., "Photochemical CO_2 Reduction Catalyzed by $[Ru(bpy)_2(CO)_2]^{2+}$ using Triethanolamine and 1-Benzyl-1,4-dihydronicotinamide as an Electron Donor", *Inorganic Chemistry*, Vol. 29, pp. 905-911 (1990).

114. Lehn, J. M., Zissel, R. and Hawecker, J., "Photochemical Reduction of Carbon Dioxide to Formate Mediated by Ruthenium Bipyridine Complexes as Homogeneous Catalysts", *Chemical Communications*, Vol. 56-58 (1985).

115. Lehn, J. M. and Ziessel, R., "Photochemical Reduction of Carbon Dioxide to Formate Catalyzed by 2,2'-bipyridine- or 1,10-phenanothroline-ruthenium(II) Complexes", *Journal of Organometallic Chemistry*, Vol. 382, pp. 157-173 (1990).

116. Hukkanen, H. and Pakkanen, T. T., "Photochemical Catalytic Reduction of Carbon Dioxide by Visible Light Using $Ru^{II}(bipy)_3$ and $Re(CO)_3(bipy)Cl$ as Photocatalysts", *Inorganica Chimica Acta*, Vol. 114, pp. 43-45 (1986).

117. Tanaka, T., Tanaka, K. and Ishida, H., "Photochemical CO_2 Reduction by an NADH Model Compound in the Presence of $[Ru(bipy)_3]^{2+}$ and $[Ru(bipy)_2(CO)_2]^{2+}$ (bpy = 2,2'-bipyridine) in H_2O / DMF", *Chemistry Letters*, pp. 339-342 (1988).

118. Durr, H. and Trierweiler, H. P., "Application of Ru-(II)-Polypyridine Sensitizers in the Reduction of CO_2 to CH_4 and H_2-Evolution using Ru-Colloids", *New Journal of Chemistry*, Vol. 14, pp. 317-320 (1990).

119. Kimura, E., Wada, S., Shionoya, M. and Okazaki, Y., "New Series of Multifunctionalized Nickel(II)-Cyclam (Cyclam = 1,4,8,11-Tetraazacyclotetradencane) Complexes. Application to the Photoreduction of Carbon Dioxide", *Inorganic Chemistry*, Vol. 33, pp. 770-778 (1994).

120. Kimura, E., Bu, X., Shionoya, M., Wada, S. and Maruyama, S., "A New Nickel(II) Cyclam (Cyclam = 1,4,8,11-Tetraazacyclotetradecane) Complex Covalently Attached to $Ru(phen)_3^{2+}$ (phen = 1,10-phenanothroline). A New Candidate for the Catalytic Photoreduction of Carbon Dioxide", *Inorganic Chemistry*, Vol. 31, pp. 4142-4146 (1992).

121. Yanagida, S., Matsuoka, S., Yamamoto, K., Ogata, T., Kusaba, M., Nakashima, N. and Fujita, E., "Efficient and Selective Electron Mediation of Cobalt Complexes with Cyclam and Related Macrocycles in the *p*-Terphenyl-Catalyzed Photoreduction of CO_2", *Journal of the American Chemical Society*, Vol. 115, pp. 601-609 (1993).

122. Ferraudi, G., Corbin, A. J. and Kutal, C., "Further Studies of the Photoinduced Reduction of Carbon Dioxdie Mediated by Tricarbonylbromo(2,2'-bipyridine)rhenium(I)", *Organometallics*, Vol. 6, pp. 553-557 (1987).

123. Kutal, C., Weber, M. A., Ferraudi, G. and Geiger, D., "A Mechanistic Investigation of the Photoinduced Reduction of Carbon Dioxide Mediated by Tricarbonylbromo(2,2'-bipyridine)rhenium(I)", *Organometallics*, Vol. 4, pp. 2161-2166 (1985).

124. Yanagida, S., Ogata, T., Yamamoto, Y., Wada, Y., Murakoshi, K., Kusaba, M., Nakashima, N., Ishida, A. and Takamuku, S., "Phenazine-Photosensitized Reduction of CO_2 Mediated by a Cobalt-Cyclam Complex through Electron and

Hydrogen Transfer", *Journal of Physical Chemistry*, Vol. 99, pp. 11916-11922 (1995).

125. Yoneyama, H., Kubo, Y. and Inoue, H., "Photocatalytic Fixation of Carbon Dioxide in Oxoglutaric Acid using Isocitrate Dehydrogenase and Cadmium Sulphide", *Journal of the Chemical Society, Faraday Transations*, Vol. 87, pp. 553-557 (1991).

126. Hirota, K., Tryk, D. A., Yamamoto, T., Hashimoto, K., Okawa, M. and Fujishima, A., "Photoelectrochemical Reduction of CO_2 in a High Pressure CO_2 + Methanol Medium at p-Type Semiconductor Electrodes", *Journal of Physical Chemistry B*, Vol. 102, pp. 9834-9843 (1998).

127. Grodkowski, J. and Neta, P., "Cobalt Corrin Catalyzed Photoreduction of CO_2", *Journal of Physical Chemistry Part A*, Vol. 104, pp. 1848-1853 (2000).

128. Behar, D., Dhanasekaran, T. and Neta, P., "Cobalt Porphyrin Catalyzed Reduction of CO_2. Radiation, Chemical, Photochemical and Electrochemical Studies", *Journal of Physical Chemistry Part A*, Vol. 102, pp. 2870-2877 (1998).

129. Ishitani, O., Hori, H., Ishihara, J., Koike, K., Takeuchi, K. and Ibusuki, T., "Photocatalytic Reduction of Carbon Dioxide using [*fac*-Re(bpy)$(CO)_3$(4-Xpy)]$^+$ (Xpy = pyridine derivatives)", *Journal of Photochemistry and Photobiology A : Chemistry*, Vol. 120, pp. 119-124 (1999).

130. Bockris, J. O. M. and Wass, J. C., "The Photoelectrocatalytic Reduction of Carbon Dioxide", *Journal of Electrochemical Society*, Vol. 136, pp. 2521-2528 (1989).

131. Ziessel, R., Hawecker, J. and Lehn, J. -C., "Photochemical Reduction of Carbon Dioxide to Formate mediated by Ruthenium Bipyridine Complexes as Homogeneous Catalysts", *Chemical Communications*, pp. 56-58 (1985).

132. Gibson, D. H., Ding, Y., Sleadd, B. A., Richardson, J. F. and Mashutta, M. S., "Photoassistance in Reactions of the *cis*-(Bis(2,2'-bipyridyl)(carbonyl)(formyl)ruthenium (II) Cation with Protic Reagents", *Journal of the American Chemical Society*, Vol. 118, pp. 11984-11985 (1996).

133. Bard, A. J., Parson, R. and Jordan, J., "Standard Potential in Aqueous Solution", *Dekker, New York, Chapter 8* (1985).

134. Gibson, D. H., "The Organometallic Chemistry of Carbon Dioxide", *Chemistry Reviews*, Vol. 96, pp. 2063-2095 (1996).

135. Hammouche, M., Lexa, D. and Savéant, J. M., "Catalysis of the Electrochemical Reduction of Carbon Dioxide by Iron(0) Porphyrins", *Journal of Electroanalytical Chemistry*, Vol. 249, pp. 347-351 (1988).

136. Bernard, C., LeMest, Y. and Gisselbrecht, J. P., "Coordination chemistry of Iron Porphycenes in the Presence of CO, CO_2, and N-methylimidazole: Electrochemical, ESR, and UV-vis Study", *Inorganic Chemistry*, Vol. 37, pp. 181-190 (1998).

137. Thom, V. J. and Hancock, R. D., "The Stability of Nickel(II) Complexes of Tetra-azamacrocycles", *Journal of the Chemical Society, Dalton Transactions*, Vol. 9, pp. 1877-1880 (1985).

138. Billo, E. J., "Kinetics of Dissociation and Isomerization of *Cis*-Ni([14]Anen4)$(H_2O)_2^{2+}$ in Aqueous Perchloric-acid Solutions", *Inorganic Chemistry*, Vol. 23, pp. 236-238 (1984).

139. Gibson, D. H., Mashuta, S., Richardson, J. F. and Sleadd, B. A., "Chloride Labilization Resulting from Nucleophilic Addition to cis-Ru(tpy)$(CO)_2Cl^+PF_6^-$: Synthesis and Characterization of New CO_2-Bridged and Formate Complexes of Ruthenium", *Organometallics*, Vol. 16, pp. 4421-4427 (1997).

140. Christensen, P. A., Hamnett, A., Timney, J. A. and Higgins, S. J., "An In-situ Fourier Transform Infrared Study of CO_2 Electroreduction Catalysed by Ni(0)-4,4'-dimethyl 2,2'-bipyridine and Ni(0)-1,10-phenanthroline Complexes", *Journal of Electroanalytical Chemistry*, Vol. 395, pp. 195-209 (1995).

141. Sullivan, B. P. and Meyer, T. J., "Photoinduced Irreversible Insertion of CO_2 into Metal-Hydride Bond", *Chemical Communications*, pp. 1244-1245 (1984).

142. Sullivan, B. P. and Meyer, T. J., "Kinetics and Mechanism of CO_2 Insertion into a Metal-Hydride Bond. A Large Solvent Effect and an Inverse Kinetic Isotope Effect", *Organometallics*, Vol. 5, pp. 1500-1502 (1986).

143. Tanaka, K., Nagao, H., Peng, S. M. and Tanaka, H., "Crystal Structure of *cis*-(Carbon Monoxide)(η^1-carbon dioxide)bis(2,2'-bipyridyl)ruthenium, an Active Species in Catalytic CO_2 Reduction Affording CO and $HCOO^-$", *Organometallics*, Vol. 11, pp. 1450-1451 (1992).

144. Whittlesey, M. K., Perutz, R. N. and Moore, M. H., "Facile Insertion of CO_2 into Ru-H Bonds of $Ru(dmpe)_2H_2$ (dmpe = $Me_2PCH_2CH_2PMe_2$): Identification of Three Ruthenium Formate Complexes", *Organometallics*, Vol. 15, pp. 5166-5169 (1996).

145. Gibson, D. H. and Yin, X., "Synthesis and Reactions of *fac*-$Re(dmbpy)(CO)_3X$ (dmbpy = 4,4'-dimethyl-2,2'-bipyridine; X = COOH, COOMe, H, OH and OCHO)", *Journal of the American Chemical Society*, Vol. 120, pp. 11200-11201 (1998).

146. Hartl, F., Stor, G. J. and Stufkens, D. J., "Spectroelectrochemical (IR, UV/Vis) Determination of the Reduction Pathways for a Series of $[Re(CO)_3(diimine)L']^{0/+}$ (L' = Halide, Otf^-, THF, MeCN, n-PrCN, PPh_3, $P(OMe)_3$) Complexes", *Organometallics*, Vol. 14, pp. 1115-1131 (1995).

147. Hartl, F., Stufkens, D. J. and Outersterp, J. W. M. V., "Variable Temperature IR Spectroelectrochemical Investigation of the Stability of the Metal-metal-bonded Tadical Anions $[(CO)_5MnRe(CO)_3(L)]^{\cdot -}$ (L = 2,2'-bipyridine (bpy), 2,2'-bipyrimidine (bpym), 2,3-bis(2-pyridyl)pyrazine (dpp)) and $[(CO)_5MnRe(CO)_3(L)Re(Br)(CO)_3]^-$ (L = bpym, dpp) Controlled by the Lowest (Diimine) Orbital Energy", *Organometallics*, Vol. 14, pp. 3303-3310 (1995).

148. Sun, S. G. and Chen, A. C., "In Situ FTIRS Features during Oxygen Adsorption and Carbon Monoxide Oxidation at a Platinum Electrode in Dilute Alkaline Solution", *Journal of Electroanalytical Chemistry*, Vol. 323, pp. 319-328 (1992).

149. Sun, S. G., Yang, D. F. and Tian, Z. W., "In Situ FTIR Studies on the Adsorption and Oxidization of Normal-propanol and Isopropanol at a Platinum-electrode in Sulfuric-acid-solutions", *Journal of Electroanalytical Chemistry*, Vol. 289, pp. 177-189 (1990).

150. Fujita, E., Creutz, C. and Sutin, N., "Photo-induced Generation of Dihydrogen and Reduction of Carbon Dioxide using Transition Metal Complexes", *Comments of Inorganic Chemistry*, Vol. 19, pp. 67-92 (1997).

151. Tanaka, K., Yoshida, T., Adachi, T., Nagao, H. and Toyohara, K., "Crystal Structure of $[Ru(bpy)_2(CO)(\eta^1\text{-}C(O)OH)]^+$ (bpy = 2,2'-bipyridine) as a Key Intermediate in CO_2/CO Conversion", *Chemistry Letters*, pp. 27-28 (1996).

152. Jameson, D. L. and Goldsby, K. A., "2,6'-Bis(N-pyrazoyl)pyridines: the Convenient Synthesis of a Family of Planar Tridentate N_3 Ligands that are Terpyridine Analogues", *Journal of Organic Chemistry*, Vol. 55, pp. 4993-4994 (1990).

153. Bard, A. J. and Faulkner, L. R., *"Electrochemical Methods, Fundamentals and Applications"*, Wiley, New York, pp. 701 (1980).

154. Churchill, M. R., Jameson, D. L., Bessel, C. A., See, R. F. and Takeuchi, K. J., "Synthesis and Characterization of Ruthenium Complexes which utilize a New Family of Terdentate Ligands based upon 2,6'-Bis(pyrazo-1-yl)pyridine", *Journal of the Chemical Society, Dalton Transactions*, pp. 1563-1576 (1993).

155. Sasaki, Y., Ito, T., Yamaguchi, T., Nagasawa, A., Koga, N. and Morokuma, K., "Redox Regulation in Ruthenium(II) Complexes of 2,6-Bis(N-pyrazoyl)pyridine Ligands: Synthetically Verstile Analogues of 2,2':6',2"-Terpyridine", *Inorganic Chemistry*, Vol. 28, pp. 4313-4314 (1989).

156. *"Acid-base Dissociation Constants in Dipolar Aprotic Solvents"*, Oxford, Boston, (1990).

157. Lambert, J. B., Shurvell, H. F., Lightner, D. A. and Cooks, R. G., *"Organic Structural Spectroscopy"*, Prentice Hall, New Jersey, (1998).

158. Kelly, J. M. and Vos, J. G., "Synthesis, Characterization, Electrochemical Properties, Photochemical Properties, and Reactivity of Bis(2,2'-bipyridyl)hydridoruthenium Complexes", *Journal of the Chemical Society, Dalton Transactions*, pp. 1045-1048 (1986).

159. Savéant, J. M., Grass, V. and Lexa, D., "Electrochemical Generation of Rhodium Porphyrin Hydrides. Catalysis of Hydrogen Evolution", *Journal of the American Chemical Society*, Vol. 119, pp. 7526-7532 (1997).

160. Gibson, D. H., "Carbon Dioxide Coordination Chemistry: Metal Complexes and Surface-bound Species. What Relationships?", *Coordination Chemistry Reviews*, Vol. 185-186, pp. 335-355 (1999).

161. Musashi, Y. and Sakaki, S., "Theoretical Study of Ruthenium-Catalyzed Hydrogenation of Carbon Dioxide into Formic Acid. Reaction Mechanism Involving a New Type of Sigma Bond Metathesis", *Journal of the American Chemical Society*, Vol. 122, pp. 3867-3877 (2000).

162. Mandal, S. K., Ho, D. M., Williams, M. T., McEachin, C. and Becker, T. M., "Synthesis and X-ray Structures of Manganese(I) and Rhenium(I) Formato Complexes, *fac*-$(CO)_3$(dppp)M-OC(H)O", *Journal of Organometic Chemistry*, Vol. 599, pp. 308-312 (2000).

163. Wayland, B. B. and Woods, B. A., "Observation of Neutral Metallo-formyl Complex Formed by the Reaction of Rhodium Octaethylporphyrin Hydride with Carbon Monoxide", *Chemical Communications*, pp. 700-701 (1981).

164. Capdevielle, P., Maumy, M. and Audebert, P., "Electroactive Polymers Exchanging Transition-metal Ions- Synthesis of New Monomers and Polymers based on 6,6'-bis(2-hydroxyphenyl) Bipyridine Complexes", *New Journal of Chemistry*, Vol. 18, pp. 519-524 (1994).

165. Masood, M. A. and Zacharias, P. S., "Electrochemical Reversibility of the Couple in Bis[2,9-di(o-substituted phenyl)-1,10-phenanthroline]-copper(I) Complexes - Stability of the corresponding Copper(0) Species", *Journal of the Chemical Society, Dalton Transactions*, Vol. 1, pp. 111-114 (1991).

166. Lin, C. C., *MSc Thesis*, National Taiwan University: Taipei (1993).

167. Balducci, G., Chottard, G., Lexa, D. and Savéant, J. M., "Electrochemistry of Iron(I) Porphyrins in the Presence of Carbon Monoxide - Comparison with Zinc Porphyrins", *Inorganic Chemistry*, Vol. 33, pp. 1972-1978 (1994).

168. Bordwell, F. G., "Equilibrium Acidities in Dimethyl Sulfoxide Solution", *Account of Chemical Research*, Vol. 21, pp. 456-463 (1988).

169. Hinman, A. S. and Jones, D. H., "In Situ Infrared Spectroelectrochemical Studies of Tetraphenylporphyrin Complexes containing Manganese, Iron, and Cobalt", *Journal of the Chemical Society, Dalton Transactions*, pp. 1503-1508 (1992).

170. Vassiliev, Y. B., Bagotzky, V. S. and Osetrova, N. V., "Electroreduction of Carbon Dioxide. 1. The mechanism and Kinetics of Electroreduction of CO_2 in Aqueous-Solutions on Metals with High and Moderate Hydrogen Overvoltages", *Journal of Electroanalytical Chemistry*, Vol. 189, pp. 271-294 (1985).

171. Darensbourg, D. D. and Kudaroski, R. A., *"Advances in Organometallic Chemistry"*, F.G.A. Stone and R.W., Academic Press, New York, Vol. 22 (1983).

172. Kristjansdottir, S. S. and Norton, J. R. in *"Transition Metal Hydrides"*, Dedien. A ed., VCH Publisher, New York, Chapter 9 (1992).

173. Savéant, J. M., Bhugun, I. and Lexa, D., "Homogeneous Catalysis of Electrochemical Hydrogen Evolution by Iron(0) Porphyrins", *Journal of the American Chemical Society*, Vol. 118, pp. 3982-3983 (1996).

174. Collman, J. P., Ha, Y., Wagenknecht, P. S., Lopez, M. A. and Gilard, R., "Cofacial Bisorganometallic Diporphyrins: Synthetic Control in Proton Reduction Catalysis", *Journal of the American Chemical Society*, Vol. 115, pp. 9080-9088 (1993).

175. Collman, J. P., Wagenknecht, P. S. and Lewis, N. S., "Hydride Transfer and Dihydrogen Elimination from Osmium and Ruthenium Metalloporphyrin Hydrides: Model Processes for Hydrogenase Enzymes and the Hydrogen Electrode Reaction", *Journal of the American Chemical Society*, Vol. 114, pp. 5665-5673 (1992).